Department of Materials Science
and Metallurgical Engineering
University of Pretoria

E.T Boshoff

Identifying critical parameters in the settling of African kimberlite slimes

A dissertation submitted in partial fulfilment of the degree Master in Engineering (Metallurgical Engineering)

Supervisors: Dr. J. Morkel, Dr. N. Naude

ABSTRACT

Kimberlite is the host rock from which diamonds are mined. The mineralogical features for kimberlites vary greatly with country, origin, depth and type of kimberlite. Kimberlites can contain various clay species with some kimberlites containing predominantly clay minerals. The presence of these clay minerals in the ore can cause difficulty in dewatering due to high flocculant demand, poor supernatant clarity and low settling rates. Identifying critical parameters that can predict the settling behaviour of African kimberlite slurries will assist the process engineer to predict the settling behaviour of different kimberlite slurries. Especially identifying the kimberlites that will most likely not settle with normal flocculant dosage rates is useful.

From first principles the settling of a particle is described by Stoke's law which incorporates the density of the particle and size of the particle as the inherent particle variables. In this case density is assumed constant and therefore the size of particles influence the settling rate of particles to a great extent. This study therefore investigated the influence of particle size on settling rate and whether the particle size distribution showed correlation with settling rate when regression modelling was fitted on the data. Other variables that were tested for correlation with settling were pH when the kimberlite is mixed in water as well as various mineralogical features of the ore. Fitting a simple model to any of these properties or combinations of these properties was attempted which would allow for prediction of settling behaviour. The mineralogical features were classified by evaluating the mineral composition, fractional elemental analysis, cation exchange capacity and the exchangeable sodium percentage of the different kimberlites.

These variables were tested as well as their settling behaviour with 18 different African kimberlite samples. The settling rate and slurry bed compaction during natural settling as well coagulant and flocculant assisted settling were measured for the kimberlite slurries. The best performing coagulant and flocculant for each kimberlite were combined to evaluate potential improvements in the settling rates and slurry bed compaction compared to current settling practices that only utilise flocculant additions. Especially the

use of coagulant for kimberlites that did not show settling with only flocculants was evaluated. For these 18 kimberlites only 2 kimberlites did not settle with the use of flocculants with settling rates varying between 10.7m/h and 25m/h. Both these kimberlites also did not settle with the combination of coagulant and flocculant, but could only settle with only coagulant additions at settling rates of 1.9 m/h and 2.2 m/h.

Regression analysis fitted to the settling rate investigated the influence of particle size, pH and mineralogical features on settling. For representation of the particle size two data points from the Particle Size Distribution (PSD) was utilised which represented the fine material and the coarser material. These two data points were taken at percentage passing 7.5 µm and 75 µm. Regression data for kimberlite with flocculant additions showed that particle size and the pH of the slurry were identified as significant parameters in predicting settling. The regression data showed a R^2 of 0.78 for the settling rate and an adjusted R^2 of 0.79 for the slurry bed depth. The regression fitting for settling rate is given by:

$$Flocculant\ settling\ rate\ (\frac{m}{h}) = -9.99pH - 0.92(7.5\ micron) + 0.63(75\ micron) + 89.52$$

No similar significant relationships could be found for coagulant assisted settling of the kimberlite slurries. The two kimberlites, AC 56-5-1 and Venetia Red, that did not settle in the presence of flocculants both showed very high Cation Exchange Capacity (CEC) and Exchangeable Sodium Percentage (ESP) values of 54 and 30% for Alto Cuilo 56-5-1 and 32 and 43% for Venetia Red. It seems that the combination of CEC and ESP values could possibly allow for identification of the non-settling kimberlites. However more kimberlites will have to be tested to confirm this hypothesis.

ACKNOWLEDGEMENT

Firstly I thank the Lord Jesus Christ for the abilities and talents He blessed me with. Also for His divine inspiration and for giving me hope in the times it felt that there was none. I thank my wife for her continued support and understanding and for always being there. I thank Dr. Jacqueline Morkel and Dr. Natassia Naude for their technical support and continued effort to improve this dissertation as well as their friendship during this time. Gratitude to my parents acting as my laboratory assistants for the settling tests and for always being there and supporting me. Gratitude to mrs. Saartjie Spies from the High School Ermelo for allowing me to make use of their measuring cylinders for the settling tests. Gratitude to Petra Diamonds, especially Mr.Andre Rogers, and to Angolan Technical Services, especially Mr. Doug Winzar, for the supply of ore resources.

Thanks to Sabine Verryn at XRD Analytical and Consulting for the hours spent on XRD work to characterise the mineralogy. My wish is that this study will really improve the understanding the parameters that influence the settling of colloidal stable kimberlite slimes. I hope wholeheartedly that this goal was achieved.

TABLE OF CONTENT

List of Figures

List of Tables

ABBREVIATIONS

CEC Cation Exchange Capacity
ESP Exchangeable Sodium Percentage
SAR Sodium Adsorption Ratio
PSD Particle Size Distribution
PZC Point of Zero Charge
XRD X-Ray Diffraction
XRF X-Ray Fluorescence

1. Background

1.1 Project Definition

The settling of clay-rich kimberlite slimes often require high dosage of flocculants to treat diamond plant processing water. The addition of these chemicals not only poses an environmental concern, it is also a large operational cost driver and as such it is important to improve the settling rate. Operations tend to increase the chemical dosage rate to try and improve the settling rate while adhering to environmental legislation, but this does not always improve the settling rate of the slimes and in some cases effective dewatering becomes almost impossible.

The settling and dewatering of fines is usually predicted by predominantly the particle size of the fine material. The word clay is used synonymously with very fine material and often clays are defined as the - 45 μm material (Klein and Hurlbut, 1993). Operations have identified that more weathered material tend to increase problems in settling, whether it is due to the fine size or mineralogical features is however not clear (Vietti and Dunn, 2003).

The project aimed to identify the critical parameters in the settling process and specifically to validate whether particle size alone can predict settling. The dewatering behaviour was characterised by utilising settling tests. The investigation included characterising the mineralogical features as well as the influence of various coagulants and flocculants on the settling behaviour. The final stages of the project investigated regression modelling of the influence of variables on settling and assessing the contribution of these variables towards the settling behaviour observed.

Understanding the critical variables in the settling process will allow for better prediction of settling behaviour and for anticipation of problematic areas. It will also allow for improved optimisation of the dewatering if the critical parameters are

known. Optimising the dewatering behaviour of clay-rich kimberlite slimes can result in a direct and indirect influence on the "triple bottom line" sustainability outcomes, (environmental, economic and social/ethical) for the mining and minerals processing industry as shown in Table 1 (McFarlane et al, 2005a) and therefore is of importance.

Table 1: Features of improved dewatering on the "triple bottom line" approach to mining and mineral processing industries (McFarlane, 2005a)

	Environmental	**Economic**	**Social/Ethical**
Increased water recycling	Increased environmental flows	Reduced acquisition and infrastructure costs	Responsible resource management
Reduce reagent usage	Reduced contamination risk	Reduced acquisition cost	
Reduced energy consumption	Reduced greenhouse emissions	Reduced energy and pumping (capital) costs	Kyoto Protocol compliance
Faster disposal site rehabilitation	Improved ecosystem recovery, decreased erosion	Decreased assessment time	Reduced geo-technical risk
Extended mine life cycle (low grade extraction)	Fewer mines for the same output, waste recovery	Extended profitability of initial capital investment.	Longer term jobs, national/global exploitation efficiency

1.2 Mineral Processing

The mineral processing industry is synonymous with water recovery and recirculation with most of the processes being water based. The current drive for environmental compliance at mineral processing plants, place a large emphasis on water recovery and tailings rehabilitation practices. The water recovery process consist predominantly of thickeners from where the water is recycled to be reused in the process, while the slimes and grits are pumped to slimes dams to recover the rest of the water still entrapped in the slimes. The current drive throughout the industry is to reduce the footprint of the slimes dams and thereby reduce the environmental accountability for the mines.

The thickener is central to the water recovery process in the mineral processing industry and large amounts of research has been spent to recover as much water as possible in this primary water recovery stage. The more water recovered in the thickener leads normally to a smaller footprint for the slimes disposal area.

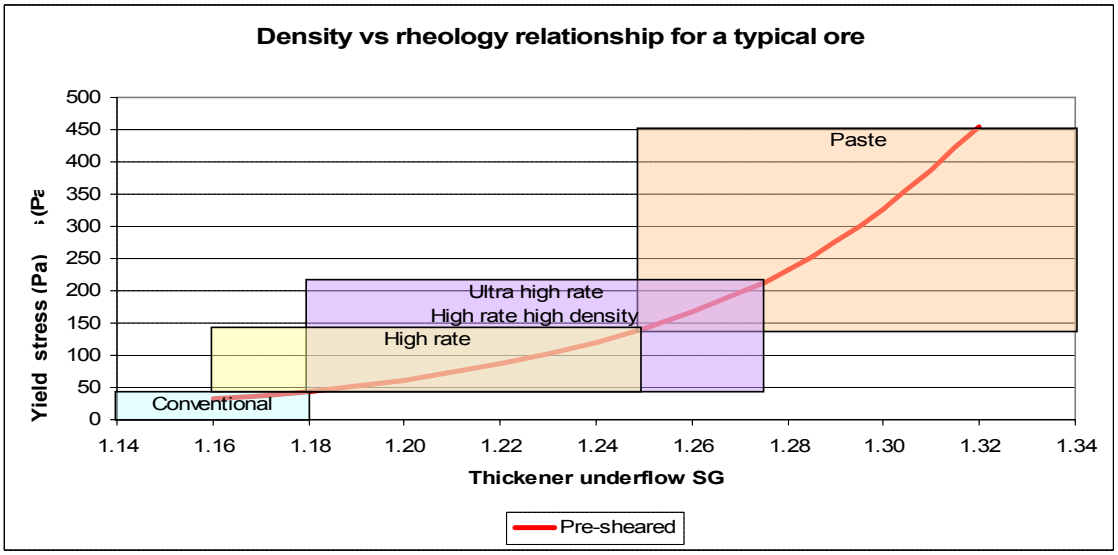

Figure 1: Density versus rheology relationship for a typical ore with the various thickener technologies to match. (Krause, B., 2008)

Currently there are 5 different type of thickeners used in industry and these types are: conventional thickeners, high rate thickeners, high rate – high density thickeners, ultra-high rate thickeners and paste thickeners (Krause, B., 2008). The density and rheology of the feed material to the thickeners determine the type of thickener best suited for the desired outcome as shown in Figure 1.

Coe and Clevenger (1916) and Talmage and Fitch (1955) developed a method to calculate thickener capacity based on batch settling tests. This method is based on a series of batch settling tests where the solids percentage is varied.

1.2.1 Diamond Processing

Diamond processing is based on the two cornerstones of minerals processing namely liberation and concentration as shown in Figure 2. The liberation process consist of two to three stages of comminution, where after the material is washed through scrubbers and screened to remove the fine clay particles adhering to the particles. The fine material is separated from the water in the water recovery section and dumped as tailings according to Hodgson (1981). The recycle of this water is critical because not only is water a costly resource but it is also scarce in the arid regions associated with the most diamond mines. The water recirculation and recovery process in most instances consists of thickeners, in various forms, to settle out the -1 mm clay rich material as quickly as possible. The thickener underflow is pumped to a slimes dam, where further water harvesting takes place. These dams require compact walls and this cannot be achieved without settling and collapsing the fine clay particles effectively and extracting the water from the voids between these particles.

The concentration step of diamond processing consist firstly of dense medium separation, where the material is separated according to its specific densities in various different processes where after the dense material containing diamonds is sent to the second concentration step. This is normally done by a first stage of X-

ray sorting machines followed by a second stage grease belts according to Hodgson (1981). The coarse material (+6mm) from the concentrate tailings stream is passed through a liberation circuit to liberate any locked diamonds in the coarser particles, while the fine particle (-6mm +1mm) stream is disregarded as waste on the tailings dumps.

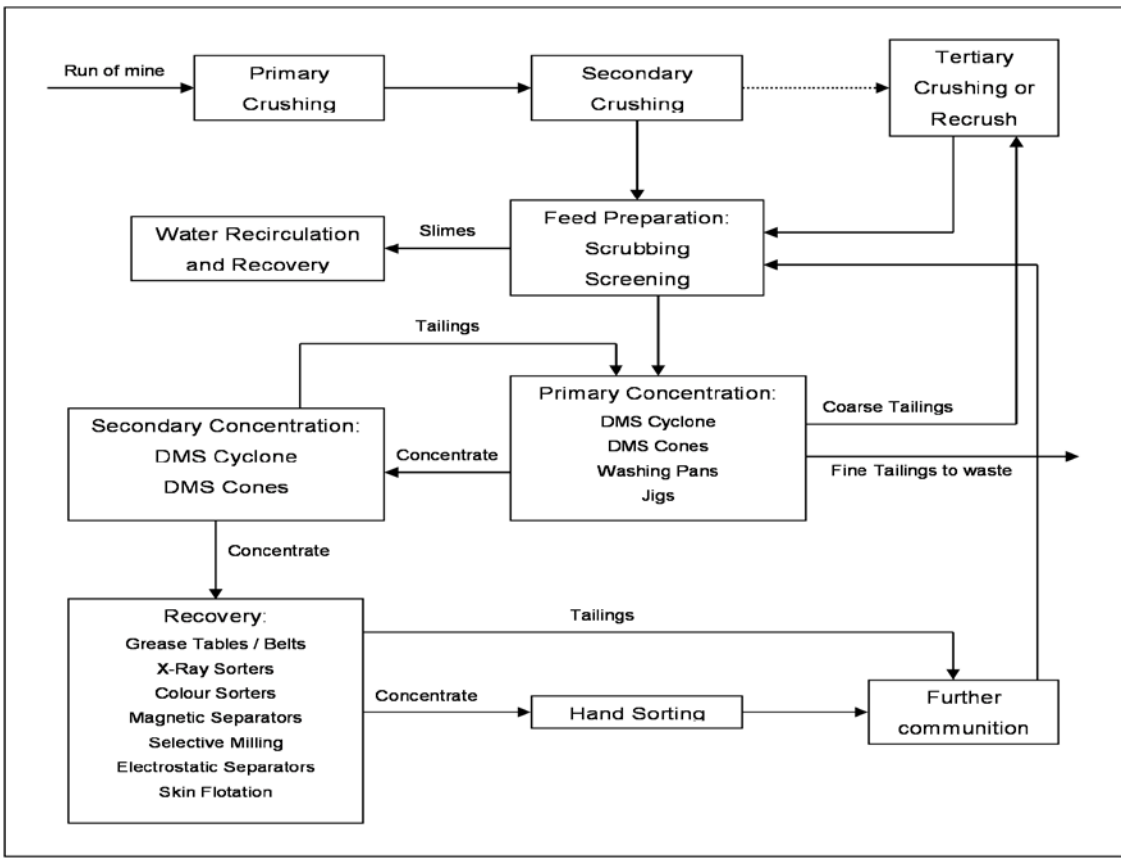

Figure 2: Generalised diamond processing flow sheet from Hodgson (1981).

1.3 Problem Statement

The project therefore ultimately aims to improve dewatering of kimberlite slimes by identifying the critical parameters that influence settling and dewatering behaviour. The focus of optimisation work was to identify parameters that have a larger influence on the settling process. The settling behaviour is usually predicted by the particle size of the fine material. Utilising only particle size is however in most

cases unsuccessful in predicting settling behaviour. One area that has been identified as a major contributor to settling is the mineralogical feature of the kimberlite and research has shown that different types of clay minerals tend to behave differently during settling (Bland and Rolls, 1998).

The negative charge surrounding the clay particles in suspension allow for possible settling through coagulation (cations that adsorb) or flocculation (long chain molecules that adsorb).

Cation adsorption on the particle surface and/or cation exchange in the particle interlayer balances out the negative charge surrounding the clay particle. The charge neutralisation improves the attraction forces between particles as well as with flocculant polymers, producing effective dewatering.

The pH of the dispersion play an important role as it dictates which hydrolysed cation species was adsorbed, while agitation could improve the settling by allowing more particle –polymer interaction (McFarlane et al, 2005 a,b).

The project therefore investigated correlation between settling and smectite content and also investigated whether the addition of coagulants (cations that can neutralise negatively charged clays) could improve settling further and whether coagulant or flocculant assisted settling could be predicted by regression modelling and what the major contributors to the settling process was. The test work aimed to identify critical parameters during the settling of kimberlites.

1.4 Hypothesis

Particle size alone cannot be used to predict the settling behaviour of kimberlite fine material. The project further aimed to identify the critical parameters in the settling process and investigated whether cation settling of clay rich kimberlites will be more efficient than settling with flocculants alone.

2. Literature Study

2.1 Kimberlite Mineralogy

Kimberlite is a rare volcanic rock and can be diamondiferous. Kimberlite volcanoes are normally found as inverted cone shapes and are known as pipes (Harlow, 1998). The process of viscous magma travelling upwards through cracks in the base rock is suggested as the formation of the kimberlite pipes. The magma breaks through at the surface at ultra-high velocities due to entrapped gasses being dislodged from the matrix and in the process diluting and fracturing the crust. This gaseous magma fluid, consisting of rock and mineral fragments, erupts at the surface forming the characteristic volcano crater zone. This crater zone is quickly eroded away by the elements due to the weathering process of kimberlite (Harlow, 1998).

The petrology of kimberlite is very complex and it is not yet defined conclusively. The definition used by Skinner and Clement (1979) is most widely accepted for kimberlite. Kimberlite is defined as diverse ultra-basic rocks consisting of xenocrysts, phenocrysts and groundmass. The principal groundmass minerals may include olivine, monticellite, clinopyroxene, pyroxene, phlogopite, calcite and serpentine (Skinner and Clement ,1979). The minerals that could be present as phenocrysts, the first crystals that starts to grow in cooling magma, are olivine, pyroxene, ilmenite, garnet, zircon and diopside. Serpentization and carbonation are some of the weathering processes that can alter the initially formed kimberlite matrix minerals. Weathering alters the mineral composition of olivine, monticellite and apatite to serpentine, chlorite, calcite smectite and diopside. The ore alteration sequence is shown in Figure 3 and Table 2 provide the chemical composition of these minerals.

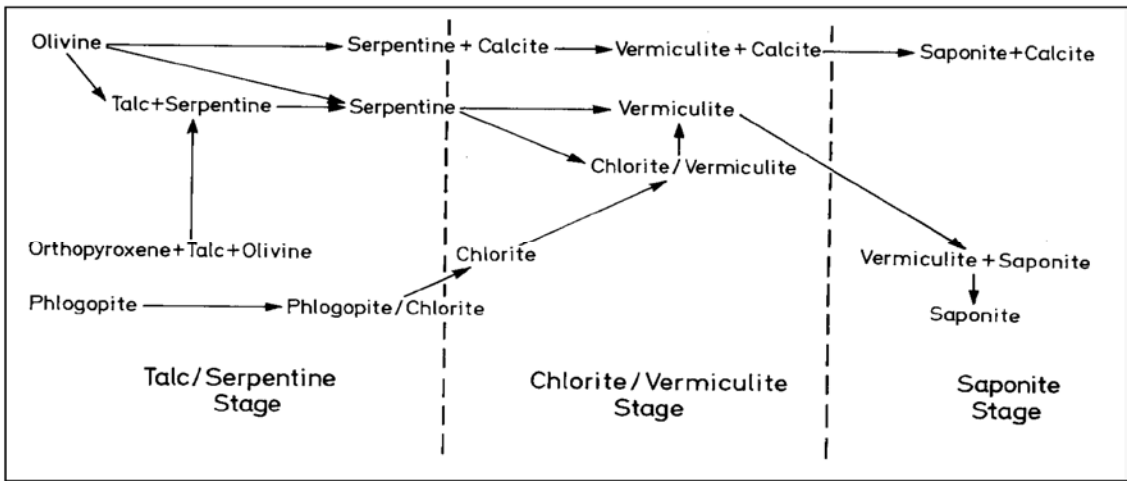

Figure 3: Schematic diagram showing the alteration of olivine, pyroxene and mica from Dawson (1980).

Table 2: Kimberlite mineral phases (Composed from Klein and Hurlbut, 1993).

Mineral Name	**Specific Gravity**	**Composition**
Apatite	3.15 – 3.2	$Ca_5(PO_4)_3$ (F_1Cl_1OH)
Calcite	2.71	$CaCO_3$
Chlorite	2.6 – 3.3	$(Mg,Fe)_3(Si,Al)_4O_{10}(OH)_2 \cdot (Mg,Fe)_3(OH)_6$
Diopside	3.2	$CaMgSi_2O_6$
Ilmenite	4.7	$FeTiO_3$
Kaolinite	2.6	$Al_2Si_2O_5(OH)_4$
Monticellite	3.2	$CaMgSiO_4$
Montmorillonite	2.4	$(Al,Mg)_8(Si_4O_{10})_4(OH)_8 \cdot 12H_2O$
Olivine	3.27 – 4.37	$(Mg,Fe)_2SiO_4$
Orthoclase	2.55 -2.63	$KAlSi_3O_8$
Perovskite	4.03	$CaTiO_3$
Phlogopite	2.86	$KMg_3(AlSi_3O_{10})(OH)_2$
Plagioclase	2.6 – 2.76	$NaAlSi_3O_8 – CaAl_2Si_2O_8$
Saponite	2.24 – 2.3	$Ca_{0.25}(Mg,Fe)_3((Si,Al)_4O_{10})(OH)_2 \cdot n(H_2O)$
Serpentine	2.3	$Mg_3Si_2O_5(OH)_4$
Talc	2.7 – 2.8	$Mg_3Si_4O_{10}(OH)_2$
Vermiculite	2.4	$(Mg,Fe,Al)_3(Al,Si)_4O_{10}(OH)_2.4H_2O$

Clay minerals form during weathering processes and these minerals are naturally soft and flaky with a low specific gravity. These clay minerals are classified in the phyllosilicates mineral group. Smectite, consisting mostly of montmorillonite and saponite, along with vermiculite, are the most common swelling clay minerals found in kimberlite. During swelling these minerals can create internal pressures which reduce the overall strength of the rock.

Diamonds are a rare constituent of kimberlite mineralogy and if any diamonds are present it is normally at a low grade of between 5 – 140 carats per hundred tons (cpht), where 1 carat = 0.2 grams (Wilson and Anhaeusser, 1998).

There are to date up to 4000 different kimberlites and lamproites intrusions identified and more are identified each year due to the systematic exploration program carried out by the various diamond exploration companies. Various attempts have been made to classify kimberlites according to the different mineralogical compositions. Mitchell (1986) classify kimberlites into three groups according to the amount of olivine, phlogopite and calcite; kimberlite (equivalent to basaltic kimberlite), micaceous kimberlite (equivalent to lamprophyric kimberlite), and calcite or calcareous kimberlite. Skinner and Clement (1979) classify kimberlites into five groups according to the predominance of diopside, monticellite, phlogopite, calcite and serpentine present.

The clay mineralogy and abundance will influence the settling behaviour and therefore is an integral part of this study. Minor minerals however are not part of this study and for more information on this the reader is referred to the work of Mitchell (1986).

2.1.1 Olivine

Olivine is the original mineral from which clay minerals form and was found at high concentrations during the early stages of the kimberlite formation. It is also the

most characteristic mineral when focusing on weathering, because it forms the basis for most of the alteration steps as shown in Figure 3. Olivine has a SG of 4.2 – 4.3. Due to its high weatherability, olivine is commonly altered along margins and fractures to several varieties (pseudo morphs) of serpentine (with or without magnetite) and also calcite. This alteration or decomposing of olivine is principally through the hydrolysis of the silicate tetrahedra and can be described as either of equations 1 or 2:

$$2Mg_2SiO_4 + 3\,H_2O \rightarrow Mg_3Si_2O_5(OH)_4 + Mg(OH)_2 \quad (1)$$

Olivine — Serpentine — Brucite

$$2Mg_2SiO_4 + 2\,H_2O \rightarrow Mg_3Si_2O_5(OH)_4 + MgO \quad (2)$$

Olivine — Serpentine

Secondary processes can locally form less prominent alteration minerals e.g. brucite, chlorite, talc, quartz, barite and pyrite (Mitchell, 1986).

Olivine is mainly present as a groundmass constituent and consists of crystals not larger than 0.5 mm. It typically varies in colour from pale green to pale yellowish brown as the iron content increases (Mitchell, 1986). The substitution of Mg^{+2} with Fe^{+2} could be up to 15% but it is seldom this high in kimberlite material.

2.1.2 Serpentine

Serpentine is formed over centuries during the alteration process of olivine and is one of the main minerals in blue ground. Blue ground is unweathered kimberlite found deeper in the volcanic pipe. Serpentine can account for 20 – 50% of the groundmass and has a SG of 2.5 – 2.6. Serpentine is the mineral that chemically breaks down during the weathering process into the clay minerals of smectite, vermiculite, calcite, chlorite and talc (Hopwood et al, 1975). The alteration to talc can be described by equation 3:

$$2Mg_3Si_2O_5(OH)_4 + 3CO_2 \rightarrow Mg_3Si_4O_{10}(OH)_2 + 3MgCO_3 + 3H_20 \quad (3)$$

Serpentine — Talc — Magnetite

The degradation products of serpentine are dependent on water and also the activity of CO_2 in the natural environment. The partial pressure of CO_2 will promote the formation of carbonates and thus provides a means of removing the magnesium. Serpentine minerals can also be weathered by the attack of hydrochloric acid that can occur even at ambient temperatures. This is probably the reason for the breakdown of serpentine in soils and this reaction is described by equation 4:

$$Mg_3Si_2O_5(OH)_4 + 2H_2 \rightarrow 3Mg^{2+} + 2Si(OH)_4 + 2H_2O \quad (4)$$

Serpentine

Most of the published papers show that the weathering process is characterised by the loss of magnesium and calcium ions associated with the emission of carbon dioxide and a gain in aluminium and iron content in the residue.

In later alteration stages the serpentine themselves can be replaced by calcite, phlogopite and magnetite (Mitchell, 1986).

2.1.3 Calcite

Calcite can report for up to 50% of the minerals in calcite rich ores. This makes it the predominant carbonaceous mineral in most of the kimberlites. It replaces mostly olivine, monticellite, apatite and phlogopite during the weathering process. Calcite is found as a rather pure mineral in kimberlites and contains low percentages of MgO and FeO as impurities. Calcite normally replaces the unstable apatite, which in some ores account for less than 1 weight percentage compared to 10 weight percentage in other ores (Klein and Hurlbut, 1993).

2.1.4 Phlogopite/Micas

Phlogopite ($KMg_3(AlSi_3O_{10})(OH)_2$) consists predominantly of silvery bronze single crystals ranging in diameter size from 5 mm to10 cm. Micas are defined as the finer fractions, smaller than 5 mm, of phlogopite. Micas are normally found in the ground mass and these mica crystals are usually between 0.05 to 1 mm in size and can be rounded, distorted and also corroded crystals. It can easily be found within calcite-serpentine segregations (Mitchel, 1986).

2.1.5 Apatite

Apatite can normally be found in calcite or carbonate rich kimberlites. It can account from 1 weight percentage up to 10 weight percentage of the groundmass consisting mainly of grains less than 0.01 mm. Apatite is not vary stable and is easily replaced by calcite (Klein and Hurlbut, 1993).

2.1.6 Clay minerals

Clay minerals are the main group in which most alteration products are grouped and are thus important in the settling of kimberlite slimes. Understanding the ionic changes that occur during the processing of kimberlite can aid in settling these clay minerals. The main clay minerals formed from the alteration of olivine, pyroxene and mica, are montmorillonite, saponite and serpentine.

Clay minerals are categorised by the structure of the sheets and also the linkage between these sheets. Clay minerals are defined as 1:1 or 2:1 clays where a 1:1 clay consist of a single octahedral and tetrahedral sheet repeated in the structure and bonded by weak intermolecular forces. A 2:1 clay is a single octahedral sheet between two tetrahedral sheets. The sheets can be formed from the linkage between SiO_4 tetrahedra and octahedra as shown in Figure 4 & Figure 5. The

enclosed ion in the tetrahedral sheet is normally Si^{4+}, but it can be replaced by Al^{3+} or Fe^{3+} (Bland and Rolls, 1998). The tetrahedral layers of the 1:1 clays are linked together by sharing their basal oxygens as shown in Figure 4. Water cannot enter between these layers and these clays are termed non-swelling clays. Examples of these clays are kaolinite with a gibbsite ($Al(OH)_3$) layer and serpentine ($Mg_3Si_2O_5(OH)_4$) with a similar structure, only the gibbsite is replaced by brucite ($Mg(OH)_2$).

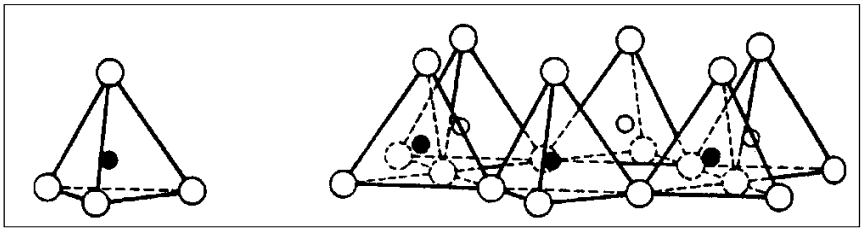

Figure 4: Illustration of a single SiO_4 tetrahedron and the sheet structure of SiO_4 tetrahedra from Bland and Rolls (1998).

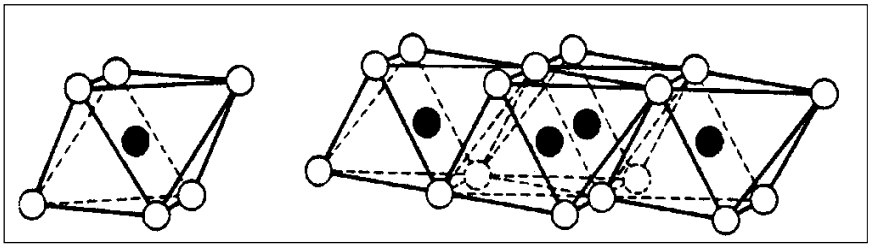

Figure 5: Illustrating a single octahedron and the sheet structure of linked octahedral from Bland and Rolls (1998).

The octahedral sheets consist of six oxygen or hydroxyl ions which link through sharing their octahedral edges as shown in Figure 5. This results in a net negative charge of –2. This negative charge are balanced out by either a single divalent cation (Mg^{2+}) for each octahedral sheet or two out of three octahedrons can be bonded to two trivalent cations such as Al^{3+}. Each octahedron requires one divalent cation (Mg^{2+}) to form a trioctahedral sheet as an intermediate layer. Two out of every three octahedrons can bond to two Al^{3+} ions to form a dioctahedral layer. This octahedral layer also represents the lower energy state for the

intermediate cations. This incorporation of cations between the layers is shown in Figure 6.

Clay minerals are defined as 1:1 or 2:1 clays where a 1:1 clay consists of a single octahedral and tetrahedral sheet repeated in the structure and bonded by weak intermolecular forces. A 2:1 clay is a single octahedral sheet between two tetrahedral sheets. The characterisation of the clay sub-groups are shown in Table 3.

Table 3: The layered silicates as published in Bland and Rolls (1998).

Main group	**Subgroup**	**Examples**
Two layers (1:1)		
Kaolinite	Kaolinite	Kaolinite, halloysite
Kaolinite	Serpentine	Chrysotile, greenalite
Three layers (2:1)		
Pyrophyllite	Pyrophyllite, talc	Pyrophyllite, talc
Smectite	Dioctahedral	Montmorillonite, beidelite
	Trioctahedral	Saponite, saucinite
Vermiculite	Dioctahedral	Vermiculite
	Trioctahedral	Vermiculite
Mica	Dioctahedral	Illite, muscovite, sericite
	Trioctahedral	Biotite
Chlorite	Trioctahedral	Corundophite, pseudothuringite, talc-chlorite

The 2:1 clay structures are constructed with 3 sheets, a single octahedral layer between two tetrahedral layers. These three layer structures are bonded together with either a cation, looking at the illite and vermiculite structures, or with brucite ($MgOH_2$) in the case of chlorite. In this brucite layer some of the Mg^{2+} is replaced by Al^{3+} cations. See Figure 6 for illustrations of the different bonding between structures.

Illite has very few interlayer cations (K^+, Ca^{2+}, Mg^{2+} and H^+) and if K^+ is the predominant interlayer cation, cation exchange and water entering between the structures are limited (Morkel, 2005). Chlorite has an electrostatic brucite sheet binding the three sheet structures. This strong bond limits swelling.

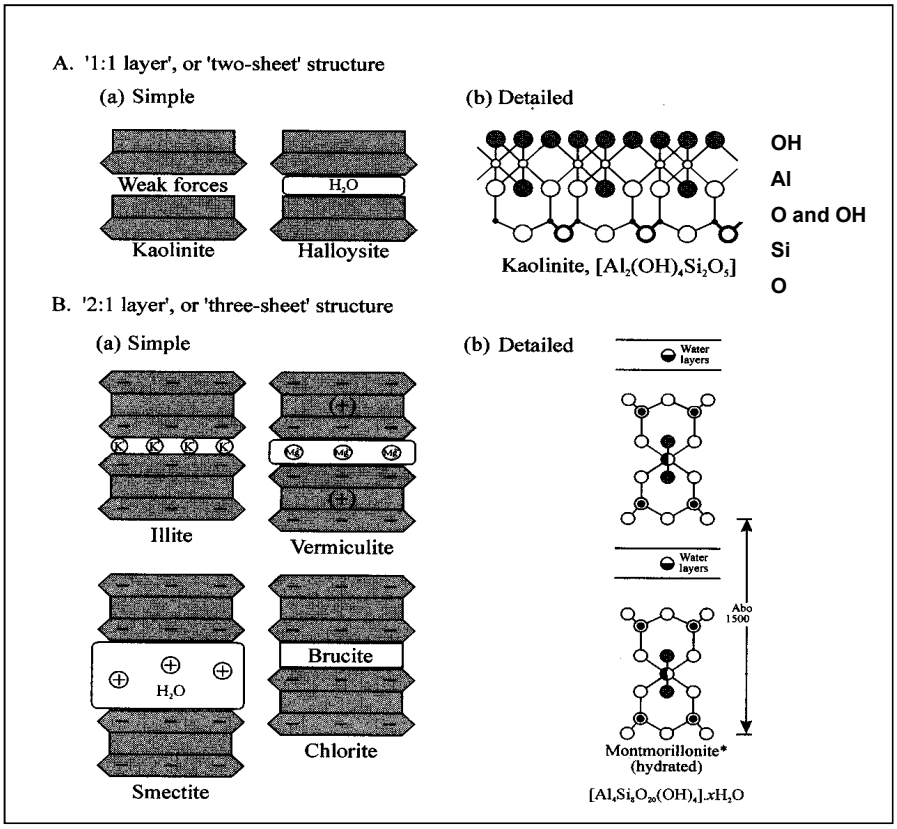

Figure 6: Structures of the clay minerals from Bland and Rolls (1998).

In the smectite group, montmorillonite is associated with the replacement of Al^{3+} with Mg^{2+} in the octahedral layer along with Na^+ being introduced as an interlayer cation. Vermiculite however experiences the replacement of Si^{4+} with Al^{3+} or Fe^{3+} and Mg^{2+} as interlayer cations. The cation exchange and the cations can readily adsorb water and is the cause of the swelling behaviour observed with these clay minerals.

2.2 Settling behaviour of kimberlite slimes

Kimberlite waste tailings typically contain various clay minerals. The presence of these clay minerals in the ore mixtures can cause difficulty in dewatering due to high flocculant demand, poor supernatant clarity and low settling rates. Handling problems like gelation and space filling “card house” structures can also occur due to the swelling of the clay minerals (Addai-Mensah, 2007). Mpofu et al (2005) have shown that it is possible to settle clay minerals at high settling rates (10-30 m/h) as well as acceptable supernatant clarity (< 50 mg.dm^3 suspended solids) with a high molecular weight flocculant, anionic polyacrylamide(PAM) in combination with hydrolysable metal ions, Mn^{2+} and Ca^{2+} acting as coagulants.

2.2.1 Surface charge on clay minerals

The settling of clay dispersions is dependent on the chemical interactions of the particle with the solution as well as the other particles. The main chemical parameters influencing the settling of the clay particles are the diffuse double layer or zeta potential (ζ) surrounding the clay particles, the pH of the solution, the hydration of the cations in solution and the cation exchange between the clay particle surfaces and the solution (Vietti, 2004).

2.2.1.1 The Electric Double Layer

The diffuse electric double layer is defined as a surface charge of a particle and a compensating counter-ion charge in solution (Van Olphen, 1977). This results in excess amounts of ions of the opposite sign accumulating close to the particle surface and the electrostatic repulsion of ions of the same sign from the particle surface as shown in Figure 7.

The zeta potential (ζ) is defined as the electrical potential at the plane of shear of the diffuse electric double layer and is the only experimentally possible

measurement of particle charge. This plane of shear is situated between the bounded ion layer, or Stern layer, and the cloud of diffuse ions extending into the solution, as shown in Figure 7. The zeta potential is dependent on the surface charge of the particles and on the concentration and charge of the counter-ions in solution (Wills, 1997). In a solution with high ionic strength the electric double layer will be compressed resulting in a low zeta potential for the particle.

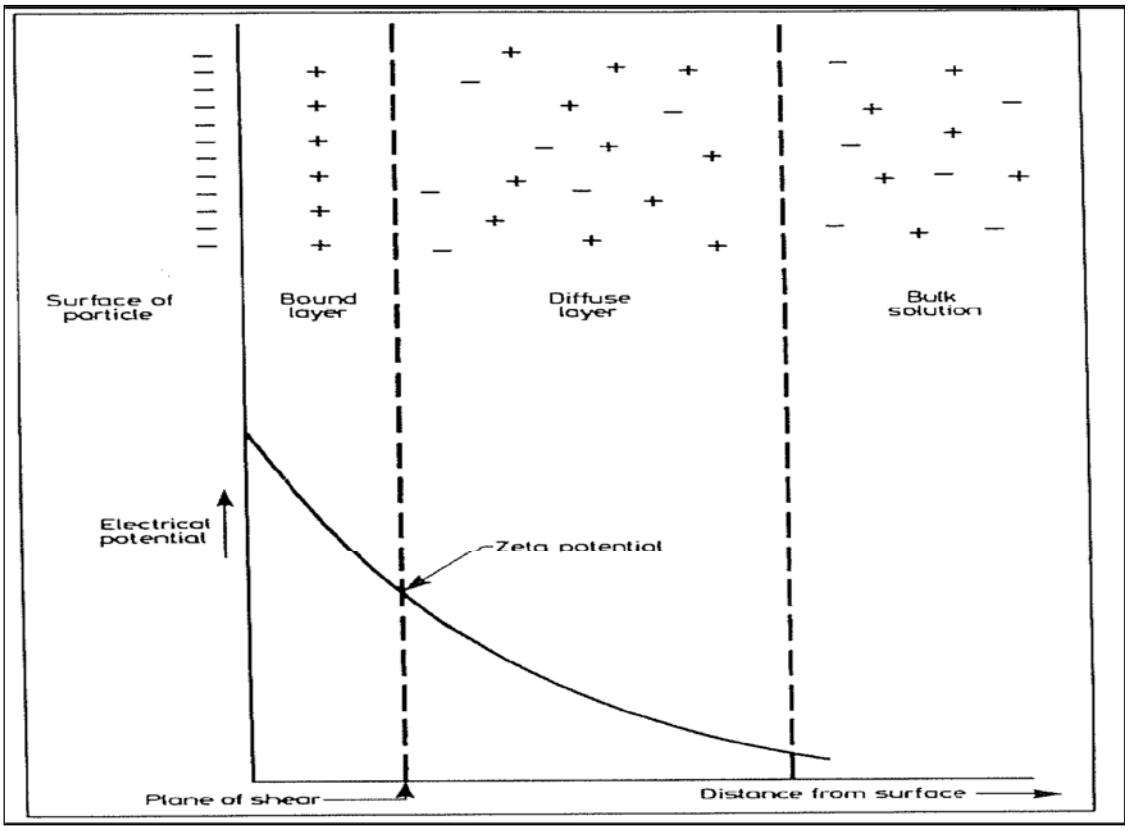

Figure 7: The zeta potential (ζ) of the diffuse double layer (Wills, 1997).

Derjaguin and Landau (1941) and Verwey and Overbeek (1948) used the double layer compression concept and independently developed a theory known as the DLVO theory for particle – particle interaction. This theory states that when two particles in solution moves closer to one another, the electric double layers will overlap and the residual attraction energy (V_T) can be predicted by adding the double layer repulsion (V_R) and van der Waal's attractive energies (V_A) as shown in Figure 8. The residual attraction energy determines whether colloidally stable

or unstable slurries are achieved. A reduction in the electric double layer repulsion force, caused by the addition of metal cations in solution, can result in a positive residual attraction energy that will lead to particle interactions.

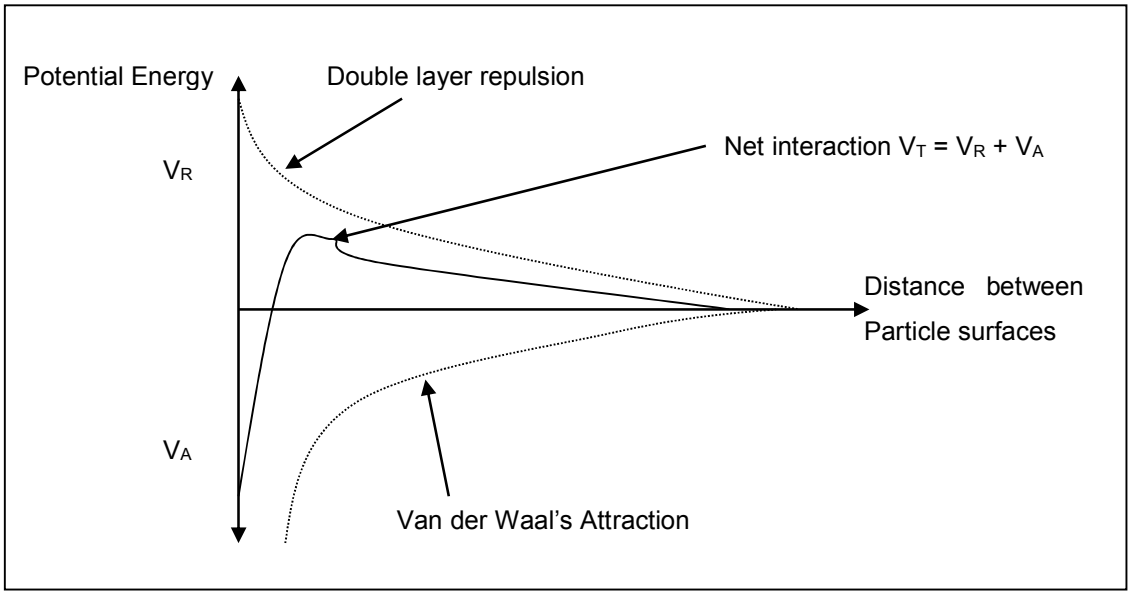

Figure 8: The net potential energy curve between two particles in suspension (Derjaguin and Landau, 1941, Verwey and Overbeek, 1948).

2.2.1.2 The compression of the electrical double layer (zeta potential)

The ζ potential measurement of colloidal particles provide information regarding the repulsive forces surrounding the particles in solution as discussed in section 2.2.1.1. Mpofu et al (2004, 2005) and McFarlane et al (2005, 2006) compared the ζ potential of 8 wt% sodium exchanged montmorillonite dispersed in a 0.01 M KNO_3 solution before and after the addition of Ca^{2+} and Mn^{2+} cations over the whole pH range. The results indicated a definite positive shift in ζ potential after the addition of the metal cations. The ζ potential did not show any significant movement after the addition of flocculants, anionic polyacrylamide copolymer (PAM) and non-ionic polyethylene oxide copolymer (PEO) to the montmorillonite dispersion treated with metal cations although the settling rates of the

montmorillonite slimes dispersion improved with the addition of flocculants. Comparing the ζ potential of the slime particles before and after the addition of cations and flocculants it is possible to predict the settling characteristics of the particular slime dispersion.

The potentiometer or accoustosizer is used to determine the ζ potential of slime dispersions through dynamic stability measurements (Kosmulski and Dahlsten, 2006). A 10^{-2} M KNO_3 solution is normally used to eliminate the surface conductance at low ionic concentrations.

2.2.1.3 Influence of pH on clay surface charge

The surface charge of clay minerals account for almost 80 percent of the exchangeable cation capacity, while the remainder is attributed to the clay particle edges (Vietti and Dunn, 2003). Under aqueous conditions the hydroxyl (OH^-) groups will attach to the exposed silicon tetrahedral and metal ion octahedral atoms at the clay edges (Svarovsky, 1981). The pH of the environment will have a major influence on the crystal lattice charge, especially under aqueous conditions where the hydroxyl (OH^-) groups will attach to the exposed octahedral and tetrahedral ions at the clay edges (Svarovsky, 1981). Acidic environments will protonate the OH^- groups to carry an overall positive charge. An increase in pH deprotonate the OH^- groups until an edge neutrality is reached and this pH is defined as the Point of Zero Charge (PZC) where zero charge exists as seen in Figure 9. A further increase in pH results in the clay edges to be dominated by an overall negative charge because of the deprotonation of the OH^- groups.

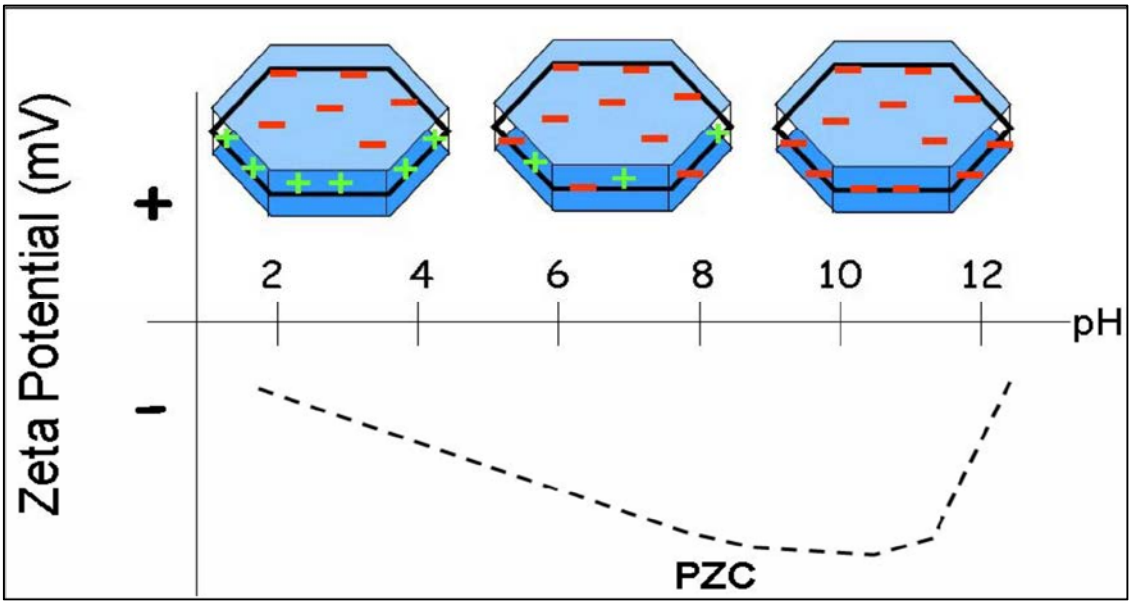

Figure 9: pH dependence of the surface electrical charge of 2:1 clays (Vietti, 2004).

2.2.1.4 Ionic concentration of the solvent

Settling difficulties are associated with repulsive forces surrounding the colloidal particles at low ionic concentrations and as the ionic concentration increases the electric double layer surrounding particles contracts and the particles can interact with one another as seen in Figure 10. The ionic concentration at which particles starts to attract one another are defined as the Critical Coagulation Concentration (CCC) and this is discussed further in section 3.1.

Research done by Mpofu et al (2005) indicated a considerable reduction in the zeta potential of smectite particles (8 wt %) with the addition Mn^{2+} and Ca^{2+} ions. This reduction takes place across the pH spectrum. It is interesting to note that with the addition of Ca^{2+} ions and at a pH value larger than 10, the zeta potential reversed from negative to positive values. This phenomenon (Healy, 1969, James and Healy, 1972a,b) can be attributed to the specific adsorption of hydrolysed Ca^{2+} species ($Ca(OH)^{+}$) and surface nucleation of $Ca(OH)_2$

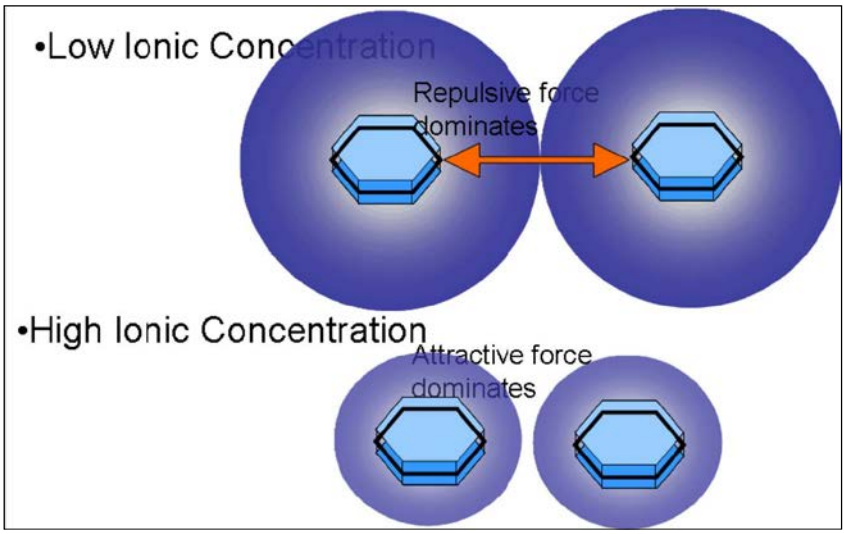

Figure 10: Illustrating the ionic strength of the solution (Vietti, 2004).

Mpofu et al (2005) also found that at certain pH values Ca^{2+} adsorption was favoured above Mn^{2+} and vice versa because the cations hydrolysed at different pH values. This is important to note, because the pH of the process water could dramatically influence the settling properties of the smectite in the presence of cations.

Research done by Kosmulski and Dahlsten (2006) indicated that the zeta potential of montmorillonite at high ionic strengths (0.1M - 2M) reduced the absolute value of the ζ potential and moved the Isoelectric potential (IEP) to higher pH values. The preferred adsorption for cations tested decreased in the series Cs> Rb > K > Na > Li. Kosmulski and Dahlsten (2006) also compared clay minerals with silica and categorised the clay minerals as “soft” compared with “hard” metal oxides. These soft surfaces attract soft ions and reject hard ions.

Research done by Kosmulski and Dahlsten (2006) indicates that at high ionic strengths, the hard cation – soft anion ($LiNO_3$) combination will result in a high absolute value of the ζ potential, while a soft cation – hard anion (CsCl) will lower the absolute value of the ζ potential. Unfortunately there is not a qualitative hard – soft scale available as noted in the reaction of KCl with kaolin and silica as a soft action – hard anion pair, while KCl acts neutral with montmorillonite.

2.2.2 Swelling of clay minerals

Serpentine, a clay mineral can contribute up to 60% or even more of the composition of kimberlite. However it is a non-swelling clay mineral due to its 1:1 structural arrangement as discussed in section 2.1.6. During the weathering process, serpentine is altered to smectite and vermiculite, which are swelling clay minerals with a 2:1 linkage between adjacent layers held together by strong columbic forces as well as weak Van der Waals forces. The swelling clay content of the ore is an important factor, because the first phase, crystalline swelling, is due to the hydration of the exchangeable cations within the dry clay structure as indicated in Figure 11. This causes the widening of the spacing between the clay particle layers to almost double the initial volume and also results in a charge balance around the clay particle. This volume change keeps on increasing as more water layers are absorbed until it reaches its maximum displacement. This displacement can relate to pressures of up to 100 N/mm^2 according to Madsen and Müller-Vonmoos (1989).

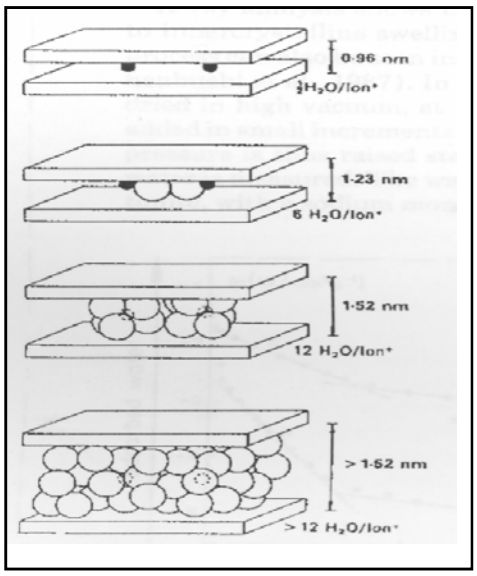

Figure 11: Inner crystalline swelling of montmorillonite as published by Madsen and Müller-Vonmoos (1989).

The second swelling phase is due to osmotic swelling in the clay minerals. According to Madsen and Müller-Vonmoos (1989), osmotic swelling can produce pressures of up to 2 N/mm^2 and can continue indefinitely. Osmotic swelling occurs because of a large concentration difference between the electro-statically bonded ions on the surface and the pore water of the rock. This result in an excess negative charge on the surface which must be corrected by positive ions close to the clay crystal surface and a resultant high concentration of positive ions close to the surface. This cloud of positive ions and the negative surface layer form the diffuse electric double layer. If the exchanged cation species are monovalent (Na^+, Li^+) the osmotic pressures can overcome the weak Van der Waals attraction. The swelling of these clays result in poor settling rates (e.g. < 0.1 m/h) as well as a low sediment solid loading (< 10 wt%) (McFarlane et al, 2005b).

2.2.2.1 Clay particle packing relationship

Clay particles can have various particle packing relationships due to the shape of the clay particles and the anisotropic charge. The main two packing relationships are the edge-face ("house of cards") and the face-face ("band structure") interactions (van Olphen, 1977; Lagaly, 1993; Luckham and Rossi, 1999). Figure 12 shows a scanning electron image of the face-to face- packing relationship. Smectites are however not normally associated with "house of cards" structure, which is dependent on a negative basal face attraction and a high angle positive edge, because the total edge face surface area is very small compared to the basal face area. The basal face negative charge is significantly larger than the edge face positive charge and the thin particles are able to bend normally to the interlayer orientation (McFarlane et al, 2005b).

Smectite particles were found to form "honeycomb" structures which retain large volumes of water in the void spaces similar to the "house of cards" structure (McFarlane et al, 2005b). It is these large volumes of water that need to be

removed for effective dewatering. A scanning electron image of the honeycomb structure is shown in Figure 13.

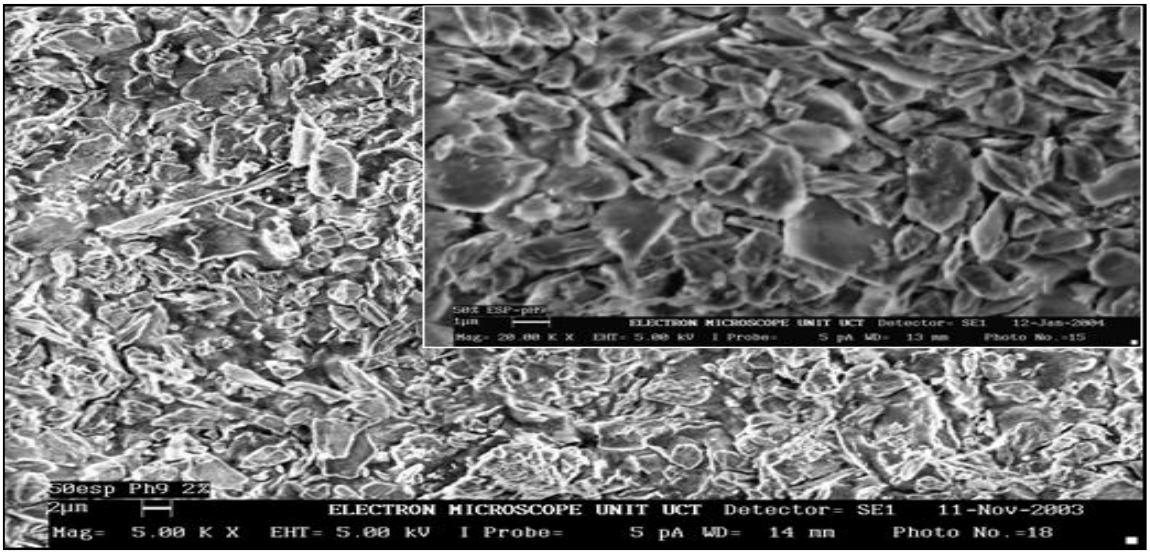

Figure 12: Scanning Electron Micrograph showing the face-to-face structure normally associated with no interaction between the smectite particles (Vietti, 2004).

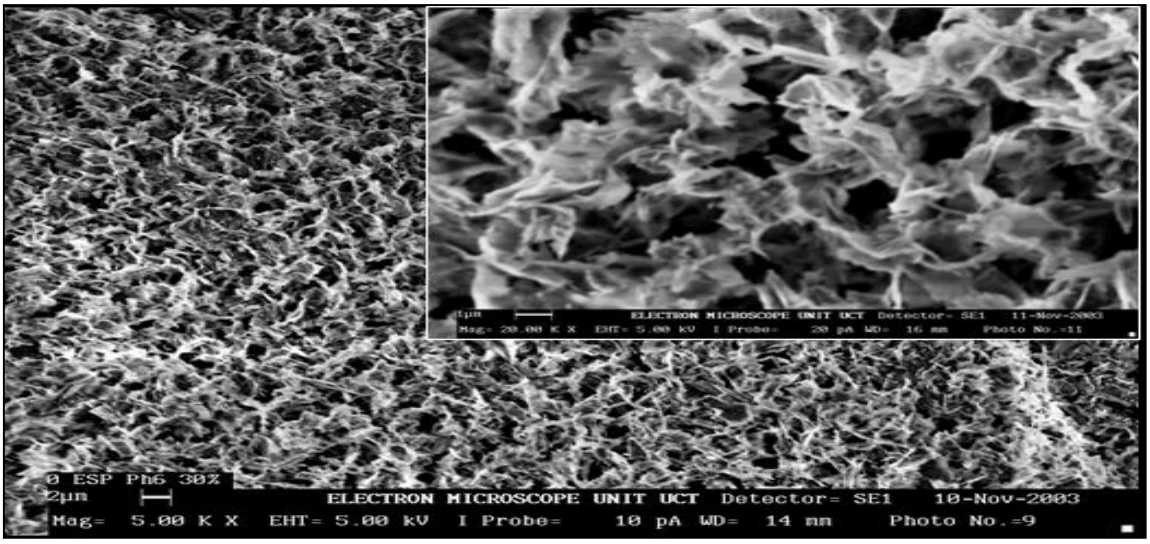

Figure 13: Scanning Electron Micrograph showing the honeycomb structure normally associated with interactive smectite particles (Vietti, 2004).

2.2.2.2 Sorption of metal ions on clay minerals

Smectites are able to adsorb organic and inorganic chemicals because of the large specific surface areas and the permanent electrostatic charge (Schlegel et al, 1999). This electrostatic charge is due to the isomorphic substitution of cations within the smectite structure (Sposito, 1984). These characteristics allow for the sorption of exchangeable cations onto or into the clay crystal structure. A cation will be adsorbed onto the exchange sites when the hydration enthalpy of the sorbate is low, when the background electrolyte concentration is low along with a high concentration of the cation in the clay (Sposito, 1984).

Electro-spin resonance (ESR), X-ray photoelectron spectroscopy and X-ray adsorption fine structure spectroscopy (EXAFS) indicates that most exchangeable divalent cations maintain a complete hydration sphere in water as shown in Figure 14. This hydration sphere could aid in the expansion of the interlayer which will result in swelling.

Cation exchange between the clay surface and the solvent is a quick process and can be completed within minutes. Outer sphere (OS) complexes are formed near the basal plane of smectite. Cation sorption studies at low cation concentrations indicate an increase in uptake of cations at higher pH values while the same trend is noted at high ionic strength conditions. Under these conditions the outer sphere surface complexes acts as a transient cation buffer, from which cations can further migrate to edge sites (Schlegal et al, 1999). Inner sphere (IS) complexes are formed on the octahedral edge sites. This migration of cations from the outer sphere to the inner sphere is a much slower process as the initial cation exchange process and this indicates that the cation exchange process will only reach equilibrium after several days.

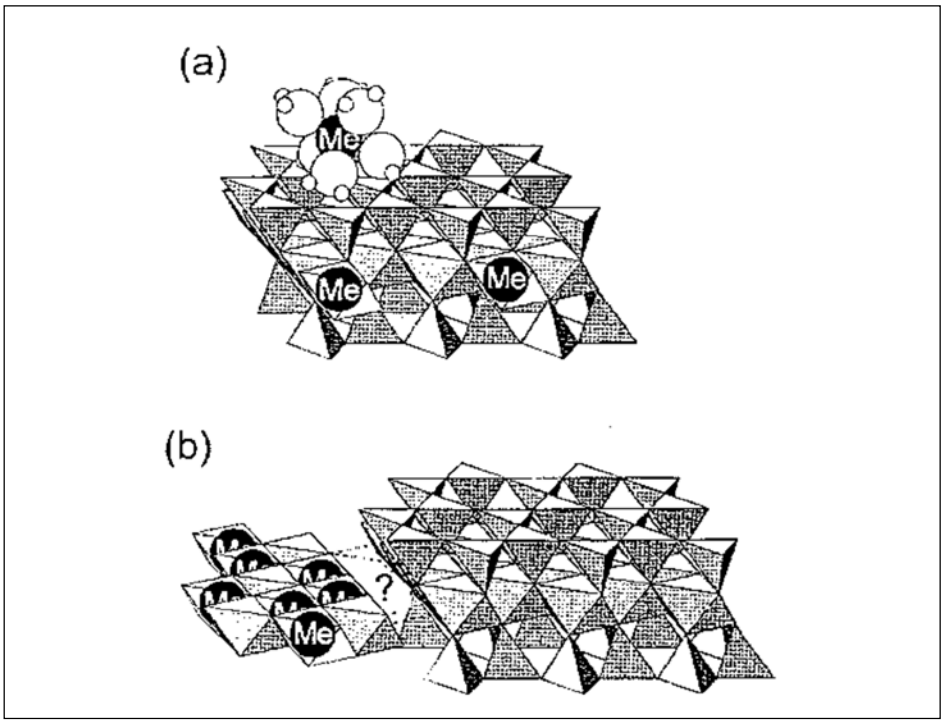

Figure 14: Illustration of different sorption mechanisms of metal ions on clay minerals (Schlegal et al, 1999). (a) Adsorption of metal ions as outer sphere surface complexes on the basal planes and as inner sphere surface complexes on crystallite edges. (b) Co precipitation of the sorbate and sorbent species liberated by dissolution.

2.2.2.3 Cation Exchange Capacity

The cation exchange capacity (CEC) of an ore is its ability to adsorb cations and is measured as the number of centimoles (cMol) of cations replaced per kilogram of ore treated (Bland and Rolls, 1998). This indicates that if an ore has a CEC of 10 Mol/100g, 100 g of ore can exchange 10 Mol of Na^+ with 10 Mol of another cation. Van Olphen (1977) found that the CEC for smectite can range from 60 – 150 mili-equivalents per 100 gram due to the high isomorphous substitution and layer charge. Research by Mpofu et al (2004) demonstrated that if the concentration of divalent cations was sufficient to complete cation exchange with

Na^+ ions, the CEC of the clay was reached and this can lead to more effective dewatering.

2.2.2.4 Sodium Adsorption Ratio

A comparison between the Sodium Adsorption Ratios of the process waters at the different De Beers kimberlite mines show a high degree of colloidally stable clays. An increase in the sodium percentage of the water results in the water becoming more alkaline and induces settling difficulties with the fine particles. The Sodium Adsorption Ratio (SAR) is defined as the ratio of sodium ions to calcium and magnesium ions in solution, see equation 3, and are derived from the chemical analysis of the water (meq/l) (Vietti and Dunn, 2003):

$$SAR = [Na^+]/ (([Ca^{2+}] + [Mg^{2+}])/2)^{1/2} \quad (5)$$

The SAR increased in all the water analysis after processing the kimberlite. A good correlation was found between the SAR of the water and the Sodium Exchange Potential (ESP) of the ore (Richards, 1969). The ESP is used as a measure to determine the percentage that sodium ions contribute to the overall cation exchange capacity.

Research done on the water used at most of the De Beers kimberlite mines in Southern Africa by Vietti (1994) showed an increase in the amount of Na^+ cations and a general decrease in the amount of Ca^{2+} and Mg^{2+} cations available in solution after contact with the ore (Vietti, 1994). The results indicate the exchangeable nature of the sodium cation of the ore.

A comparison of the cation constituents in the raw water and process water of the various Mines are shown in Table 4. Results show a definite trend in the exchanging of Na^+ with Mg^{2+} and Ca^{2+} cations (Vietti, 1994). This cation exchange not only increases the sodium adsorption ratio of the process water but also

increase the pH of the water. Unfortunately the mineralogical composition of the ore treated during the water sampling is not available to compare these values with the amount of clay minerals present.

At an ESP of more than 15% the colloidal stability of the slimes increases rapidly (Vietti, 1994). The high degree of colloidal stability could be ascribed to reduction of the divalent cation constituent and an increase in the Na^+ concentration in the process water, possibly due to cation exchange in the kimberlite slimes. The comparison between the SAR of the raw water and process water can be a quick and affordable reference to not only determine the colloidal stability of the slimes but also to give an indication of the amount of higher order cations required to settle the slimes.

Table 4: Comparison of Ca^{2+}, Mg^{2+}, Na^+ and the sodium adsorption ratios for the raw water and process water at the different De Beers Kimberlite Mines 1990 - 1993. (Composed from Vietti, 1994).

Analysis (mg/l)	Premier Mine		Venetia Mine		Kimberley Mine		Finsch Mine		Koffiefontein Mine		Jwaneng Mine		Orapa Mine	
Water type	Raw	Process	Raw	Process	Raw	Process	Raw	Process	Raw	Process	Raw	Process	Raw	Process
pH	7.8	10.0	8.3	9.0	8.2	8.3	9.3	10.0	8.0	9.6	8.0	8.5	7.9	9.0
Ca^{2+}	13	4	25	7	86	63	76	83	82	42	71	6	78	70
Mg^{2+}	10	1	16	33	113	70	19	5	22	0.5	27	20	50	51
Na^+	11	240	31	307	530	748	255	283	335	725	57	168	550	620
SAR (meq/l)	0.6	25.5	1.2	11.2	9.2	16.0	7.1	8.5	8.8	31.8	1.5	7.6	12.4	14.3

2.2.2.5 Hydration

Salts dissolving in water ionise into cations and anions. These cations and anions are hydrated to some extent in water. This hydration reaction is associated with the release of energy due to its exothermic nature. The released energy is defined as the hydration enthalpy of the cation or anion. Hydration enthalpy is dependent on the size of the ion and also the charge density. The smaller the ion size and the larger the charge density, the larger the hydration enthalpy according to Greenwood and Earnshaw (1997). Ion exchange takes place during the settling process of clay-rich kimberlite slimes and therefore the extent of hydration of the cations is of particular importance. The hydrated cation form the outer sphere complexes on the clay particle surface as described in section 2.2.2.2.

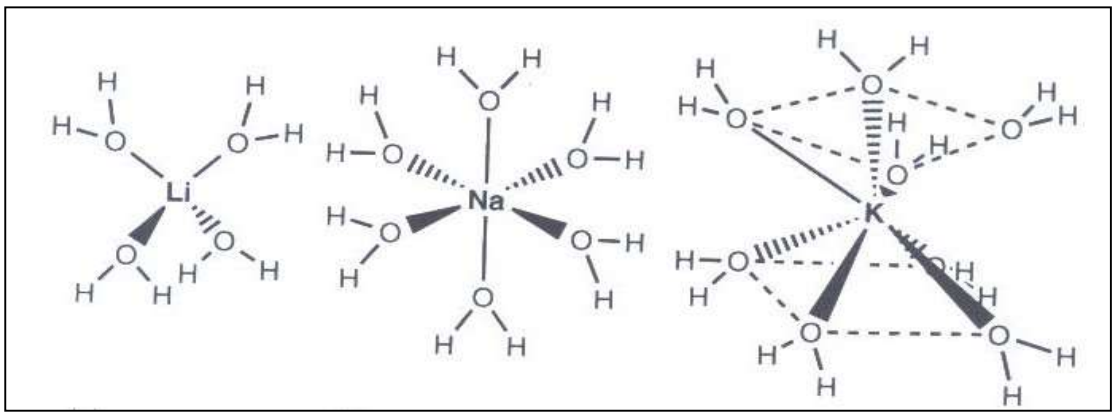

Figure 15: Hydration structures of lithium, sodium and potassium (Richens, 1997).

Table 5 list the most common cations and their metal hydroxide bond size together with the hydration enthalpy. It is expected that the larger the metal hydroxide bond size and the lower the hydration enthalpy of a specific cation, the greater the effect on the settling process according to Greenwood and Earnshaw (1997) and Richens (1997).

Table 5: Metal and ionic radii from Greenwood and Earnshaw (1997) and hydration bond size from Richens (1997).

Element	**Cation Charge**	**Metal radius**	**Ionic radius**	**M-OH bond size**	**Hydration Enthalpy**
		pm	pm	pm	KJ/mol
Ag	+ 1	144	115	240	-475.3
Li	+ 1	152	76	195-228	-514.1
Na	+ 1	186	102	240-250	-405.4
K	+ 1	227	138	260-295	-320.9
Ca	+ 2	197	100	241-246	-1592.4
Cr	+ 2	128	80	230	-1849.7
Cu	+ 2	128	77	196-200	-2100.4
Fe	+ 2	124	78	213	-1920
Mg	+ 2	112	27[a]	200-215	-1922.1
Mn	+ 2	118	83	218	-1845.6
Al	+ 3	143	53.5[b]	187-190	-4659.7
Cr	+ 3	128	80	196	-4401.6
Fe	+ 3	124	78	200	-4376.5
Ga	+ 3	135	62	215	-4684.8

I. Monovalent cations:

Comparing the hydration enthalpies of Na^+(-400KJ/mol) and K^+(-320KJ/mol) with that of the hydronium ion, H_3O^+(370KJ/mol), it can be noted that the Na^+ is a medium hydrated cation while K^+ is a weakly hydrated cation. Li^+(514KJ/mol) is however a strongly hydrated cation according to Richens (1997). Comparison of the degree of hydration between these cations is shown in Figure 15. The hydration enthalpies of these cations correspond with their metal hydroxide bond

size, where K^+ has the largest bond size and Li^+ the smallest. The larger the bond size the smaller the double layer size.

II. Divalent cations:

Comparing the metal hydroxide bond size and hydration enthalpies of the divalent cations in Table 5 it is noted that Cu^{2+} have the smallest bond size and the highest hydration enthalpy. It is expected that Cu^{2+} will have the smallest effect on the settling of weathered clay-rich kimberlite slimes, followed by Fe^{2+}, Mg^{2+}, Mn^{2+}, Cr^{2+} and lastly the large cation Ca^{2+} according to Richens (1997). The transition metals, Cu^{2+}, Ni^{2+}, Co^{2+} and Zn^{2+} have similar characteristics, as shown in Figure 16, and would be expected to show similar behaviour in the settling of kimberlite slimes.

III. Trivalent cations:

Al^{3+} has the smallest metal-hydroxide bond size and the highest hydration enthalpy of the shown trivalent cations according to Richens (1997). Al^{3+} is followed by Ga^{3+}, Cr^{3+} and Fe^{3+}.

To conclude the trivalent cations are expected to be the most effective in the settling of clay-rich kimberlite slimes, then the divalent cations and the monovalent cations the least effective. This can be seen in Figure 16.

2.2.2.6 Swelling of the clay interlayer with cations

Yamanaka and Brindley (1977) investigated the metal hydroxide interlayer of montmorillonite. This investigation focused on the complex formation of the transition metals, Cu^{2+}, Cr^{3+} and Ni^{2+}. The research they showed a difference in the amount of water molecules with which the cations associate during hydration.

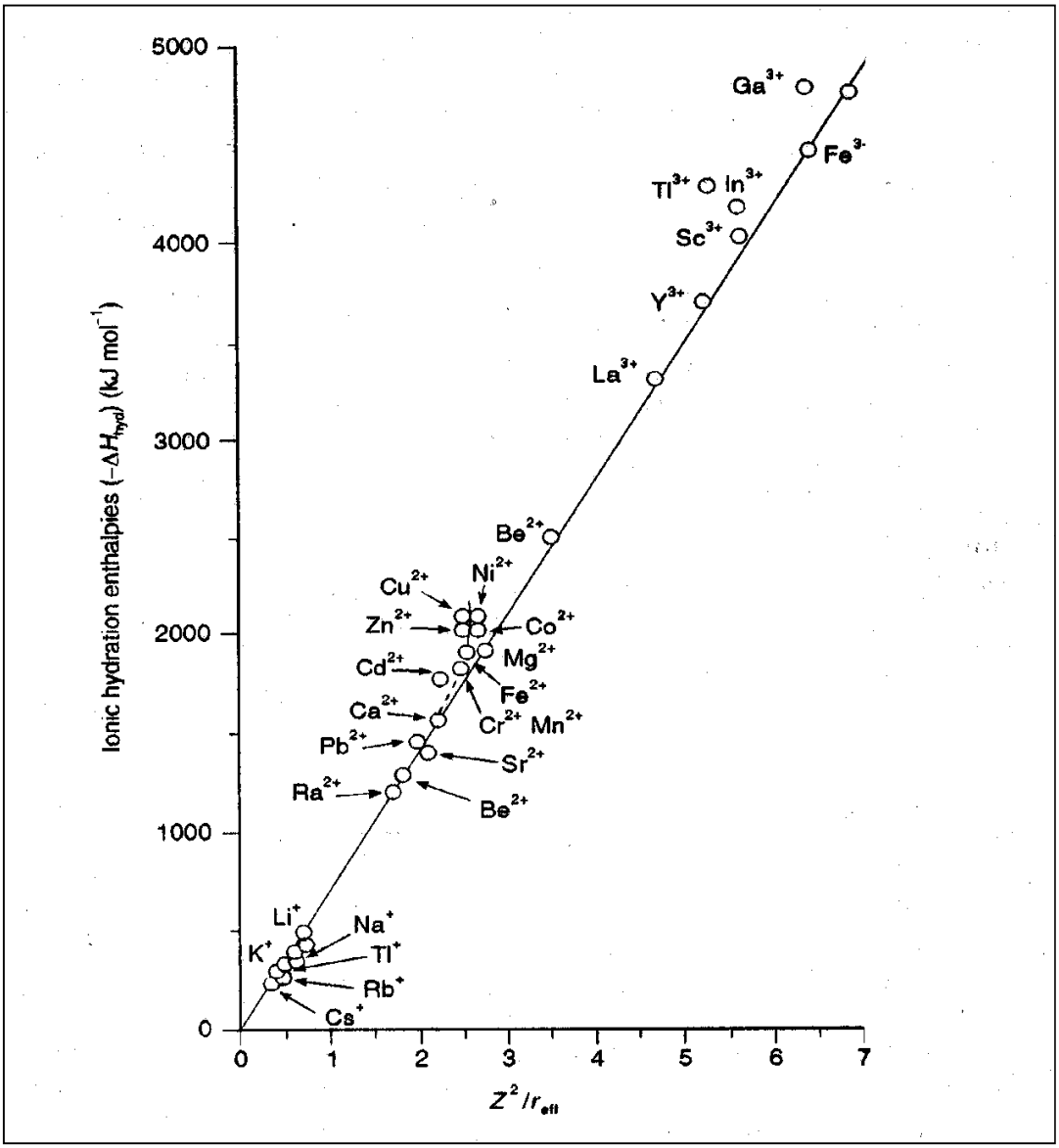

Figure 16: Correlation between ionic hydration enthalpy and metal-hydroxide bond (Richens, 1997).

Yamanaka and Brindley (1977) found that Cu^{2+} associate with 14 H_2O molecules to form the Cu-arene complexes, while Ni^{2+} only associate with 6 H_2O molecules. From this it can be seen that the Cu^{2+} complex takes up the most H_2O molecules and would induce the greatest pressure on the silicate layers, creating swelling in the clays. This was also confirmed by Yamanaka et al (1987).

Grim (1968) determined the amount of water molecules associated with certain cations, shown in Table 6. Grim (1968) also noted that the amount of water molecules associated with the cation is related with the amount of swelling that can occur. For faster settling the cations with smaller amounts of hydration moles associated with it could reduce the swelling and improve the settling of the clay particles.

Table 6: Ionic hydration data from Grim (1968).

Ion	**Hydration moles H_2O**	**Ion**	**Hydration moles H_2O**
Li	10	Mg	33
Na	5	Ca	22
K	1	Sr	21
Rb	0.5	Ba	17
Cs	0.2		

Figure 17 shows data on complex formation for various cations. It can be seen that with the monovalent cations Li^+ forms a complex the quickest while Cu^{2+} and Gd^{3+} are the quickest of the divalent and the trivalent cations respectively.

2.2.3 Organic compounds

During the water treatment of acid dyes montmorillonite clays are used in conjunction with anionic surfactants. Clay minerals are normally negatively charged and show no affinity for the anionic acid dyes. The only possible way to activate adsorption of these anionic dyes onto the clay surface was to alter the surface characteristics by exchanging inorganic cations (Ca^{2+}, Na^+) with organic cations (Wang et al, 2004). The size of the quaternary ammonium compounds (QAC) cation influenced the adsorption mechanism. The smaller tetramethylammonium (TMA) chloride is isolated from one another when adhering to the interlammellar surface of the clays, restricting particle interactions, while the larger hexadecyltrimetylammonium (HDTMA) bromide hydrophobic tails interact with one another and form an organic phase. This organic phase can result in the

partitioning of non-ionic organic molecules and settling of the particles. A positive surface charge is developed on the clay surface, due to the hydrophobic bonding by conglomeration of the C_{16} alkyl groups associated with (HDTMA), adsorbing the acid dyes and settling out of suspension (Wang et al, 2004).

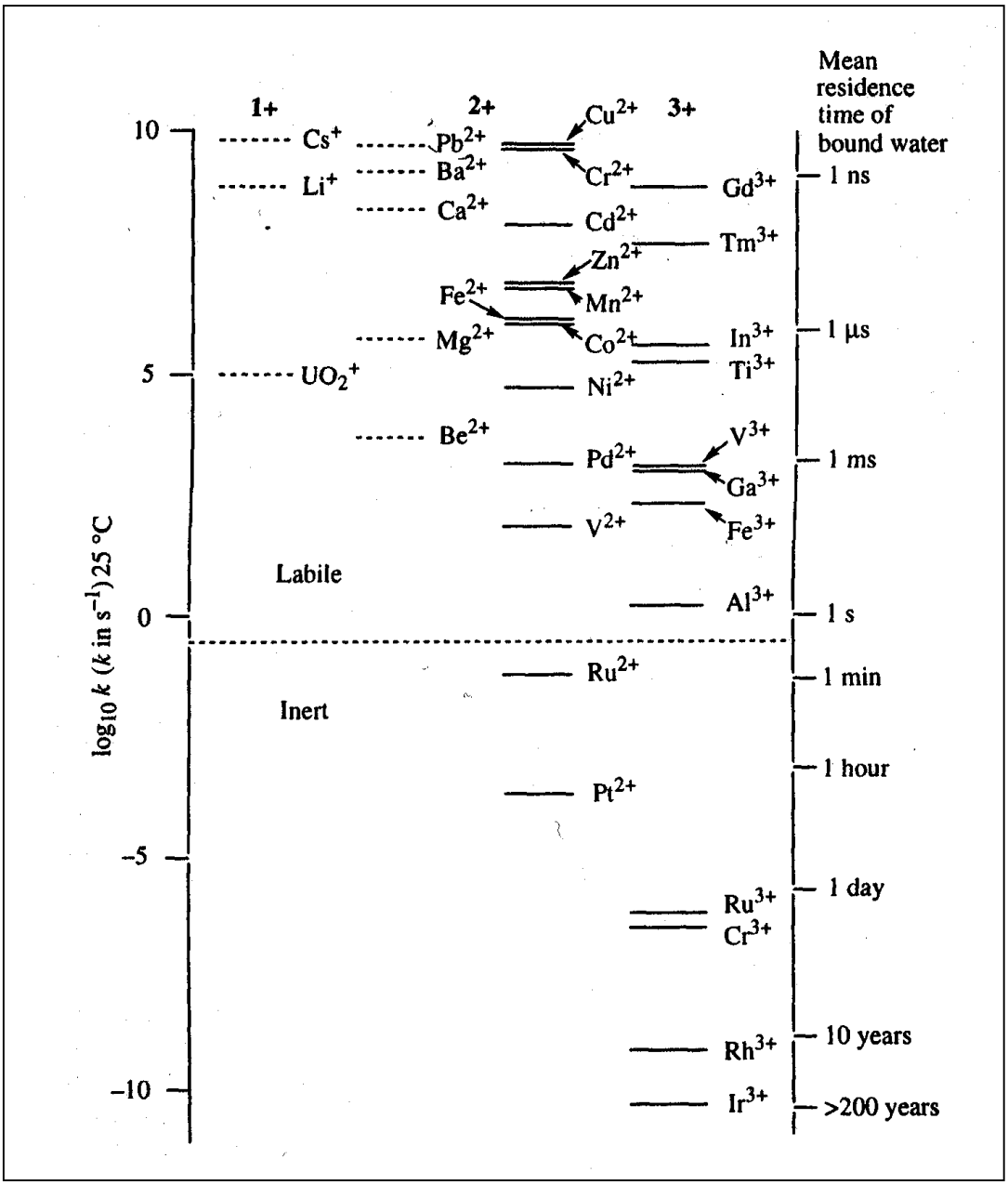

Figure 17: Indication of the ease at which complexes are formed between cations and water (Richens, 1997).

Research done by Pieters (2006) on the effect of organic compounds on 30 percent clay–rich kimberlite weathering indicated that most of the organic functional groups resulted in decelerated weathering, whereby a collapse of the clay interlayer is indicated. Carboxylic acid and carboxylic acid anhydride were the only two functional groups that caused swelling of the clay interlayer and caused accelerated weathering. Ester and aldehyde functional groups indicated the most effective decelerated weathering of the kimberlite slimes. The possible collapse of the clay interlayer caused by most of the organic functional groups could give an indication of potential settling possibilities.

2.2.4 Environmental cation limits

The worldwide shift to a more environmental conscious population necessitates the need to adhere to the most stringent environmental limits with regards to water used. In the design of any new processing plant it is important to consider beforehand the implications of environmental aspects of the effluent produced. According to Vatta (2001) water quality guidelines are important because it influences the selection of water sources, treatment processes and design criteria for current and future treatment processes.

The Department of Water Affairs and Forestry (DWAF) uses four broad categories for the usage of water in the South African Water Act. These four categories are for domestic, industrial, agricultural and recreational purposes. Water used for domestic use has the stringiest limits since this water is consumed by living beings and cannot jeopardise their health. Vatta (2001) compare the industrial waste water regulation and disposal between South Africa, Europe (Germany and Switzerland), Canada and Australia. There are no major differences between the various legislations regarding the limits set. The major concern with the industrial water limits is that it does not define the limits for the various cations as explicitly as is the case for domestic usage. It would therefore seem appropriate to use the domestic water usage limitations for cations as set out by DWAF to produce a recipe for a combination of the various cations intended in the accelerated

weathering process. It would be appropriate to adhere to the limits for industrial usage regarding total suspended solids, pH, colour, conductivity, odour, salinity, temperature and turbidity.

The limitations and effects of common cations for domestic usage along with the major anions Cl^-, SO_4^{2-}, and CO_3^{2-}, and exchangeable cations Na^+, K^+ and Al^{3+} are stipulated in Table 7.

2.3 Methods to settle clay-rich kimberlite slimes

In conventional kimberlite processing plants, the ore is normally crushed and scrubbed before the material is sized and processed through the dense medium circuits. The diamond industry utilizes inter particle crushing to try and minimize diamond breakage but this results in soft friable flakes released from the conglomerate (O' Gorman & Kitchener, 1972). Difficulty in settling of slimes can normally be attributed to these flakes. The crushed material first interact with water during the scrubbing stage of the process where the aim is to wash of the fine particles adhering to the larger rocks. The material and water passes over screens where the -1.0 mm material is separated with the water in a low density slurry stream.

The slurry stream can be divided into two fragments, grits and slimes. Grits are defined as the larger particles, 75 µm – 1.0 mm, and slimes are particles smaller than 75µm. Grits settle out quickly due to gravitational forces dominating, while the slimes are mostly stable in suspension. Then slimes can further be divided into particles that are large enough to settle out given enough time and the colloidal stable particles. The colloidal stable slimes fraction is predominantly clay minerals and is responsible for most of the settling problems in the diamond industry. O' Gorman and Kitchener (1972) noted that these slime particles did not adhere, but rather collided with one another, resulting in a vigorous Brownian motion where particles stay separate in suspension.

Table 7: The ion health limits and possible effects on humans (Department of Water Affairs and Forestry, 1996).

Ion	Maximum Limit (mg/l)	Maximum Limit (mM)	Effects
Al^{3+}	< 0.5	0.0185	Aesthetic / No health effects
Ca^{2+}	80 - 400	2 – 10	Severe scaling at certain pH
Cl^{-}	< 200	< 5.64	Corrosion problems
Cu^{2+}	30 - 200	0.47 – 3.2	Nausea & Vomiting / staining problems
Fe^{2+}/Fe^{3+}	30 - 100	0.54 – 1.8	Acute health effects increase / Iron overload possible / Slimy coatings in pipelines
K^{+}	> 400	> 10.2	Nausea, vomiting and irritation of mucous membranes
Mg^{2+}	> 400	> 16.45	Diarrhoea in new users / Severe scaling
Na^{+}	600 – 1000	26.1 – 43.5	Salty taste / possible health effects
SO_4^{2-}	400 – 600	4.2 – 6.25	Diarrhoea in non-adapted individuals
Zn^{2+}	10 – 50	0.15 – 0.76	Bitter taste / Possible chronic toxicity

The settling rate of particles in a fluid is mostly dependant on particle size and hence the smaller the particles the longer the time required for the particles to settle out. This necessitates the addition of chemicals to agglomerate the particles and increase the settling rate of the fine particles. Flocculation and cation salts could increase the settling rate.

Flocculation and coagulation are settling mechanisms that interrelate with each other, but these mechanisms are easily confused with each other. Flocculation is

the process where high molecular weight particles form bridges between particles, uniting these particles to form larger particles that will settle out quicker.

Coagulation is an electrostatic mechanism where the chemical reduces the repulsion potential at the diffuse double layer (O' Gorman and Kitchener (1972)). This allows the adhesion of colloidal particles to each other due to the domination of the attractive forces or Van der Waals forces surrounding these particles. Coagulation forms much finer and closer agglomerates compared to flocculation with open agglomerates where suspended particles are linked with molecules of the reagent.

Coagulants and flocculants are used in combination to settle out fine suspended solids with the coagulant adhering particles together and the flocculent forming bridges between these particles. This increases the settling rate of the particles dramatically. Cations could be added to increase the settling process, decrease the cost of reagents and ensure clean recyclable water.

2.3.1 Coagulation

Coagulation is required to settle the colloidal stable clay-rich kimberlite slimes by reducing the overall repulsive negative charge that surround these particles and enable the attractive Van der Waals forces to dominate. The immergence of these clay particles in solution lead to the formation of an electric double layer around each particle due to the migration of ions to balance out the surface charge. This electric double layer consists of the Stern layer, which are bounded ions next to the particle surface and a diffuse ionic cloud further away from the surface (Vietti, 1994). A graphical presentation of the electric double layer can be seen in Figure 18.

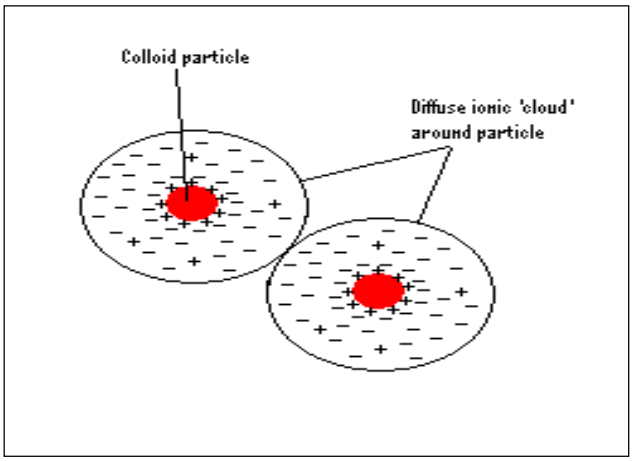

Figure 18: Colloid particle in suspension (Vietti, 1994).

The repulsive forces caused by the double layers prevent the particles to interact with one another and results in stable colloidal particles. It is therefore necessary to destabilize the suspension to create the opportunity for particles to attract one another, form aggregates and settle out (Kemmer, 1988).

Coagulants are used to neutralise the negative particle surface charge of the particles and create the opportunity for the particles to form aggregates and settle out of suspension. The most effective coagulation occurs when the particles have a ζ potential of zero and this results in a zero surface charge in relation with the suspension. Positive ions form the bound layer onto the negative surface charge of the particle and a diffuse layer extends outward as seen in Figure 7. Movement of the particle through the solution creates a plane of shear just on the outside of the bound positive ion layer.

2.3.1.1 Coagulation mechanisms

Two different coagulation mechanisms can be used to reduce the surface charge of the particles. Inorganic salts are normally used as ‘electrolyte’ coagulants, where the inorganic salts separate into cations and anions in solution, which undergo various hydrolysis processes and form various different hydrolysed products. The

different hydrolysed products are dependent on pH and temperature (Ye et al, 2006). The Ca^{2+} and Mn^{2+} hydrolysis reactions take place in the pH range 7-10 forming various different species as the pH increase. This could indicate that optimum coagulation can be dependent on the cation that hydrolyses at that specific pH.

The hydrolysed multivalent cations are adsorbed onto the particle surface to reduce the negative surface charge as shown in Figure 19. Comparing the microstructures before and after coagulation with hydrolysed cations shows that the surface charge, specifically on the basal planes, reduces. Familiar 'electrolyte' coagulants used are sodium chloride (NaCl), calcium chloride ($CaCl_2$), ferric chloride ($FeCl_2$) and aluminium sulphate ($Al_2(SO_4)_3$). Test work done by Olivier (2006) on the influence of cations (Na^+, K^+, Ca^{2+}, Cu^{2+}, Mg^{2+}, Al^{3+}) on settling behaviour of 30 percent clay-rich kimberlite slimes indicated that Ca^{2+}, Cu^{2+} and Al^{3+} showed the best settling results when used as coagulant. It was also noted that the higher the cation valence, the lower the concentrations of the cation required to achieve the critical coagulation concentration (CCC) and an improved clarity was observed.

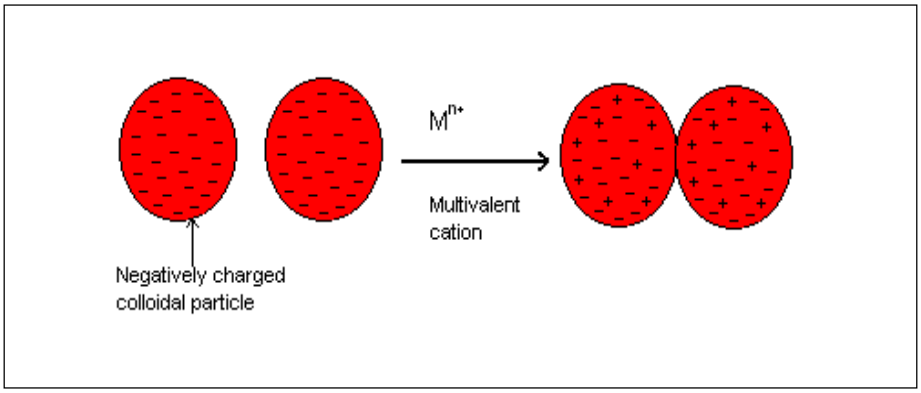

Figure 19: Particle surface charge reduction through the adsorption of multivalent cations (Klimpel, 1997).

Poly-electrolyte coagulation takes place when the surface charge is reduced through 'charge-patch attraction'. Poly-electrolytes are low molecular cationic

polymers consisting of short chains. The polymers attach to the negative charged particle and reduce the overall surface charge as shown in Figure 20. Examples of these polymers are PAC (Poly Aluminium Chloride) and XD 100.

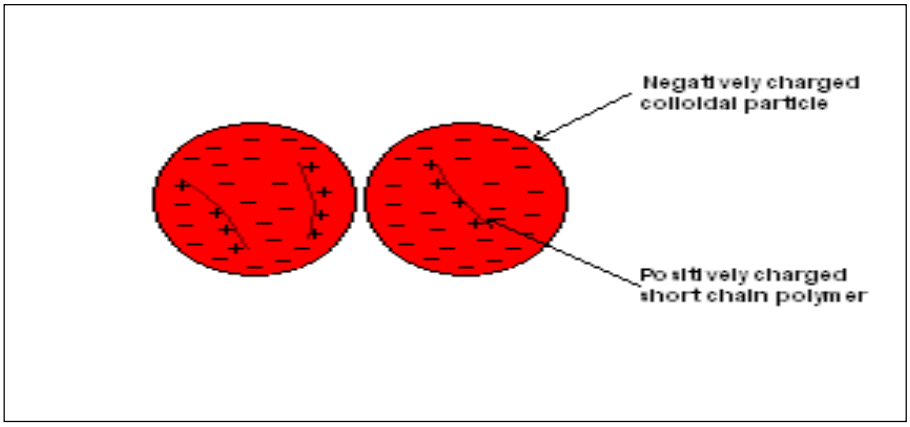

Figure 20: Particle surface charge reduction through charge patch reduction (Klimpel, 1997).

Coagulation often cannot achieve efficient settling behaviour and therefore is followed by flocculation to increase the settling rate of the clay-rich slimes.

2.3.2 Flocculation

Effective flocculation of slime particles are influenced by the flocculation mechanism, whether it is bridging of particles or charge neutralisation, the type and demand of the flocculant and whether agitation occur or not. The parameters influencing the flocculation process are discussed further.

2.3.2.1 Flocculation mechanism

Flocculants are high molecular weight polymers and are available with a positive (cationic), negative (anionic) or a neutral charge. Flocculants are mostly based on polyacrylamide monomers and normally consists of significant polymer chain

lengths. These chains enable a segment of the chain to be adsorbed on a particle surface, leaving the rest of the chain free to float, swerve and attach to various different particles. These loops and tails of the polymer enable the formation of multi-particle aggregates and this enable the quick settling of the slimes as shown in Figure 21. The longer the polymer chain the more effective is the bridging between the particles and the quicker large flocs are formed that can settle.

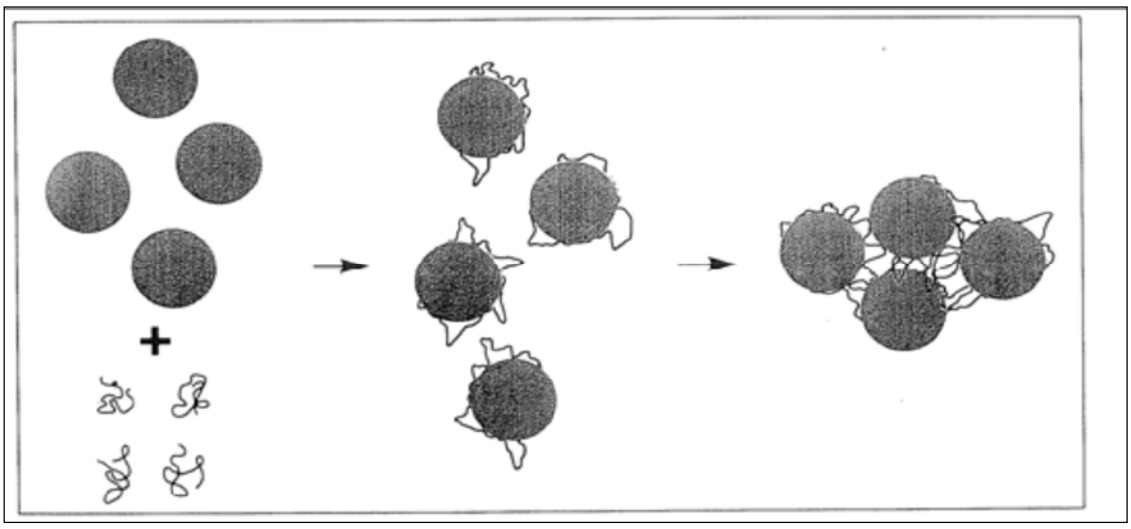

Figure 21: Polymers form loops and tails on particles surface leading to aggregates (Moss & Dymond, 1978).

Charge neutralisation or compensation is another frequently encountered mechanism during flocculation with high molecular weight polyelectrolytes or non-ionic polymers (Besra et al, 2002). Other possible flocculation mechanisms that could improve dewatering are polymer-particle surface complex formation and depletion flocculation (Gregory, 1985, 1987). A combination of flocculation mechanisms can also occur.

2.3.2.2 Influence of flocculant type

Clay-rich kimberlite slimes have a large negative charge on the particle surface and therefore it is assumed that cationic flocculants will be the most effective. O' Gorman and Kitchener (1972) proved the latter assumption by test work conducted on Premier Mine slimes at a pH of 9.8, with a mineral composition of 50-60 % saponite, 10-20 % talc and minor amounts of chlorite, illite and quarts. It was found that excessive amounts of cationic flocculant were required to settle the slimes. Further test work also indicated that neutral flocculants resulted in little flocculation of the solution and anionic flocculants had no effect. Huang and Dixon (2000) studied the dewatering and flocculation of Na^+ exchanged smectite and found that flocculation was easily achieved with cationic polydiallyldimethyl-ammonium chloride (PAM) while anionic PAM was ineffective.

Test work by O' Gorman and Kitchener (1972) indicated that less flocculants is needed after partial coagulation occurred first. Tests also indicated that anionic flocculants showed the best results in the presence of divalent cations. Research done by de Kretser (1995) indicates that complete cation exchange of Na^+ with Ca^{2+} must take place before flocculation and dewatering takes place with anionic polyacrylamide copolymer (PAM) or the unconventional polyethylene oxide (PEO). Results by Scheiner and Smelly (1984) indicated that the interlayer cation play a significant role in the effective flocculation of smectite particles with PEO or anionic PAM. Mpofu et al (2003 a) found that lower dosages of PEO polymers was required to dewater smectite particles compared to anionic PAM with hydrolysable metal ion addition. The flocs produced by PEO were larger and more robust and less sensitive to shear. The addition of metal ions, especially Ca^{2+}, Mg^{2+}, Ba^{2+} and Al^{3+} before PEO flocculation, ensured effective dewatering of the smectite particles. Mpofu et al (2003 a) also discovered that the addition of divalent cations at critical pH values and concentrations has a marked improvement on flocculation.

The molecular structures of the polymers play an important part in the flocculation process and will have theoretical and practical implications on the dewatering

process of mineral waste tailings. An effective dewatering process is dependent on the surface chemistry of the clay particles, the polymer structure as well as on the chain flexibility and particle interaction during moderate shear or compression (Mpofu et al, 2003 a, b).

2.3.2.3 Flocculant demand

The particle size and solids weight percentage in the slimes determine the amount of flocculant required to settle the slimes. Previous test work by Vietti (1994) indicated that the amount of -20μm material determine flocculant demand. For particles in this size range it is more difficult to link and bridge with one another before a large enough aggregate can be formed to settle under gravity. The larger the slimes particle distribution, less particles is required to form settling aggregates and less flocculant is required. A minimum amount of flocculant is required to allow effective settling by providing enough polymers to bridge between the particles in suspension. Over-flocculation can stabilize the solution due to too many polymer chains coating the surface of the particles and preventing aggregation between particles to take place. This result is defined as 'steric stabilization' (Klimpel, 1997).

Solid concentrations in excess of 15 percent by volume reduces the settling rate dramatically and increases the flocculant demand due to hindered settling in the solution and more particle surfaces available for aggregate formation (Vietti, 1994).

Flocculant dosage has a significant effect on the surface properties of the smectite particles. Research by Mpofu et al (2004) indicated a decrease in the ζ potential of smectite in solution at a pH of 10.5 with an increase in the dosage of the anionic PAM up to a certain point where an actual increase in ζ potential occurs as the flocculant dosage of anionic PAM is increased further. This is expected as the smectite particles are charged negatively and less anionic PAM was adsorbed. This clearly indicates that the settling rate of the smectite particles with anionic PAM peaks at a certain dosage and then decrease again due to the influence on

the surface characteristics of the smectite particles. The settling rate of PEO treated smectite particles continued to increase as the flocculant dosage increased.

Mpofu et al (2004) found that at a pH of 7.5, an increase in the dosage of anionic PAM did not decrease the zeta potential of the smectite in solution. Increasing the dosages of PEO did reduce the zeta potential of the smectite in solution to zero. This effect is attributed to a greater adsorption of layers of polymer chains onto the smectite surface, shifting the plane of shear away from the particle. This indicated that the ζ potential is not only pH and metal cation type dependant but can also be dependent on the flocculant dosage.

2.3.2.4 Influence of agitation on flocculation

Efficient flocculation requires proper mixing of the flocculant with the solution, to create enough opportunities for collisions between the polymer chains and the suspended solid particles and also to distribute the flocculant throughout the solution. As soon as the first flocs start to form the mixing intensity should be reduced to prevent shear of newly formed aggregates, because sheared aggregates seldom return to optimal size (Kemmer, 1988). Agitation in processing plants is achieved first in the feed launder of the thickener and thereafter in the feed well of the different thickeners. This result in a 20-25 wt% solids loading of the underflow.

This agitation rate of the solution helps to improve the consolidation of the settling particles and to recover as much water from the sediment bed as possible. Research done by Mpofu et al (2004) investigated the influence of increasing agitation on the consolidation of the sediment bed of smectite particles after flocculation with anionic PAM and PEO flocculants. There was only a slight improvement in the consolidation of the sediment bed with anionic PAM after agitation at moderate shear rates, while further increases in agitation rate led to

the destruction of the formed flocs. Consolidation of the sediment bed after flocculation with PEO and at moderate shear rates improved with 10 percent compared to no agitation. Further increases in agitation rate led to a maximum value of sediment bed height where after consolidation started to decrease again due to floc rupture.

McFarlane et al (2005a) studied the difference in consolidation of Ca-exchanged smectite particles after flocculation with anionic PAM and non-ionic PAM at different agitation rates and times. It was found that shorter agitation (15 seconds), a moderate agitation rate (200-300 rpm) and anionic PAM rather than non-ionic PAM produced optimum orthokinetic flocculation. According to McFarlane (2005a) this is believed to be caused by the additional carboxylate group electrostatic repulsion effect that induced an expanded anionic polymer conformation size.

3. Variables that influence settling behaviour

The analytical techniques used to quantify mineralogical features and settling behaviour is discussed further.

3.1 X-ray Diffraction Analysis

X-ray diffraction (XRD) is commonly used as an analysing technique to determine the mineral constituents that are present in a specific ore. This technique can only be used with crystals because characteristic identity periods exist along the crystallographic axes of the three-dimensional crystal structure (Klein and Hurlbut, 1993). When this three dimensional structure is x-rayed it results in electron vibration at the same frequency of incident X radiation. The electrons scatter X radiation of the same wavelength and frequency to balance out the adsorbed x-ray energy. Most of the waves undergo destructive interferences, unless Bragg's law is fulfilled causing constructive interference producing the scattering effect called diffraction. More detail discussions can be obtained from Klein and Hurlbut (1993). XRD tend to be a quantitative analysis and only mineral contents of more than ~ 5% can be accurately reported.

3.1.1 X-ray Diffraction of clay minerals

The XRD analysis of clay minerals is challenging and tedious because a lot of overlapping reflections. Bühmann (1998) and Moore and Reynolds (1989) completed research that discusses how to determine accurately the clay minerals present along with a detail description of the XRD analysis of clay minerals. The difficulty in analyzing the ore can be overcome by treating the ore and using the concentrated clay fraction (< 2 μm) for optimal XRD results. This is however not a good representation of the total sample mineralogy. Bühmann (1998) suggests an

air-dry scan of the clay fraction followed by an ethylene glycol and / or glycerol treatment to aid the identification of the clay minerals vermiculite and smectite. A XRD scan is completed before continuing the process to identify kaolinites. Another treatment of the sample with hydrazine and formamide allow for identification of kaolinites. The sample is hereafter treated at 500ºC to collapse the swelling clays and destroy or transform minerals such as chlorite and kaolinite. The XRD scans from the different treatments can be compared and then reveal the main clay groups in the ore. If more accurate identification of clay minerals is required the ore can be treated with Na, K, Mg or Ca and these XRD scans can be compared to accurately identify the specific clay species. Bühmann (1998) and Moore and Reynolds (1989) give a full description of these treatments.

3.2 X-ray Fluorescence analysis

X-Ray Fluorescence (XRF) analysis is used to determine the chemical composition of the ore. The ore is grounded into a fine powder where after it is pelletised with a binder. The pellet is bombarded by X-rays, generated by a high intensity X-ray tube. An X-ray emission spectrum is created characterising each element in the ore sample because of the adsorption and release of the X-ray energy. The spectral lines occur at specific wavelengths and these wavelengths are used to quantify the different elements. Klein and Hurlbut (1993) discuss the analysis method and equipment in detail if more information is required.

XRF allows for accurate determination of the chemical composition of inorganic material, but cannot quantify the mineral phases present. The standard detection limits for specific cation detection during XRF analysis on glass fusion disks can be seen in
Table 8. XRF can be used to measure the cation exchange that take place during the settling process of the kimberlite slimes particles.

Table 8: The standard detection limits of the main elements during XRF analysis on glass fusion disks (Klein and Hurlbut (1993)).

Cation	Standard deviation (%)	Limit of detection
Na2O	0.11	0.0265
K2O	0.06	0.005
CaO	0.07	0.01
MgO	0.1	0.0118
CuO	0.0037	0.0003
Fe2O3	0.3	0.0097
Al2O3	0.3	0.01
MnO	0.0065	0.0013

3.3 Particle size distribution

The most accurate method to determine the particle size distribution of a dry sample is with Low Angle Laser Light Scattering (LALLS) (Rawle, 2012). This analysing technique determines the particle size by measuring the diffraction angle. The diffraction angle of the particle is inversely proportional to the particle size. LALLS enable a large size range, 0.02 µm – 2000 µm, to be accurately measured. He-Na gas lasers, with a fixed wave length, λ = 0.63 µm, are used as the source of a coherent intense light (Rawle, 2012). The dried sample are blown through the laser beam by means of pressure and sucked into a vacuum cleaner afterwards.

Vietti (2004) defined the slimes fraction of kimberlite slurries to be smaller than 75 µm and the clay mineral fraction, smaller than 2 µm would form part of this fraction. Stokes law predicts the settling velocity of small spheres in a fluid, whether it is air or water as shown in equation 6. The expectation would be that the smaller average particle size, the lower the settling velocity of the particles and the more difficult it would be to settle the slurry.

$$\omega = \frac{2(\rho_p - \rho_f)gr^2}{9\mu} \quad (6)$$

ω = settling velocity (m/s), ρ_p = particle density, ρ_f = fluid density, g = gravity (m/s^2), r = radius of the particle (m), μ = dynamic viscosity of fluid

Stokes law identifies only two parameters pertaining to the particle properties namely size and density. Fine kimberlite particles from different Mines that have similar particle sizes and relative densities would be expected to show similar settling velocities during the settling process.

Settling particles in a thickener experience free settling, hindered settling as well as compression settling. Stokes law is based on the free settling regime and it should be noted that the settling velocities of hindered and compression settling, Newton's law for settling, use the settling velocity from Stokes law as a reference in the equations. Lester et al (2005) did research on determining the interfacial drag for colloidal suspensions and how this function influence the settling velocity of the slimes.

3.4 The settling rate of the clay particles over time

The most common method for determining the settling rates of slime solutions is the standard jar test methods. The critical concentration slimes in solution at which effective coagulation starts to take place was found at 7 wt% (O'Gorman and Kitchener, 1974). Vietti (2004) recorded that slurries with a solid loading of more than 15 wt % experienced ineffective settling rates attributed to delayed settling between the particles. The slimes solution is poured first into the measuring cylinder where after the flocculant dosage is added. The measuring cylinder is inverted a couple of times and the solution is left to settle. The mud-water interface is tracked over time by marking the distance travelled at certain times on a strip of masking tape on the side of the measuring cylinder. The settling rate is determined by plotting the time versus settled distance of the dispersion.

McFarlane et al (2005a) compared the settling rate of smectite particles under orthokinetic flocculation conditions in the laboratory, which utilise a controlled agitation rate at a fixed duration, with the more conventional pulp mixing/flocculation methods of inversion and plunging, used to determine feed flocculant mixtures in processing plants. The findings were that settling rates under orthokinetic flocculation conditions, using a low flocculant dosage, was almost a magnitude higher compared with the inversion and plunging flocculant/ pulp mixing method, using a higher flocculant dosage. This clearly indicates that the orthokinetic flocculation methods mimic plant operations much more accurately.

A concern was raised by McFarlane et al (2005b) that there is a variation in settling rate as a function of orthokinetic flocculation. The settling behaviour of slime particles could be changed detrimentally using a certain polymer dosage and agitation. This will lead to low solids content in the underflow of the thickener because most thickeners operate at residence times less than that required for optimum bed consolidation.

3.5 Changes in the particle size of the settling medium before and after the introduction of cations and flocculants.

Settling of kimberlite slimes is dependent on the particle size during the various stages of dewatering. The faster a particle can overcome the inner solution forces and settle under gravity, the more efficient the settling process. A high resolution field emission scanning electron microscope can be used to examine particle structures before and after cation and flocculant additions along or without agitation (Mpofu et al, 2004). This can give an indication of the differences in compaction of the particle structures when the various chemicals are added to the settling medium.

Slurry samples should be rapidly vitrified to avoid drying that can lead to rearrangement of the particles. Vitrification is achieved by taking microgram samples and placing the samples in copper rivets (7 mm length and 1 mm diameter) with a micro-syringe. The copper rivets are mounted on a cryo transfer rod and submerged into liquid propane, cooled by submersion into liquid nitrogen, to arrest all supra-molecular motion and retain clay microstructures (Mpofu et al, 2004). The vitrified samples are stored in liquid nitrogen until the samples are fractured under vacuum by breaking the top copper rivet and removing the vitrified water through sublimation at -90ºC. The samples are kept at this temperature for 5 minutes before cooling down to -180ºC, to prevent any further sublimation. The samples are sputter coated with a platinum layer of 3 nm at high resolution and analysed at an accelerating voltage range of 5 -10 kV.

The scanning electron micrographs can be compared and it would be possible to track the rearrangement of the clay particles to facilitate more particle – particle and polymer – particle interactions. The closer the particle stacking the more water is excluded and the more efficient the dewatering process.

3.6 The critical coagulation concentration of the slurry

The critical coagulation concentration (CCC) is the minimum cation concentration in solution necessary to induce double layer compression and create clay particles coagulation. In the minerals processing industry the CCC of the slurry compared with the specific cation concentration of the water indicates whether additional cations are necessary or if the cation concentration is sufficient for the efficient settling of the slurry.

The critical coagulant concentration determination requires a visual coagulation test with the parameters shown in Table 9 (Vietti and Dunn, 2003). The prepared kimberlite ore, 10 weight % solids, is added to various measuring cylinders with

similar dimensions and volume, while the cation concentration of the solution is increased in every cylinder. After two hours the cylinders was visually analysed and ranked according to the following categories as shown in

Figure 22:

Table 9: Visual coagulation test parameters (Vietti & Dunn 2003).

No coagulation	-
Partial coagulation	+
Complete coagulation	++

Figure 22: Example of coagulant test (Vietti & Dunn 2003).

3.7 Characterisation of the sediment bed after settling

The greatest challenge which confronts the efficiency of chemical additives-assisted tailings dewatering methods is not only faster settling rates; it is pulp consolidation and specifically enhanced rapid pulp compaction (McFarlane et al, 2006). Optimisation of flocculant performance, using conventional polymeric flocculants and respective dosages, cannot guarantee that the optimum flocculant structures and improved settling behaviours will result in sediment bed compact consolidation. The sediment bed is characterised by determining the solids weight percentage or by measuring the yield stress. According to McFarlane (2005b), smectite thickener underflow pulps consolidate to 20% - 22% weight percentage solids. Measuring the yield stress of the sediment bed can give an indication of the compaction of the sediment bed. The more compact the sediment bed is, the higher the yield stress could be and a higher solids concentration of the sediment bed can be achieved according to the DLVO theory as discussed in section 2.2.1.1. Mpofu et al (2005) found that the yield stress decreased as the cation

concentration increased at a constant sediment loading of 25 wt% smectite. This result, which is a discrepancy according to the DLVO theory reflects the specific influence of metal ions on the various edge-basal faces, basal-basal faces and edge-edge faces interactions of the anisotropic charge properties of the smectite particles. The lower the yield stress and the higher the sediment bed compaction the more effective the dewatering of the slimes.

The yield stress of the sediment bed is measured using the vane technique (Nguyen et al, 1985) by inserting a six blade vane into the sediment bed. The vane is rotated slowly at a constant rate of 0.2 rpm. At this rate the shear yield stress is expected to be independent of the speed of rotation (Johnson et al, 1999). The yield stress is calculated from the maximum torque reading using established formulae for submerged conditions.

3.8 Prediction of kimberlite settling properties

Vietti (2004) investigated the settling behaviour of various kimberlite slurries. Based on this work a model was developed that predicted colloidal stability of kimberlite e.g. natural settling based on the Exchangeable Sodium Percentage of the ore and the pH of the solution. The model therefore suggests that these two parameters can be used to predict the settling behaviour. This work will investigate whether these two parameters alone or in combination with other parameters can successfully accomplish prediction of colloidal stability.

3.9 Polymer type

The smectite particles have a negative surface charge and the specific polymer type will have various effects on the settling of the smectite particles depending if coagulants are used or not. Cationic polymers could be effective but potentially at

high polymer dosage, while cationic coagulants could enable the usage of non-ionic or anionic polymer flocculants as discussed in section 2.3.2.2.

3.10 Polymer dosage

To achieve optimum dewatering conditions it is important to find the correct flocculant dosage that will ensure that over or under flocculation does not take place. Flocculant dosage is furthermore one of the main cost drivers in the dewatering circuits on most mineral processing plants and over flocculation is detrimental to dewatering while increasing the processing costs.

3.11 Coagulant salt

Smectite slimes are known for adsorbing cation to balance the negative surface charge of the particles. If easily hydrolysable cations are used the coagulation of the smectite particles can take place in a shorter time, improving the efficiency of the dewatering process. The cation exchange process is discussed in detail in section 2.2.2.3.

3.12 Coagulant dosage

Coagulation can only take place once the critical coagulation concentration (CCC, section 3.6) is reached and complete cation exchange or adsorption could take place to reduce the ζ potential of the particles to enable particle – particle attraction. The coagulant dosage is dependent on the ionic concentration of the process water.

3.13 pH

The pH of the solution plays a critical role in the settling characteristics of kimberlite slimes. A shift in the pH of the process water can result in settling difficulties because the ζ potential could increase, the hydrolysable cation product could change and become ineffective and the polymer effectiveness could decrease leading to higher dosages required. The effect of pH on surface charge is discussed in section 2.2.1.3.

3.14 Agitation

Agitation can improve the settling behaviour of the dispersion by increasing the flocculant – particle interactions, while it can be just as detrimental by rupturing the flocculant structures and hinder the settling process. McFarlane et al (2005a) indicated a marked improvement in laboratory settling results by agitating the medium which lead to a reduction in flocculant demand.

4. Experimental Procedure

Drill core samples were received from 3 different kimberlite locations in Angola called Alto Cuilo, Itengo and Tchegi and from 1 location in South Africa, called Venetia Red. Thickener samples were not available as the kimberlite deposits have only been explored as yet and drill core extracted during the experimental phase. A rod mill was used to control the size range of the product. The use of drill core samples instead of thickener samples necessitated certain assumptions in order to add credibility to the data generated from the test work. The assumptions made were as follows:

- A crushed drill core sample will have the same clay mineral composition as the kimberlite ore at the same depth;
- Stirring the milled drill core in water for 15 minutes will simulate the sheared slime particles due to pumps and cyclones in the processing plant; and
- The average density of kimberlite is 2.65 g/cm^3.

Further test work is discussed in the following sections.

4.1 Sample Analysis

The drill core samples (1kg) from Alto Cuilo, Itengo and Tchegi were dry milled in a rod mill together with the Venetia Red sample until eighty percent of the sample passed the hundred micron (-100 μm) size fraction for the settling tests. The -75 μm fraction was not screened out separately as it is important to simulate plant conditions. Each sample was split utilising a rotary splitter into smaller bags for analytical tests and settling tests.

4.1.1 Particle Size Analysis

From the splitted samples a small sample was submitted for Low Angle Laser Light Scattering (LALLS) analysis by using the Malvern Mastersizer 2000 at the University of Pretoria to determine the particle size analysis. The light diffraction of the particle passing through the laser beam is inversely proportional to the particle size. The sizing analysis was done dry to ensure that there could not be any interaction with water, which in return can result in swelling of the clay particles as well as changes in the chemical composition.

4.1.2 XRF and XRD analyses

The kimberlite samples submitted for XRF analyses were ground to < 75 µm in a Tungsten Carbide milling vessel, roasted at 1000ºC to determine the Loss On Ignition value and after adding a 1 g sample to 6 g $Li^2B^4O^7$ fused into a glass bead. Major element analysis was executed on the fused bead using the ARL9400XP+ spectrometer at the University of Pretoria. Another aliquot of the samples was pressed in a powder briquette for trace element analyses.

Similarly the kimberlite samples were submitted for XRD analysis at the University of Pretoria. XRD analysis was done at the University of Pretoria on a Siemens D501 instrument utilising a copper lamp on a 4 – 70° 2θ range. The samples were in some cases air-dried, glycol and temperature treated for more accurate identification of the clay species.

4.1.3 Cation exchange capacity

Samples from each kimberlite were sent to the Agricultural Research Centre in Pretoria where the cation exchange capacity for every sample was determined

through the Ammonium Acetate method for soil analyses. Sodium, potassium, calcium and magnesium were reported in centimol(+) per kilogram.

4.1.4 Natural settling

The settling and colloidal stability of the 18 different kimberlites was investigated without the addition of any coagulants or flocculants. The settling tests were performed with distilled water to eliminate the potential influence of impurities normally found in process water. For comparison it was necessary to ensure that the same solid loading was used throughout all test work conducted. There is an optimum solid concentration associated with effective settling through coagulation and flocculation of any slurry. O' Gorman and Kitchener (1974) found that diluted clay slurries tend to form a gel state during coagulation and this characteristic is attributed to platy particles orientating themselves in the shear gradient. The critical concentration slimes in solution at which effective coagulation starts to take place was found at 7 wt% (O'Gorman and Kitchener, 1974). Vietti (2004) recorded that slurries with a solid loading of more than 15 wt% experienced ineffective settling rates attributed to delayed settling between the particles. The tests were performed by mixing 50 g of kimberlite with 450 ml of distilled water where after the slurry was stirred with a magnetic stirrer at a 1000 rpm for 15 minutes. The slurry was poured into a 500 ml measuring cylinder, inverted 3 times, where after the solid – liquid line was traced for 1 hour as described in section 4.4.

4.1.5 pH values of the slurries

The pH of the different kimberlite slurries were measured 1 hour after the natural settling tests were conducted as discussed in section 4.1.4. A calibrated pH meter probe was inserted in the liquid face of the slurry and the pH values were recorded.

4.2 Critical coagulant concentration

The critical coagulation concentration (CCC) is defined as the minimum amount of cations required to settle clay minerals in dispersion as discussed in section 3.6. The critical coagulant concentration was used to determine the effectiveness of the cations in settling clay-rich kimberlite slimes. Previous test work by Olivier (2006) indicated that the best settling rate on 30 percent clay rich kimberlite slimes was achieved at critical coagulation concentrations of 0.005M Al^{3+}, 0.02M Ca^{2+}, 0.01M Cu^{2+} and 0.01M Mg^{2+}. It was decided to test monovalent, divalent and trivalent cations to determine if there is any difference in the settling behaviour of the different cations.

Ga^{3+}, Cr^{3+}, Ag^{+}, Cr^{2+} and Mn^{2+} are extremely expensive and toxic and as such economic and environmental reasoning indicated that these cations would be excluded from test work.

The coagulation solution were prepared by dissolving chloride salts of the cations (Al^{3+} , Fe^{3+}, Ca^{2+}, Cu^{2+} and Mg^{2+}, K^{+}) in distilled water at concentrations 0.005 M, 0.01 M, 0.02 M, 0.035 M, and 0.05 M.

The coagulation tests were performed using 500 ml measuring cylinders filled with 250 ml of the various coagulant solutions and adding 25 g of the milled kimberlite to each cylinder. The tests were visually quantified after 120 minutes as described in section 3.6.

4.3 Flocculant test work

Anionic and non-ionic polydiallyldimethyl-ammonium (PAM) was tested as this is the most commonly used in the industry. The magnafloc range from Senmin is commonly used in the industry in South Africa where clay problems arise. The different flocculants used to conduct the settling tests are shown in Table 10. Two

non-ionic flocculants were used together with 8 different anionic flocculants from Senmin's Magnafloc range.

Table 10: Different flocculants used to conduct settling tests.

Flocculant - Magnafloc	Type of Flocculant
10	Anionic
155	Anionic
333	Non -ionic
336	Anionic
340	Anionic
342	Anionic
345	Anionic
351	Non -ionic
356	Anionic
919	Anionic

The concentration of the flocculants was varied from a low to a high dosage. The maximum flocculant dosage rate (gram of flocculant /per ton of ore) can be determined with the aid of equations 7 – 9 where ρ_{solids} = 2.65 S.G, T = 25g, W = 250ml and Flocculant Concentration = 0.025 wt%.

$$Flocculant-dose(g/t)=\frac{\frac{Flocculant\_concentration}{100}*Volume\_flocculant(ml)}{\frac{\%solids}{100}*\left\{\frac{\rho_{slurry}(g/cm^3)*Volume\_of\_slurry(ml)}{10^6}\right\}} \quad (7)$$

$$\rho_{slurry}(g/ml)=\frac{(T+W)(g)}{M(ml)} \quad (8)$$

$$M(ml)=\frac{T(g)}{\rho_{solids}(g/ml)}+W(ml) \quad (9)$$

4.3.1 Flocculant make up

Effective flocculant activity in solution is dependent on the prevention of aging of the flocculant along with poor flocculant preparation. Powder flocculants require about two hours to fully hydrate before being added to slurries. The flocculant powder, 0.025 g, was mixed with the 100 ml of water and agitated for an hour at 1000 rpm before leaving it for 24 hours to ensure flocculant activation. It was not required to dilute the flocculant solution afterwards as it was made up on 0.025 percent strength. High molecular weight flocculants are hydrophobic and tend to form ball-like structures if enough time is not allowed for the flocculant to uncoil and relax in solution (Klimpel, 1997).

'Fish-eyes' or polymer gels are the result of reduced activity of flocculants when poor mixing causes the flocculant powder molecules to stick and swell together in lumps. Gentle agitation is required to distribute the flocculant powder and create dissolution. Excessive agitation should be prevented as flocculant particles are susceptible to shear degradation in diluted solution.

Flocculant solutions become less viscous with time due to the disentanglement of the polymer molecules in solution resulting in a reduction in flocculant activity. This aging phenomenon happens normally after two weeks, but to ensure that flocculant solutions remain fresh and active it is preferable to use flocculant solutions within 3 days of mixing (Addai-Mensah, 2007).

The flocculant tests were performed utilising a flocculant strength of 0.025 percent (0.025 g of flocculant added to 100 ml of distilled water). The optimum flocculant strength according to Vietti (2004) is between 0.025 percent and 0.05 percent. Testing at the lower limit of the optimum flocculant strength range ensures that the flocculant demand is as low as possible, reducing the operating costs of the water recovery in the processing plant. The flocculant solution needs to be stirred for one

hour to ensure efficient hydration of the flocculants. The flocculant solution was used within three days after preparation of the solution.

4.4 Coagulant and flocculant optimisation test work

The cation and flocculant that gave the best results for every kimberlite were combined during a settling test to compare the difference in settling rate and bed depth between the cation, flocculant and a combination of cation and flocculant assisted settling of the kimberlite slimes.

4.4.1 Settling rate determination

The effect of a specific cation or flocculant or a combination of these on the settling rate of clay-rich kimberlite slimes was determined by plotting the mud line (solid-liquid interface) against time as indicated in Figure 23. The settling rate was determined by using the following formula:

$$Settling\_rate(m/h) = \frac{hi - hf}{time\_taken\_to\_settle} * \frac{3600s}{1000mm} \quad (10)$$

with hi = height initial and hf = height final.

The cation was mixed with 500 ml distilled water in a measuring cylinder. The kimberlite ore, 50 g, was added to the coagulant mixture, 450 ml, and stirred for 15 minutes at 1000 rpm to simulate the shear experienced during plant processing. After complete mixing of the ore with the water, the flocculant can be added if needed and stirred at 200 revolutions per minute for 15 seconds to ensure effective distributions of the flocculant throughout the slurry as discussed in section 2.3.2.4.

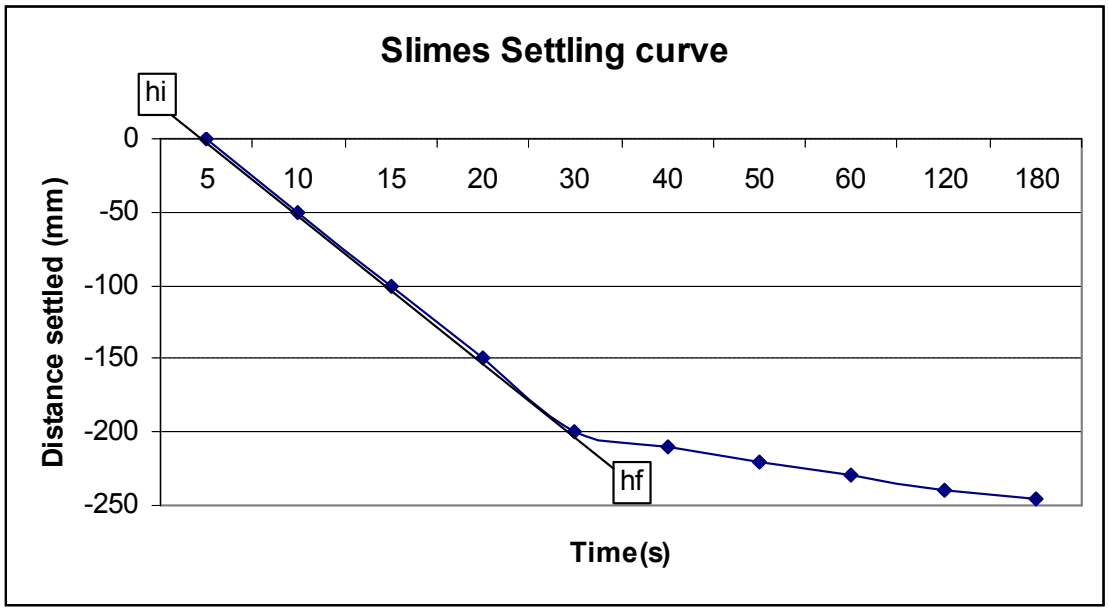

Figure 23: Example of a settling curve.

The solid-liquid interface was tracked for one hour and the consolidated sediment bed height was recorded after 24 hours. The pH of the solution was recorded after completion of the settling tests.

4.4.2 Bed Depth Determination

The bed depth for each sample was determined by measuring the volume in millilitre (ml) of the settled slurry bed after 24 hours. The percentage solids was calculated by determining the mass of the slurry bed from the volume of the settled slurry bed. The mass of the kimberlite was divided by the mass of the sediment bed and the percentage solids calculated accordingly.

4.5 Repeatability of results

Triplicate settling tests were done on kimberlite sample AO 322 using the best cation, flocculant and a combination of the cation and flocculant to investigate the repeatability of the results and investigate the error range.

4.6 Regression modelling

Regression modelling is the process of developing a predictive equation from data (Napier-Munn, 2008). Multiple linear regression determines the coefficients or parameters in the linear model as shown in equation 11:

$$y_i = a_i x_i + \varepsilon_I \qquad (11)$$

Where y_i is the dependant variable, a_0, a_1 and a_2 are the parameters, x_1 and x_2 are the independent variables or predictors, i represent the ith value of the data set and ε represents the error, the variation in the data that is not explained by the regression.

The least squares method was used to minimise the sum of squares of the differences between the observed values of the dependant variables and the values predicted by the model (Napier-Munn, 2008).

Regression modelling was used to evaluate the critical parameters in the settling of kimberlite slimes. The regression modelling tested whether particle size, CEC, ESP, or chemical or mineralogical features could predict the settling behaviour. To represent particle size, the -7.5 µm and -75 µm data was used. From XRF the Na, K, Ca, and Mg content of the ore was used for the model and from the XRD data the smectite content was incorporated as variables. As output for the model, correlation with natural settling, coagulant settling, flocculant settling and

combined coagulant and flocculant settling was specified as well as slurry bed depth of the kimberlite slurries.

An online software package, Business Spreadsheets, Multiple Regression Analysis and Forecasting, was used for regression modelling. The regression model was evaluated in terms of its standard error, σ, and R^2 adjusted where after the significance of the model was determined by the significance of F through the analysis of variance. The coefficients were evaluated on their respective P-values, where a P-value smaller than 5% was significant, based on a 95% confidence level. Coefficients with values larger than 5% were insignificant and the regression was run again with the remaining variables. This process was repeated until a significant model was found with significant coefficients.

5. Experimental results and discussion

5.1 Sample analysis

Samples were received from 3 different kimberlite locations in Angola and from 1 location in South Africa. The classifications of the different areas are shown in Table 11. The classifications of the type of kimberlite from which the samples originate are shown in Table 12. The Itengo and Tchegi samples were similar in geological features and therefore similarly named. The Itengo and Tchegi samples were selected to have 2 or more samples at different depths for a specific kimberlite. This was done to investigate the change in the mineralogy of the kimberlite as depth increases and the influence on slimes settling. The samples were compared to a South African sample, Venetia Red, which causes problems with settling. The colour of the kimberlite suspended in water was noted and compared and ranged from grey, green, brown to orange and red.

Table 11: Sample name allocation

Kimberlite Location	**Sample name allocation**
Alto Cuilo	AC
Itengo	AO
Tchegi	AO
Venetia	Venetia Red

Table 12: Sample classification and sample extraction depth.

Sample number	Kimberlite type	Colour	From (m)	To (m)
AC-1-1-1	Hypabyssal kimberlite	Grey		
AC-4-1A-1	Tuffisitic kimberlite	Red		
AC-5-5-1	Hypabyssal kimberlite	Green		
AC-5-5-2	Tuffisitic kimberlite	Light red		
AC-16-11-1	Tuffisitic kimberlite	Brown		
AC-56-5-1	Resedimented Volcaniclastic kimberlite	Dark red		
AC-197-1-1	Volcaniclastic kimberlite	Dark brown		
AO 319	Primary Volcaniclastic kimberlite	Green	115.43	116.41
AO 320	Resedimented Volcaniclastic kimberlite	Grey-Brown	29.56	30.37
AO 321	Volcaniclastic kimberlite	Red	136.36	137.16
AO 322	Sandy Resedimented Volcaniclastic kimberlite	Red - Orange	91.72	92.56
AO 323	Crater Facies Sediment	Red	29.56	30.59
AO 324	Primary Volcaniclastic kimberlite	Grey-Brown	339.70	340.98
AO 325	Crater Facies Sediment	Red-Grey	103.74	104.56
AO 326	Primary Volcaniclastic kimberlite	Grey-Green	89.41	90.76
AO 327	Resedimented Volcaniclastic kimberlite	Orange	100.36	101.14
AO 328	Primary Volcaniclastic kimberlite	Grey	163.03	163.64
Venetia Red	Red kimberlite	Red		

5.1.1 Particle Size Analysis

Samples were dry milled and screened in order to prevent any change in the mineralogical features of the kimberlite. Agglomerates can however be formed during dry milling and this can lead to a coarser size distribution being reported. Possible agglomeration formation in the -75 μm fraction is not seen as a problem as the diamond processing industry disregard the -1mm fraction as slurry.

Particle size is usually regarded as the most important variable in particle settling where especially fine particles will cause very slow settling or colloidally stable suspensions. The most colloidally stable and hence most difficult size ranges to settle in slurries are typically below 75 μm. The clay minerals are usually

concentrated in this size fraction. Figure 24 to Figure 26 show the particle size distributions of the kimberlite samples that were determined through the Low Angle Laser Light Scattering (LALLS) analysis used by the Malvern Mastersizer 2000 at the University of Pretoria. The light diffraction of the particle passing through the laser beam is inversely proportional to the particle size. Figure 24 shows the particle size analyses of the Alto Cuilo samples. Samples range between 20 - 40% passing 7.5 µm, 60 – 80% passing 75 µm, and all samples have 100% of the particles passing 100 µm. This could also be indicative of harder kimberlite mineralogy. A coarser range in a sample could lead to higher settling rate due to an increased influence of gravity on the settling of the particles in the kimberlite slurries. The particle size distribution of all the samples was compared against the known colloidally stable Venetia Red.

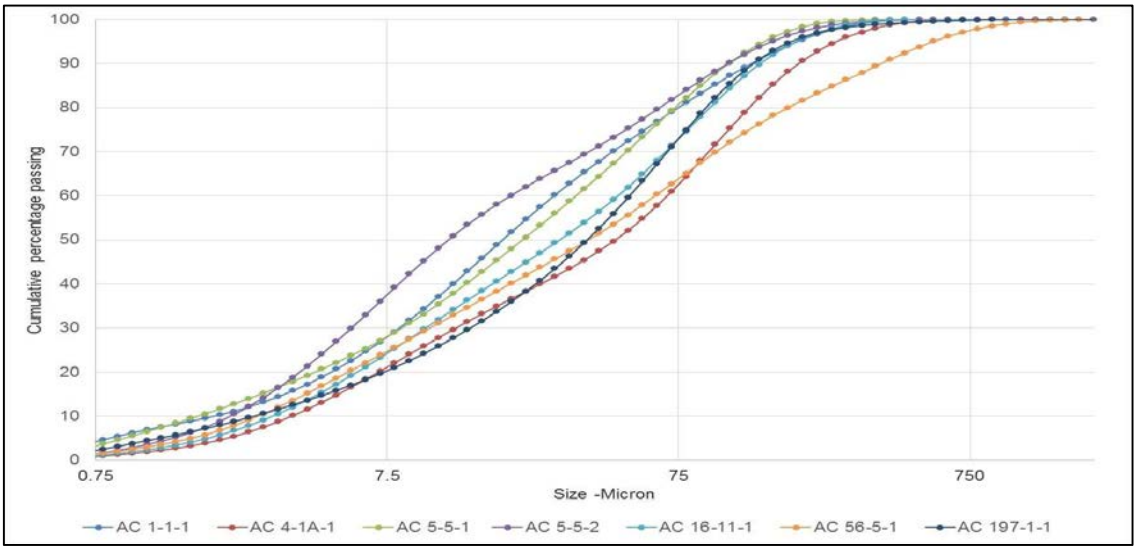

Figure 24: AC particle size analysis – Cumulative percentage passing micron.

Figure 25 shows the particle size analyses of kimberlites AO 319 to AO 323 compared to Venetia Red. 20 – 40% of the particles from the samples are passing 7.5 µm and 80 – 95% of the samples are passing 75 µm, except with AO 323 where 7% of the particles are passing 75 µm. This size range is known to be colloidally stable.

Figure 26 shows the particle size analyses of kimberlites AO 324 to AO 328 compared to Venetia Red. 20 – 40% of the particles from the samples are passing

7.5 µm. It can be seen that all the samples have 80% of the sample size smaller than 75 µm while AO 327 and AO 328 have a size range where more than 90% are smaller than 75 µm.

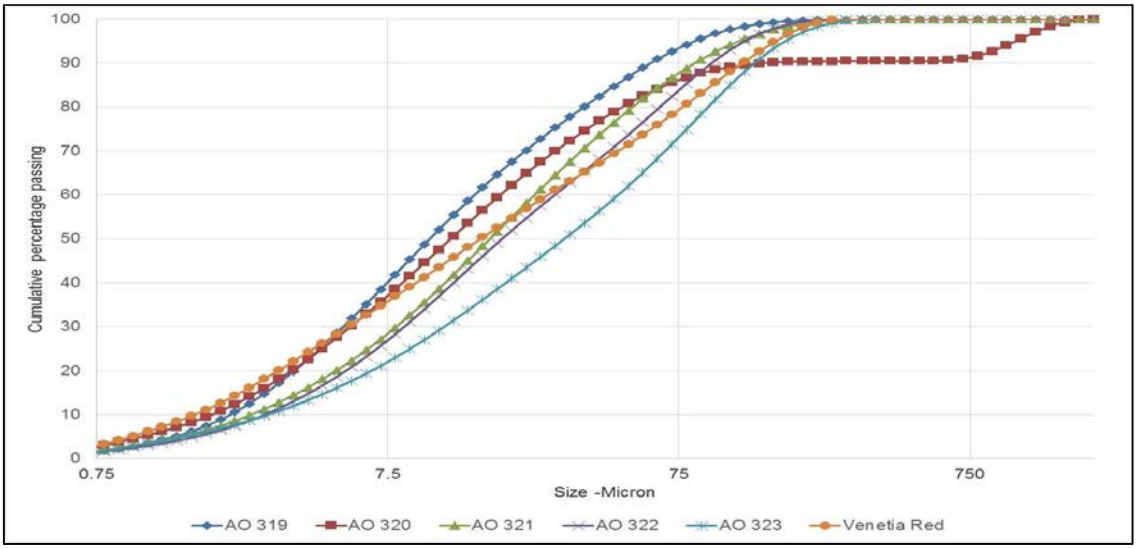

Figure 25: AO particle size analysis – Cumulative percentage passing micron.

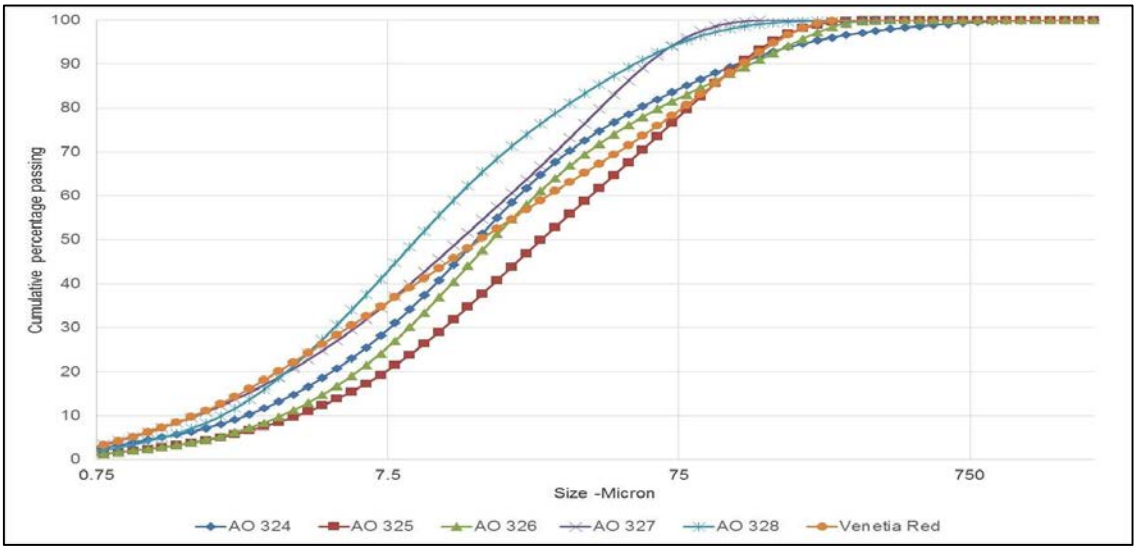

Figure 26: AO particle size analysis – Cumulative percentage passing micron.

The cumulative % passing 7.5 µm and 75 µm was obtained from the particle size distribution data and is shown in Table 13. These values were utilised for prediction regression analysis. The sample with the finest size distribution was AO328 at 43% passing 7.5 µm and 95% passing 75 µm. The coarsest size distribution were AC-4-1A-1 with 20% passing 7.5 µm and 62% passing 75 µm as well as AC-197-

1-1 with 20% passing 7.5 μm and 63% passing 75 μm. We would expect the samples to follow Stokes law where samples with a finer particle size distribution to show more problematic settling compared to samples with a coarser particle size distribution.

Table 13: The cumulative % passing 7.5 μm and 75 μm from the particle size distribution data.

	Particle size distribution			Particle size distribution	
Sample name	- 7.5 μm	-75 μm	Sample name	- 7.5 μm	-75 μm
AC-1-1-1	28	80	AO319	40	94
AC-4-1A-1	20	62	AO320	37	86
AC-5-5-1	28	80	AO321	27	89
AC-5-5-2	38	83	AO322	29	88
AC-16-11-1	24	73	AO323	27	84
AC-56-5-1	24	65	AO324	30	84
AC-197-1-1	20	63	AO325	20	78
Venetia Red	35	80	AO326	25	82
			AO327	35	95
			AO328	43	95

5.1.2 XRF and XRD analysis

The XRF analyses were completed at the University of Pretoria and are shown in Table 14. The XRD data was also performed at the University of Pretoria and results are summarised in Table 15 and
Table 16. The original XRD scans are shown in Figure 171 to Figure 187 in Appendix A.

Kimberlites usually show high quantities of magnesium and silica because of the predominance of silicate minerals. These kimberlites contain between 0-30% MgO and up to 80% SiO_2. Other major constituents in these ores are calcium (0-18% CaO), iron (2-15% Fe_2O_3), aluminium (2-13% Al_2O_3) and to a lesser extent, potassium (0-5% K_2O) and sodium (0-2% Na_2O).

The XRD results show 10% - 75% smectite in these kimberlite samples. Other predominant minerals are chlorite (up to 30%), calcite (up to 30%), quartz (~ 10% - 20%), pyroxene (~10%), plagioclase and orthoclase (up to 15%). Differences in the mineralogical features was noted with AO324 which consists of 20- 25% pyroxene, AO325 which contain up to 50% quartz, AO321 contain ~ 25% plagioclase and AO326 contain 10 - 20% talc which can also reduce the efficiency of settling drastically. The South African Venetia Red contains Feldspar. Quartz (SiO_2) would result in a high Si content, Calcite ($CaCO_3$) would results in a high Ca content, orthoclase ($KAlSi_3O_8$) would result in a high K and Al content. Plagioclase is a feldspar mineral with chemistry ranging between $NaAlSi_3O_8$ to $CaAl_2Si_2O_8$. Chlorite was classified as chlinochlore with chemical formula ($(Mg_5Al)(AlSi_3)O_{10}(OH)_8$). Annite is a Fe rich mica mineral with chemical formula $KFe_3^{2+}AlSi_3O_{10}(OH,F)_2$. Actinolite is an amphibole silicate mineral with the chemical formula $Ca_2(Mg,Fe)_5Si_8O_{22}(OH)_2$.

Table 14: Results of XRF analysis done on the ore samples tested (proportions by mass).

Sample name	Na_2O	MgO	Al_2O_3	SiO_2	P_2O_5	K_2O	CaO	TiO_2	Fe_2O_3	MnO
	%	%	%	%	%	%	%	%	%	%
AC-1-1-1	0.01	20.63	4.10	25.54	1.36	0.61	15.34	4.70	15.18	0.27
AC-4-1A-1	0.01	17.47	2.71	62.81	0.15	0.23	3.19	0.86	5.25	0.06
AC-5-5-1	0.01	29.35	3.73	35.33	0.66	0.15	5.91	1.03	9.49	0.14
AC-5-5-2	0.01	25.82	4.12	38.99	0.56	0.25	7.19	0.90	8.50	0.10
AC-16-11-1	0.00	24.52	2.30	41.29	0.18	0.26	6.73	1.44	9.60	0.18
AC-56-5-1	0.58	18.92	7.15	51.10	0.34	1.68	4.54	1.16	6.27	0.10
AC-197-1-1	0.00	20.68	2.89	26.01	1.19	0.21	17.24	1.35	9.50	0.47
AO319	0.60	18.69	6.16	44.45	0.20	0.82	5.72	2.16	13.70	0.18
AO320	0.55	17.86	4.57	43.71	0.49	1.47	8.16	1.99	11.07	0.23
AO321	1.98	4.14	10.99	65.44	0.09	1.96	2.89	0.54	8.80	0.06
AO322	0.85	10.97	7.12	56.61	0.14	1.25	5.37	0.56	8.51	0.12
AO323	0.82	0.65	8.65	80.49	0.23	4.05	0.81	0.34	2.38	0.05
AO324	0.98	15.29	6.96	41.59	0.66	0.46	11.77	1.89	12.35	0.16
AO325	0.97	2.53	7.24	80.04	<0.01	1.89	2.23	0.26	2.20	0.03
AO326	0.72	15.70	6.93	52.37	0.14	2.49	3.89	0.84	9.58	0.11
AO327	0.88	1.77	12.72	65.29	0.07	5.40	3.86	0.53	4.82	0.08
AO328	0.11	16.10	6.04	45.15	0.21	0.75	10.12	1.21	14.11	0.18
Venetia Red	1.09	19.60	8.37	51.10	0.18	1.86	4.46	0.72	8.79	0.10

Table 15: The XRD analyses of the Alto Cuilo kimberlites

Sample	**AC 1-1-1**	**Sample**	**AC 4-1A-1**
Mineral group / mineral identified	Estimated quantity Quantity[Mass %]	Mineral group / mineral identified	Estimated quantity Quantity[Mass %]
Smectite	40 - 50	Smectite	70 - 75
Chlorite	30 -35	Quartz	~ 10
Calcite	10 - 15	Annite	6 - 8
Pyroxene	~ 5	Calcite	~ 6
Serpentine	~ 5	Kaolinite	< 4
		Hematite	< 3
Sample	**AC 5-5-1**	**Sample**	**AC 5-5-2**
Mineral group / mineral identified	Estimated quantity Quantity[Mass %]	Mineral group / mineral identified	Estimated quantity Quantity[Mass %]
Smectite	40 - 50	Smectite	60 - 70
Chlorite	30 -35	Kaolinite	~ 10
Calcite	10 - 15	Calcite	< 10
Pyroxene	~ 5	Annite	< 10
Serpentine	~ 5	Pyroxene	~ 5
Hematite	~ 5	Orthoclase	< 5
		Plagioclase	< 2
Sample	**AC 16-1-1**	**Sample**	**AC 56-5-1**
Mineral group / mineral identified	Estimated quantity Quantity[Mass %]	Mineral group / mineral identified	Estimated quantity Quantity[Mass %]
Smectite	65 - 70	Smectite	55 - 65
Chlorite	10 - 15	Talc	~ 8
Calcite	~ 10	Annite	~ 7
Annite	~ 5	Quartz	~ 7
Serpentine	< 5	Calcite	~ 5
Hematite	< 2	Plagioclase	~ 5
Quartz	~ 1	Orthoclase	~ 3
		Hematite	2 – 3
		Diopside	2 – 3
		Chlorite	~ 2
		Kaolinite	< 1
Sample	**AC 197-1-1**	**Sample**	**Venetia Red**
Mineral group / mineral identified	Estimated quantity Quantity[Mass %]	Mineral group / mineral identified	Estimated quantity Quantity[Mass %]
Smectite	35 – 40	Smectite	~ 40
Calcite	25 - 30	Quartz	~ 25
Chlorite	5 - 10	Calcite	~ 10
Kaolinite	5 - 8	Feldspar	~ 10
Hematite	~ 5	Serpentine	~ 10
Serpentine	< 5	Mica	~ 5
Pyroxene	< 3	Amphibole	< 5
Annite	< 3	Magnetite	< 5
Orthoclase	< 2		

Table 16: The XRD analyses on the Itengo/Tchegi kimberlites

Sample	**AO 319**	**Sample**	**AO 320**
Mineral group / mineral	Estimated quantity	Mineral group / mineral	Estimated quantity
Smectite	55 - 60	Smectite	55 - 60
Pyroxene	10 – 15	Annite	~ 10
Actinolite	~ 10	Pyroxene	~10
Annite	~ 10	Actinolite	6 - 8
Calcite	~ 3	Calcite	~ 6
Orthoclase	~ 3	Orthoclase	< 5
Plagioclase	< 3	Plagioclase	< 5
		Hematite	< 3
Sample	**AO 321**	**Sample**	**AO 322**
Mineral group / mineral	Estimated quantity	Mineral group / mineral	Estimated quantity
Smectite	30 - 35	Smectite	55 - 60
Plagioclase	30 - 35	Quartz	~ 13
Quartz	20 - 25	Plagioclase	~ 10
Pyroxene	~ 4	Calcite	~ 7
Annite	~ 4	Annite	~ 6
Hematite	~ 3	Pyroxene	~ 3
Calcite	2 - 3	Orthoclase	~ 3
		Hematite	~ 2
Sample	**AO 323**	**Sample**	**AO 324**
Mineral group / mineral	Estimated quantity	Mineral group / mineral	Estimated quantity
Quartz	40 - 50	Smectite	50 - 55
Orthoclase	~ 20	Pyroxene	20 -25
Smectite	~ 15	Annite	~ 10
Plagioclase	10 - 15	Calcite	~ 5
Annite	~ 3	Plagioclase	< 5
Pyroxene	~ 2	Hematite	< 4
Hematite	< 2	Actinolite	< 3
		Orthoclase	< 2
		Quartz	< 1
Sample	**AO 325**	**Sample**	**AO 326**
Mineral group / mineral	Estimated quantity	Mineral group / mineral	Estimated quantity
Quartz	45 - 50	Smectite	50 - 55
Smectite	~ 30	Talc	10 – 20
Plagioclase	10 -15	Annite	~ 8
Calcite	~ 5	Plagioclase	5 – 10
Orthoclase	< 4	Orthoclase	~ 5
Pyroxene	< 2	Pyroxene	~ 5
Hematite	< 2	Actinolite	< 5
		Calcite	~ 3
Sample	**AO 327**	**Sample**	**AO 328**
Mineral group / mineral	Estimated quantity	Mineral group / mineral	Estimated quantity
Quartz	~ 25	Smectite	55 - 60
Smectite	20 – 25	Pyroxene	~ 15
Plagioclase	15 – 20	Actinolite	10 - 12
Orthoclase	15 – 20	Annite	~ 9
Calcite	~ 5	Calcite	~ 4
Annite	~ 5	Orthoclase	< 4
Pyroxene	< 3	Hematite	~ 2
Actinolite	< 3	Plagioclase	< 2
Hematite	< 2		

Changes in chemical and mineralogical properties with depth

Figure 27 shows the XRF results for Tchegi 31 Hole 6 at a depth of 30 meters (sample 320) compared to a depth of 116 m (sample 319). Based on the XRD results both these kimberlite contain 60% smectite and show very similar mineralogical properties. A reduction in the amount of Al^{3+}, - 1.5%, Mg^{2+}, - 0.8%, and Fe^{3+}, - 2.6% cations are observed closer to the surface together with an increase in the amount of Ca^{2+}, 2.5% and K^{+}, 0.7% cations, which indicate that a small degree of cation exchange has taken place closer to the surface.

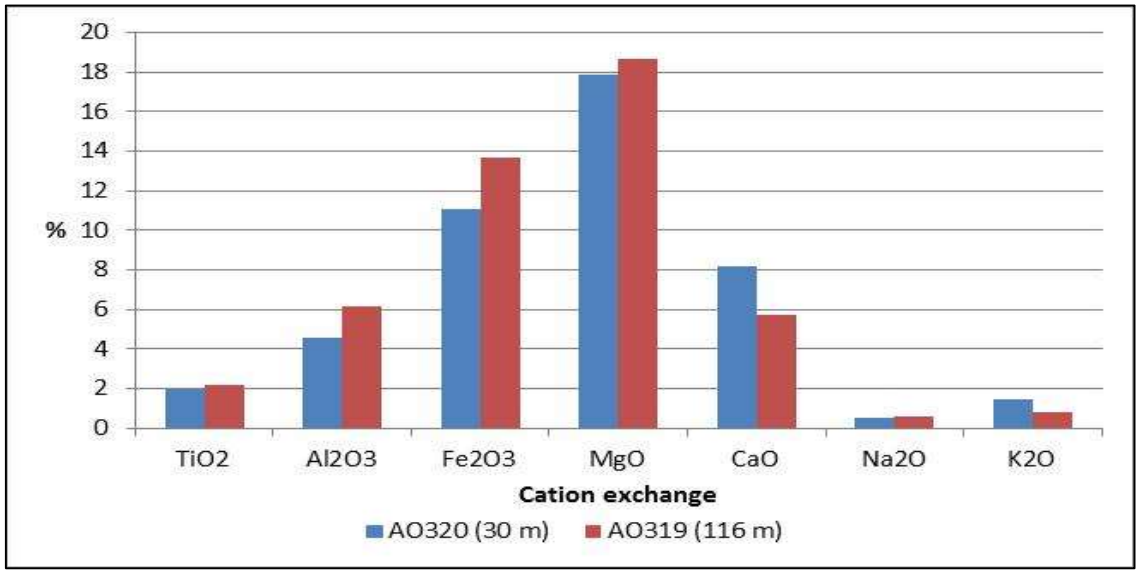

Figure 27: The changes in cation percentages, as measured by XRF analyses, with depth of hole 6 of the Tchegi 31 kimberlite.

The XRD and XRF results for Tchegi 32 Hole 1 are shown in Figure 28 and Figure 29 respectively for depths of 137 m (sample AO321), 92 m (sample AO322) and 30 m (sample AO323). The XRD shows very different mineralogical features at these three depths suggesting a different type of kimberlite especially at 30 m with the very high quartz content at 50% compared to 13% at 92 m and 25% at 137 m. The smectite content varies from 15% at 30 m to 60% at 92 m and 35% at 137 m. The plagioclase is highest at a depth of 137 m at 35% and reduces to 10 % at 92 m and 15% at a depth of 30 m. The orthoclase is reported as 20% at 30 m compared to < 5% at 92 m and absent at 137 m. The high amount of orthoclase

($KAlSi_3O_8$) at 30 m would suggest a high potassium content which agrees with the observed XRF results.

The XRF results show an increase in magnesium and calcium cations which is commonly found in smectite. Cation exchange also took place, moving from 137 meters to 92 meters as the sodium and aluminium cations reduced with subsequent sharp increases in calcium and magnesium cations.

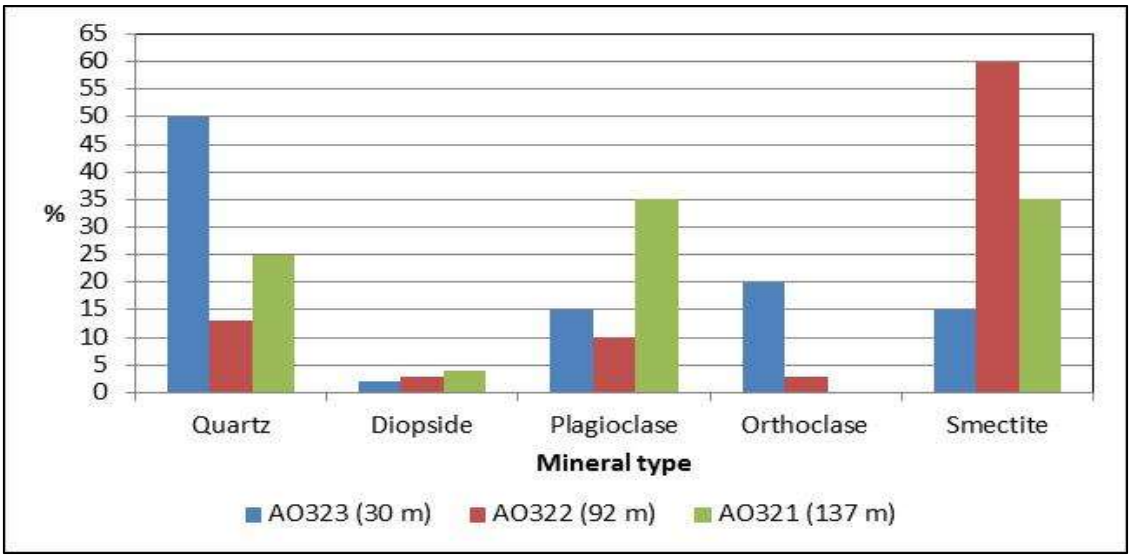

Figure 28: The changes in mineral types with depth of Tchegi 32 Hole 1 kimberlite.

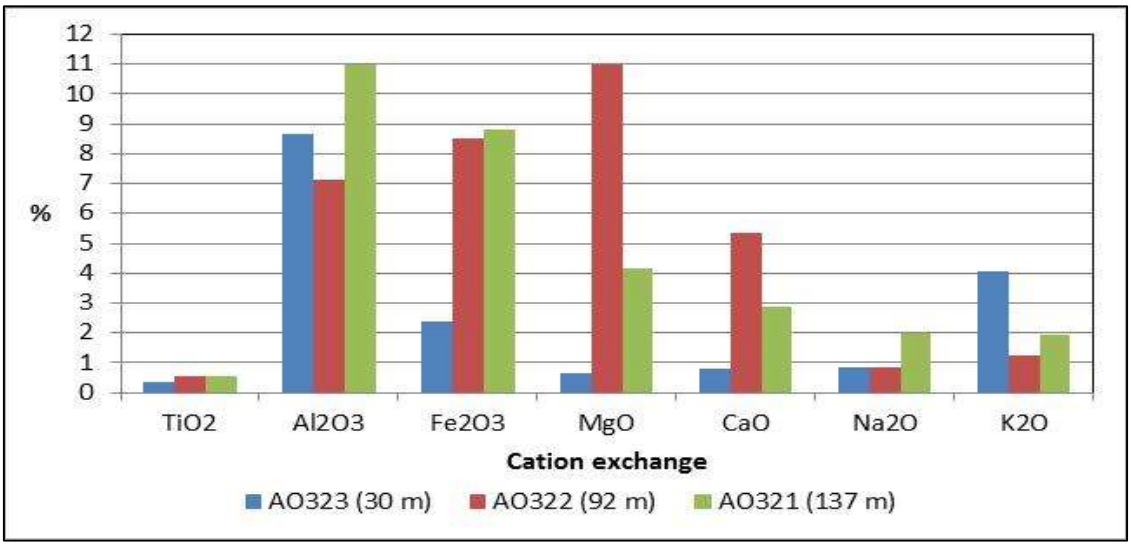

Figure 29: The changes in cation percentages, as measured by XRF analyses, with depth of hole 1 of the Tchegi 32 kimberlite.

The XRD and XRF results for Itengo 66 Hole 1 are shown in Figure 30 and Figure 31 respectively for depths of 340 m (sample AO324) and 104 m (sample AO325). The XRD results shows very different mineralogical features at the two different depths suggesting a different type of kimberlite at 104 m with the very high quartz content at 50% compared to 0% at 304 m. The smectite content varies from 30% at 104 m to 55% at 304 m. The plagioclase is highest at a depth of 104 m at 15% and reduces to 5% at a depth of 304 m. The diopside is reported as 25% at 304 m compared to < 5% at 104 m. The high amount of diopside ($CaMgSi_2O_6$) and smectite at 304 m would suggest a high calcium and magnesium content which agrees with the observed XRF results.

The XRF results show an increase in magnesium, and calcium cations which is commonly found in smectite. Cation exchange also took place, moving from 304 meters to 104 meters as the potassium, calcium, magnesium and ferric cations showed a sharp reduction while there was a small increase in aluminium cations.

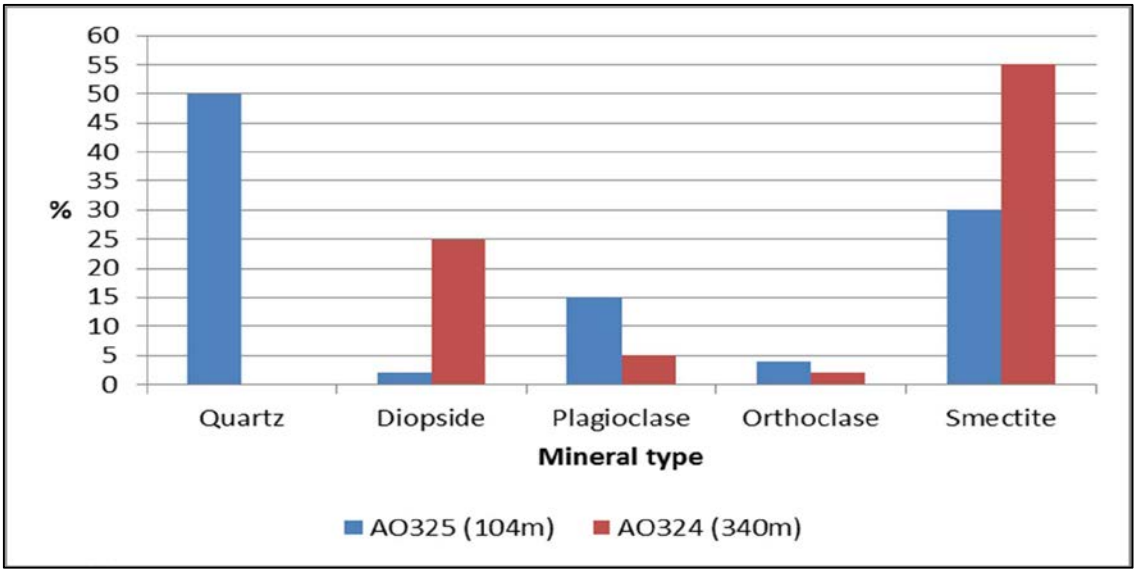

Figure 30: The changes in mineral types with depth of hole 1 of the Itengo 66 kimberlite.

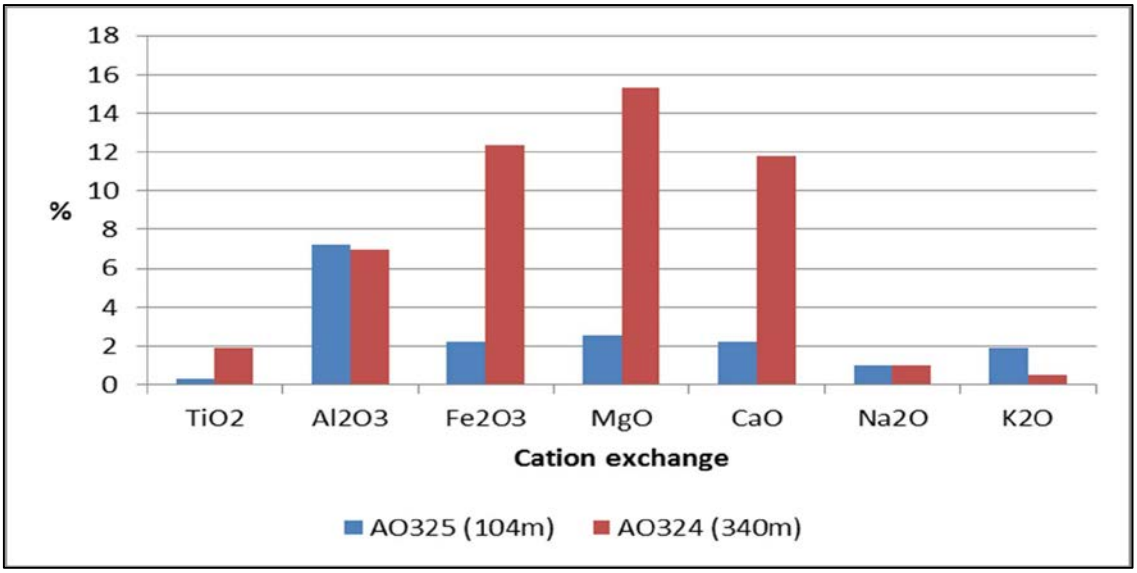

Figure 31: The changes in cation percentages, as measured by XRF analyses, with depth of hole 1 of the Itengo 66 kimberlite.

The XRD and XRF results for Tchegi 30 Hole 1 are shown in Figure 32 and Figure 33 respectively for depths of 100 m (sample AO327) and 163 m (sample AO328). The XRD shows very different mineralogical features at the two different depths suggesting a different type of kimberlite at 100 m with the high quartz content at 25% compared to 0% at 163 m. The smectite content varies from 25% at 100 m to 6% at 163 m. The plagioclase is highest at a depth of 100 m at 20% and reduces to < 5% at a depth of 163 m. The diopside is reported as 15% at 163 m compared to < 5% at 100 m. The high amount of diopside ($CaMgSi_2O_6$) and smectite at 163 m would suggest a high calcium and magnesium content which agrees with the observed XRF results.

The XRF results show an increase in magnesium and calcium cations which is commonly found in smectite. Cation exchange also took place, moving from 163 meters to 100 meters as the calcium, magnesium and ferric cations showed a sharp reduction while there was an increase in aluminium, sodium and potassium cations.

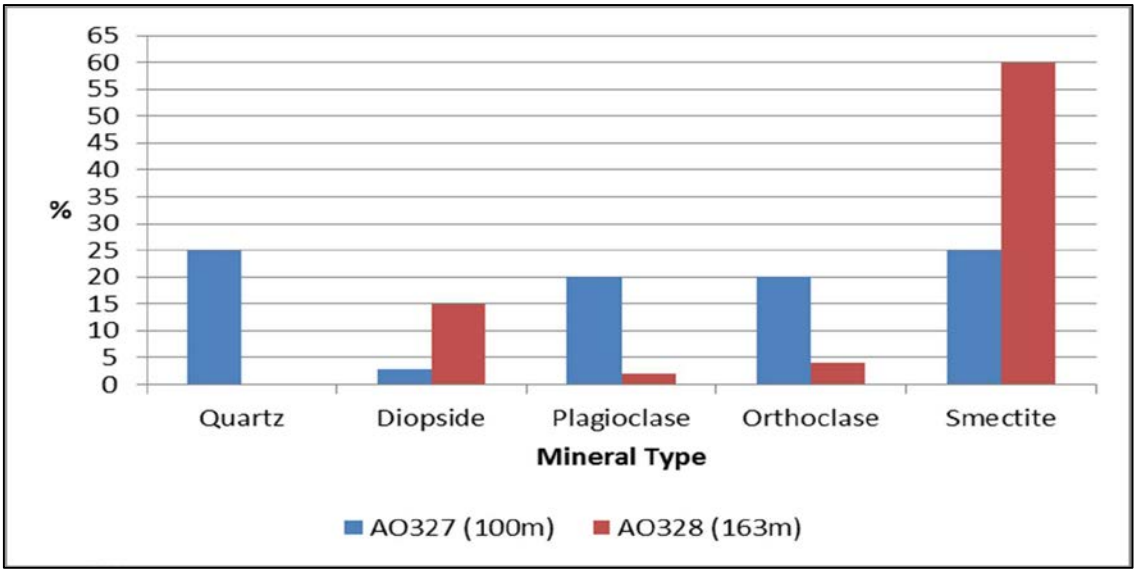

Figure 32: The changes in mineral types with depth of hole 1 of the Tchegi 30 kimberlite.

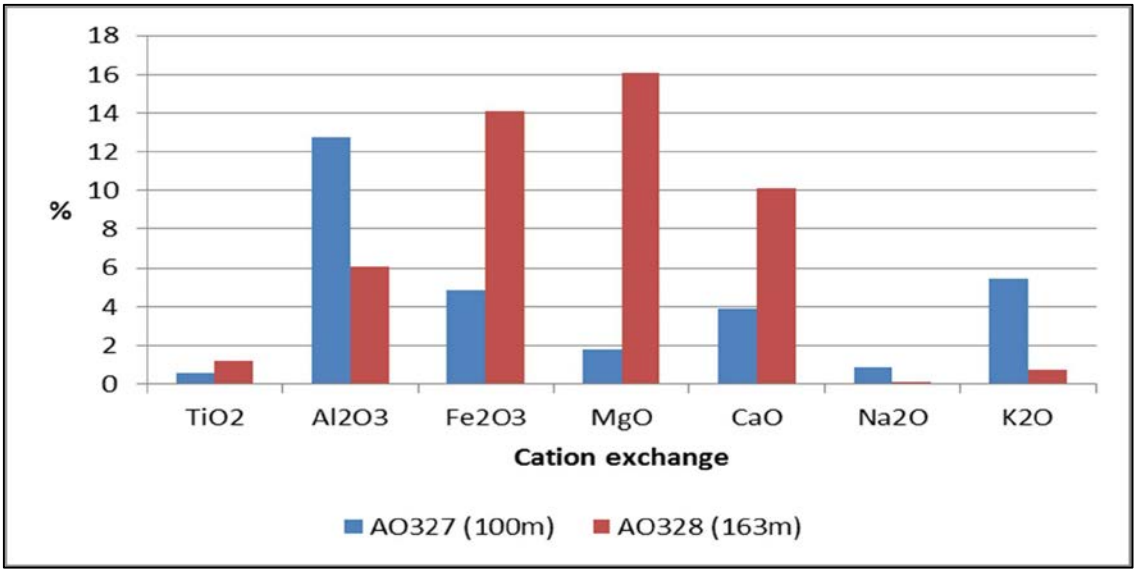

Figure 33: The changes in cation percentages, as measured by XRF analyses, with depth of hole 1 of the Tchegi 30 kimberlite.

Drill core samples from different depths of kimberlite deposits presented insight into mineral changes that took place along the depth of the kimberlite and how this would influence the settling characteristics of the kimberlite ore during the life cycle of the mine. It was observed that there was a decrease in the percentage of Na^{+}, Mg^{2+}, Ca^{2+}, Ti^{4+} and Fe^{3+} as the depth of the kimberlite and the smectite percentage increases, while the percentage of potassium and aluminium

increases closer to the surface. Divalent and trivalent cations were exchanged with potassium as natural weathering of the kimberlites takes place. It was evident that as the percentage of smectite decreases closer to the surface, there is an increase in the percentages of the minerals, plagioclase and orthoclase. Comparing the exchangeable cations with the depth of the various kimberlites it was noted that there was a reduction in the cation exchange capacity as well as the exchangeable sodium percentage of the kimberlite. This occurred as the percentage of smectite decreased and the cations were locked in other minerals such as plagioclase, orthoclase and diopside.

5.1.3 Cation exchange capacity

Samples from each kimberlite were analysed to determine the cation exchange capacity for every sample through the Ammonium Acetate method for soil analyses as shown in Table 17. Sodium, potassium, calcium and magnesium were reported in centimol(+) per kilogram. Calcium and magnesium cations are the predominantly exchangeable cations.

The cation exchange capacity and the smectite percentage of the different kimberlites are shown in Figure 34. It is seen that kimberlites that have a smectite content of less than 30% will also have a low cation exchange capacity. The red dots on the graphs indicate the two samples, AC 1-1-1 and AC 5-5-1, which settled out naturally. Figure 35 show the comparison of the exchangeable sodium percentage for the different kimberlite samples against the smectite percentage for each kimberlite. The red dots on the graphs indicate the two samples, AC 1-1-1 and AC 5-5-1, which settled out naturally. Looking at Figure 35 it is seen that samples with high smectite content have a low percentage of exchangeable sodium percentage and it would be expected that no colloidal stability will be experienced. Only two samples, AC 1-1-1 and AC 5-5-1 settled out naturally.

Table 17: The cation exchange capacity of the different kimberlites compared to the smectite and exchangeable sodium percentage.

cmol(+)/kg	Na	K	Ca	Mg	CEC	Smectite %	ESP %
AC-1-1-1	0.1	0.2	12.3	6.4	5	50	2
AC-5-5-1	0.3	0.3	16.2	7.7	10	50	3
AC-4-1A-1	0.3	0.6	35.1	20.9	45	75	1
AC-5-5-2	0.3	0.4	42.1	7.9	48	70	1
AC-16-11-1	1.8	0.5	26.6	13.4	31	70	6
AC-56-5-1	16.3	0.8	37.7	5.4	54	65	30
AC-197-1-1	3.2	0.2	19.8	6.8	19	40	17
AO319	13.8	1.1	51.2	5.9	67	60	21
AO320	1.9	1.6	47.9	19.1	59	60	3
AO321	3.4	1.0	62.7	12.8	68	35	5
AO322	0.6	0.7	28.0	10.3	31	60	2
AO323	0.2	0.7	8.7	4.1	13	15	1
AO324	9.7	0.5	52.9	4.2	56	55	17
AO325	0.3	0.5	24.1	6.5	22	30	2
AO326	1.6	0.9	46.4	14.8	53	55	3
AO327	1.5	1.8	21.8	4.9	18	25	8
AO328	15.8	1.1	53.6	10.6	77	60	21
Venetia Red	14.0	0.9	22.6	3.9	32	40	43

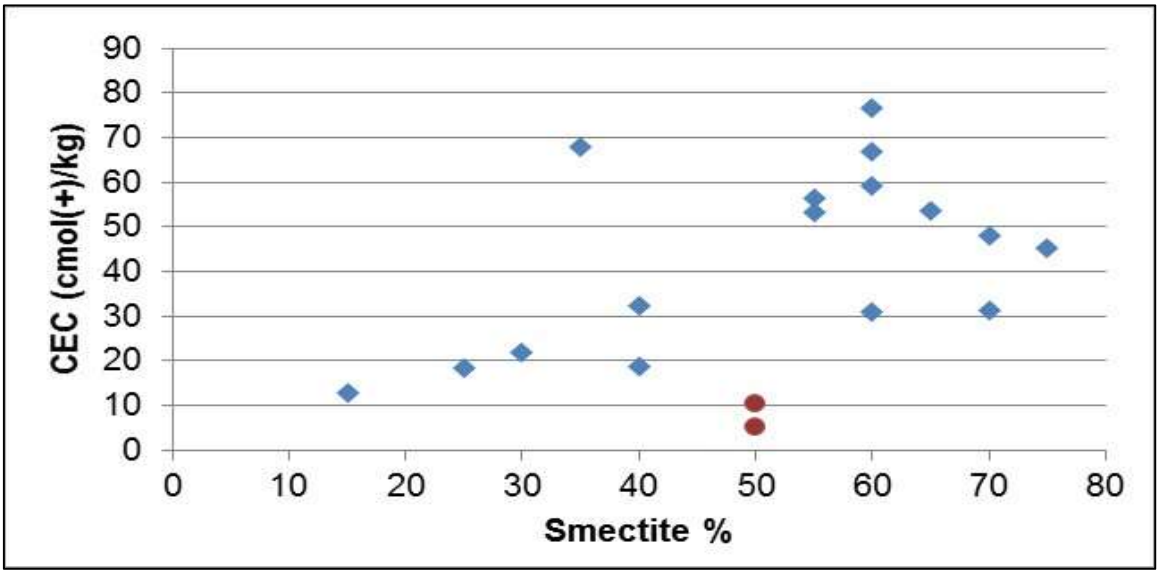

Figure 34: Cation exchange capacity versus percentage smectite for the various kimberlites.

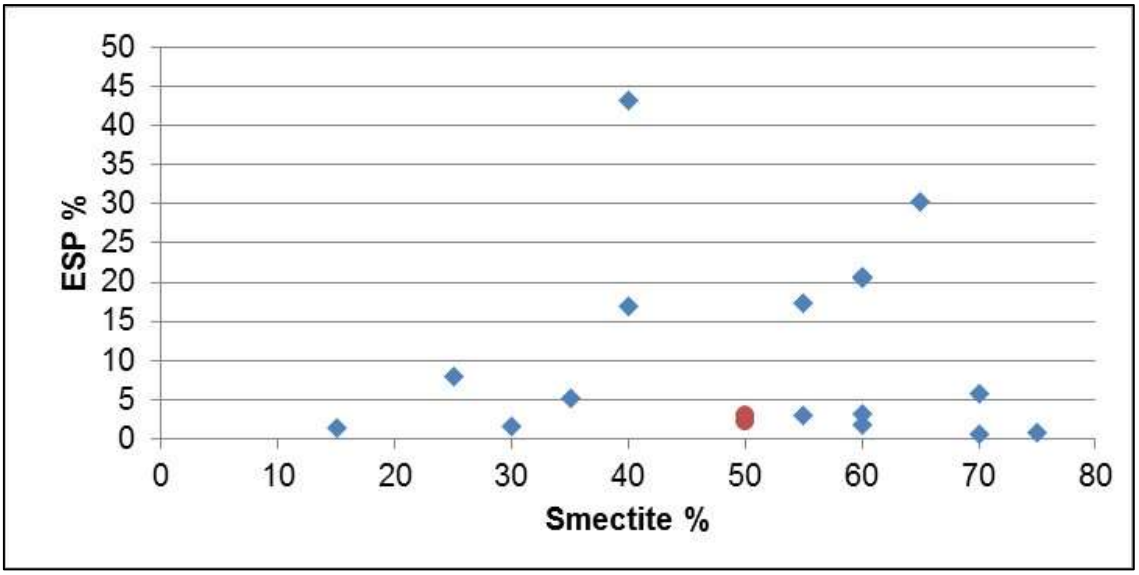

Figure 35: Exchangeable sodium percentage versus percentage smectite of the various kimberlites.

Table 24 in Appendix A shows the cation exchange capacity and the exchangeable sodium percentage along with the clarity of the natural settling process of the kimberlites. Vietti (2004) proposed that kimberlites will experience colloidal stability when the exchangeable sodium percentage in the kimberlite is higher than 15% and the pH of the slurry is between 9 and 11 as shown in Figure 36. The exchangeable sodium percentage of the kimberlites however ranged from 0.6% to 43%. The two kimberlites that settled out naturally, AC 1-1-1 and AC 5-5-1, had ESP values of 2.1% and 2.9% respectively, which conform to proposed model of Vietti (2004). Six kimberlites experienced colloidal stability and had ESP values higher than 15% confirming the proposed model by Vietti (2004). The remaining 10 kimberlites had ESP values ranging between 0.6% and 8% and experienced colloidal stability during natural settling. These results indicate that the Exchangeable Sodium Percentage of a kimberlite cannot be used as a critical parameter to predict whether natural settling will occur or not.

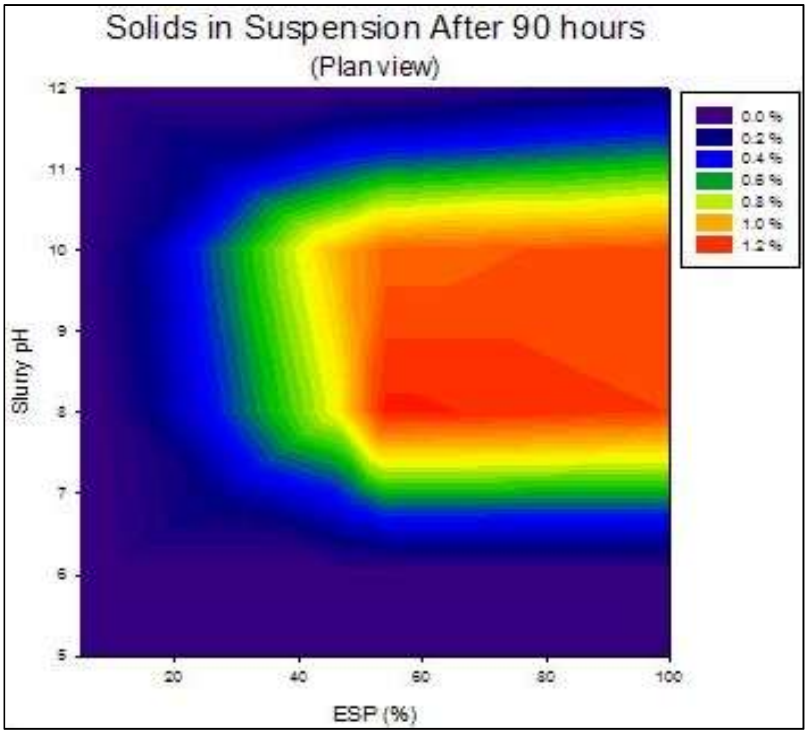

Figure 36: Model for Describing the Suspension Behaviour of Naturally Settling Low-Density Kimberlitic Clay Slurries (Vietti, 2004)

5.1.4 Natural settling

The natural settling of the different kimberlite samples is shown in Figure 37 to Figure 41. Figure 37 shows the natural settling for sample AC 1-1-1, AC 4-1A-1, AC 5-5-2 and AC 16-1-1 after 60 minutes. It can be seen that only sample AC 1-1-1 settled out naturally after 60 minutes. AC 1-1-1 had a similar particle size distribution when compared to AC 5-5-2 with 80% of the material passing through 75 µm, while AC 4-1-4A and AC 16-1-1 have coarser size distributions with 65% and75 % of the particles smaller than 75 µm respectively. This indicated that AC 1-1-1 did not settle out naturally as the result of a coarser size fraction compared to the other samples. AC 1-1-1 did however have the lowest smectite content of 50% when compared to the other kimberlite slurries that showed colloidal stability in this time period, with smectite contents ranging between 70% and 75%.

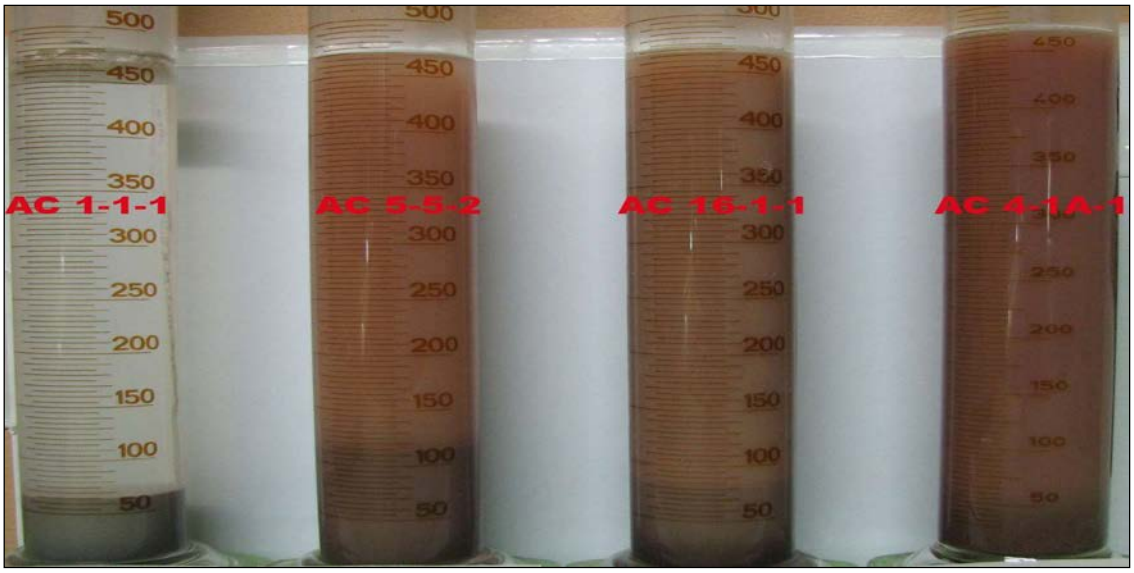

Figure 37: Natural settling of AC 1-1-1, AC 5-5-2, AC 16-1-1 and AC 4-1A-1 after 60 minutes.

Figure 38 shows the natural settling for sample AC 5-5-1, AC 56-5-1 and AC 197-1-1 after 60 minutes. It can be seen that kimberlite sample AC 5-5-1 settled out naturally after 60 minutes while AC 56-5-1 and AC 197-1-1 experienced colloidal stability. AC 5-5-1 had 80% of the particles passing through 75 µm, compared to 65% for AC 56-5-1 and 75% for AC 197-1-1. AC 5-1-1 and AC 197-1-1 contained similar smectite percentages of between 50% and 40% respectively while AC 56-5-1 contained 65% smectite.

Colloidal stability was experienced after 60 minutes during the natural settling of Venetia Red, AO 319, AO 327 and AO 328 kimberlite samples as shown in Figure 39. Venetia Red had a size distribution of 80% passing 75 µm, while the AO 319, AO 327 and AO 328 had more than 90% of the particles passing 75 µm. AO 327 had the lowest smectite content at 25%, while Venetia Red contained 40% smectite and AO 319 and AO 328 contained 60% smectite each.

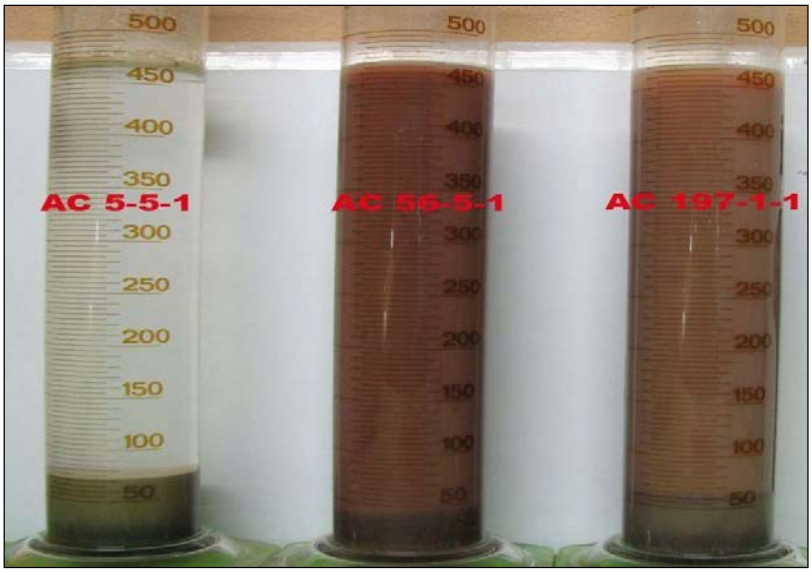

Figure 38: Natural settling of AC 5-5-1, AC 56-5-1 and AC 197-1-1 after 60 minutes.

Figure 39: Natural settling of Venetia Red, AO 319, AO 327 and AO 328 after 60 minutes.

Natural settling did not occur after 60 minutes for AO 320, AO 322, AO 324 and AO 326 kimberlite samples as shown in Figure 40. AO 326 had a size distribution of 83% passing 75 µm, while the AO 320, AO 322 and AO 324 showed that between 85% and 90% of the particles passed 75 µm. The smectite percentage of the different kimberlites ranged between 55% and 60%.

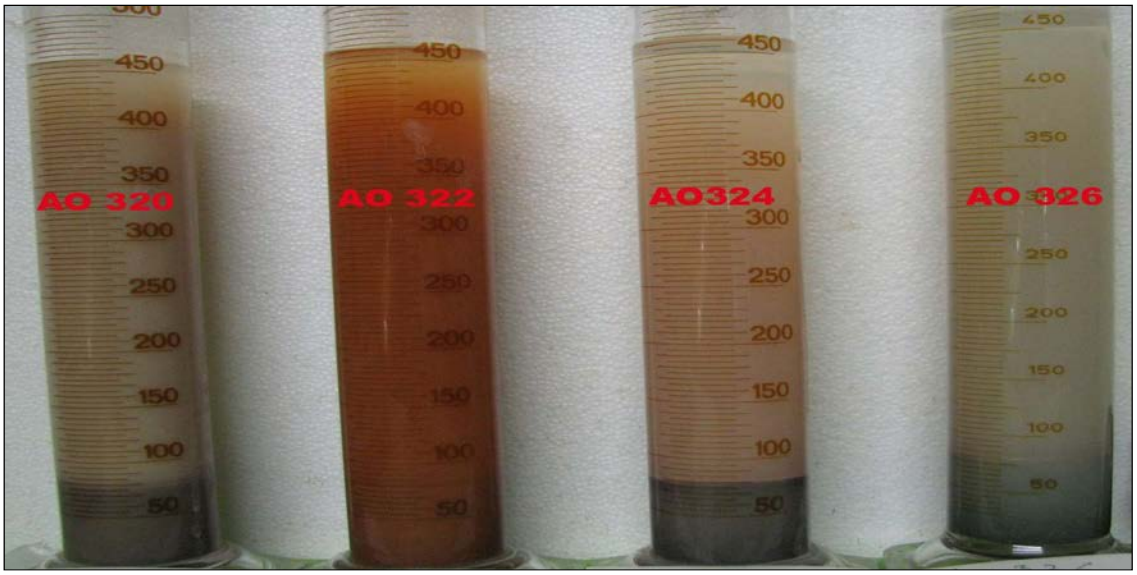

Figure 40: Natural settling of AO 320, AO 322, AO 324 and AO 326 after 60 minutes.

Figure 41 shows the colloidal stability of AO 321, AO 323 and AO 325 after 60 minutes of natural settling. All three samples had between 80% and 88% of the material passing 75 µm. AO 321 had a smectite content of 35% and a quartz content of 20% and colloidal stability was still experienced. AO 323 had a smectite content of 15% while AO 325 had a smectite content of 30%.

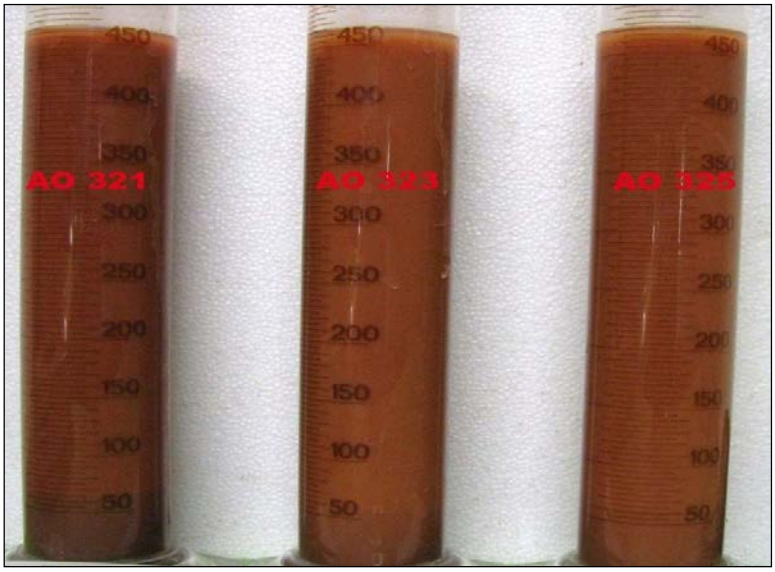

Figure 41: Natural settling of AO 321, AO 323 and AO 325 after 60 minutes.

Settling behaviour is usually predicted by particle size and Stokes law, for the settling of particles, indicates that the finer, the particle size distribution of a kimberlite slurry, the more difficult it would be to settle the slurry. On average 27% of the slurry particles were passing 7.5 micron and 80% of the particles were passing 75 micron. Two kimberlites, AC 1-1-1 and AC 5-5-1, settled out naturally with 27% of the fine particles passing 7.5 micron and 81% and 82% of the fine particles passing 75 micron. The other 16 kimberlites, with coarser and finer particle size distributions than AC 1-1-1 and AC 5-5-1, experienced colloidal stability, indicating that Stokes law cannot be used alone to predict whether settling will occur or not.

5.1.5 pH of the kimberlite slurry solutions

Table 18 show the pH values of the kimberlite slurries after 60 minutes of natural settling. The pH values of the kimberlite slurries are all between 9 and 11, which is higher than the point of zero charge. Vietti (2004) defined the pH range, between 9 and 11, as the range where kimberlite slurries could be colloidally stable if the exchangeable sodium percentage of the kimberlite is more than 15%.

Table 18: The pH values of the kimberlite slurries after 60 minutes of natural settling.

Sample	pH	Sample	pH
AC-1-1-1	9.3	AO321	9.9
AC-4-1A-1	9.3	AO322	9.7
AC-5-5-1	9.5	AO323	9.3
AC-5-5-2	9.5	AO324	10.3
AC-16-11-1	9.7	AO325	9.8
AC-56-5-1	10.6	AO326	9.8
AC-197-1-1	10.1	AO327	10.0
AO319	9.4	AO328	10.1
AO320	9.7	Venetia Red	10.6

Figure 42 shows the pH values of the various kimberlite slurries against the smectite percentage of these. It can be seen that the pH values range from 9 to 11 which is higher than the zero potential charge clay crystal edge as discussed in section 2.2.1.3. The result is negative repulsive forces that exist on the clay surface charges, rendering the slurries colloidally stable. The data indicates that the lower the pH value, the lower the chance that colloidal stability will be experienced.

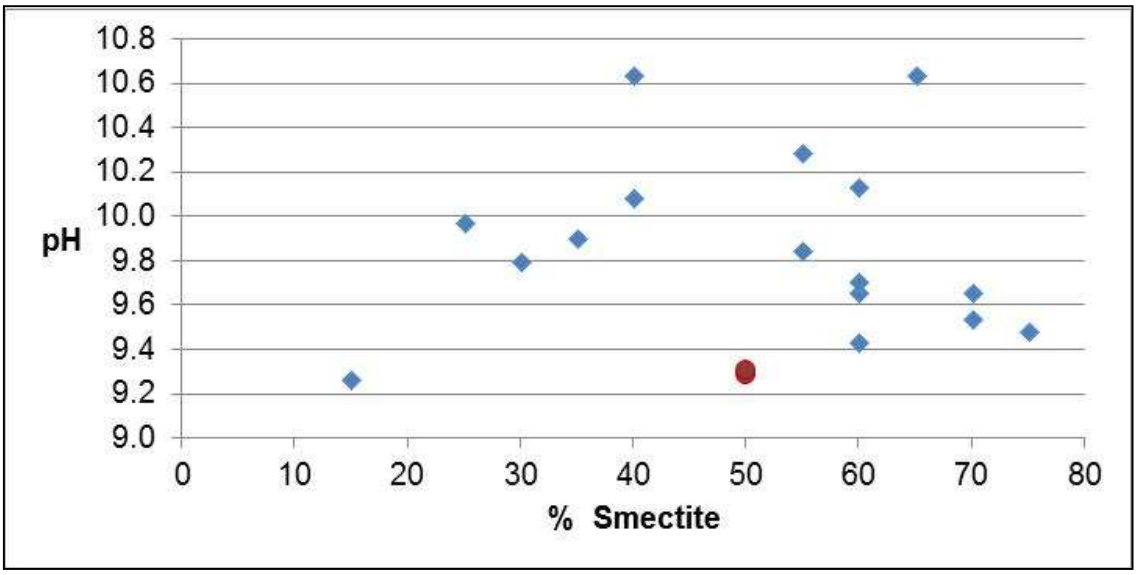

Figure 42: pH values of the kimberlite slurries against the smectite percentage of the kimberlites.

Figure 43 show the pH versus % ESP data. The proposed model by Vietti (2004) predicts that 10 kimberlites with ESP values of less than 15% and pH values between 9 and 11, will settle naturally. Of these 10 kimberlites, only two kimberlites, AC 1-1-1 and AC 5-5-1, shown as the red dots, settled naturally. The other 8 kimberlites experienced colloidal stability and this is in contradiction with ESP and pH model proposed by Vietti (2004). There were eight kimberlites with ESP values of more than 15% and pH values between 9 and 11 and all of these kimberlites experienced colloidal stability and conformed to the ESP and pH model of Vietti (2004). The test work confirmed that colloidal stability is experienced with kimberlites slurries where the pH of the solution range between 9 and 11 but the ESP cannot be used together with the pH to predict colloidal stability of kimberlite slurries. There are other parameters that need to be taken into consideration before determining colloidal stability.

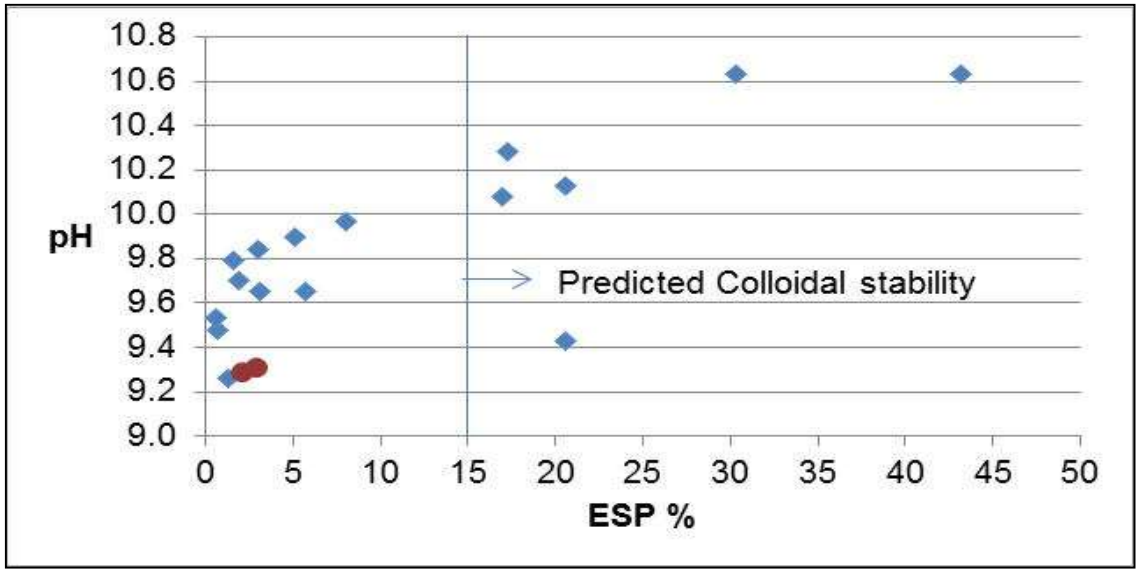

Figure 43: pH values of the kimberlite slurries versus the exchangeable sodium percentage of the kimberlites.

Figure 44 shows the pH values of the kimberlite samples against the respective cation exchange capacities. The red dots represent samples AC 1-1-1 and AC 5-5-1 which settled out naturally.

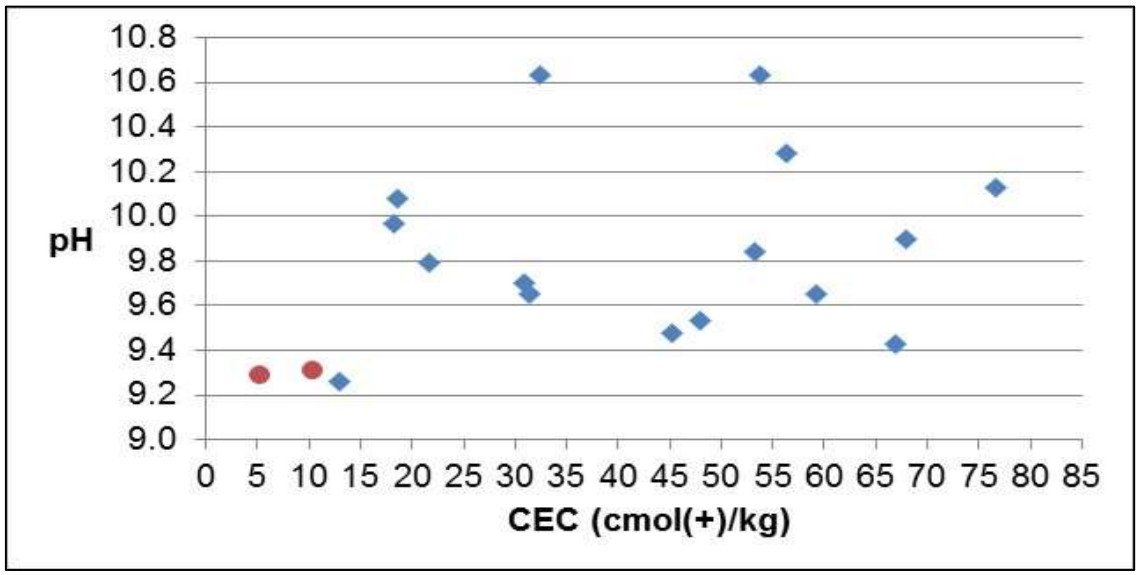

Figure 44: pH values of the kimberlite slurries versus the cation exchange capacity of the kimberlites.

The Cation Exchange Capacity of the kimberlite was compared with pH values of the kimberlite slurries but no definite trend could be identified to use the CEC as critical parameter in predicting the settling behaviour of kimberlite slurries.

5.2 Critical coagulant concentration (CCC)

The critical coagulant concentrations for the various kimberlites, as shown in Table 25 and Table 26 in Appendix A, were used to conduct settling rate test work and determine the most efficient cationic coagulant. This was determined by investigating the settling rate of the different kimberlite slurry samples after 10 minutes, and determining the slurry bed depth after 24 hours. The cation that produced the fastest settling rate and the lowest slurry bed depth for the different kimberlite slurries was selected for further test work. Divalent and trivalent cations contributed to the most efficient settling rates. Settling rates varied between 0.6 m/h to 3 m/h between the different kimberlites, and the most compacted sediment bed weight percentage varied between 20% and 58%. The settling rate graphs for the different kimberlites at the various critical coagulant concentrations can be seen in Figure 137 to Figure 154 in Appendix A.

The best settling result for AC 1-1-1, as shown in Figure 45 and Figure 46, was achieved with $CaCl_2$ where the initial settling rate was 2.7 m/h and the final slurry bed weight percentage was 58% after 24 hours. AC 1-1-1 had the lowest cation exchange capacity of all the kimberlites at 5 cmol/kg and an exchangeable sodium percentage of 2%. Settling rates of more than 2 m/h were achieved with mono-, di- and trivalent cations and the weight percentage of kimberlite in the slurry was more than 5% for all the cations tested. The negative forces surrounding the particles are very small since AC 1-1-1 did settle naturally as well. The packing relationship of these particles can only be face-to-face to result in a very good slurry bed compaction comprising of a high slurry bed weight percentage. It is important to note, however, that the XRD results indicate 50% smectite content.

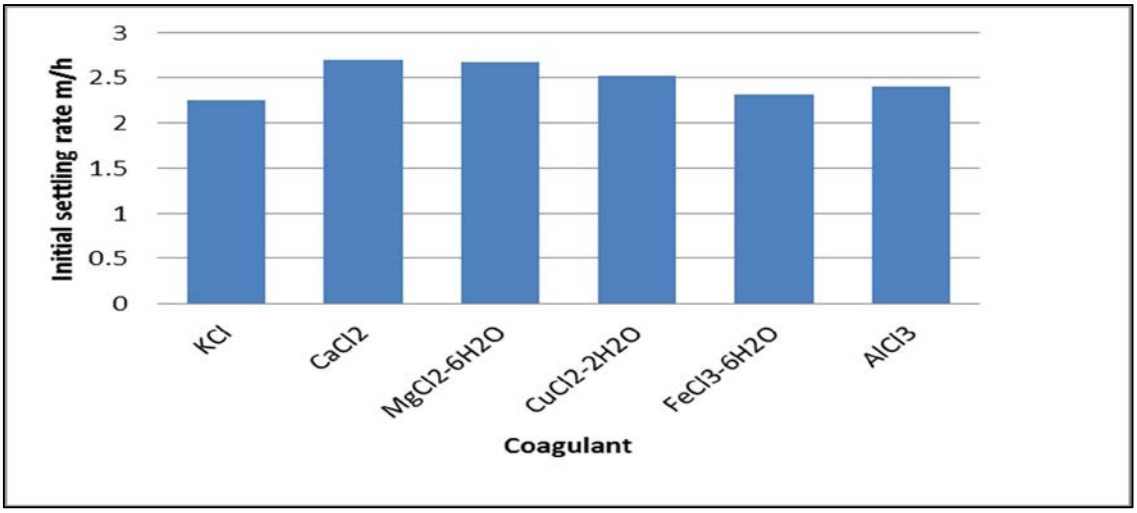

Figure 45: Critical coagulant concentration settling graph for AC 1-1-1.

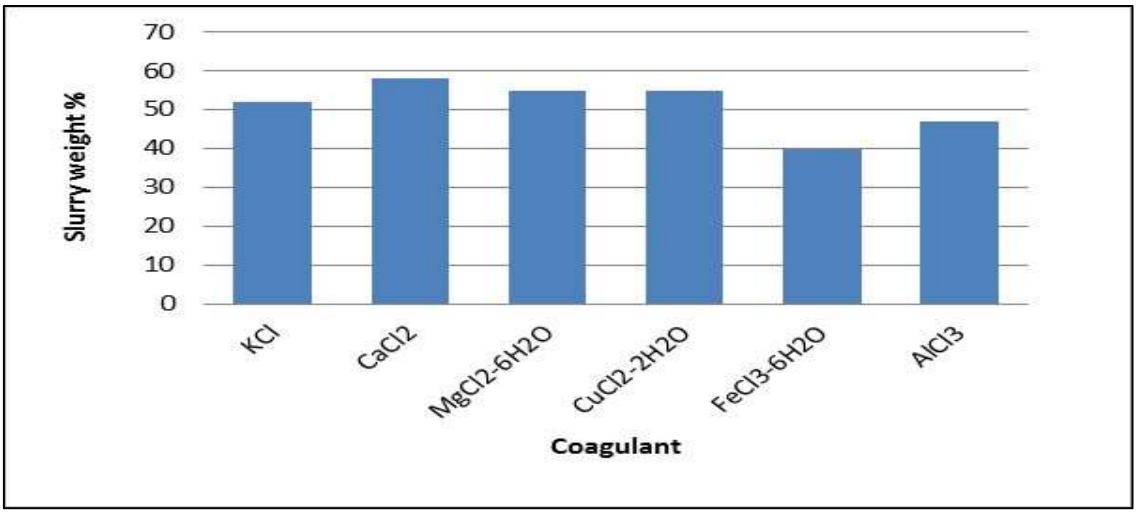

Figure 46: Critical coagulant concentration slurry weight percentage graph for AC 1-1-1.

AC 4-1A-1 has a smectite content of 75% and a cation exchange capacity of 45 cmol/kg. The best settling results for AC 4-1A-1, as shown in Figure 47 and Figure 48, were achieved with $FeCl_3$ where the initial settling rate is 1.35 m/h and the final slurry bed weight percentage was 35% after 24 hours. This was expected as the trivalent cations have a higher positive charge to neutralise the negative charges surrounding the particles. There is a 20% slurry bed weight reduction between AC 1-1-1 and AC 4-1A-1, and this could be contributed to the house-of-card packing relationship dominating the slurry bed.

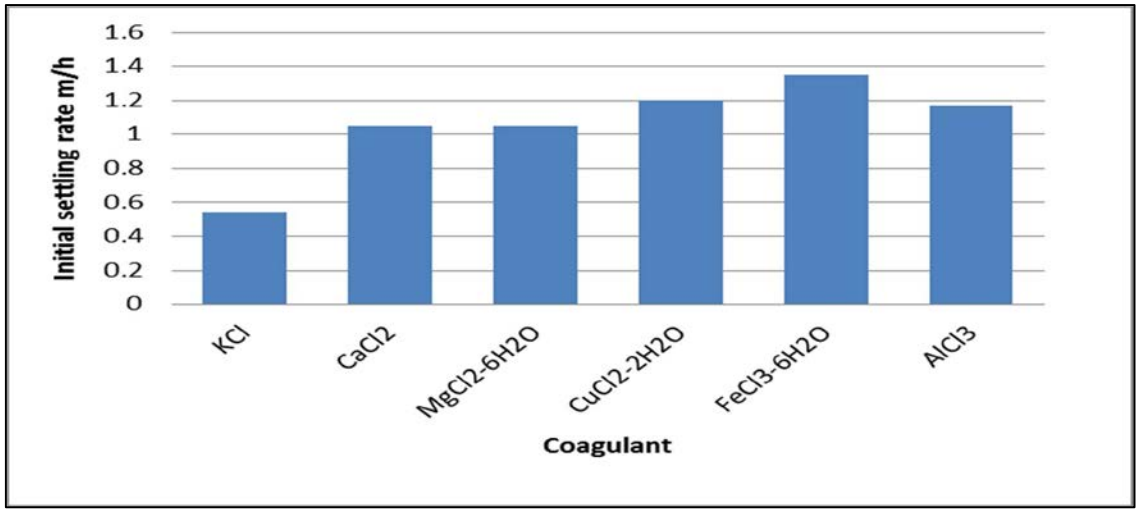

Figure 47: Critical coagulant concentration settling graphs for AC 4-1A-1.

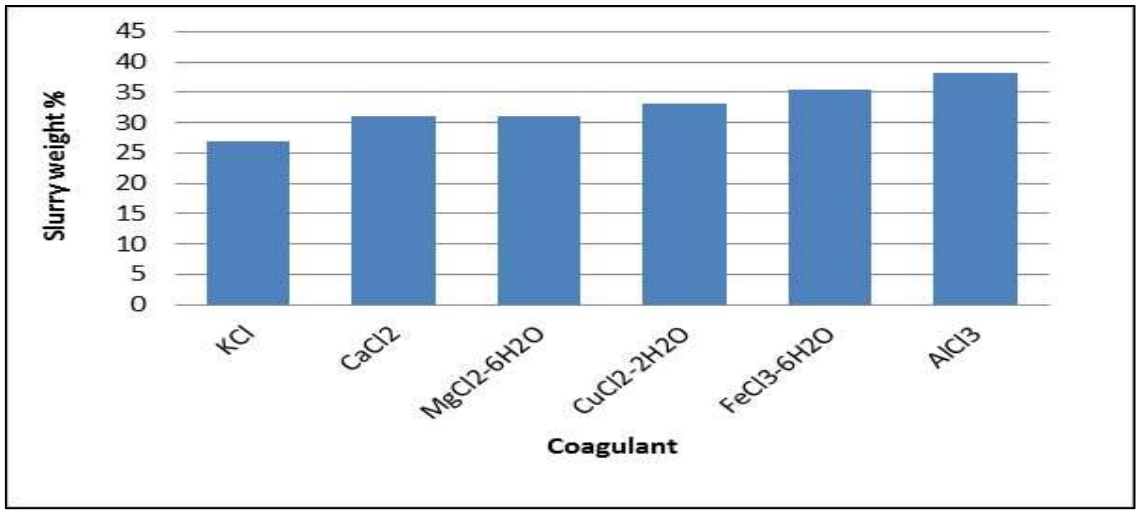

Figure 48: Critical coagulant concentration slurry weight percentage graph for AC 4-1A-1.

AC 5-5-1 reacted similarly to AC 1-1-1 with a high settling rate, with more than 2 m/h and a slurry bed compaction of at least 45% regardless whether there were mono-, di-, or trivalent cations used to do the settling tests. The best settling results for AC 5-5-1, as shown in Figure 49 and Figure 50, were achieved with $CaCl_2$ where the initial settling rate was 2.49 m/h and the final slurry bed weight percentage was 55% after 24 hours.

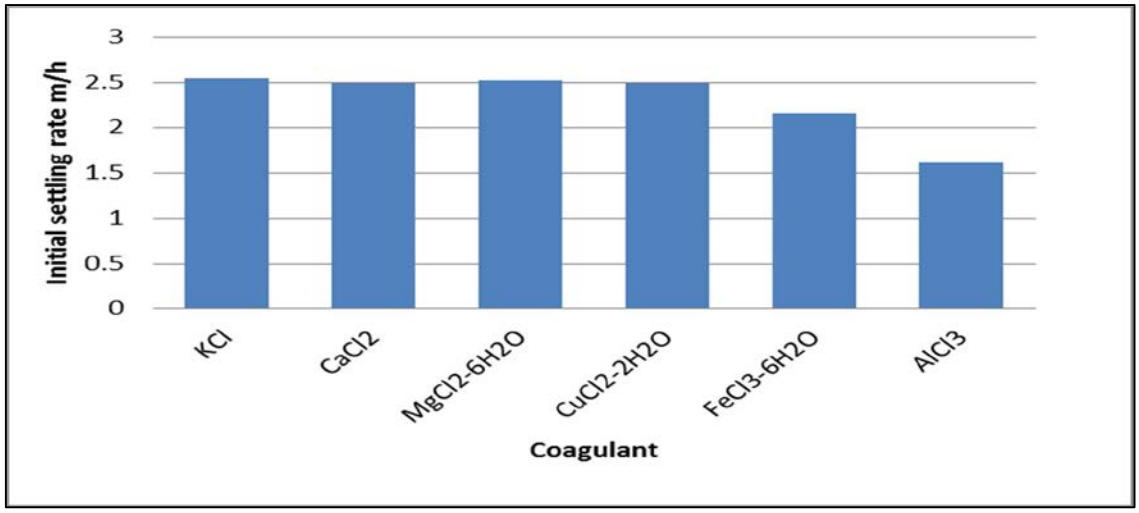

Figure 49: Critical coagulant concentration settling graphs for AC 5 -5-1.

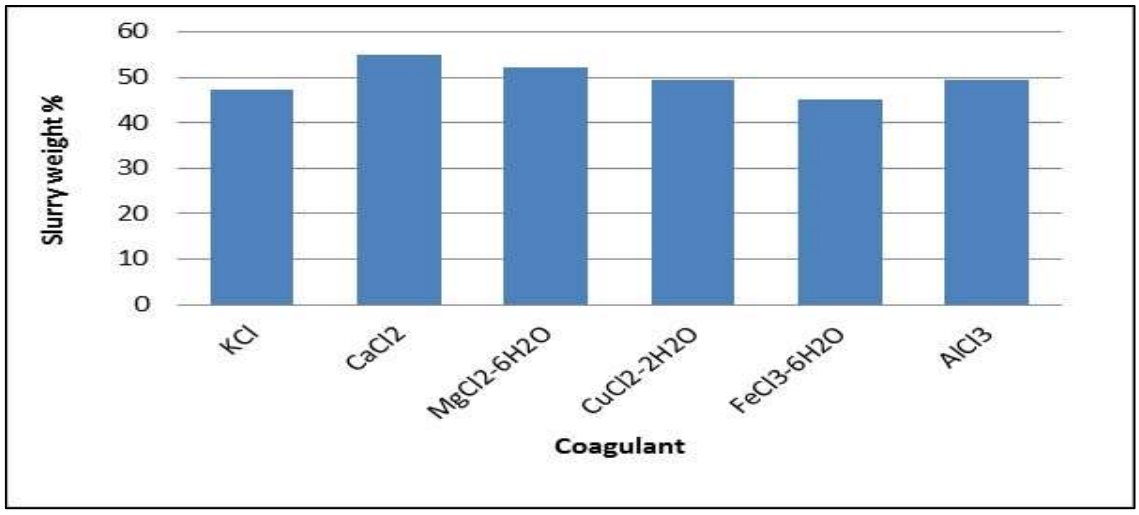

Figure 50: Critical coagulant concentration slurry weight percentage graph for AC 5-5-1.

The best settling results for AC 5-5-2, as shown in Figure 51 and Figure 52, were achieved with $CuCl_2$ where the initial settling rate was 1.56 m/h and the final slurry bed weight percentage was 37% after 24 hours. AC 5-5-2 had its highest settling rate with KCl at 1.62 m/h, but also presented the lowest slurry bed weight percentage of 33%, while the highest slurry bed weight percentage was achieved with $AlCl_3$. The fast settling rate with KCl can be explained in terms of that the potassium cations did not exchange with any cations in the crystal lattice but attached themselves to the crystal lattice. This would have reduced the negative repulsive forces surrounding the particles compared to the di- and trivalent cations

where cation exchange in the crystal structure would have taken place first resulting in swelling of the clay particles instead of reducing the negative forces.

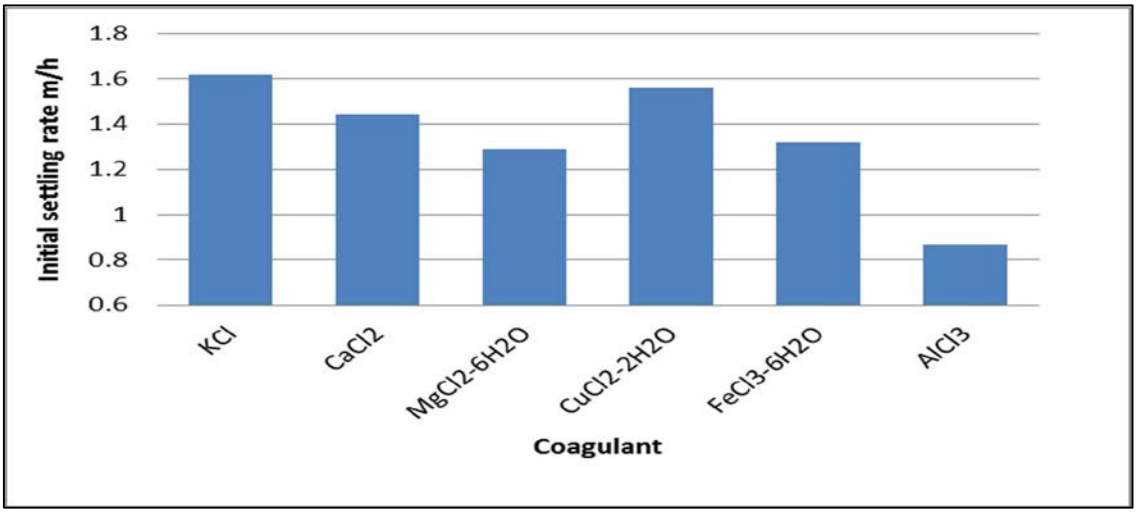

Figure 51: Critical coagulant concentration settling graphs for AC 5 -5-2.

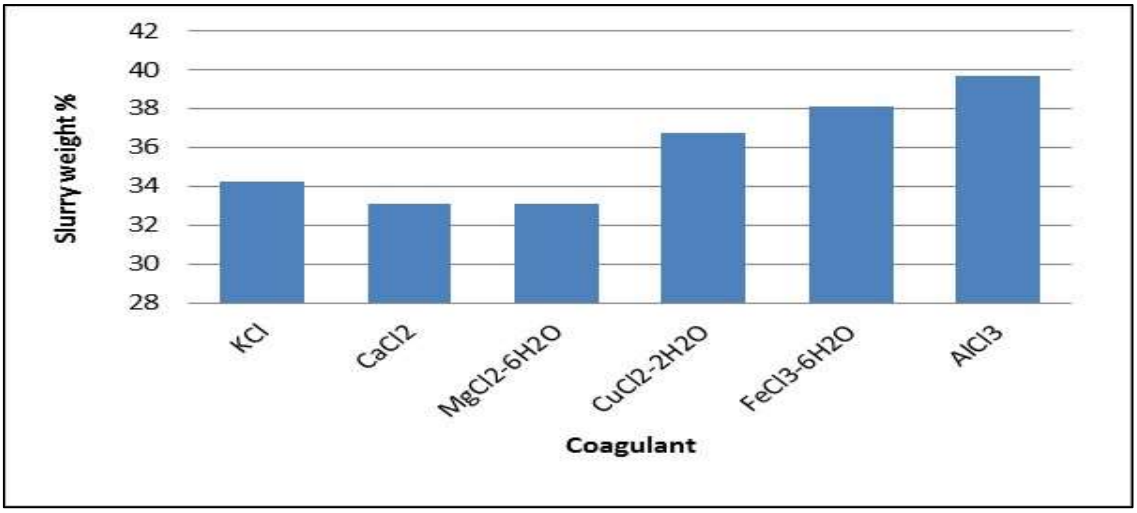

Figure 52: Critical coagulant concentration slurry weight percentage graph for AC 5-5-2.

AC 16-1-1 achieved an initial settling rate of 1.5 m/h with $CaCl_2$ and a final slurry bed weight percentage of 33% after 24 hours as shown in Figure 53 and Figure 54. The results for the di- and trivalent cations behaved very similarly with only a 1% or 2% change in the slurry bed weight percentage and only marginal improvements on the settling rates.

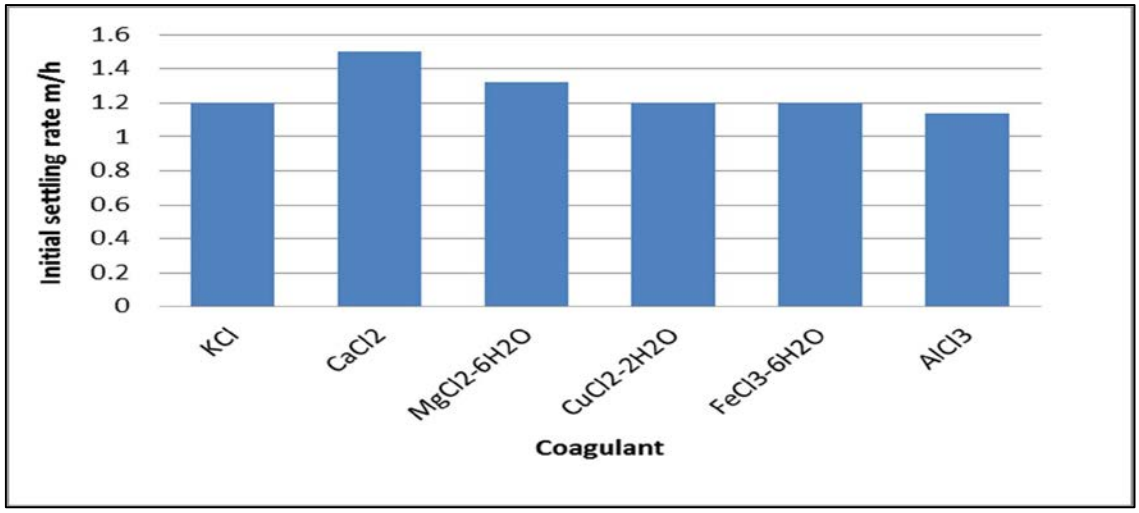

Figure 53: Critical coagulant concentration settling graphs for AC 16-1-1.

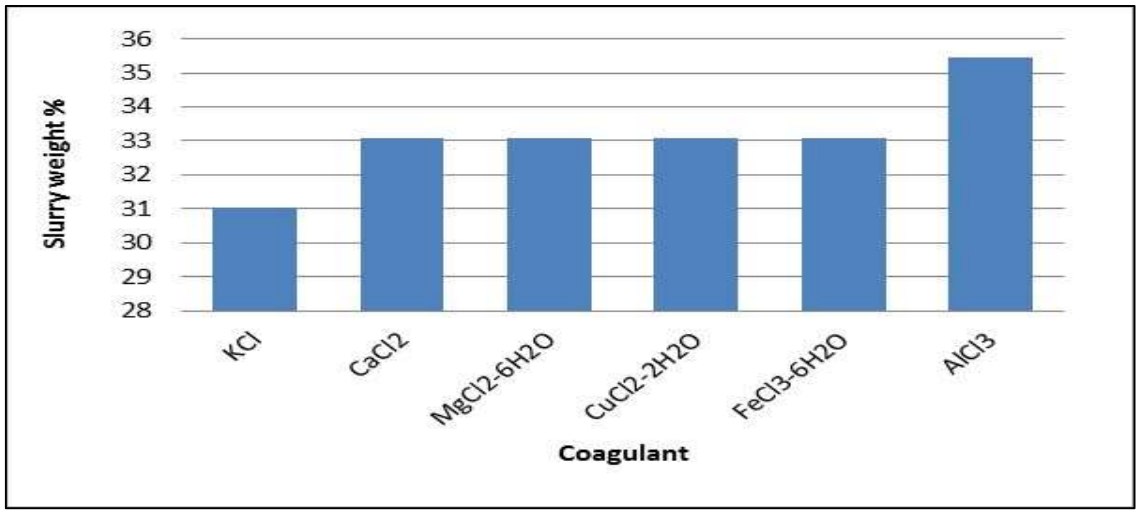

Figure 54: Critical coagulant concentration slurry weight percentage graph for AC 16-1-1.

The best settling results for AC 56-5-1, as shown in Figure 55 and Figure 56, were achieved with $AlCl_3$ where the initial settling rate was 1.86 m/h and the final slurry bed weight percentage was 35% after 24 hours. It is interesting to note the very high slurry bed depth and slow settling rates for KCl, $CaCl_2$ and $MgCl_2$-$6H_2O$ compared to the other kimberlite slurries and against the cupric, ferric and aluminium settling rates and slurry bed depth. The smectite content of AC-56-5-1 is at 65% and is not exceedingly higher than some of the other kimberlites, but it contains an 8 – 10% talc content which could explain this occurrence as talc is non-ionic and has a very low cation exchange capacity. Talc is a stable 2:1 clay,

and exchanges cations only on the edges, and not inside the layers unless the hydration energy is high enough as is the case with the cupric, ferric and aluminium ions.

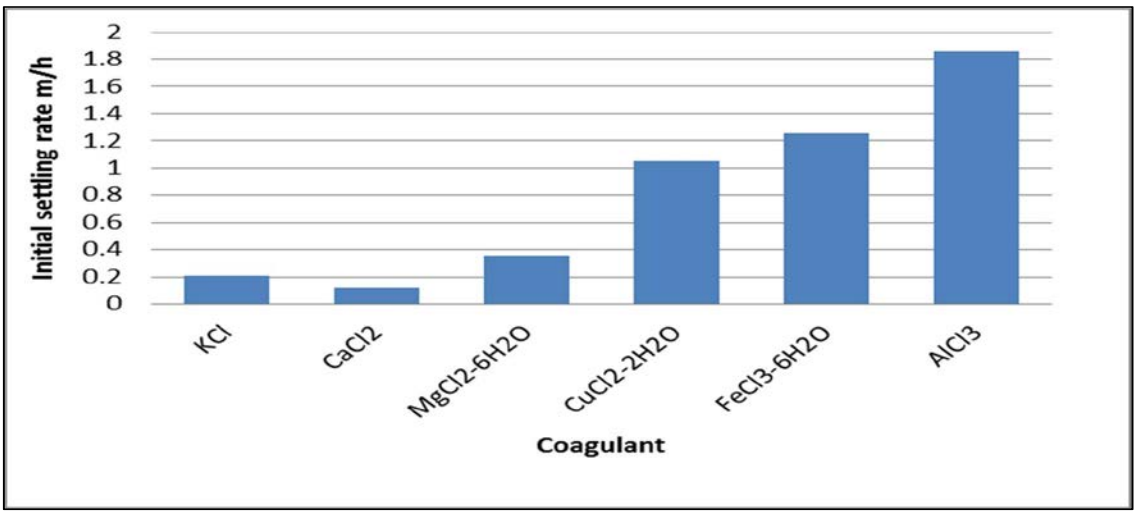

Figure 55: Critical coagulant concentration settling graphs for AC 56-5-1.

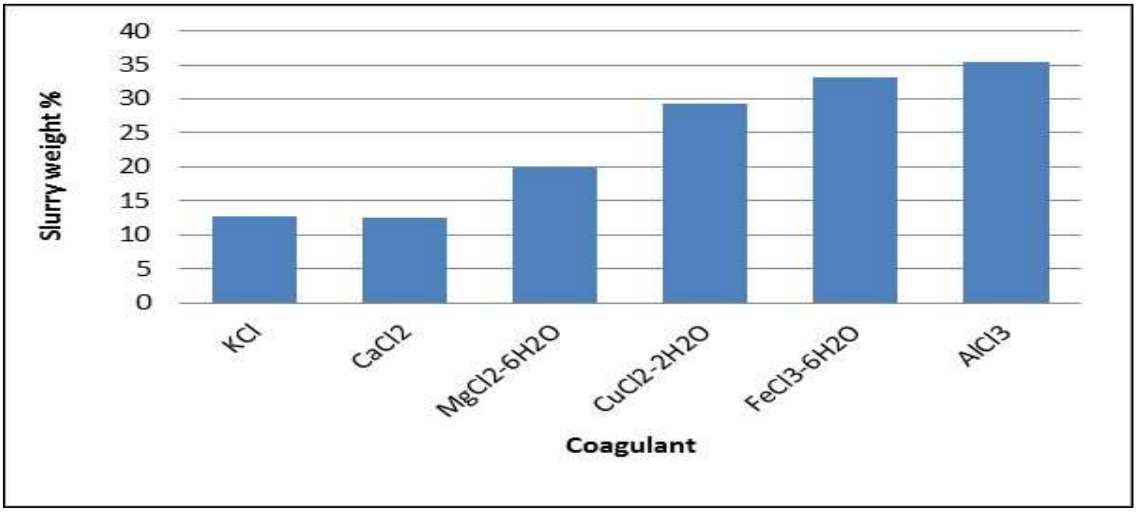

Figure 56: Critical coagulant concentration slurry weight percentage graph for AC 56-5-1.

The best settling results for AC 197-1-1, as shown in Figure 57 and Figure 58, were achieved with $CaCl_2$ where the initial settling rate was 1.83 m/h and the final slurry bed weight percentage was 38% after 24 hours. AC 197-1-1 has a smectite content of 40% along with a lower cation exchange capacity of 19 cmol/kg and a high sodium exchange percentage of 17%. The higher exchangeable sodium percentage may explain why the potassium settling test had such poor results

compared to the di-and trivalent cations, as sodium is more easily exchanged by di- and trivalent cations. The house-of-card packing relationship is also more dominant with the monovalent cation exchange of potassium as the negative repulsive forces dominate around the particles compared to the divalent and trivalent cations.

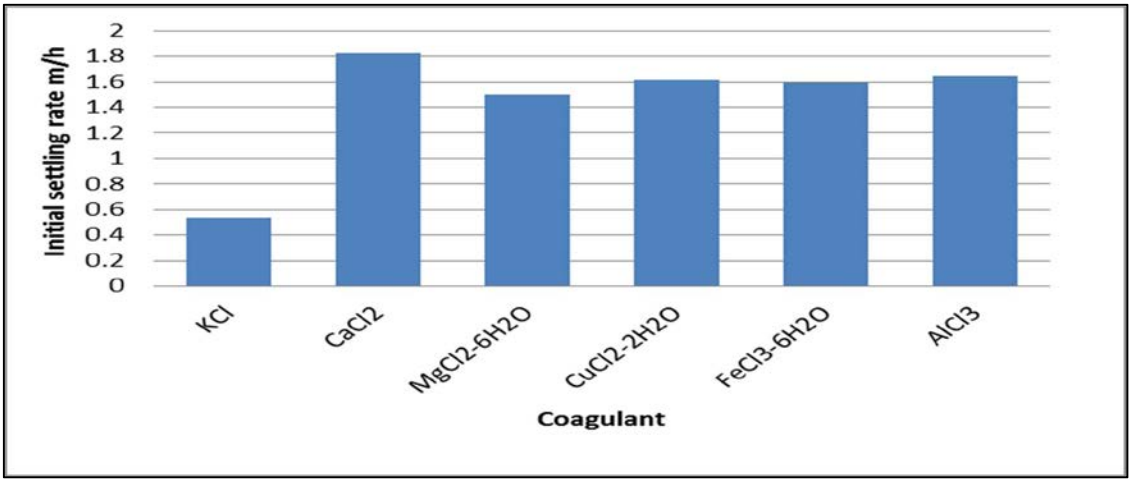

Figure 57: Critical coagulant concentration settling graphs for AC 197-1-1.

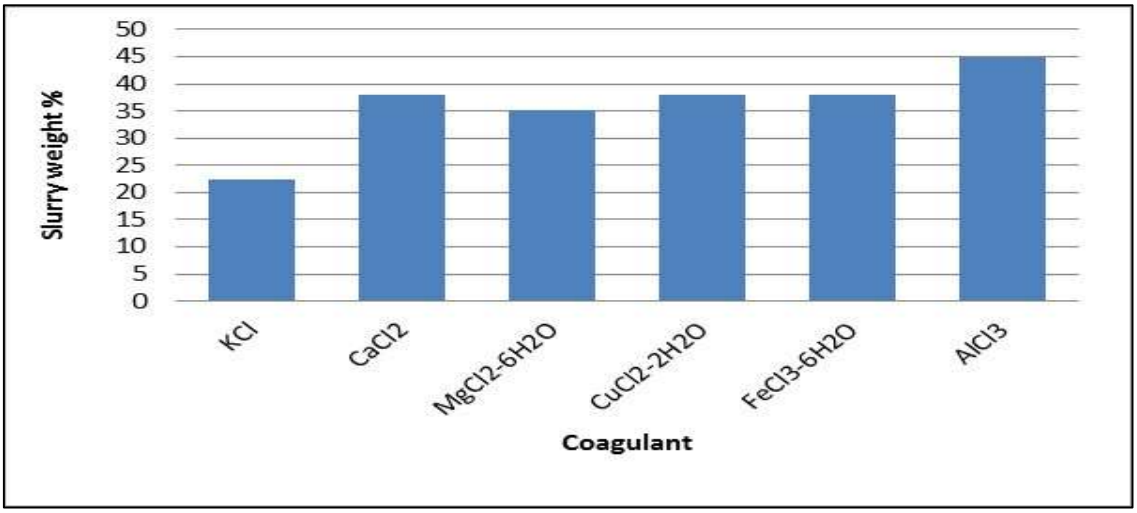

Figure 58: Critical coagulant concentration slurry weight percentage graph for AC 197-1-1.

The best settling results for Venetia Red (VR) as shown in Figure 59 and Figure 60 were achieved with $AlCl_3$, where the initial settling rate was 2.22 m/h and the final slurry bed weight percentage was 52% after 24 hours. Venetia Red has a smectite content of 40% with a cation exchange capacity of 32 cmol/kg and the highest exchangeable sodium percentage of 43% of the 18 kimberlite samples

tested. The lower the smectite content, the higher the expected slurry weight percentage. This can be seen with Venetia Red where the slurry weight percentage for all the cations was above 45%. The higher settling rate of more than 2 m/h can be attributed to lower smectite content along with a reduced cation exchange capacity. This can also be seen with AC 1-1-1, AC 5-5-1 and AC 197-1-1 which all have low cation exchange capacities.

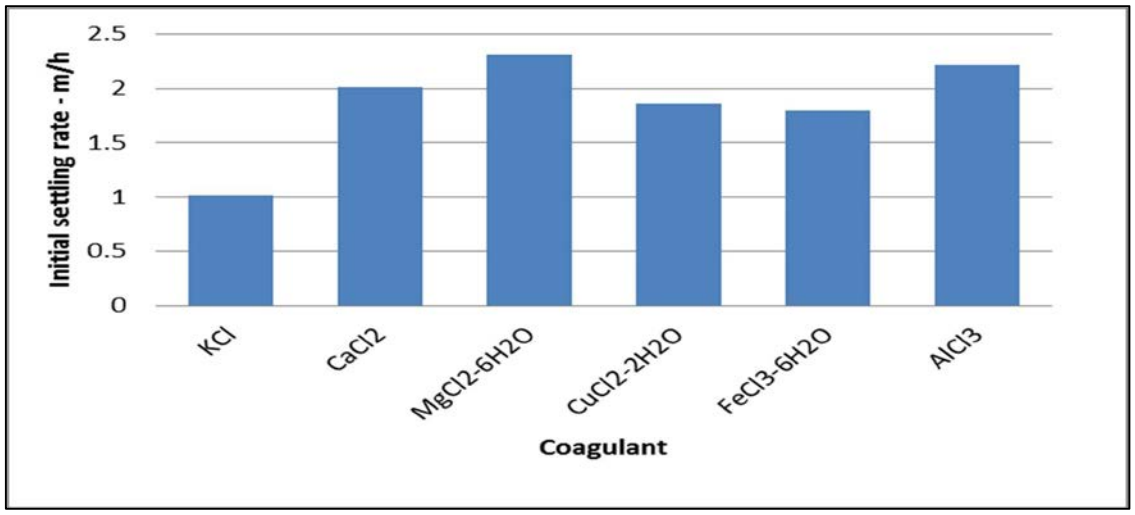

Figure 59: Critical coagulant concentration settling graphs for Venetia Red.

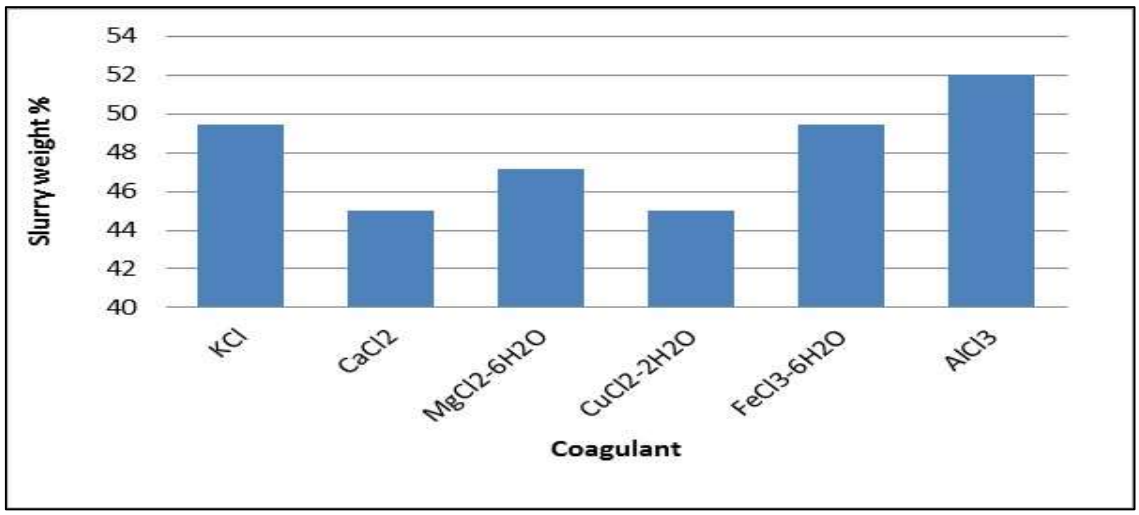

Figure 60: Critical coagulant concentration slurry weight percentage graph for Venetia Red.

AO 319 and AO 320 were kimberlite samples extracted from 116 m and 30 m within the same borehole of the same kimberlite. The mineral composition of the

two samples are similar except for 5% more diopside in AO 319. Looking at the critical coagulant concentration settling graphs of AO 319 in Figure 61 and Figure 62 and for AO 320 in Figure 63 and Figure 64 the best settling results for AO319 were achieved with $AlCl_3$ where the initial settling rate was 0.55 m/h and the final slurry bed weight percentage was 28% after 24 hours. For AO 320 the best settling results were achieved with $MgCl_2$ where the initial settling rate was 0.78 m/h and the final slurry bed weight percentage was 28% after 24 hours. AO 320 settled at a rate that was almost 50% more than that of AO 319 for the same di- and trivalent cations, while potassium cations showed the same results. The higher exchangeable sodium percentage of 21% for AO319 compared to the 3% exchangeable sodium percentage for AO 320 may possibly explain this, as more divalent and trivalent cations were first exchanged in the crystal lattice, leaving sodium cations in solution. This will reduce the effect of the di- and trivalent cations in solution on the negative repulsive forces surrounding the particles, resulting in a slower settling rate.

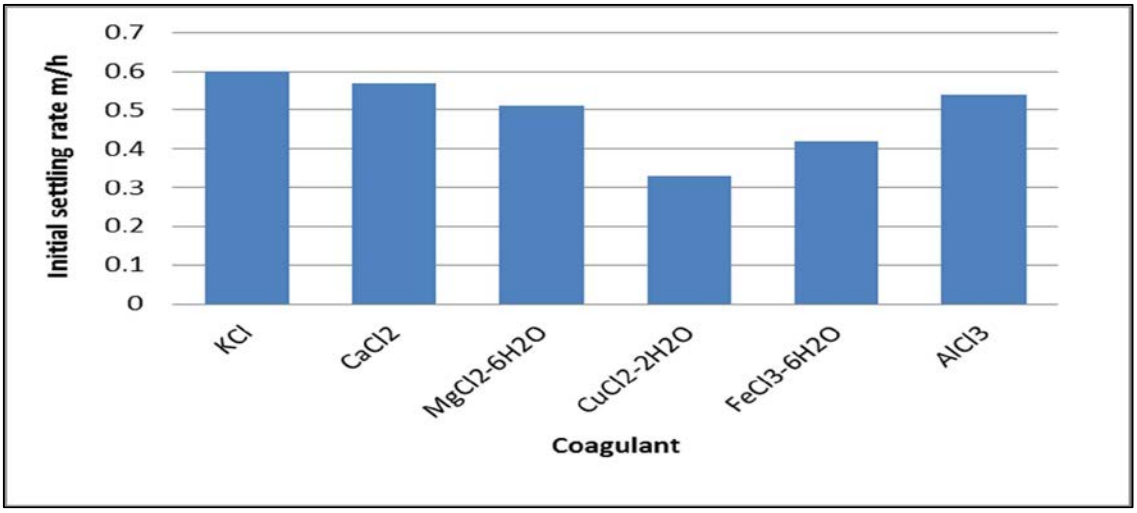

Figure 61: Critical coagulant concentration settling graphs for AO 319.

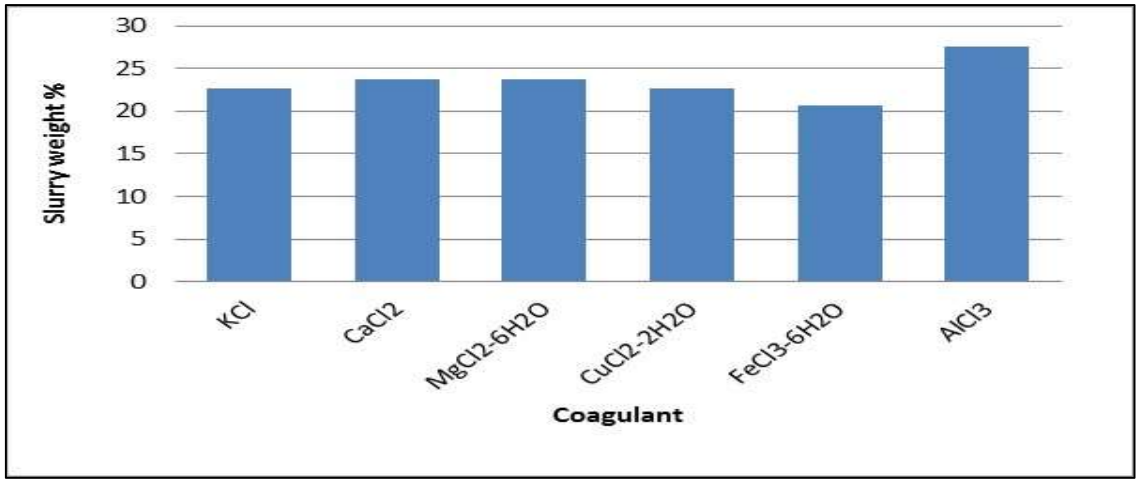

Figure 62: Critical coagulant concentration slurry weight percentage graph for A0 319.

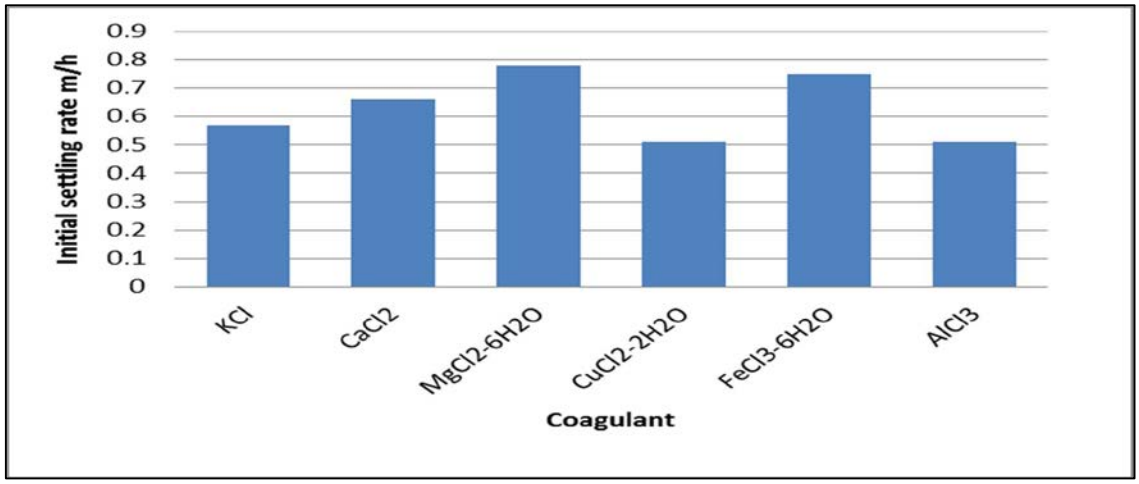

Figure 63: Critical coagulant concentration settling graphs for AO 320.

AO 321, AO 322 and AO 323 were samples extracted from Tchegi kimberlite 32 at depths of 137 m, 92 m and 30 m respectively. The critical coagulant settling rates for these 3 samples are shown in Figure 65 and Figure 66, Figure 67 and Figure 68 and Figure 69 and Figure 70. The best settling results for AO 321 were achieved with $CuCl_2$ where the initial settling rate was 1.5 m/h and the final slurry bed weight percentage was 41% after 24 hours, and for AO 322 the best settling results were also achieved with $CuCl_2$ where the initial settling rate was 1.2 m/h and the final slurry bed weight percentage was 41% after 24 hours. AO 323 achieved its best settling results with $FeCl_3$ where the initial settling rate was 2.01 m/h and the final slurry bed weight percentage was 49% after 24 hours. Comparing the slurry bed weight percentage of all the cations tested of the 3 samples, it can

be seen that AO 322 has the lowest slurry weight percentage while AO 323 contains the highest slurry weight percentage. This can be attributed to the amount of smectite present in each sample where AO 323 contains only 15% smectite, AO 321 contains 35% smectite and AO 322 contains 60% smectite. AO 323 also contains 50% quartz in its mineral structure and this resulted in the achievement of a higher settling rate of 2 m/h.

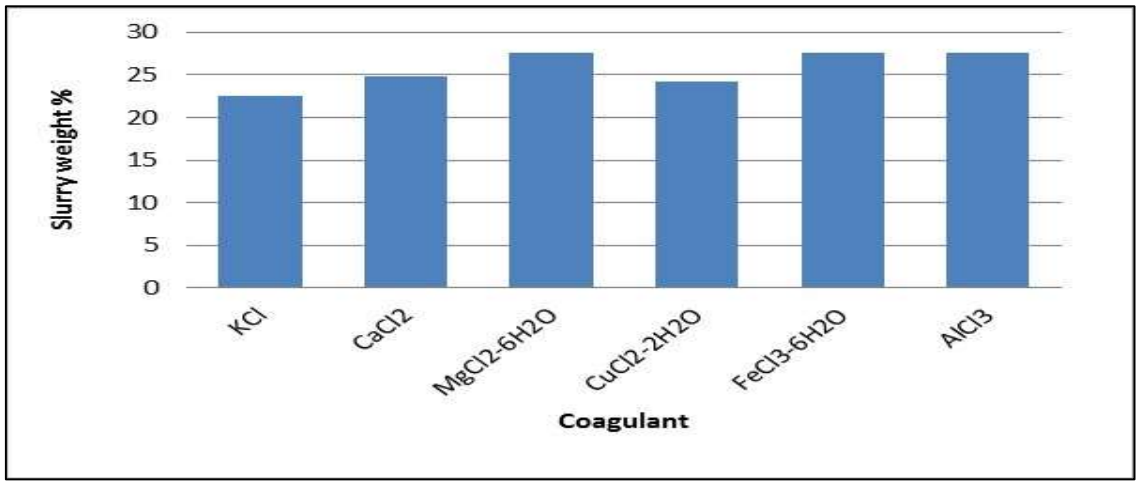

Figure 64: Critical coagulant concentration slurry weight percentage graph for AO 320.

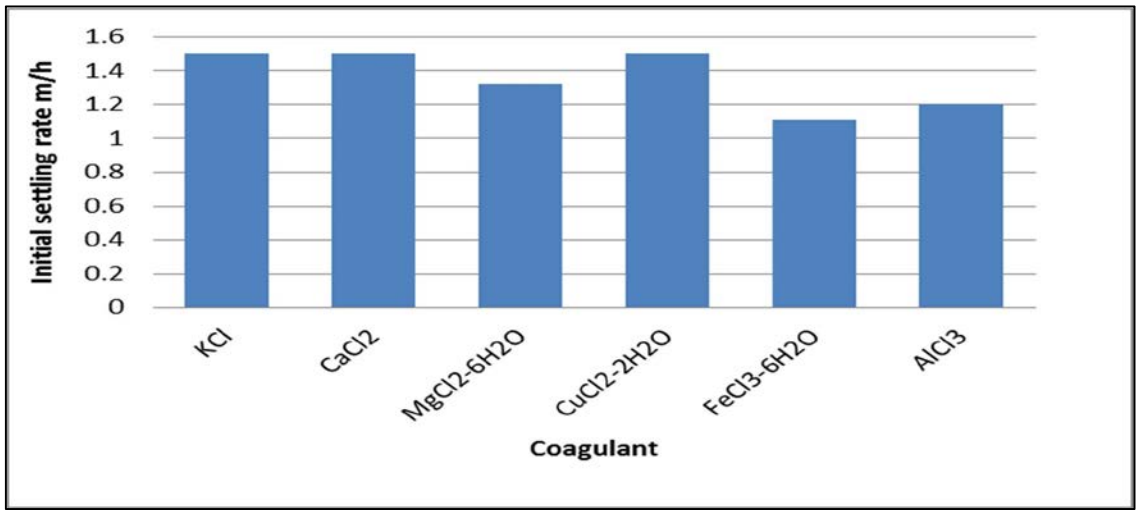

Figure 65: Critical coagulant concentration settling graphs for AO 321.

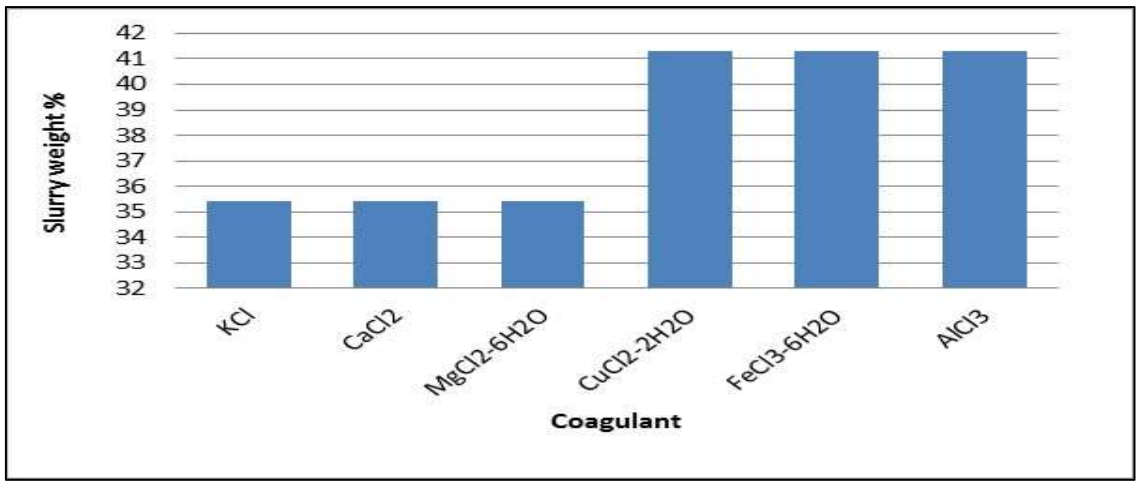

Figure 66: Critical coagulant concentration slurry weight percentage graph for AO 321.

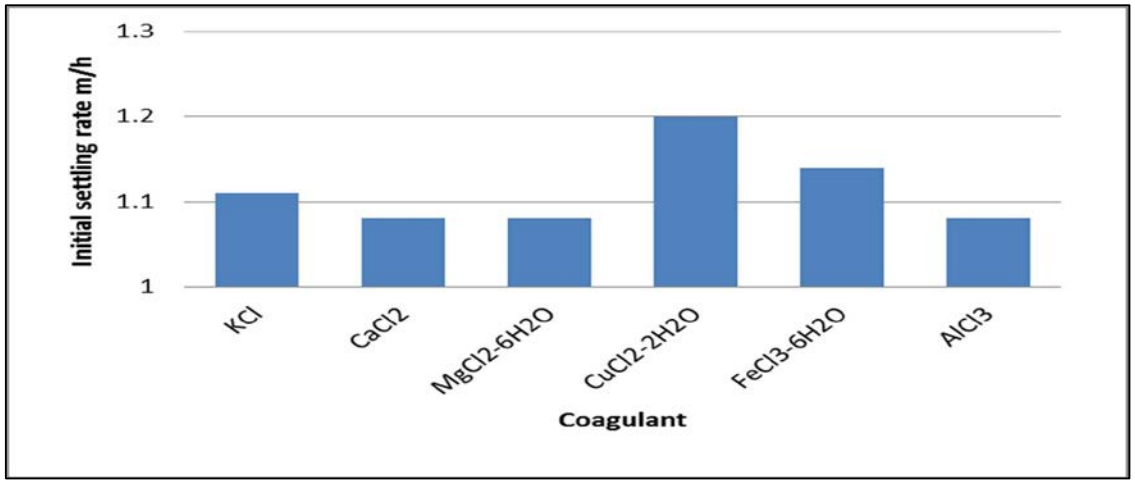

Figure 67: Critical coagulant concentration settling graphs for AO 322.

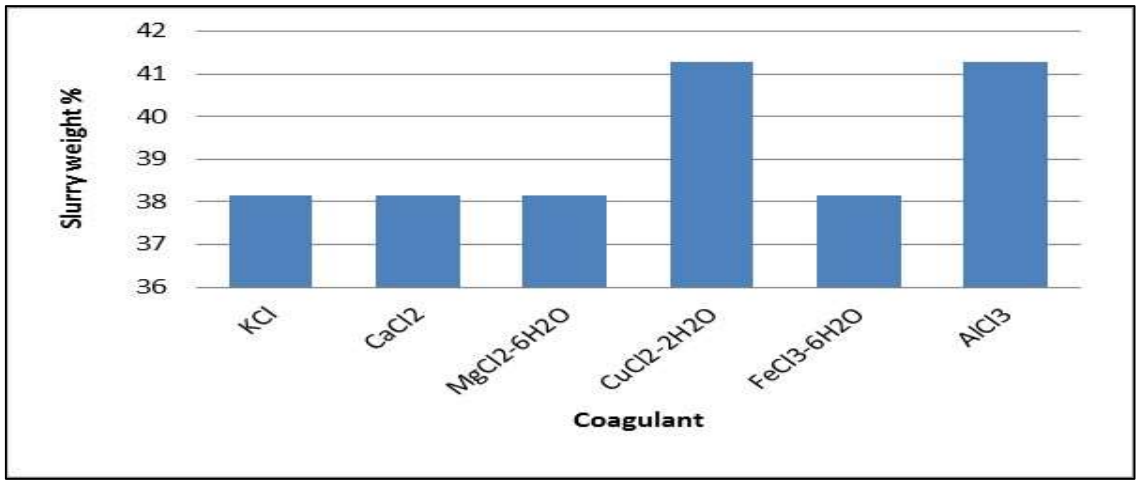

Figure 68: Critical coagulant concentration slurry weight percentage graph for AO 322.

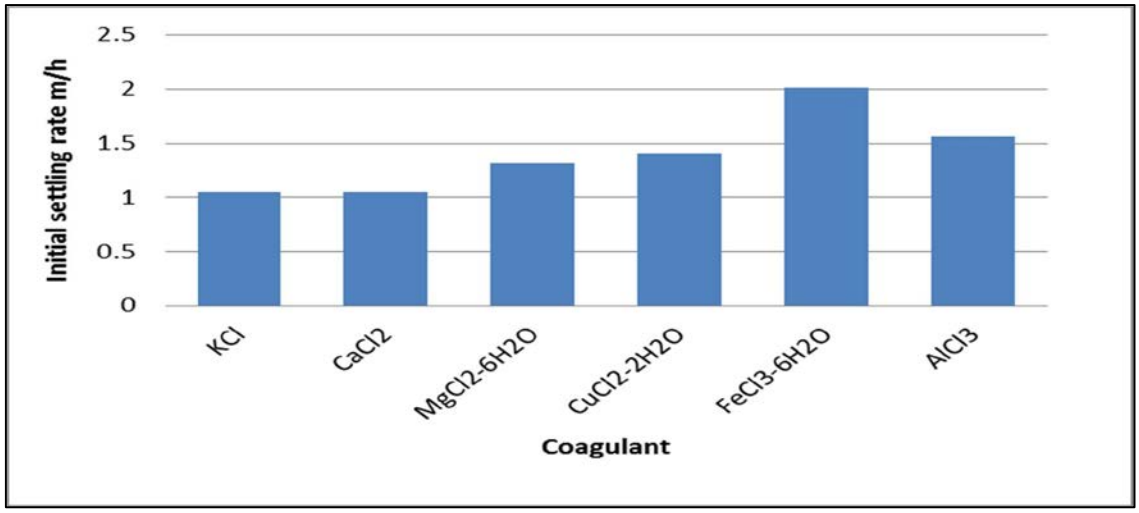

Figure 69: Critical coagulant concentration settling graphs for AO 323.

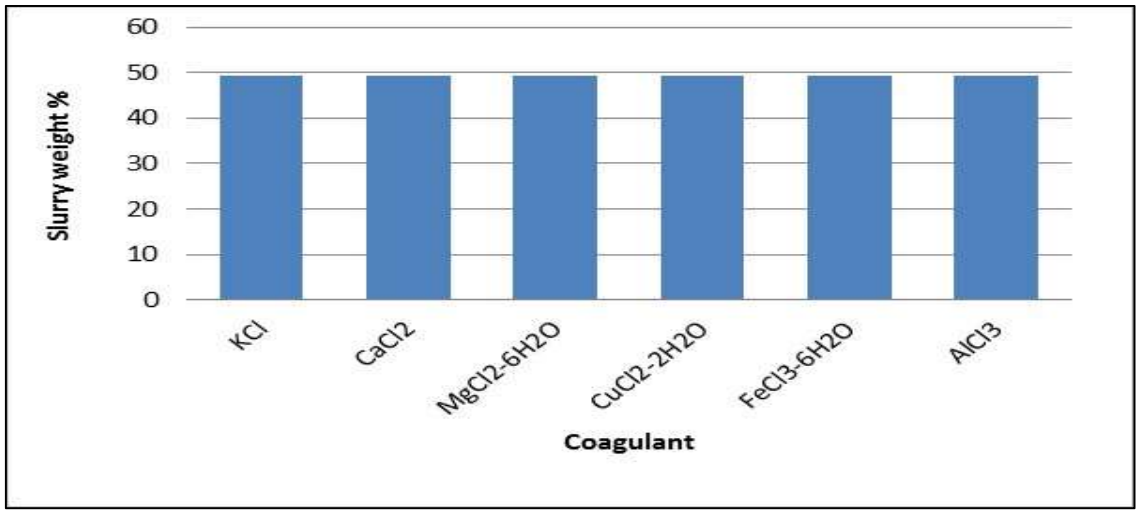

Figure 70: Critical coagulant concentration slurry weight percentage graph for AO 323.

The best settling results for AO 324, as shown in Figure 71 and Figure 72, were achieved with $CaCl_2$ and $MgCl_2$, where the initial settling rate was 2.1 m/h and the final slurry bed weight percentage was 41% after 24 hours. For AO 325 the best settling results were achieved with $CaCl_2$ and $MgCl_2$, where the initial settling rate was 1.5 m/h and the final slurry bed weight percentage was 45% after 24 hours as shown in Figure 73 and Figure 74. The AO 324 sample has 55% smectite content and was extracted at a depth of 340 metres while AO 325 has smectite content of 30% and was extracted from 104 metres of the same kimberlite. AO 324 had high settling rates of more than 1.8 m/h to 2 m/h when the divalent cations were used

as coagulants, and this could be due the high percentage exchangeable sodium in the crystal lattice as the sodium is more easily replaced with a divalent cation than a trivalent cation. This will reduce the negative charge at the crystal lattice edges allowing more interaction of the particles resulting in a better settling rate.

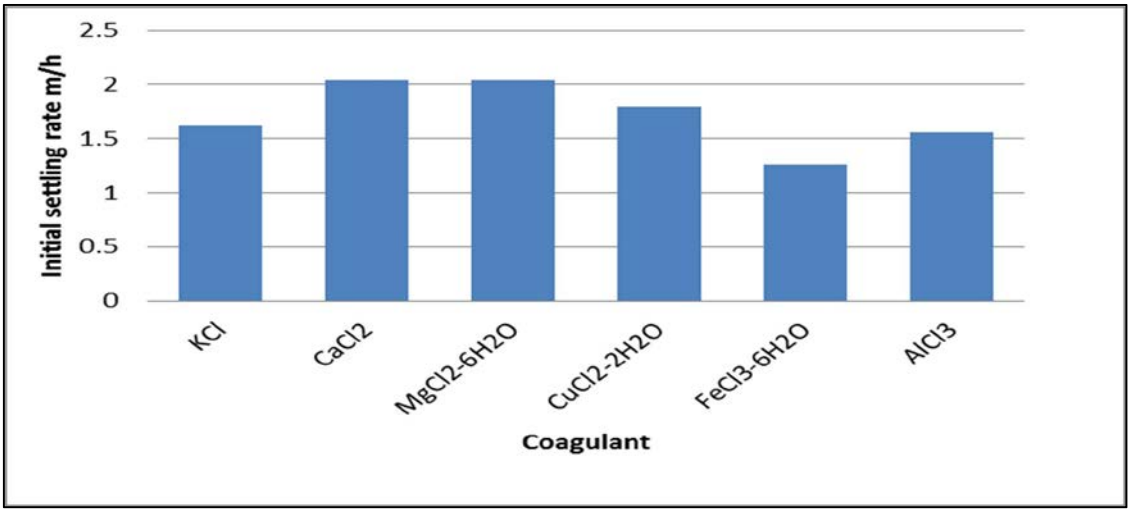

Figure 71: Critical coagulant concentration settling graphs for AO 324.

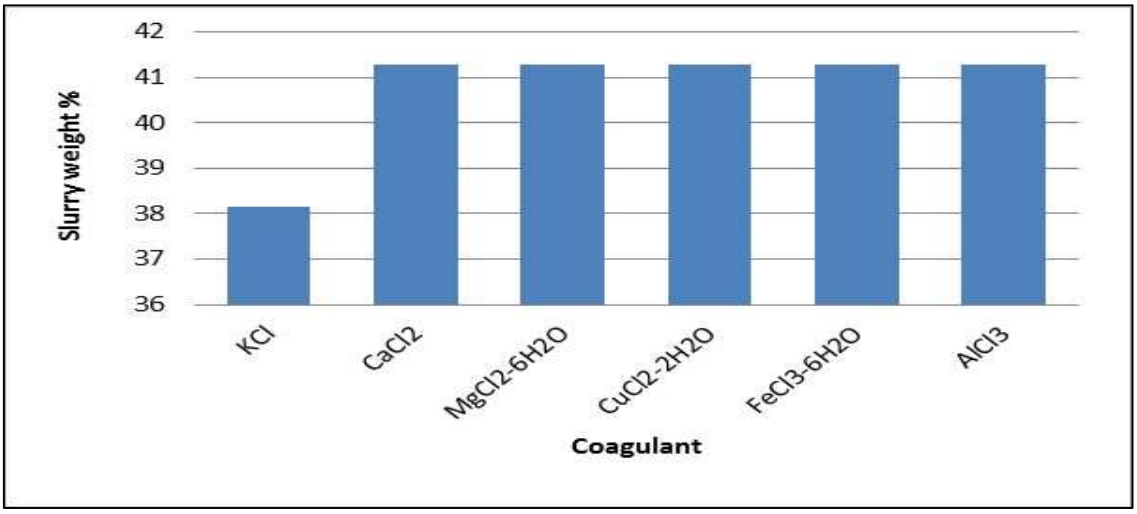

Figure 72: Critical coagulant concentration slurry weight percentage graph for AO 324.

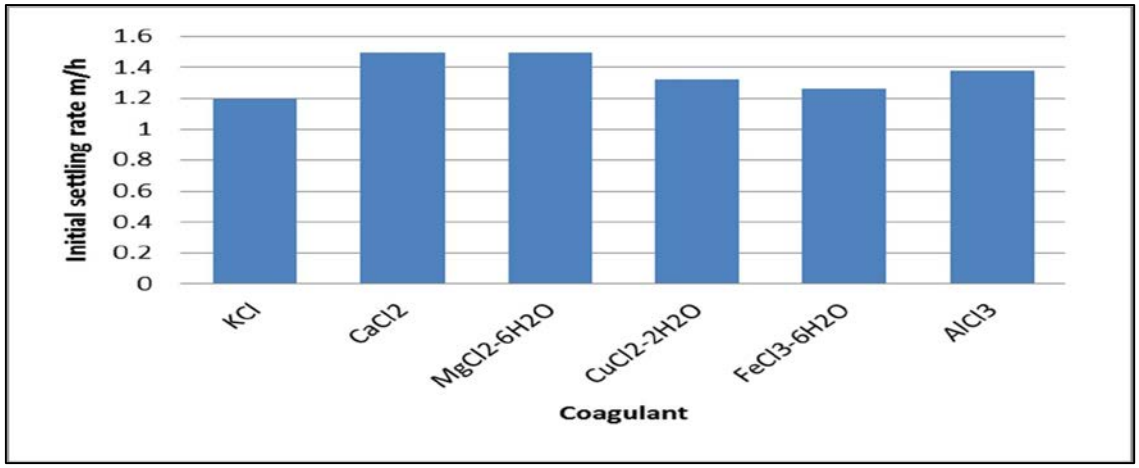

Figure 73: Critical coagulant concentration settling graphs for AO 325.

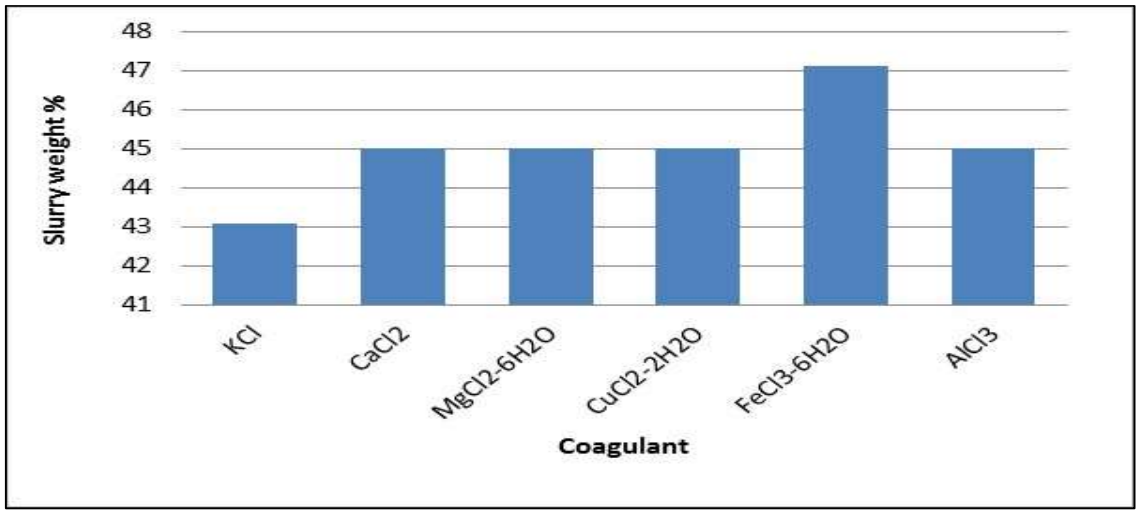

Figure 74: Critical coagulant concentration slurry weight percentage graph for AO 325.

The best settling results for AO326, as shown in Figure 75 and Figure 76, were achieved with $AlCl_3$ where the initial settling rate was 2.07 m/h and the final slurry bed weight percentage was 41% after 24 hours.

The AO 327 sample was extracted from a depth of 100 metres and AO 328 from a depth of 163 metres in the same borehole. AO 327 contains 25% smectite while AO 328 contains 60% smectite. The best settling results for AO327, as shown in Figure 77 and Figure 78, were achieved with $FeCl_3$ where the initial settling rate was 1.2 m/h and the final slurry bed weight percentage was 41% after 24 hours, while the best settling results for AO328, as shown in Figure 79 and Figure 80 were

achieved with $CaCl_2$ where the initial settling rate was 0.6 m/h and the final slurry bed weight percentage was 25% after 24 hours. It is clear that the higher the smectite content of a kimberlite the lower the slurry weight percentage of the slurry bed due to the house-of-card packing relationship associated with smectite.

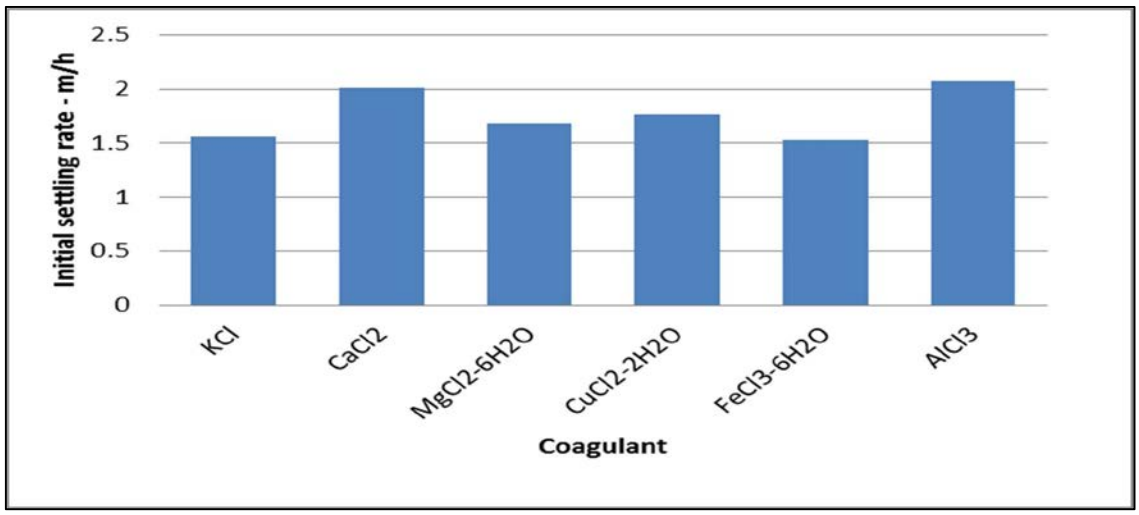

Figure 75: Critical coagulant concentration settling graphs for AO 326.

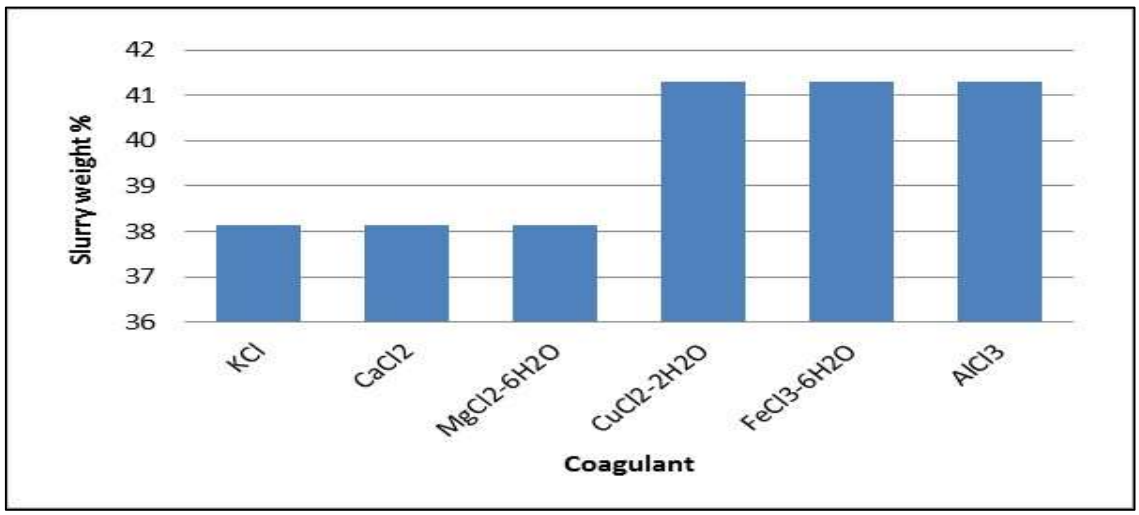

Figure 76: Critical coagulant concentration slurry weight percentage graph for AO 326.

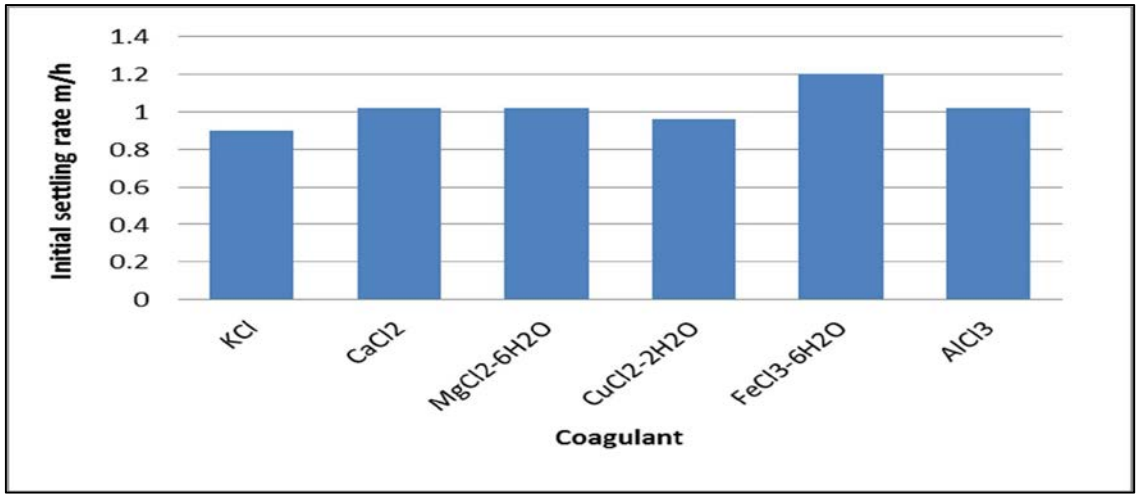

Figure 77: Critical coagulant concentration settling graphs for AO 327.

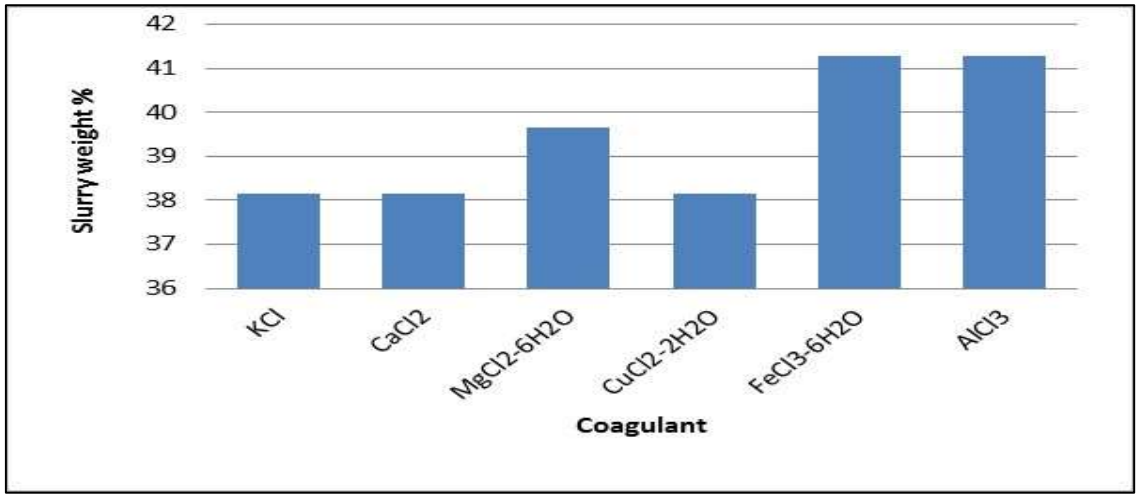

Figure 78: Critical coagulant concentration slurry weight percentage graph for AO 327.

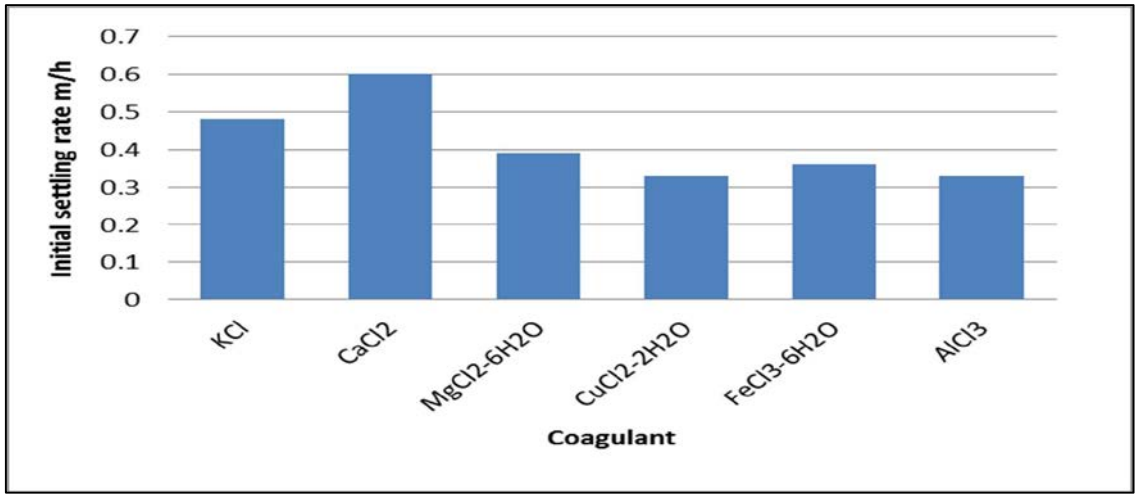

Figure 79: Critical coagulant concentration settling graphs for AO 328.

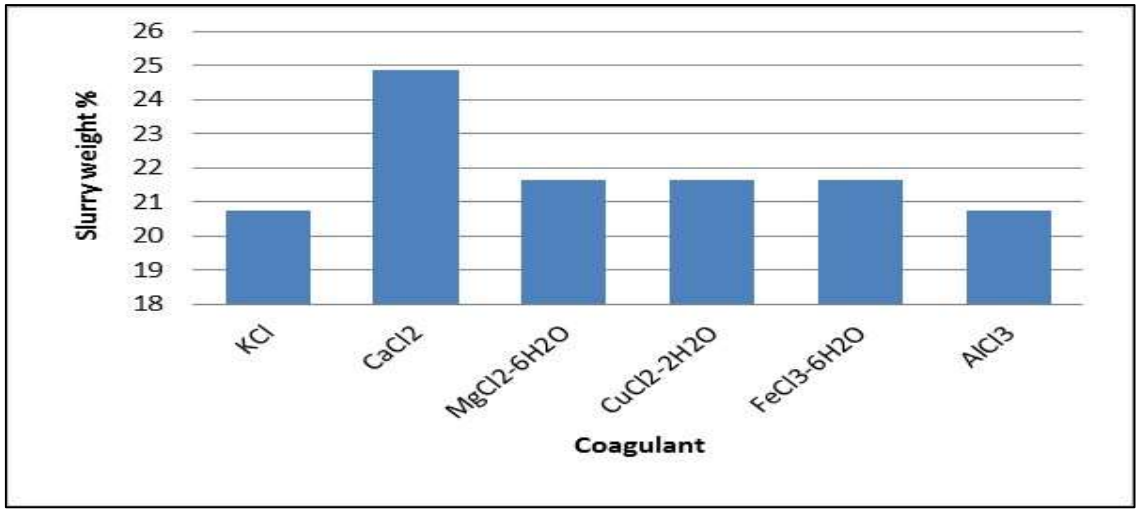

Figure 80: Critical coagulant concentration slurry weight percentage graph for AO 328.

Figure 81and Figure 82 show the fastest cationic settling rate and accompanied slurry bed weight percentage for the different kimberlites. The settling rate and slurry bed weight percentage for every kimberlite sample increased when di- and tri-valent cations, as opposed to monovalent cations, were used as coagulants. Settling rates of between 0.5 m/h and 2.5 m/h were achieved for coagulant settling, which is less than the industry norm of 10m/h (Nguyen and Boger, 1998; de Kretser, 1995; O Gorman and Kitchener, 1974). Slurry bed weight percentages ranged between 28% and 52% with an average slurry bed weight percentage of 40%, which is almost twice as much as the industry norm of 20% to 22% (Nguyen and Boger, 1998; de Kretser, 1995; O Gorman and Kitchener, 1974). The slowest settling rate, 0.5 m/h, and least compaction in the slurry bed, less than 30%, were found with kimberlites AO 319, AO 320 and AO 328. These kimberlites consist of 60% smectite and between 10% and 15% diopside. Comparing the settling rates and slurry bed weight percentages of the three kimberlites with AO 322, which has 60% smectite in its mineral structure but with only 3% diopside, the settling rate is almost double at 1.2 m/h and with a slurry bed weight percentage of 41%. None of the other kimberlites have any diopside in their mineral structures and it appears as if the diopside can have a detrimental effect on the settling rates of these kimberlites with cations as coagulants.

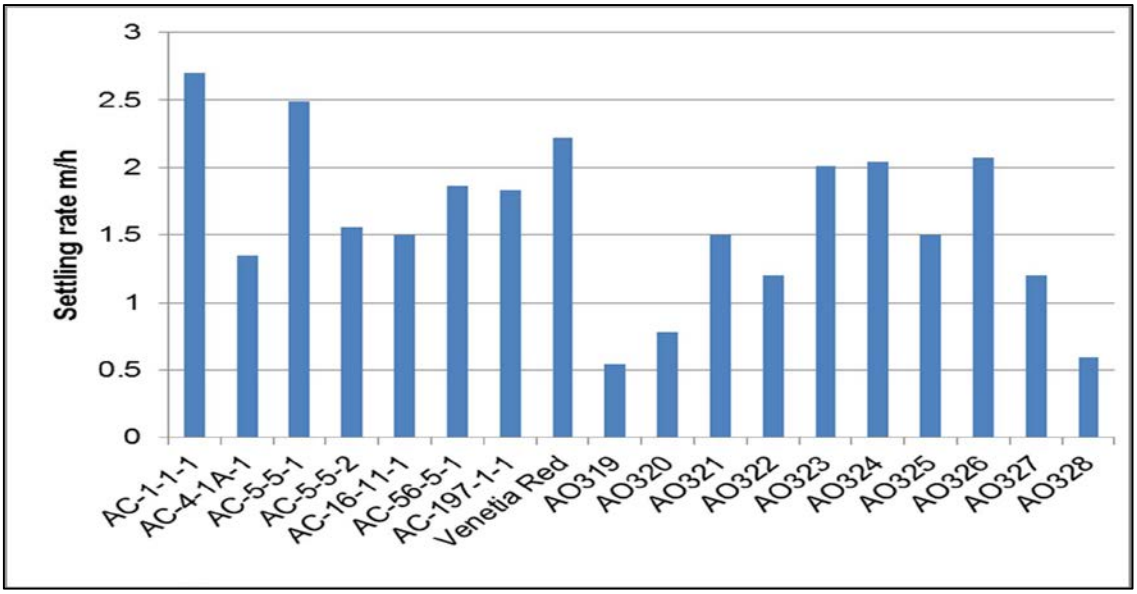

Figure 81: The fastest cationic settling rate for the different kimberlites.

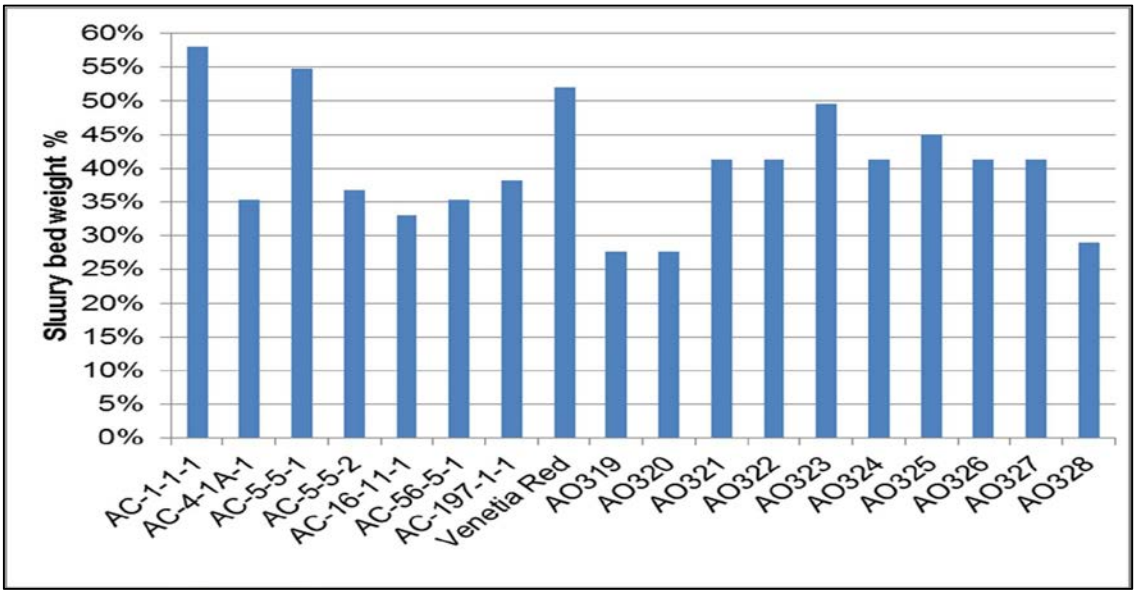

Figure 82: The lowest cationic slurry bed weight % for the different kimberlites.

Figure 83 and Figure 84 show the relationships between the critical potassium concentration settling rates of the different kimberlites plotted against the cation exchange capacity (CEC) and the sodium exchange percentage (ESP) of the kimberlites. The data indicates that a high settling rate is only possible if the kimberlite has a low CEC or ESP.

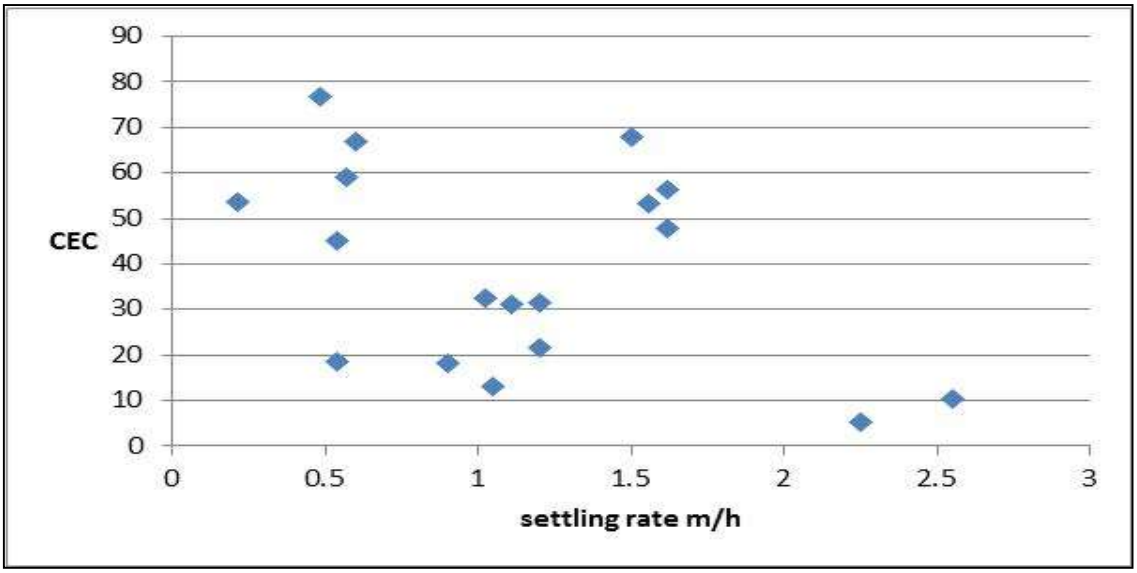

Figure 83: Cation exchange capacity (CEC) versus the initial settling rate of the critical potassium concentrations of the various kimberlites.

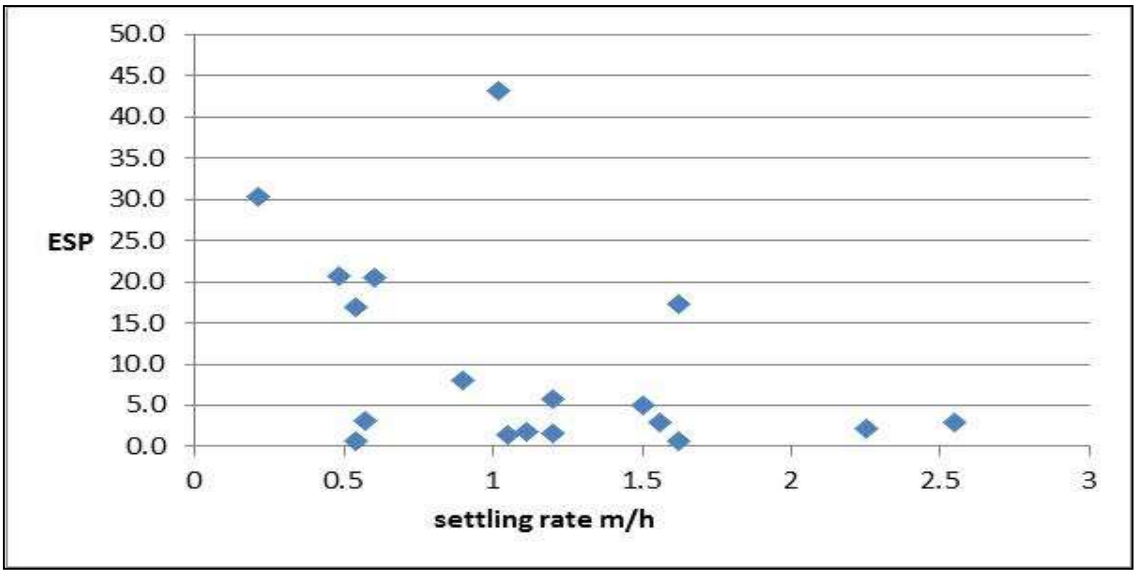

Figure 84: Sodium exchange capacity (ESP) versus the initial settling rate of the critical potassium concentrations of the various kimberlites.

The relationship between the CEC and ESP of the different kimberlites and the settling rate of the critical calcium concentration is seen in Figure 85 and Figure 86. A similar trend, compared with the potassium settling rates, is noted where a high settling rate is only possible when the kimberlite has a low ESP. No definite trend can be noted with critical calcium concentration settling rates of the kimberlites against the CEC of the different kimberlites. The outlier in Figure 86 is

Venetia Red where a higher settling rate was achieved even though the kimberlite has a high ESP value.

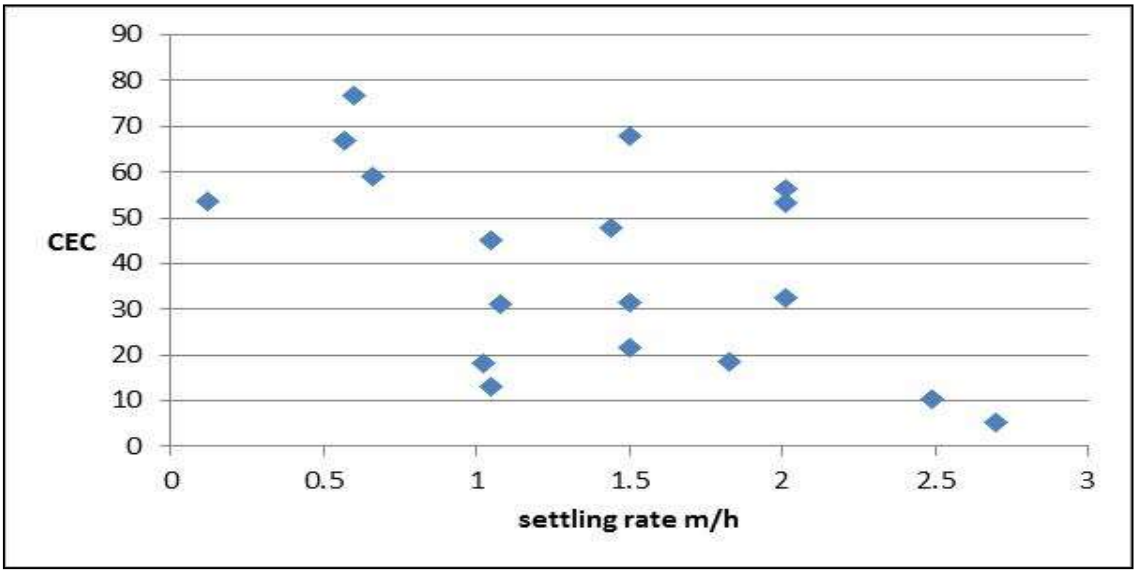

Figure 85: Cation exchange capacity (CEC) versus the initial settling rate of the critical calcium concentrations of the various kimberlites.

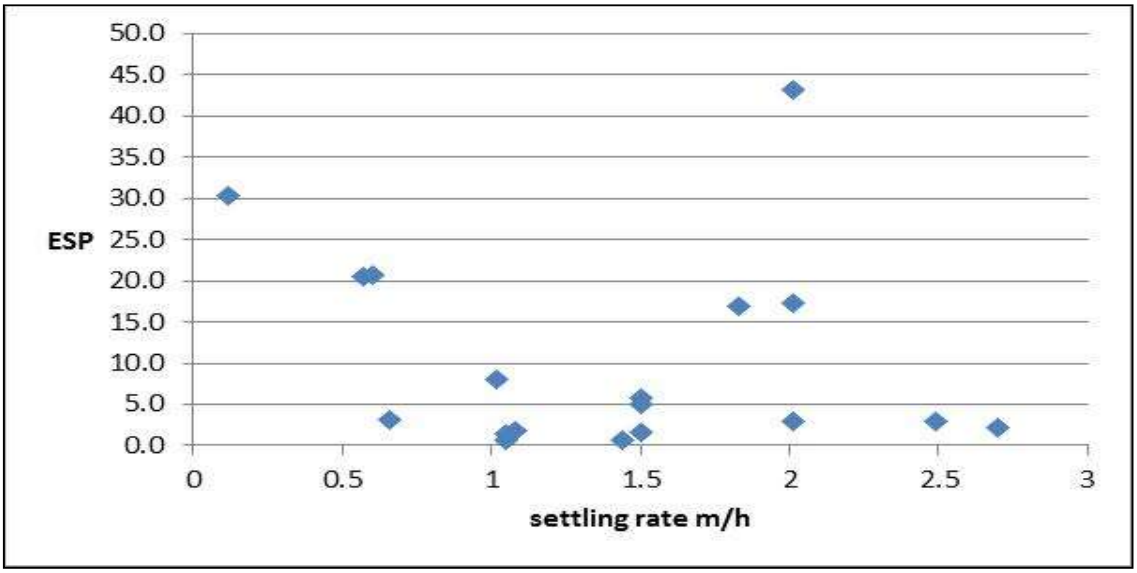

Figure 86: Sodium exchange capacity (ESP) versus the initial settling rate of the critical calcium concentrations of the various kimberlites.

The settling rate comparison for the critical magnesium concentration of the kimberlites and the CEC and ESP values of the kimberlites are shown in Figure 87 and Figure 88. A high settling rate is achieved when the ESP value of the kimberlite

is low. The outlier in Figure 88 is Venetia Red where a high settling rate was achieved even when the ESP value was high. No definitive trend can be established between the CEC of the kimberlite and the critical magnesium concentration settling rates of the different samples.

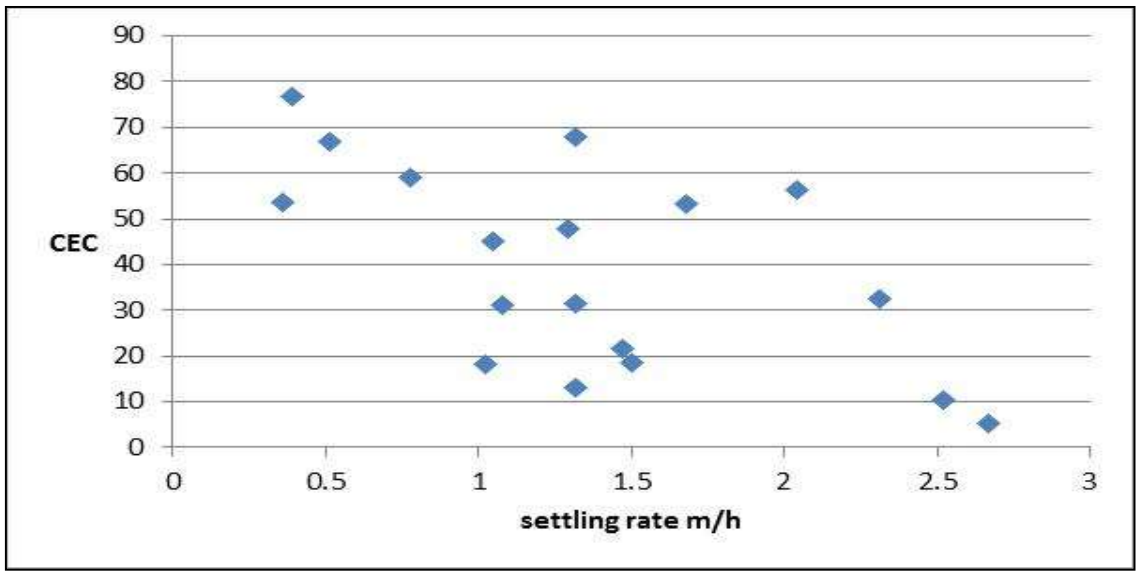

Figure 87: Cation exchange capacity (CEC) versus the initial settling rate of the critical magnesium concentrations of the various kimberlites.

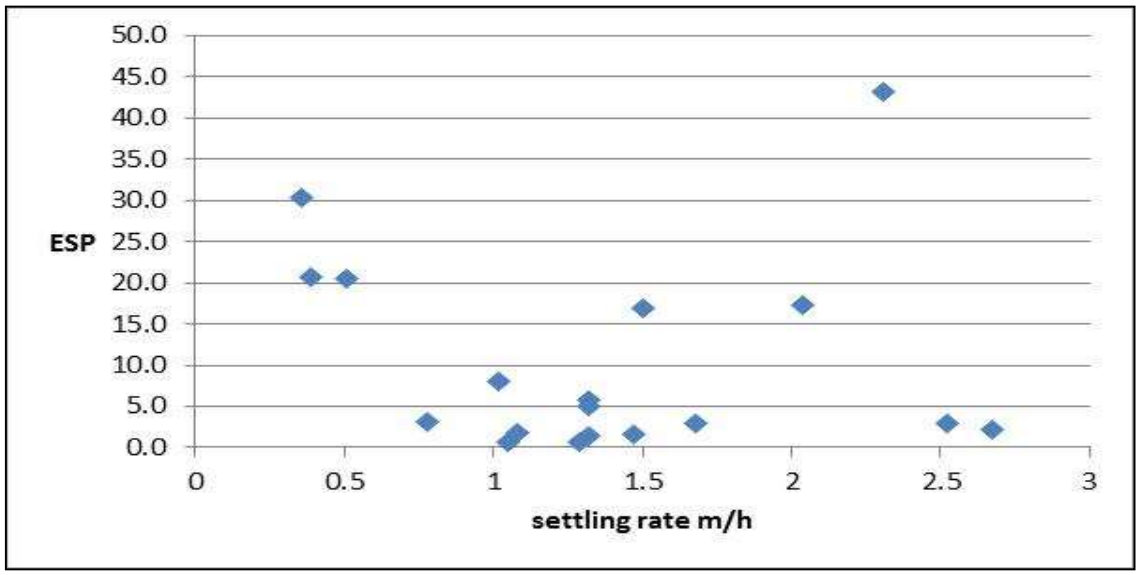

Figure 88: Sodium exchange capacity (ESP) versus the initial settling rate of the critical magnesium concentrations of the various kimberlites.

Figure 89 and Figure 90 show the settling rates of the critical cupric concentrations of the different kimberlites against the CEC and ESP values of the respective kimberlites. The CEC and the critical cupric concentration of the kimberlites are showing a possible exponential trend where the CEC increases exponentially as the settling rate of the kimberlite decreases. Figure 90 shows that it is possible to attain a high settling rate when the ESP of the sample is low. Three outliers are noted where a higher settling rate is achieved although the ESP value of the kimberlite is high. This can be attributed to the exchange of copper cations with the sodium cations in the crystal lattice, lowering the overall negative charge surrounding the particles which then leads to higher settling rates.

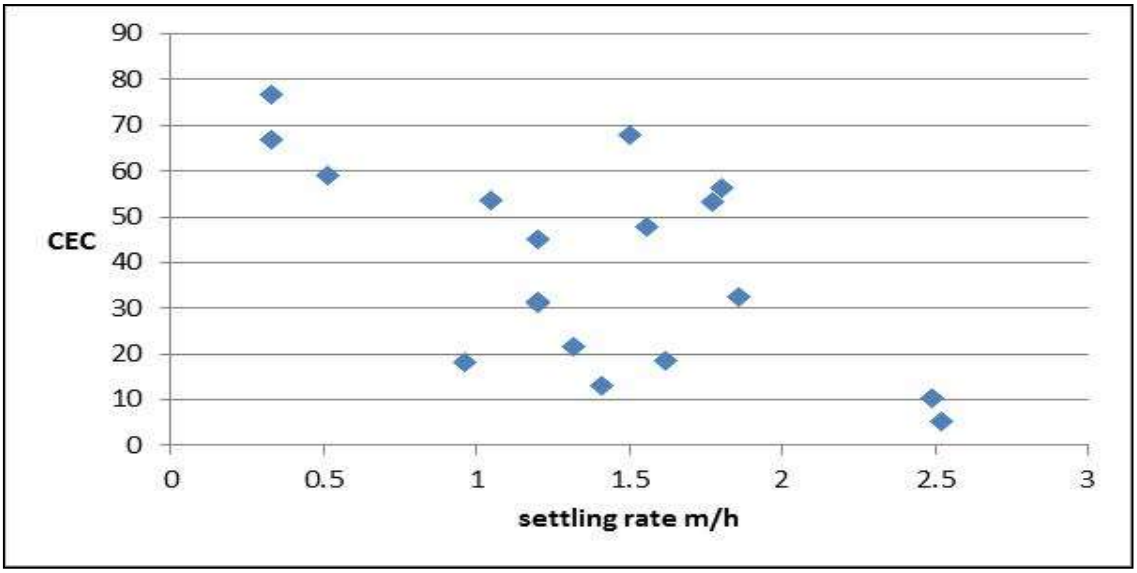

Figure 89: Cation exchange capacity (CEC) versus the initial settling rate of the critical copper concentrations of the various kimberlites.

The CEC and the ESP values of the different kimberlites are plotted against the respective settling rates achieved when the critical ferric concentration was added to the slurry as shown in Figure 91 and Figure 92. The CEC and critical ferric concentration settling rates of the kimberlites show no trend although the CEC increases sharply as the settling rate decreases as shown in Figure 91. Figure 92 shows that a high settling rate is possible when the critical ferric concentration is added, as long as the kimberlite has a low ESP value. Four outliers are noted where kimberlites had a high settling rate although the ESP value of the kimberlite

is high. This is due to the sodium cations being exchanged with ferric cations in the smectite layers, reducing the overall negative charge.

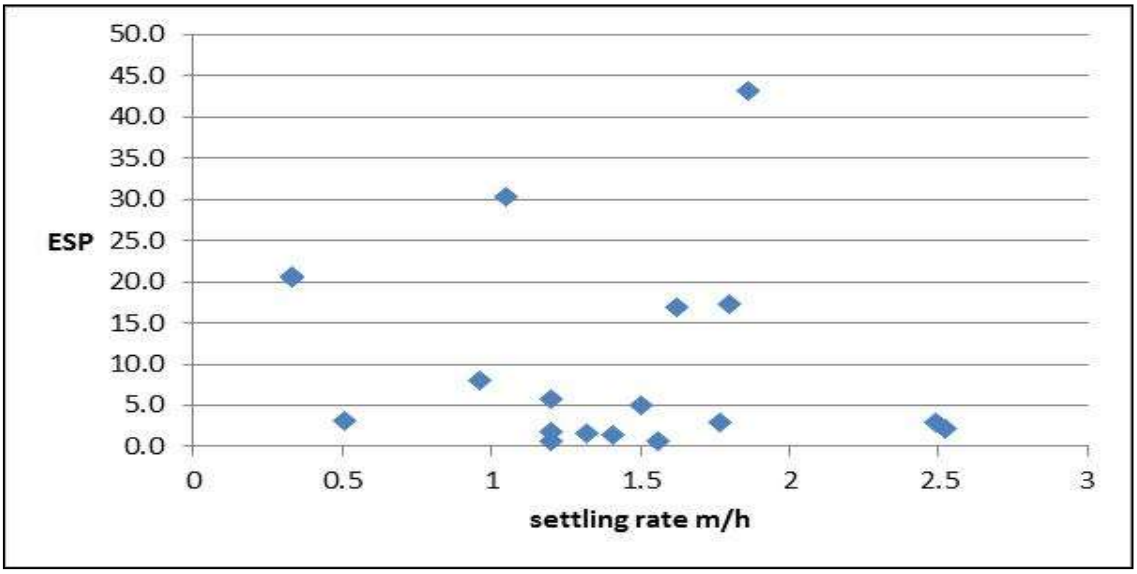

Figure 90: Sodium exchange capacity (ESP) versus the initial settling rate of the critical copper concentrations of the various kimberlites.

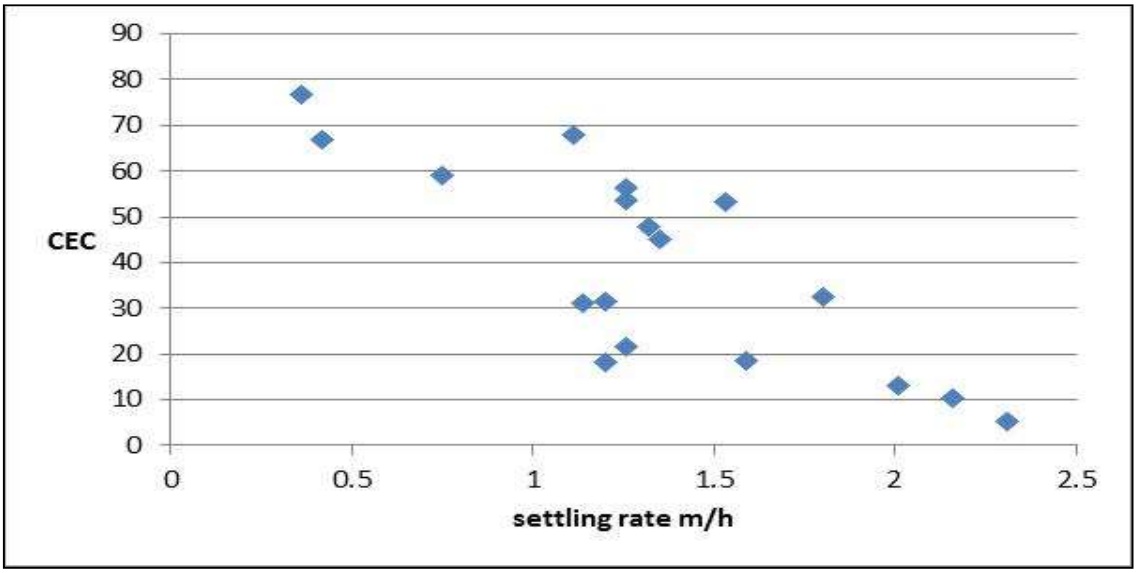

Figure 91: Cation exchange capacity (CEC) versus the initial settling rate of the critical ferric concentrations of the various kimberlites.

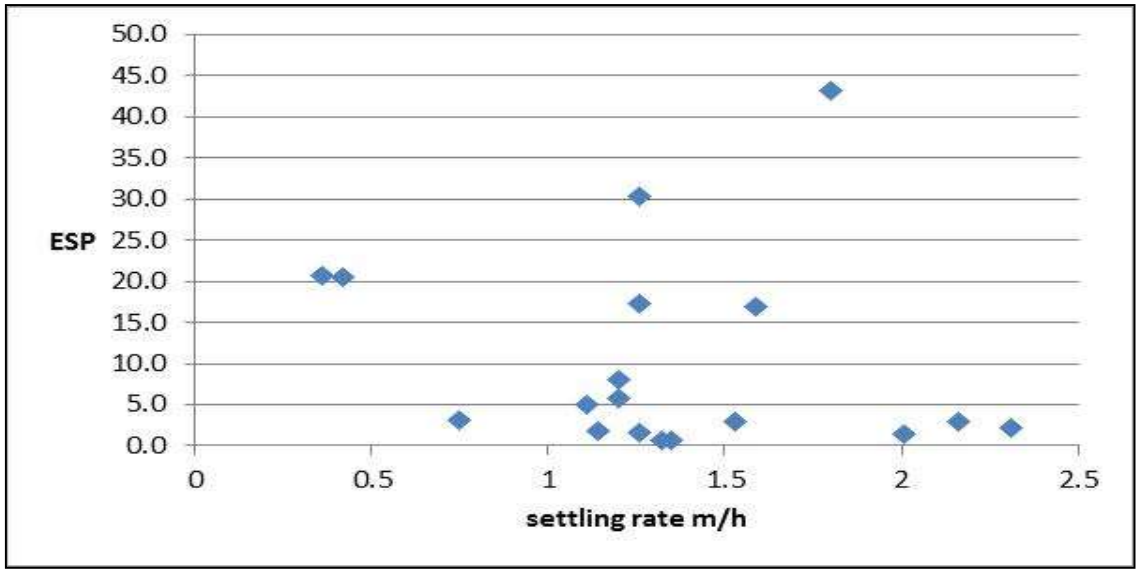

Figure 92: Sodium exchange capacity (ESP) versus the initial settling rate of the critical ferric concentrations of the various kimberlites.

Figure 93 and Figure 94 show the CEC and ESP of the different kimberlites plotted against the settling rate that was achieved with the addition of the critical aluminium concentration to the different slurries. No definitive trend could be established between the settling rate of the critical aluminium concentration and the CEC of the different kimberlites as shown in Figure 93. Figure 94 shows that a low ESP value is required to achieve a higher settling rate. There are more outliers with the critical aluminium concentration settling rates against the ESP value of the kimberlite where higher settling rates are experienced with high ESP values. This can be contributed to the exchange of the trivalent aluminium cation with the monovalent sodium cation, whereby the overall negative charge of the solution is reduced, resulting in higher settling rates.

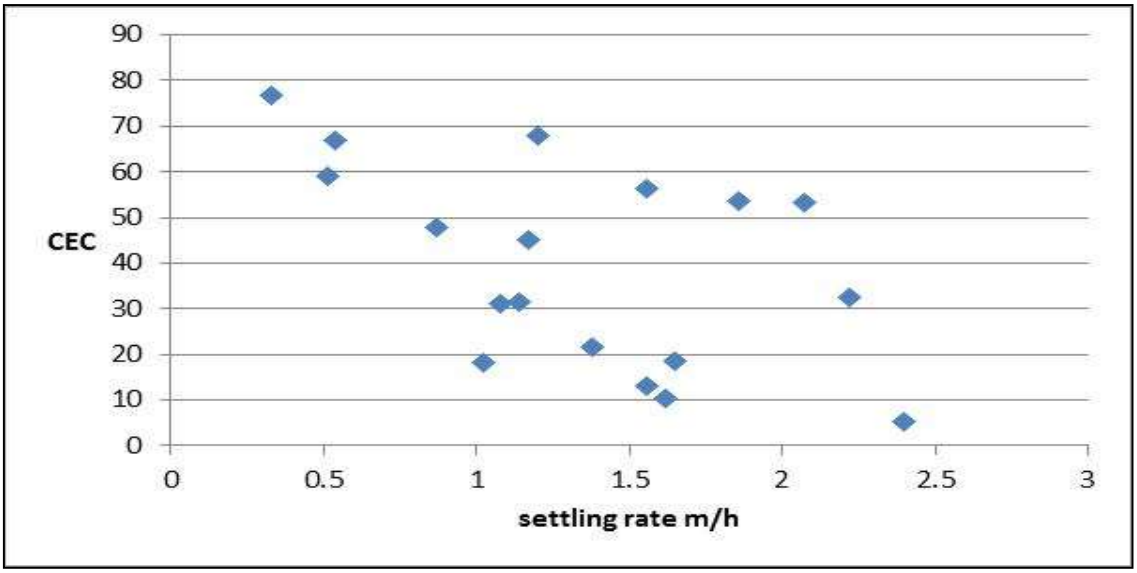

Figure 93: Cation exchange capacity (CEC) versus the initial settling rate of the critical aluminium concentrations of the various kimberlites.

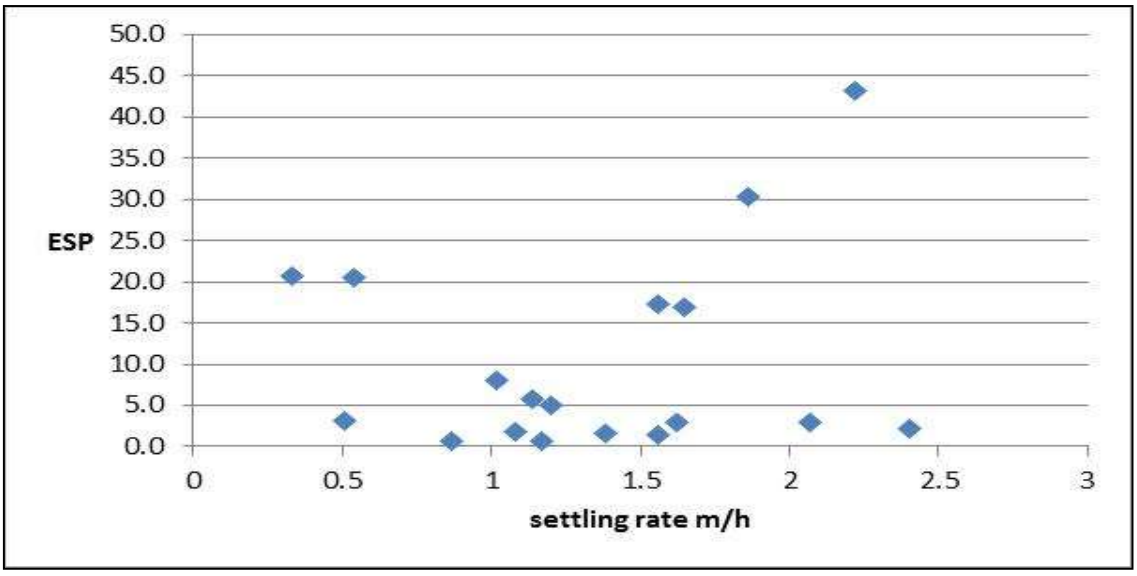

Figure 94: Sodium exchange capacity (ESP) versus the initial settling rate of the critical aluminium concentrations of the various kimberlites.

It is very difficult to establish a trend between the critical coagulant concentrations and the exchangeable sodium percentage with the settling rates of the different kimberlites. The settling rates of the critical coagulant concentrations and the cation exchange capacities did not show any trends. The higher cation exchange capacities allow for more absorption of the copper, ferric and aluminium cations into the clay structure, reducing the cationic strength of the solution and thus

resulting in a faster settling rate. The lower the ESP value of the kimberlites the higher the settling rate of the kimberlites when the critical cation concentration is added to the slurry. Exceptions were noted where kimberlites with high ESP values experienced faster settling rates when cupric, ferric or aluminium ions were added to the slurries. This happens when the sodium ion in the crystal lattice of the smectite is exchanged by the divalent or trivalent cations due to a smaller hydration bond size and a higher hydration enthalpy.

5.3 Flocculant test results

The different Magnafloc flocculants from Senmin were screened with a 10% solids loading and the settling rate determined after 30 ml of settling. The flocculent polymer structure was determined visually and categorised as large, medium or small while the supernatant clarity was determined by using a clarity wedge where 0 is equal to no clarity, 1 to 29 is equal to poor clarity, 30 to 40 is good clarity and 41 to 46 is equal to exceptional clarity. The results for every kimberlite are tabled in Table 22 to Table 39 in Appendix A. The non-ionic flocculants resulted in very slow settling rates of less than 7 m/h for kimberlites with a cation exchange capacity of more than 10 cmol/kg. Kimberlites with a cation exchange capacity of less than 10 cmol/kg, AC 1-1-1 and AC 5-5-1, had low settling rates of less than 5 m/h.

The flocculant screening process highlighted the 3 fastest flocculants for each kimberlite, and these flocculants were used to conduct the settling tests and determine the slurry bed depth after each settling test. The settling test graphs for the different kimberlites were recorded and these graphs are shown in Figure 155 to Figure 170 in Appendix A. The flocculants were made up to strength of 0.025% and 2 ml drops were added to the sample in the 500 ml measuring cylinder before mixing occurred. The initial settling rates were determined after 30 seconds and the slurry bed depth determined after 24 hours.

The settling rate and slurry bed depth of the 3 most effective flocculants for AC 1-1-1 are shown in Figure 95, and Magnafloc 10 gave the best results with a settling

rate of 25 m/h and a slurry bed weight percentage of 47%. Although the XRD scan indicated a smectite content of 50%, the settling behaviour of the kimberlite is showing similar settling rates for hyperbyssal kimberlites which are known to settle naturally. AC 1-1-1 is the kimberlite with the lowest cation exchange capacity of 5 cmol/kg and this will reduce the possibility of a negative charge at the slurry particles which will result in faster settling rates. The lower cation exchange capacity will contribute to a reduction in the basal edge and face charges. Lower face and edge charges will enable a face-to-face packing relationship between the particles allowing for more compaction in the slurry bed.

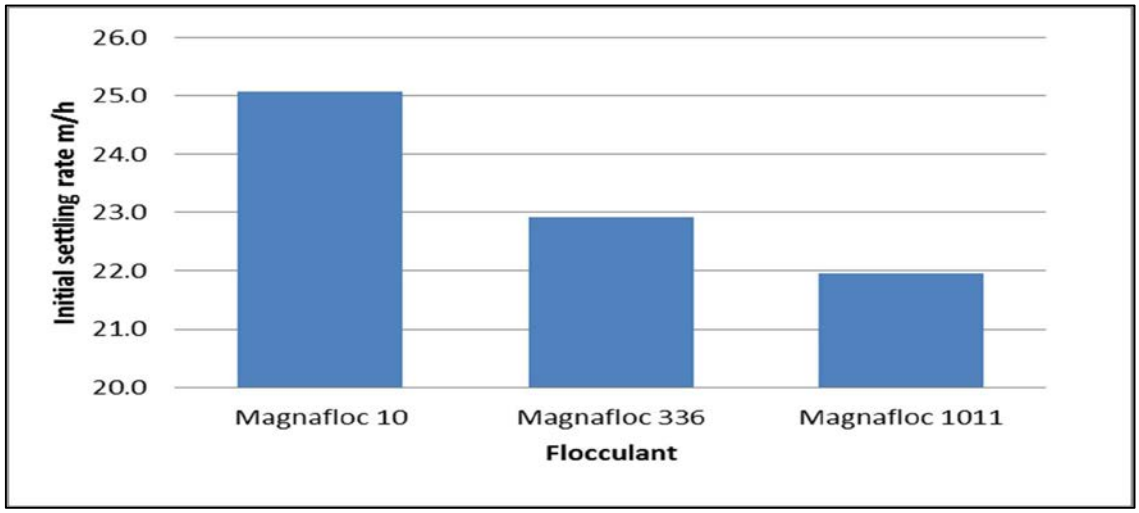

Figure 95: Settling rate of the 3 most effective flocculants for AC 1-1-1.

The settling rate and slurry bed depth of the 3 most effective flocculants for AC 4-1A-1 are shown in Figure 97 and Figure 98 and Magnafloc 5250 gave the best results with a settling rate of 16 m/h and a slurry bed weight percentage of 34%. AC 4-1A-1 has a cation exchange capacity of 45 cmol/kg that increase the possibility of more negative charge surrounding the slurry particles reducing the settling rate of the slurry as compared to AC 1-1-1. The higher negative charge surrounding the particles will reduce the slurry bed compaction due to the honeycomb structure being formed.

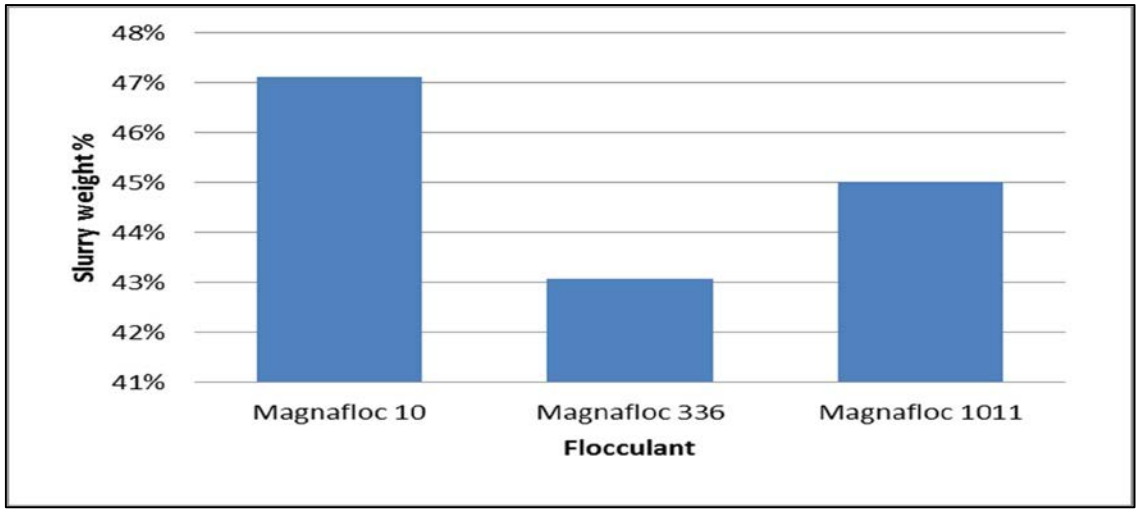

Figure 96: Slurry bed percentage of 3 most effective flocculants for AC 1-1-1.

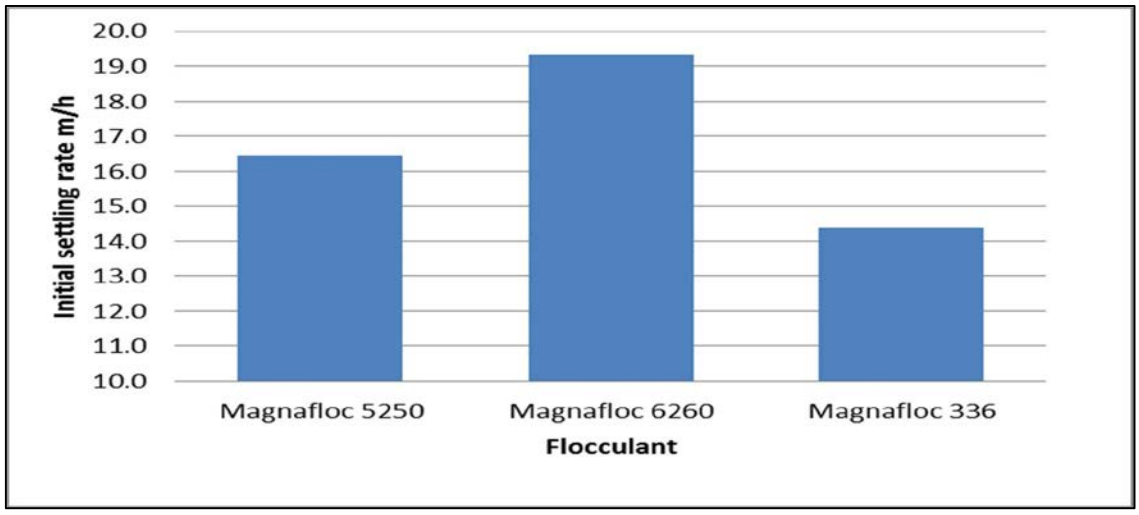

Figure 97: Settling rate of the 3 most effective flocculants for AC 4-1A-1.

The settling rate and slurry bed depth of the 3 most effective flocculants for AC 5-5-1 are shown in Figure 99 and Figure 100 and Magnafloc 340 gave the best results with a settling rate of 21 m/h and a slurry bed weight percentage of 41%. Although the XRD scan indicated a smectite content of 50%, the settling behaviour of the kimberlite is showing similar settling rates for hypabyssal kimberlites which are known to settle naturally. AC 5-5-1 has a low cation exchange capacity of 10 cmol/kg, which reduces the possibility of a high negative charge surrounding the slurry particles, resulting in faster settling rates and more compact slurry beds.

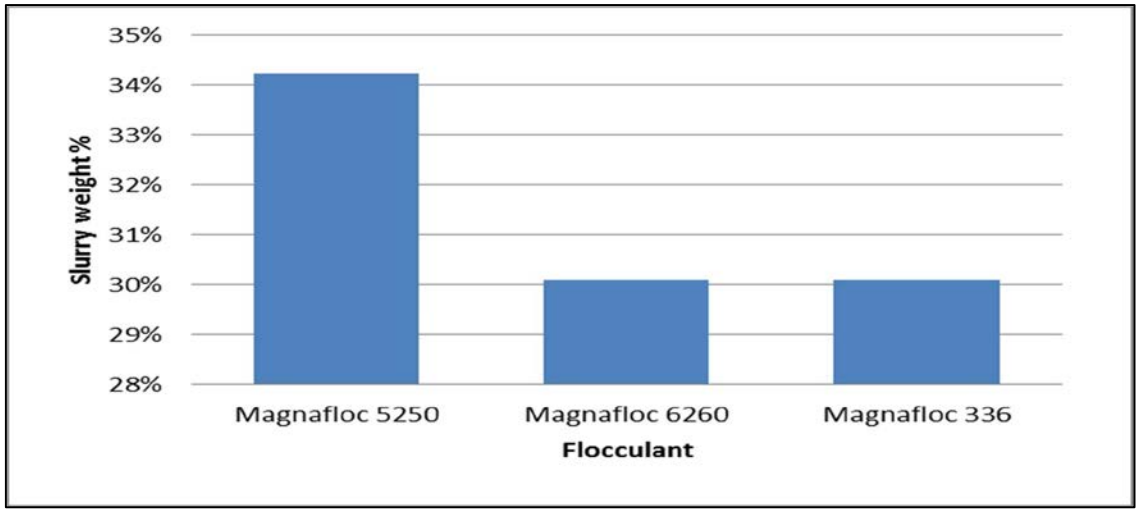

Figure 98: Slurry bed percentage of 3 most effective flocculants for AC 4-1A-1.

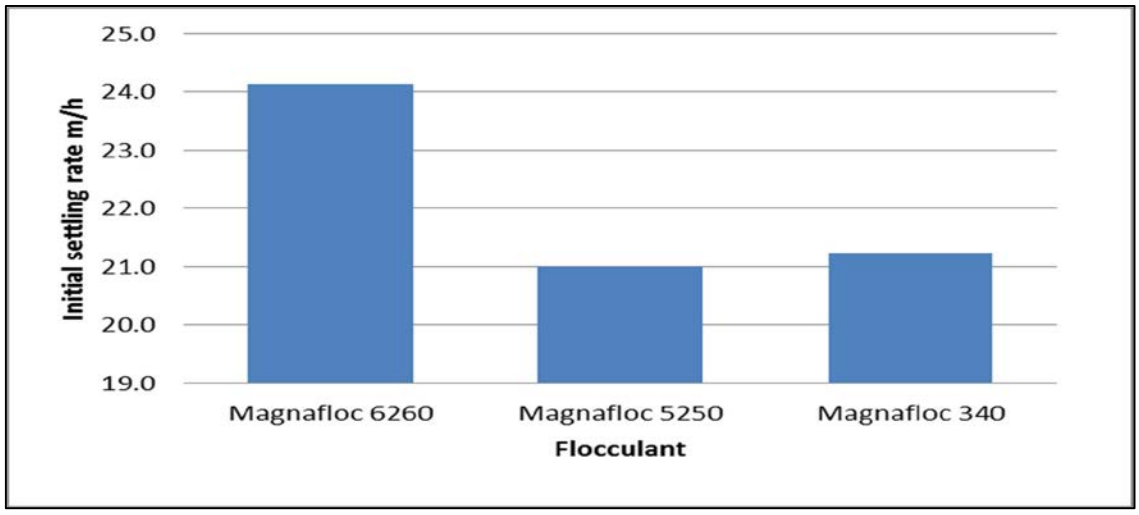

Figure 99: Settling rate of the 3 most effective flocculants for AC 5-5-1.

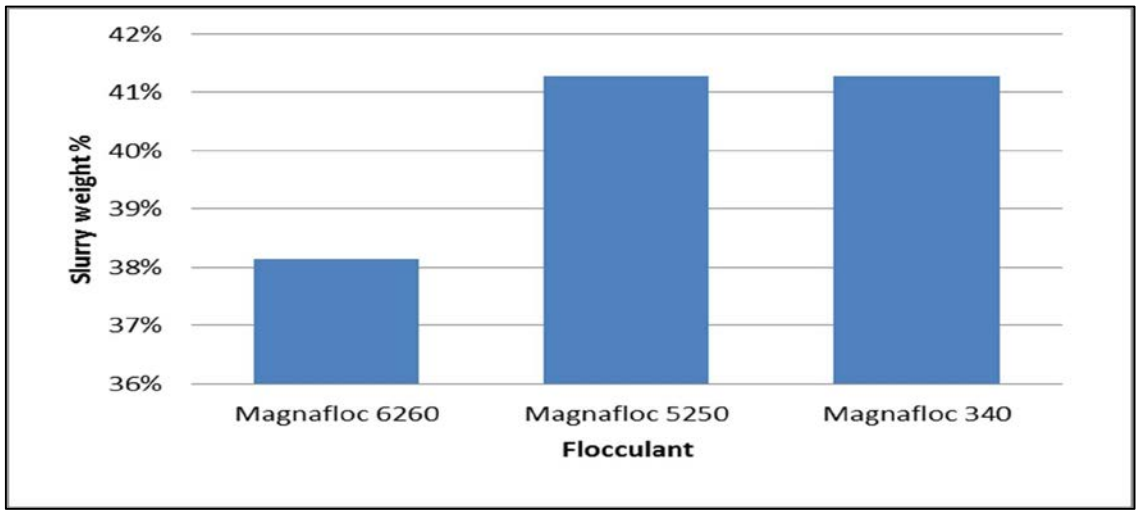

Figure 100: Slurry bed percentage of 3 most effective flocculants for AC 5-5-1.

The settling rate and slurry bed depth of the 3 most effective flocculants for AC 5-5-2 are shown in Figure 101 and Figure 102, and Magnafloc 5250 gave the best results with a settling rate of 12 m/h and a slurry bed weight percentage of 30%. A lower settling rate is achieved along with less compaction in the slurry bed and this is expected because of the higher smectite content of 70% and a higher cation exchange capacity of 48 cmol/kg.

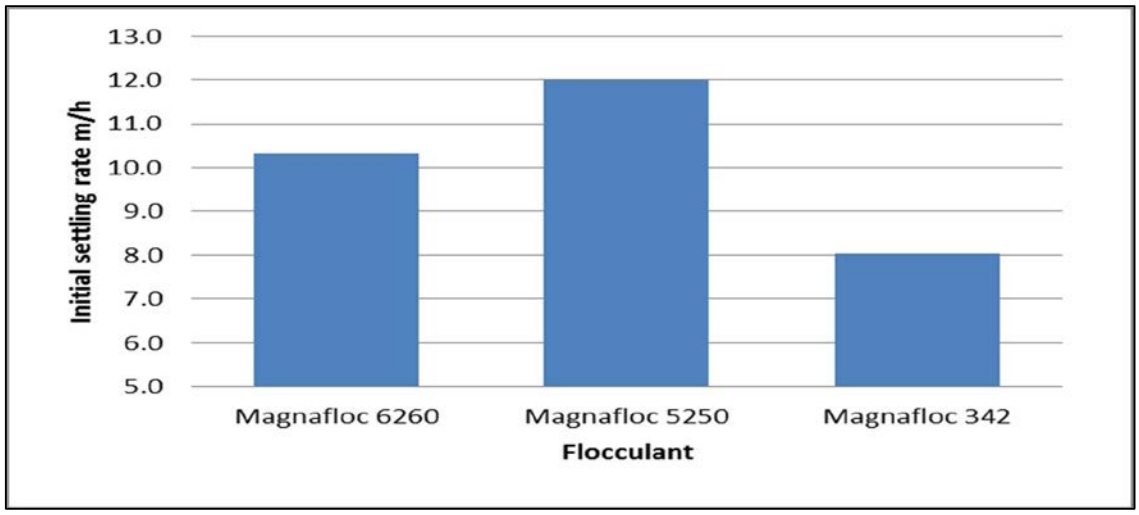

Figure 101: Settling rate of the 3 most effective flocculants for AC 5-5-2.

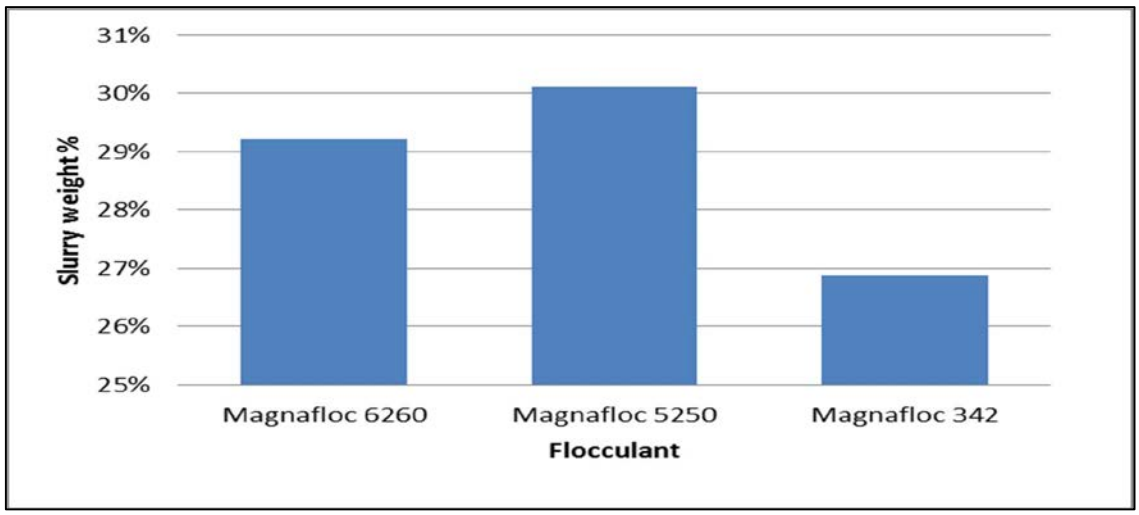

Figure 102: Slurry bed percentage of 3 most effective flocculants for AC 5-5-2.

The settling rate and slurry bed depth of the 3 most effective flocculants for AC 16-1-1 are shown in Figure 103 and Figure 104, and Magnafloc 5250 gave the best results with a settling rate of 10.5 m/h and a slurry bed weight percentage of

29%. A lower settling rate is achieved along with less compaction in the slurry bed and this is expected because of the higher smectite content of 70% and a higher cation exchange capacity of 31 cmol/kg.

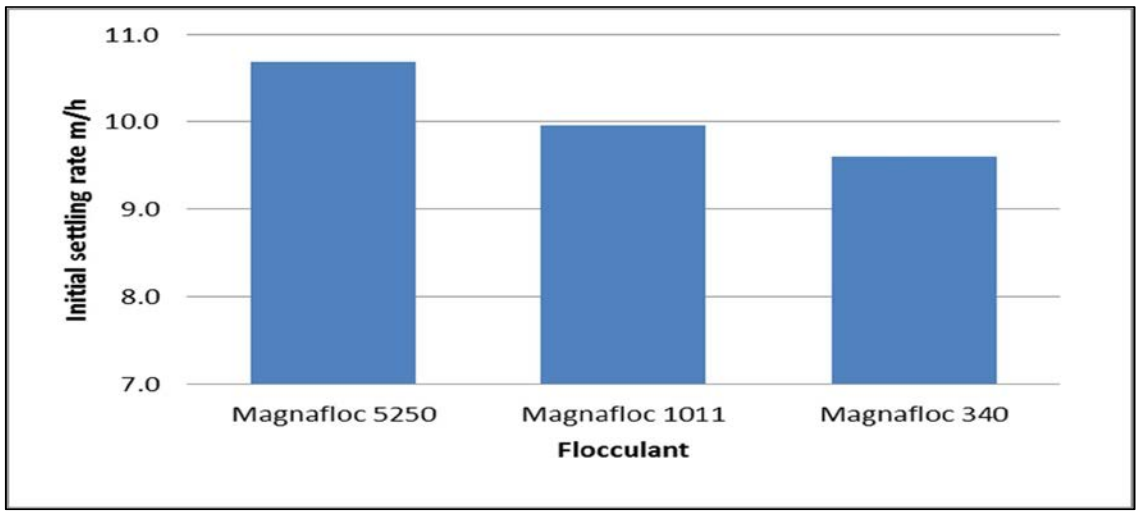

Figure 103: Settling rate of the 3 most effective flocculants for AC 16-1-1.

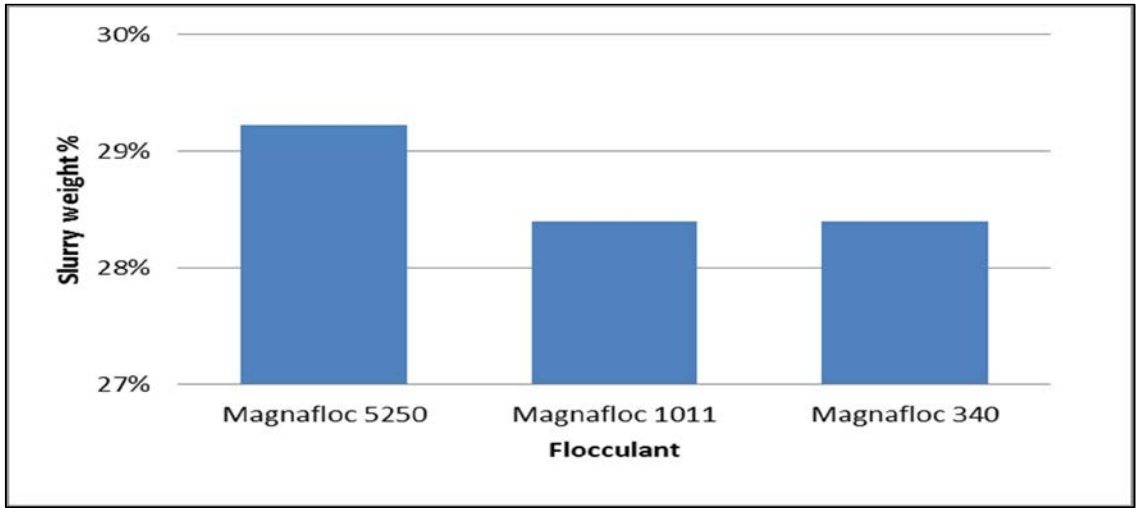

Figure 104: Slurry bed percentage of 3 most effective flocculants for AC 16-1-1.

The settling rate and slurry bed depth of the 3 most effective flocculants for AC 197-1-1 are shown in Figure 105 and Figure 106, and Magnafloc 340 gave the best result with a settling rate of 16.5 m/h and a slurry bed weight percentage of 33%. Although the Magnafloc 1101 gave a higher settling rate of 18 m/h, the slurry bed weight percentage was also the highest and therefore it was decided to

choose Magnafloc 340 as it has a slightly lower settling rate together with the best slurry bed compaction depth.

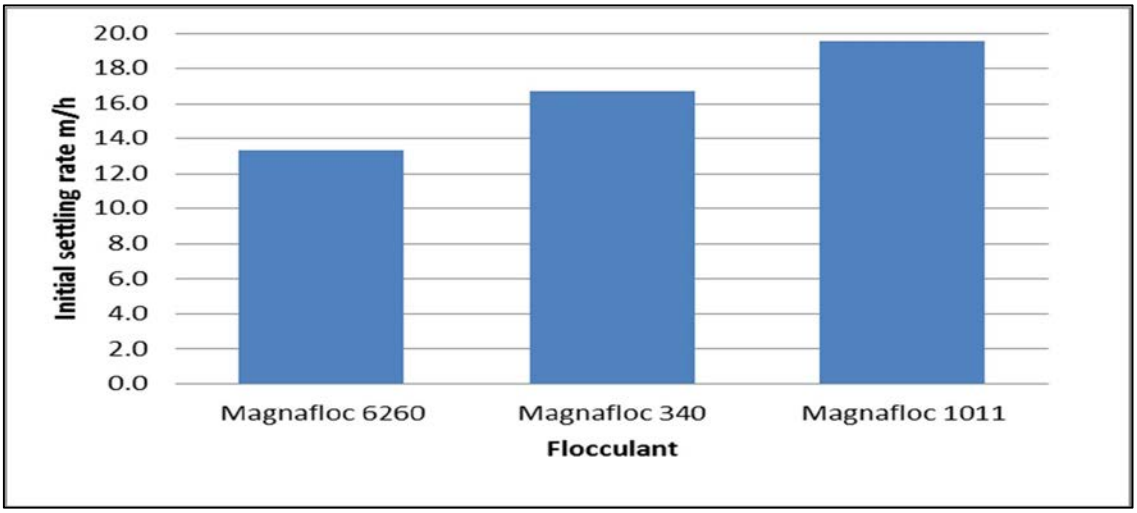

Figure 105: Settling rate of the 3 most effective flocculants for AC 197-1-1.

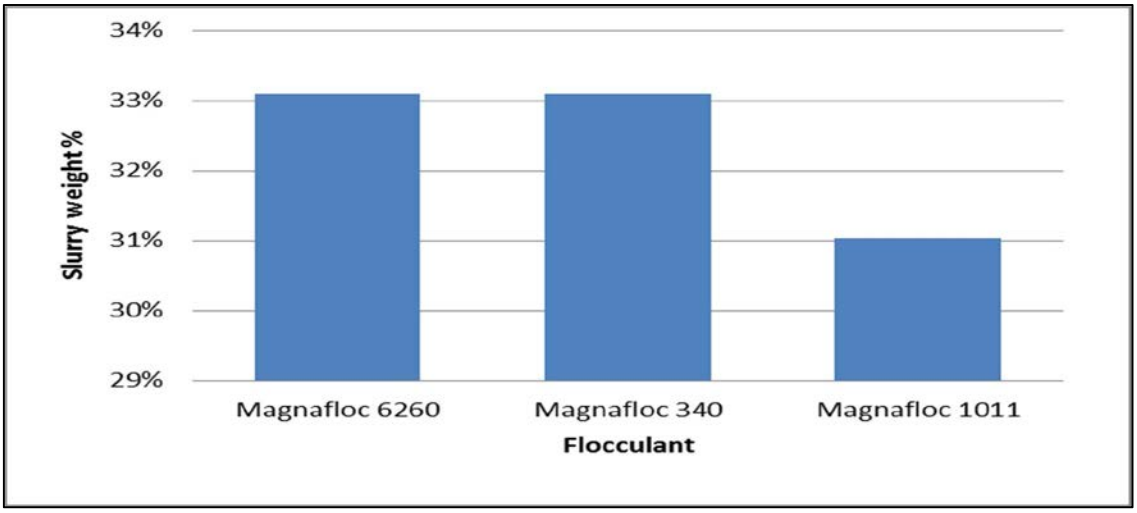

Figure 106: Slurry bed percentage of 3 most effective flocculants for AC 197-1-1.

AC 56-5-1 kimberlite and Venetia Red kimberlite did not settle out with any of the flocculants. These two kimberlites have high cation exchange capacities, 56 cmol/kg for AC 56-5-1 and 32 cmol/kg for Venetia Red, and have the highest sodium exchange percentages of the 18 kimberlites at 30% ESP for AC 56-5-1 and 43% for Venetia Red. The two kimberlites had the highest pH value of 10.6 of all the kimberlite slurries. The combination of the high cation exchange capacity along with the high sodium exchange percentages along with a high pH value

could possibly counteract the anionic flocculants and non-ionic flocculants which in turn results in no settling taking place.

The settling rate and slurry bed depth of the 3 most effective flocculants for AO 319 are shown in Figure 107 and Figure 108, and Magnafloc 10 gave the best results with a settling rate of 18.5 m/h and a slurry bed weight percentage of 32%.

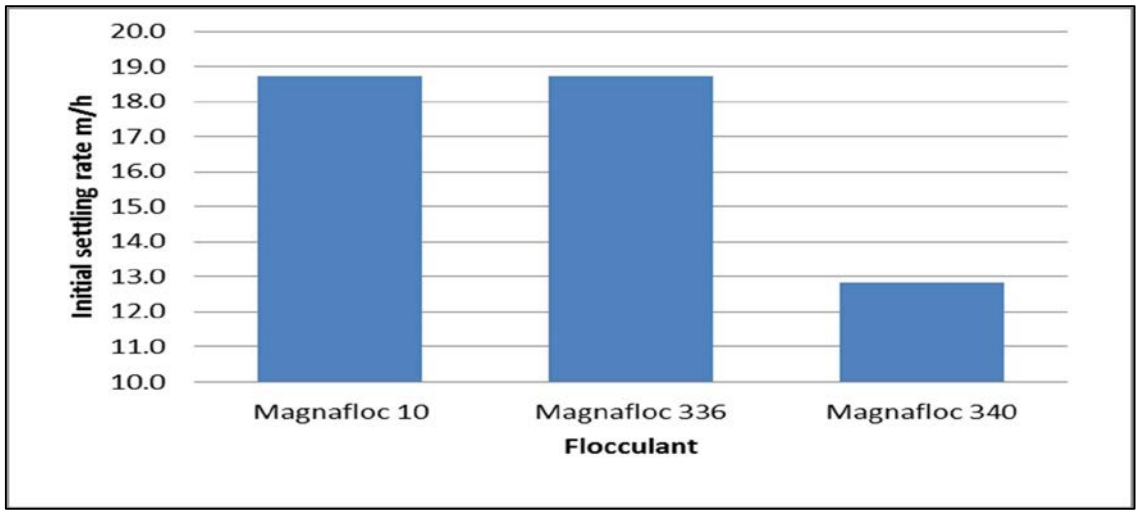

Figure 107: Settling rate of the 3 most effective flocculants for AO 319.

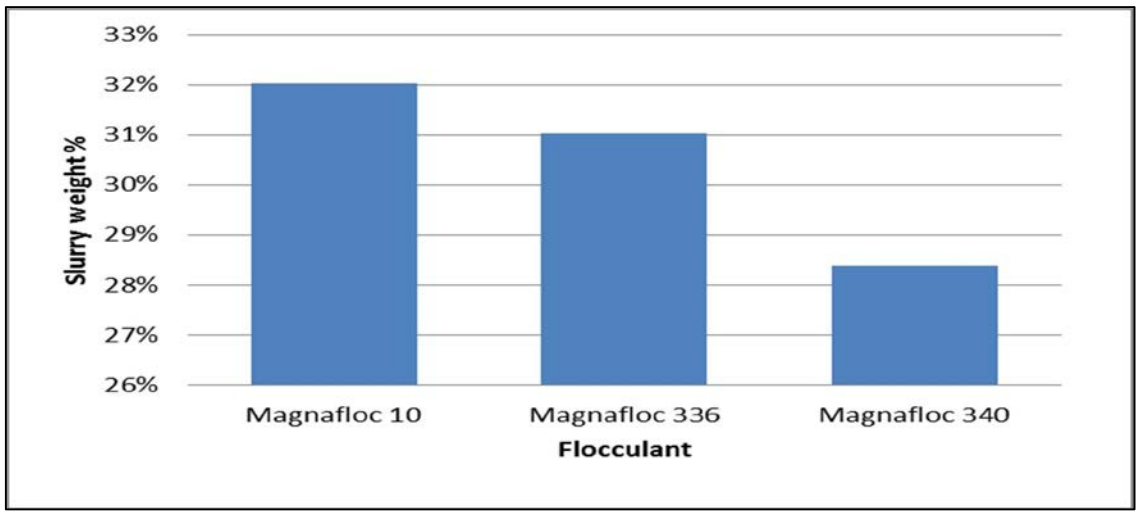

Figure 108: Slurry bed percentage of the 3 most effective flocculants for AO 319.

Figure 109 and Figure 110 show the settling rate and slurry bed depth of the three most effective flocculants for AO 320, and Magnafloc 1011 gave the best results with a settling rate of 12 m/h and a slurry bed weight percentage of 29%. The AO

319 kimberlite sample was taken at a depth of 116 metres and AO 320 was taken at a depth of 30 metres from the same drill core hole. It is interesting to note that there are different sets of flocculant that gave the best results for different depths, and that a faster settling rate and higher slurry bed compaction are achieved as the depth of the kimberlite is increased. This is due to cation exchange that has already taken place closer to the surface of the kimberlite.

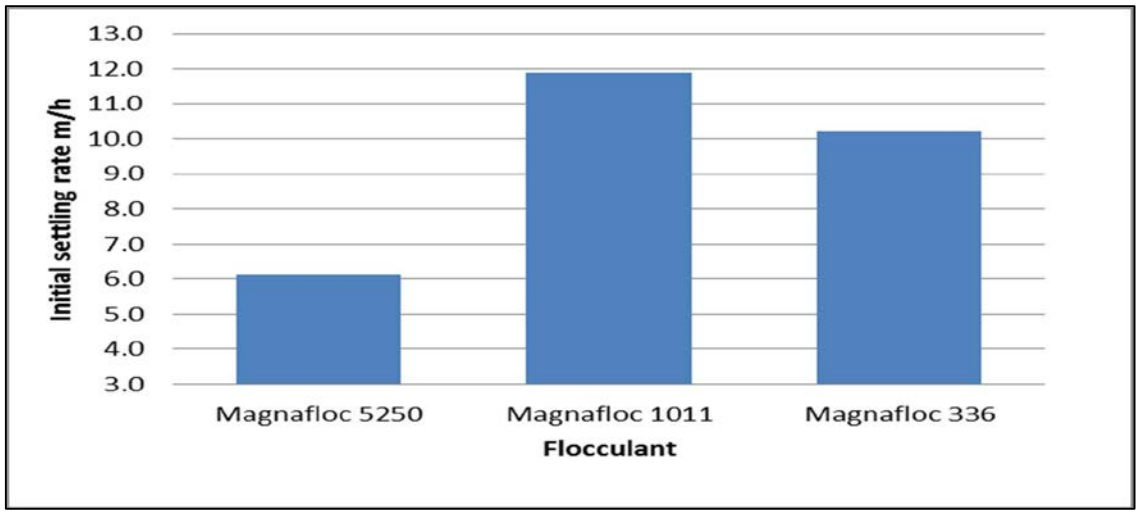

Figure 109: Settling rate of the 3 most effective flocculants for AO 320.

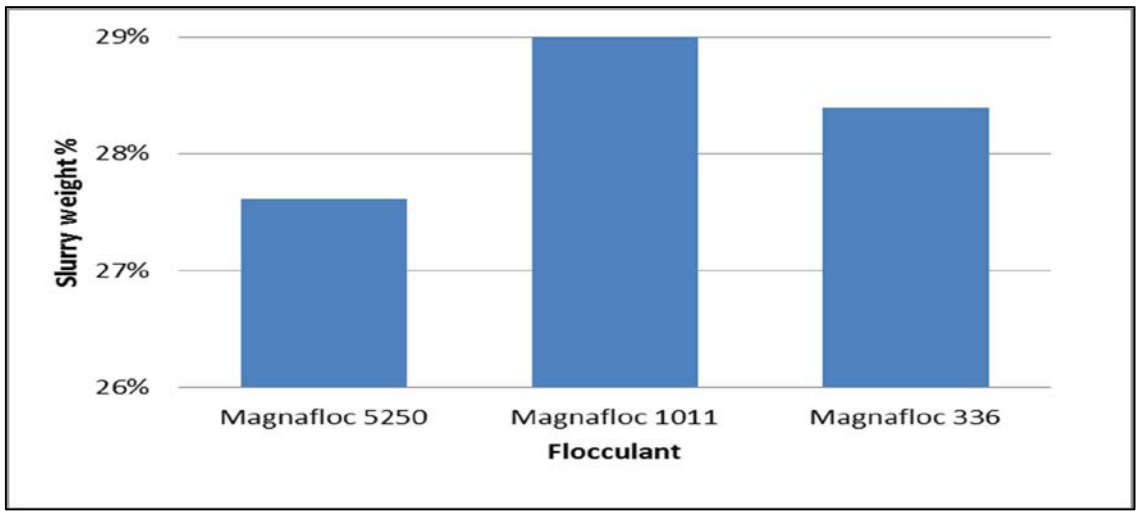

Figure 110: Slurry bed percentage of the 3 most effective flocculants for AO 320.

The AO 321, AO 322 and AO 323 samples were all taken from the same kimberlite but at different depths with AO 321 taken at 137 metres from surface, AO 322 at 90 metres and AO 323 at 30 metres. Comparing the settling rates and of these

samples, as shown in Figure 111, Figure 113 and Figure 115, and the slurry bed weight percentages, as shown in Figure 112, Figure 114 and Figure 116 it can be seen that the best settling rate for AO 321 were achieved with Magnafloc 336 at a rate of 21.5 m/h and a slurry bed weight percentage of 38%. The best settling rate for AO 322 was achieved with Magnafloc 336 at a rate of 17.5 m/h and slurry bed weight percentage of 33%, while AO 323 had the best results with Magnafloc 155 at a settling rate of 22.6 m/h and slurry bed weight percentage of 43%. AO 322 has the highest smectite content of the three samples at 60% while AO 321 has a smectite content of 35%, and AO 323 has a smectite content of 15%. It can be seen how an increase in the percentage of smectite leads to a reduced settling rate and less compaction of the slurry bed. This is possibly due to the house-of-card structure dominating the packing relationship for AO 322 due to the high smectite content while the face-to-face packing relationship dominates when less smectite is found in a kimberlite.

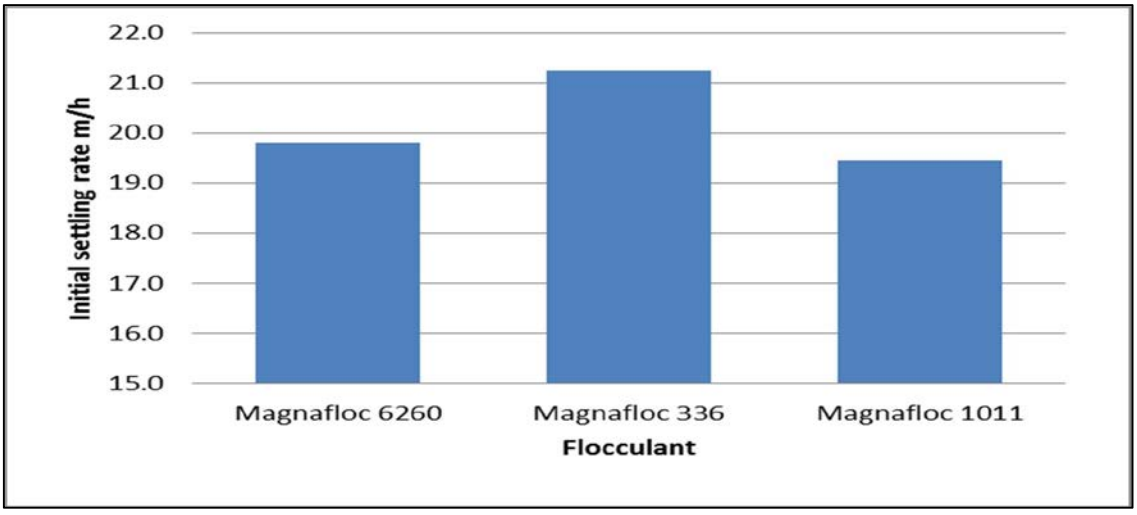

Figure 111: Settling rate of the 3 most effective flocculants for AO 321.

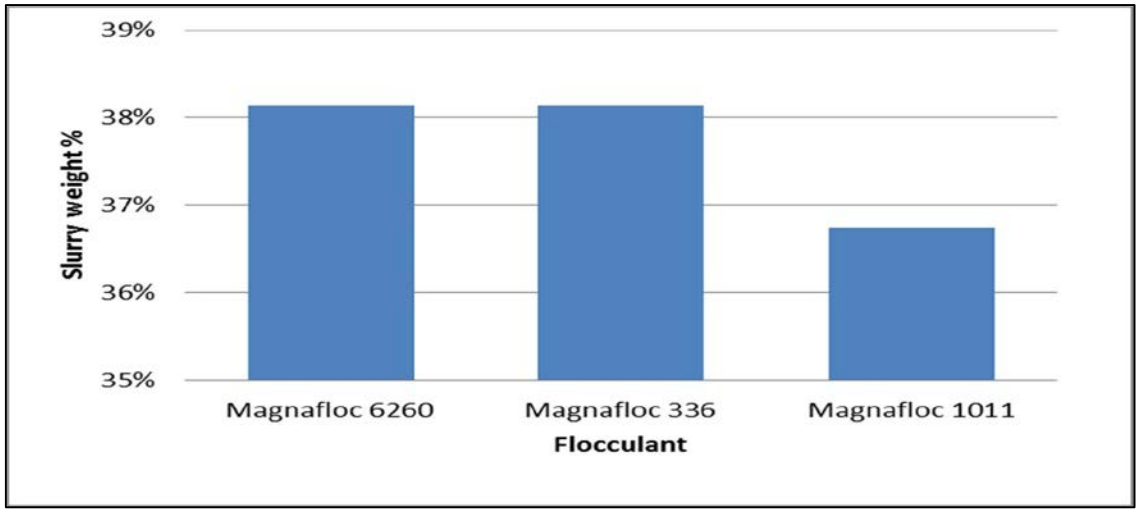

Figure 112: Slurry bed percentage of the 3 most effective flocculants for AO 321.

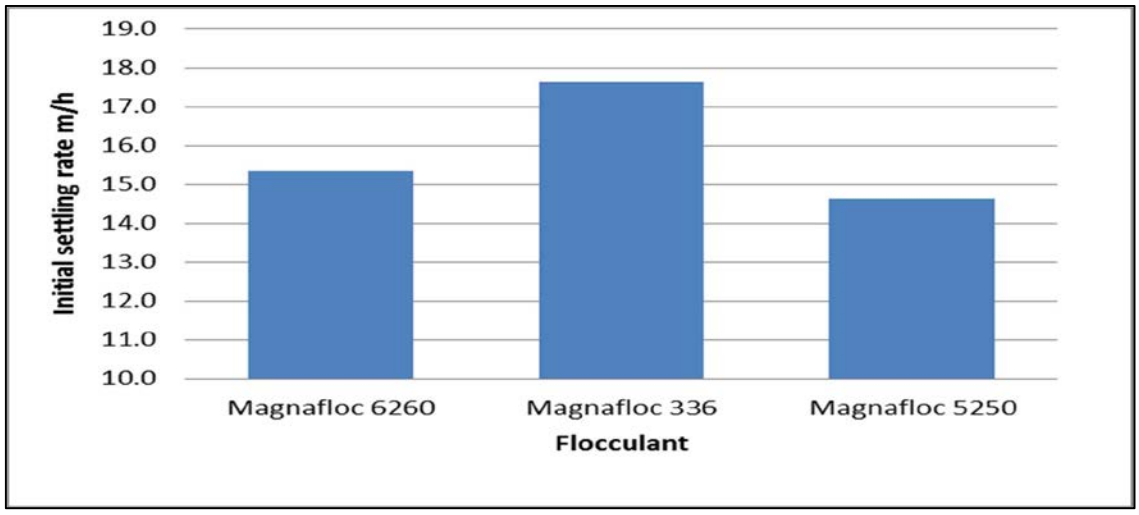

Figure 113: Settling rate of the 3 most effective flocculants for AO 322.

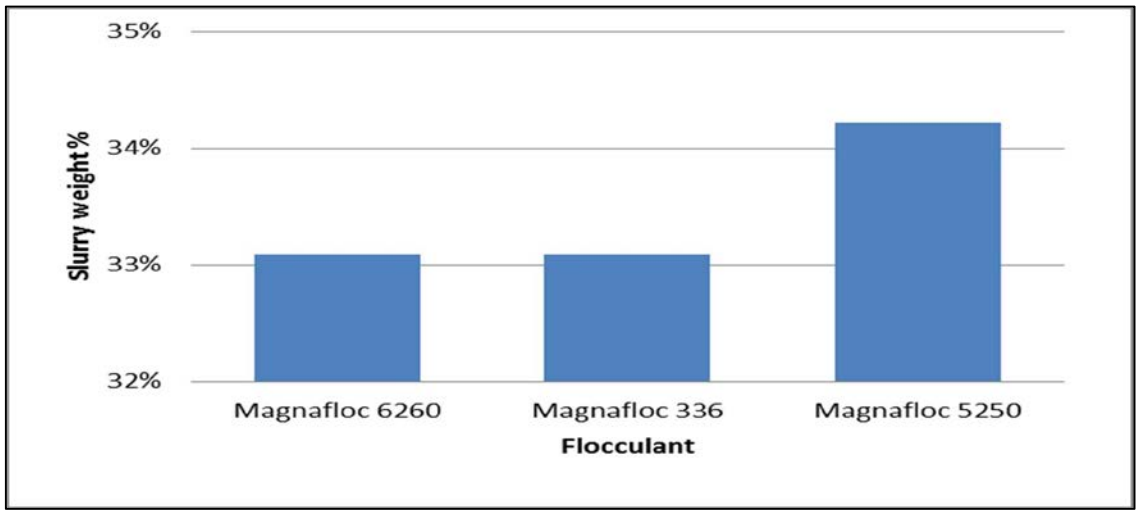

Figure 114: Slurry bed percentage of the 3 most effective flocculants for AO 322.

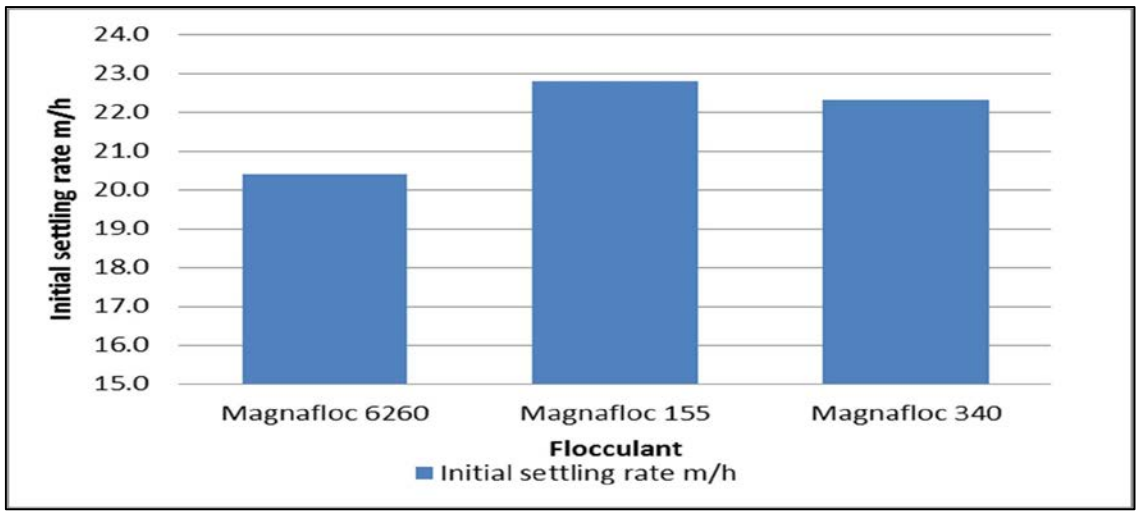

Figure 115: Settling rate of the 3 most effective flocculants for AO 323.

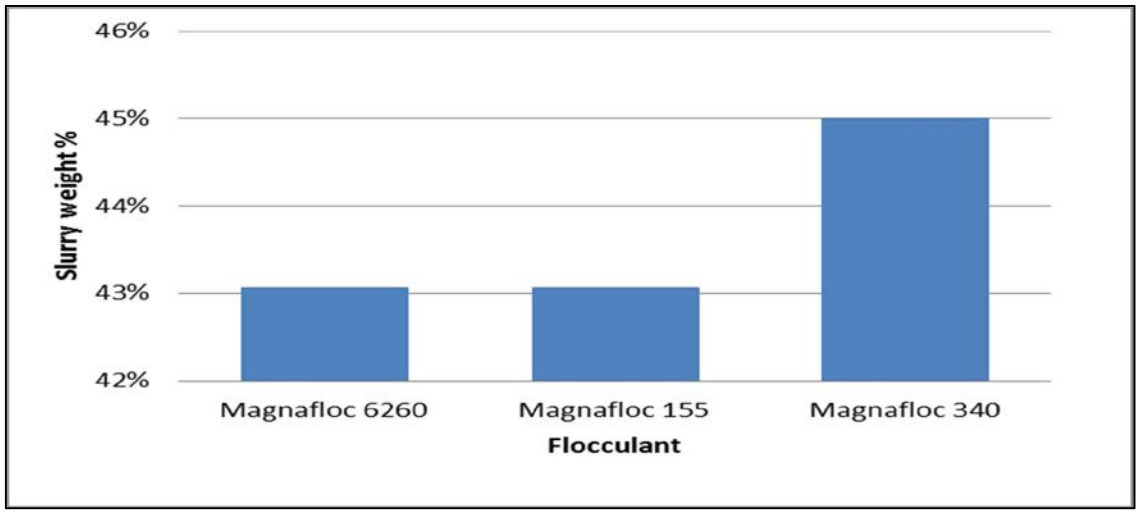

Figure 116: Slurry bed percentage of the 3 most effective flocculants for AO 323.

Figure 117 and Figure 119 show the 3 fastest flocculant settling rates for AO 324 and AO 325 while Figure 118 and Figure 120 show the slurry bed weight percentages after settling. The AO 324 kimberlite sample was taken at a depth of 340 metres and the AO 325 kimberlite sample was taken at a depth of 104 metres of the same kimberlite. The best settling rate for AO 324 was achieved with Magnafloc 342 at a settling rate of 17.8 m/h and slurry bed weight percentage of 35%, while the best settling rate for AO 325 was achieved with Magnafloc 336 at a settling rate of 20.6 m/h and a slurry bed weight percentage of 40%. A similar trend is seen where AO 324, with a smectite content of 55%, as a lower settling rate and slurry bed compaction compared to AO 325 that has a smectite content of 30%.

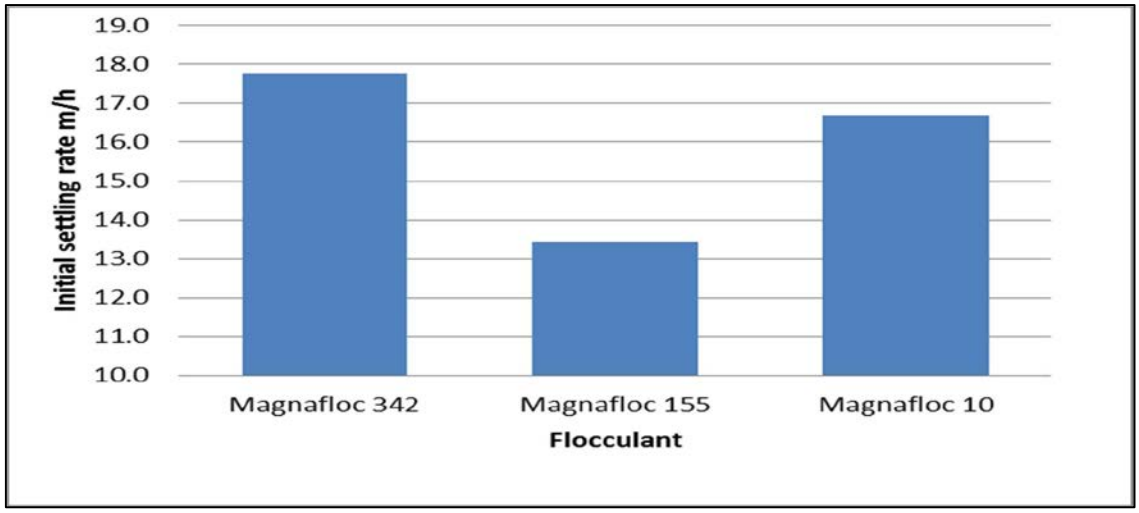

Figure 117: Settling rate of the 3 most effective flocculants for AO 324.

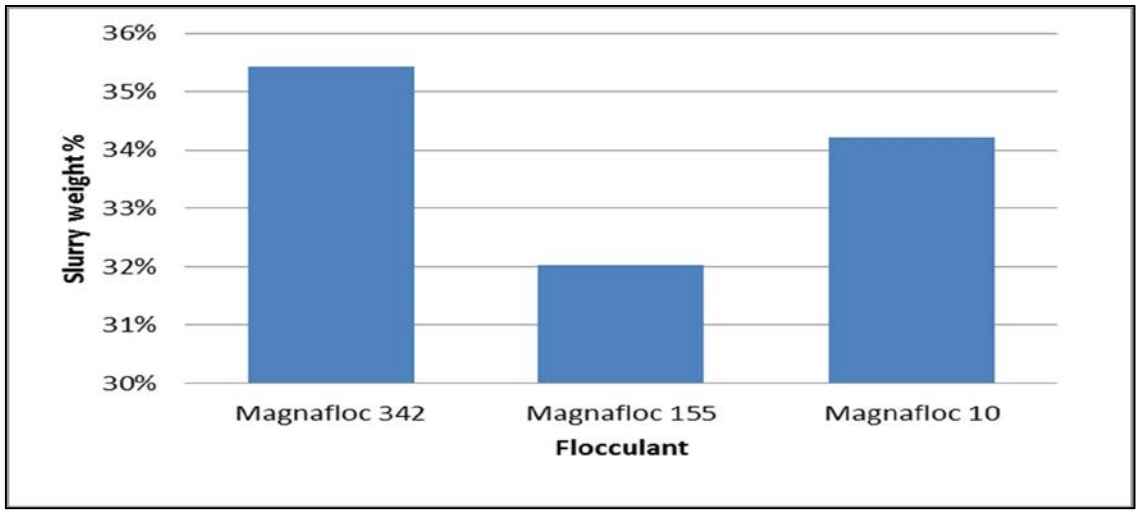

Figure 118: Slurry bed percentage of the 3 most effective flocculants for AO 324.

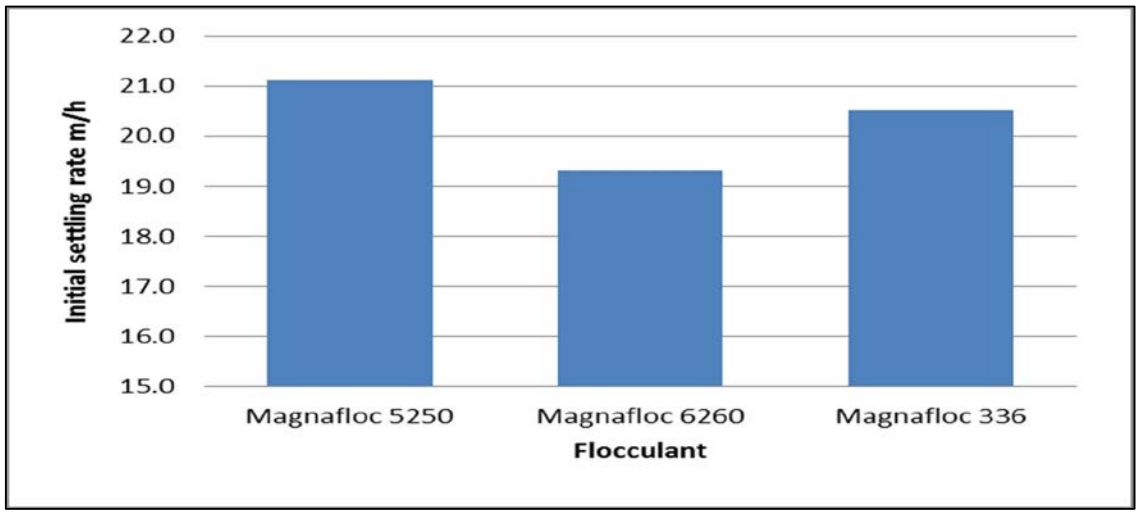

Figure 119: Settling rate of the 3 most effective flocculants for AO 325.

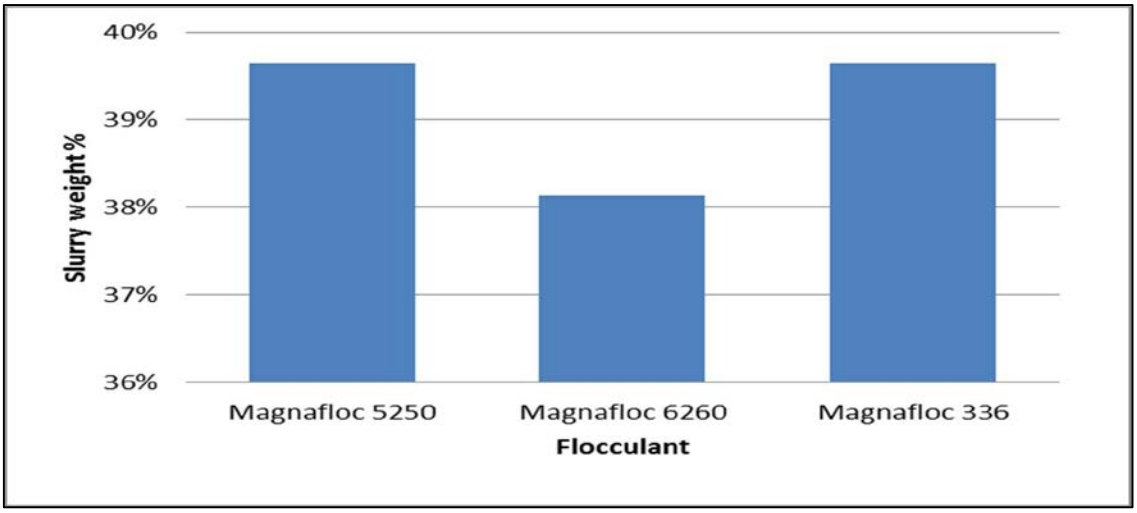

Figure 120: Slurry bed percentage of the 3 most effective flocculants for AO 325.

The settling rates and slurry bed depth of the 3 most effective flocculants for AO 326 is shown in Figure 121 and Figure 122, and Magnafloc 5250 had the best settling rate of 20 m/h along with a slurry bed weight percentage of 40%.

Kimberlite samples AO 327 and AO 328 were taken at different depths of 100 metres and 163 metres respectively within the same drilled hole. The settling rates and slurry bed compaction of the 3 most effective flocculants are shown in Figure 123 and Figure 124 for AO 327 and Figure 125 and Figure 126 for AO 328. Magnafloc 1011 had the best settling rate of 15 m/h and a slurry bed weight percentage of 30% for AO 327 while Magnafloc 10 achieved the best settling rate of 14 m/h and a slurry bed weight percentage of 28% for AO 328. The same trend is seen within this kimberlite where the slurry bed compaction increases when the smectite content is less, where AO 327 has a smectite content of 25%, while AO 328 has a smectite content of 60%.

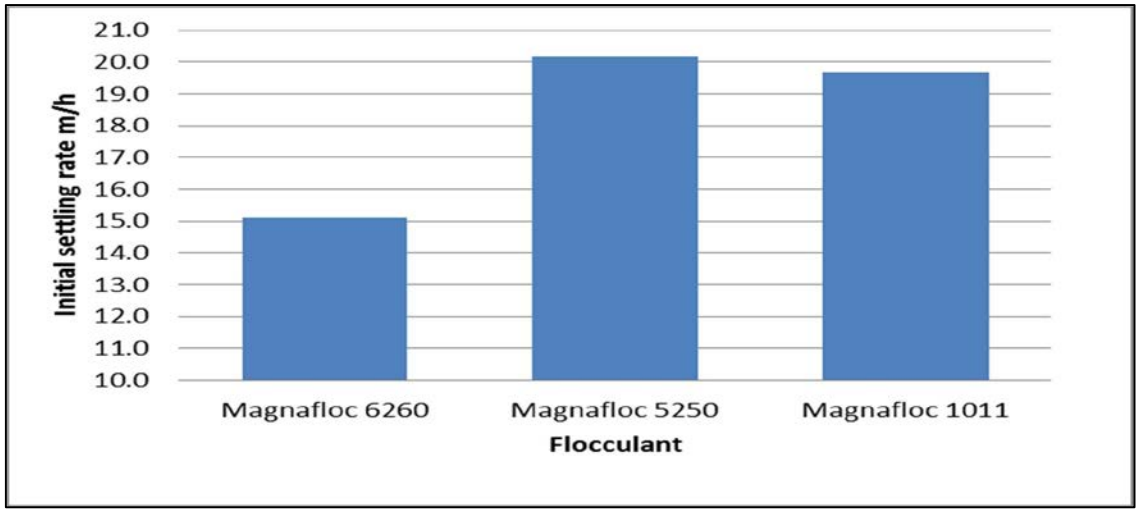

Figure 121: Settling rate of the 3 most effective flocculants for AO 326.

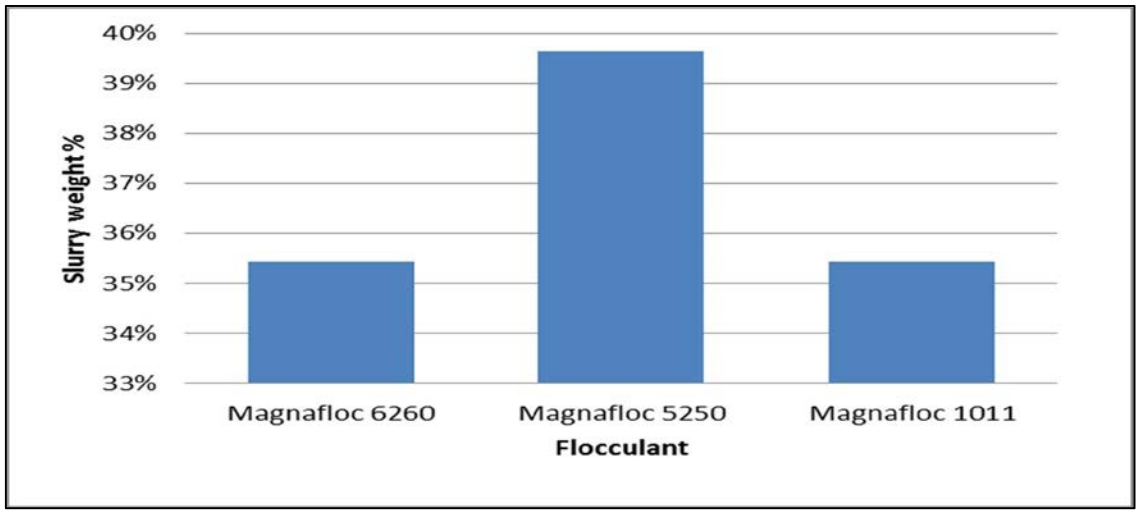

Figure 122: Slurry bed percentage of the 3 most effective flocculants for AO 326.

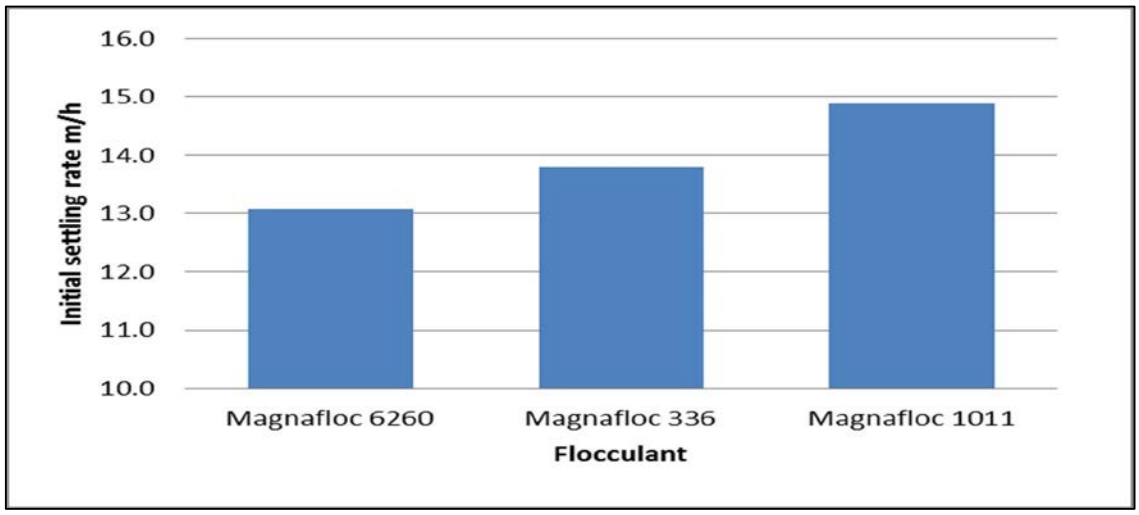

Figure 123: Settling rate of the 3 most effective flocculants for AO 327.

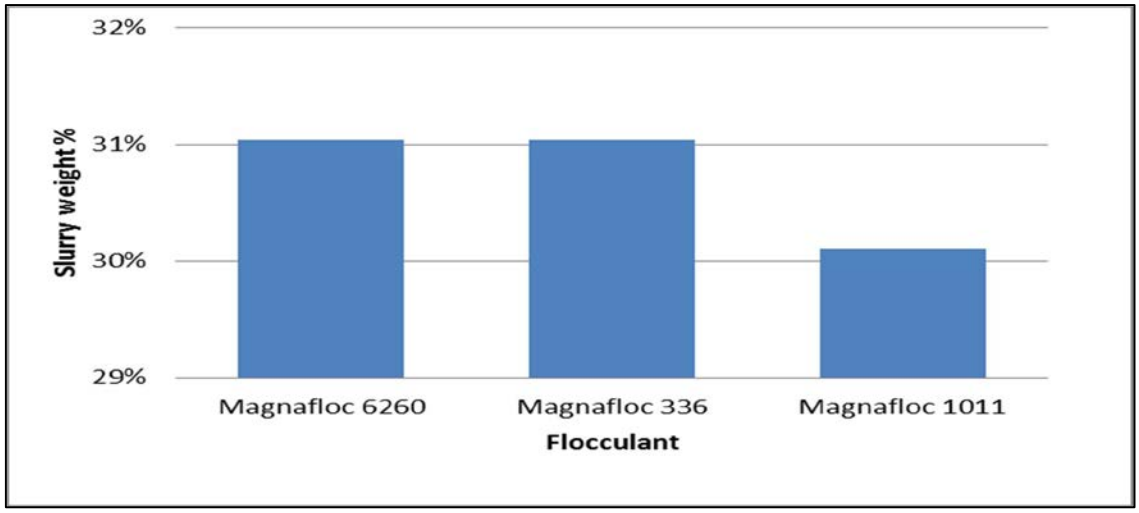

Figure 124: Slurry bed percentage of the 3 most effective flocculants for AO 327.

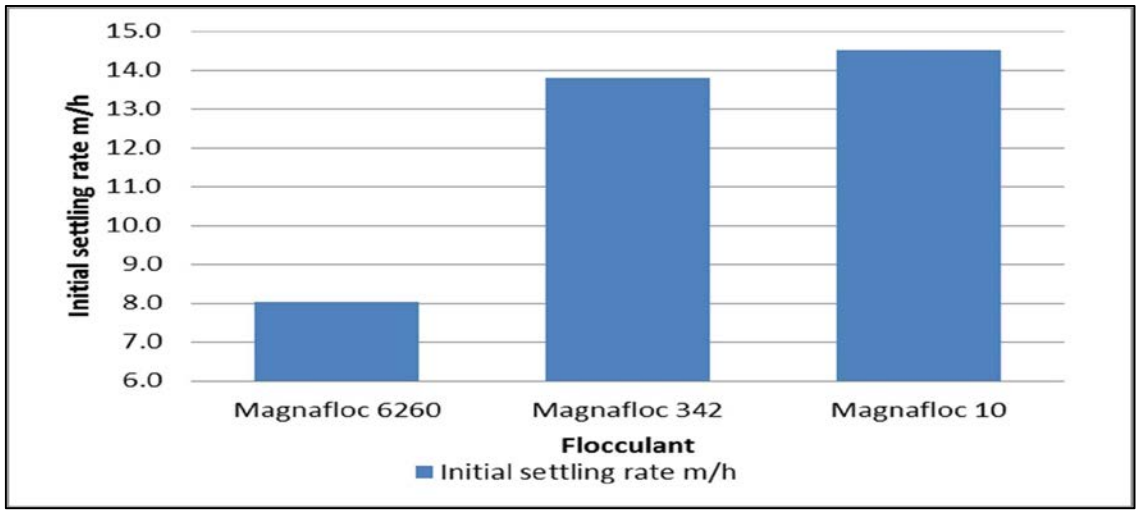

Figure 125: Settling rate of the 3 most effective flocculants for AO 328.

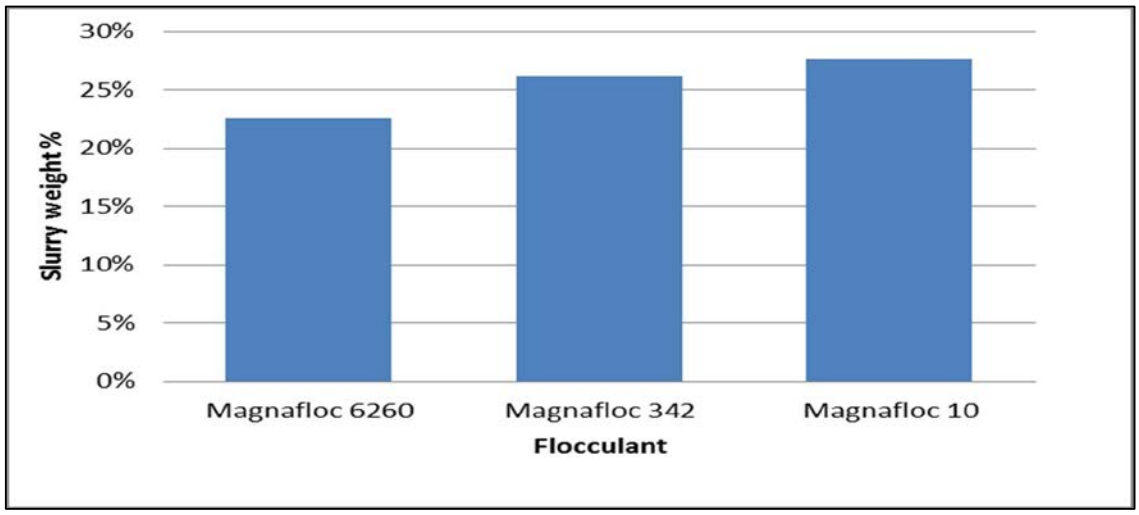

Figure 126: Slurry bed percentage of the 3 most effective flocculants for AO 328.

Two kimberlite samples, AC 56-5-1 and Venetia Red, did not settle with any of the flocculants. These two kimberlites have the highest ESP values of 30% and 43% respectively as well as high slurry pH values of 10.6. Anionic flocculants produced faster settling rates than the non-ionic flocculants, regardless of the smectite percentage in the kimberlite. Anionic flocculants produced acceptable settling rates of more than 10 m/h (Nguyen and Boger, 1998; de Kretser, 1995; O Gorman and Kitchener, 1974) for every kimberlite sample with the lowest being 12 m/h and the highest being 25 m/h. The slurry bed weight percentages ranged between 28% and 48% with an average slurry weight percentage of 35%, which is significantly higher than the industry norm of between 20% and 22% weight percentage (Nguyen and Boger, 1998; de Kretser, 1995; O Gorman and Kitchener, 1974). The smectite percentage with depth within the kimberlite did however influence the slurry bed weight percentage of the kimberlite samples tested. The higher the smectite content in the kimberlite the lower the slurry bed weight percentage was.

5.4 Coagulant and flocculant optimisation test results

The cation and flocculant that had the fastest settling rate along with a high slurry bed weight percentage for each kimberlite sample is combined in order to conduct settling tests to try and find a correlation that can predict the settling behaviour of the kimberlite slurries. Figure 127 shows the settling rate comparison between the best cation, flocculant and a combination of the cation and flocculant during the settling tests for the AC kimberlites. A 10 m/h or higher settling rate is the accepted norm in the industry (Nguyen and Boger, 1998; de Kretser, 1995; O Gorman and Kitchener, 1974), and we can see that this was achieved when settling was done with only the flocculants for AC 1-1-1, AC 4-1A-1, AC 5-5-1, AC 5-5-2, AC 16-1-1 and AC 197-1-1. AC 56-5-1 and Venetia Red did not settle down with any of the flocculants. It was expected that the cation combined with the flocculant would also give acceptable settling rates of more than 10 m/h because of the combined effect of reducing the negative repulsive forces surrounding the particles and allowing more flocculant interaction, but this only occurred during the settling of AC 1-1-1 and AC 5-5-1, which had the lowest cation exchange capacities of all the kimberlites of 5 cmol/kg and 10 cmol/kg. This indicates that cation exchange or

cation charge balance could be detrimental to the settling behaviour of high smectite content kimberlites as the lowest smectite percentage is found in Venetia Red with 40% smectite content, while all the other samples range between 50% and 70% of smectite.

The weight percentages of the slurries for the cation, flocculant and the combined cation and flocculant settling tests for the AC kimberlite samples are shown in Figure 128 while the results for the AO kimberlites are shown in Figure 129. It was expected that the cation settling would have the highest slurry bed weight percentage followed by the cation/flocculant combination and the worst result would be the flocculant due to the different settling mechanisms of cation and flocculant assisted settling. This is evident in the results, as a 4% to 7% weight increase was found between the cation/flocculant combinations compared to the flocculant alone. All the slurry bed weight percentages were higher than the industry acceptable standard of between 20% and 22%.

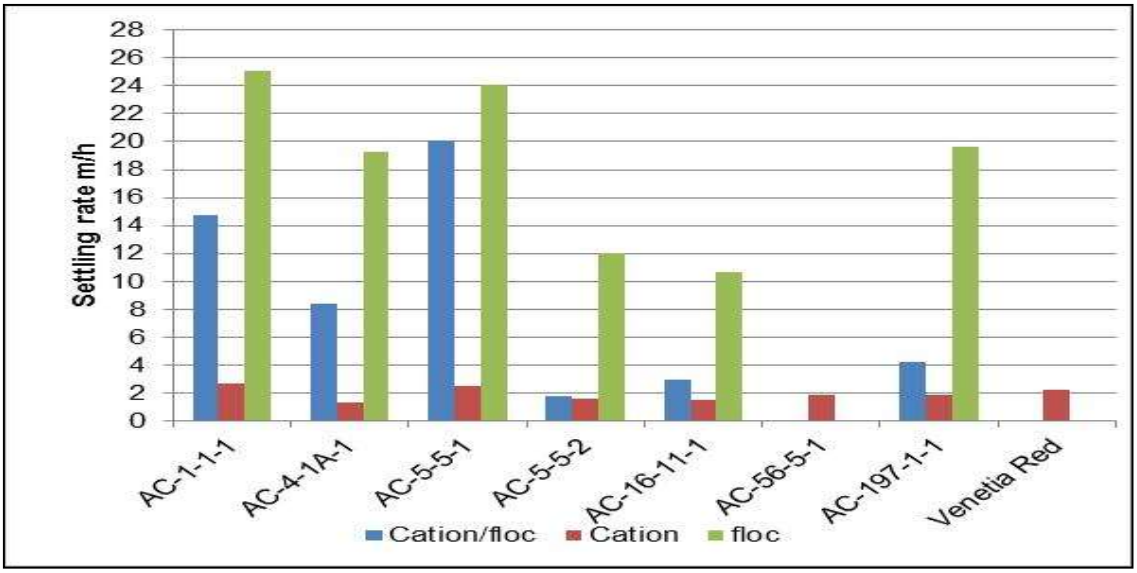

Figure 127: Comparison of the best cation, flocculant and a combination of the cation / flocculant settling rates of the AC kimberlites.

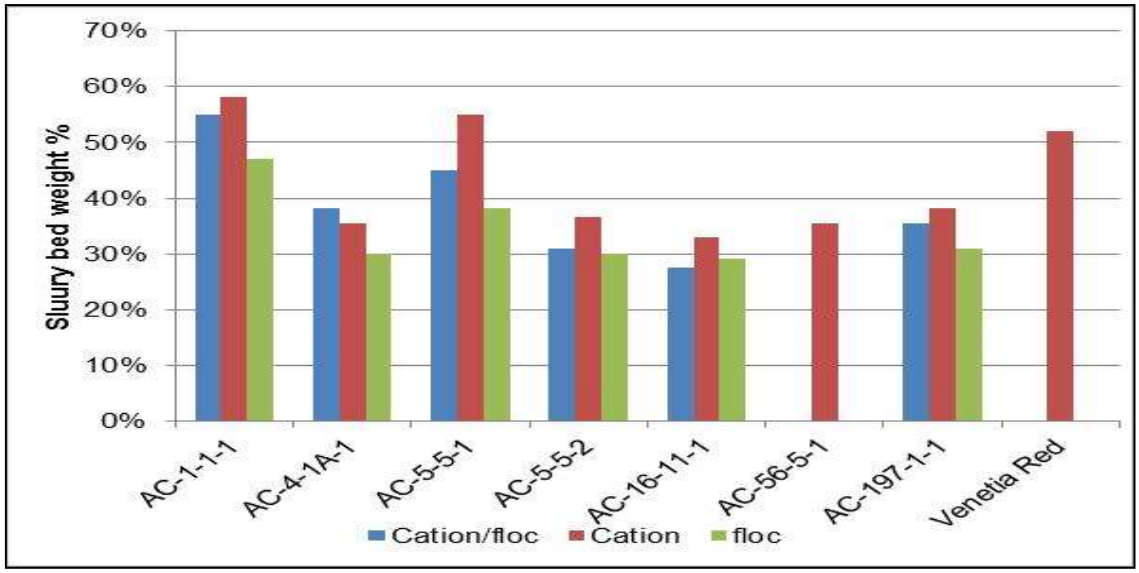

Figure 128: Comparison of the best cation, flocculant and a combination of the cation / flocculant bed depth of the AC kimberlites.

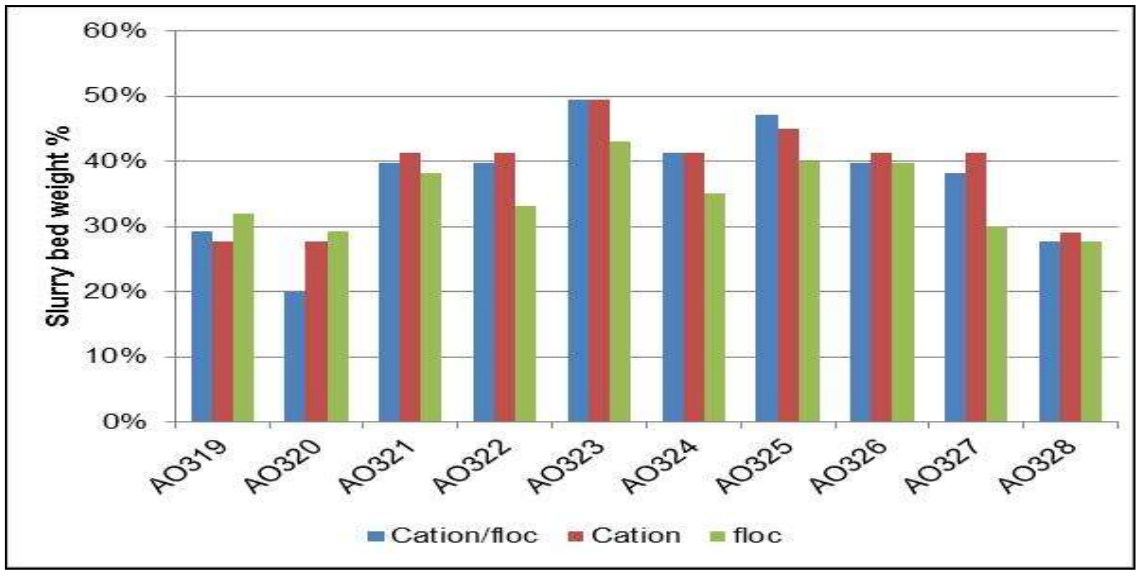

Figure 129: Comparison of the best cation, flocculant and a combination of the cation / flocculant bed depth of the AO kimberlites.

Figure 130 shows the settling rates for the most effective cation, flocculant and cation/flocculant combination for the AO kimberlite samples. The coagulant settling rates of the kimberlites were remarkably lower than the settling rates achieved with flocculant addition. As with the AC kimberlites we see that there are large differences in settling rates between the flocculant settling tests and the cation/flocculant settling tests, although we do note that AO 321, AO 324, AO 325

and AO 326 achieved acceptable settling rates of more than 10 m/h for the cation/flocculant combination while AO 327 reached a settling rate of 9.6 m/h. This trend could be related to the smectite percentage as the smectite content for these 4 kimberlites varies from 30% to 55%. AO 319, AO 320, AO 322 and AO 328 have smectite percentages of 60%, which is similar to the smectite percentages for the AC kimberlites, and this could indicate that cation addition to flocculant settling of kimberlites with more than 60 % smectite could be detrimental to the slurry settling rate.

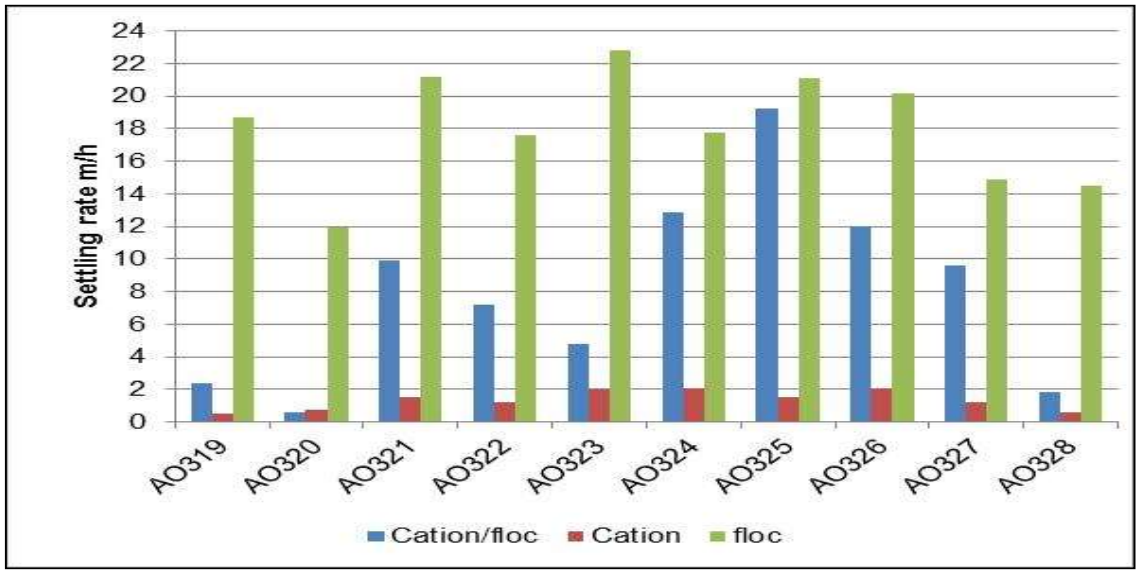

Figure 130: Comparison of the best cation, flocculant and a combination of the cation / flocculant settling rates of the AO kimberlites.

5.5 Repeatability of results

The repeatability of the test work was done by testing the settling rate in triplicate and slurry bed weight percentage of AO 322 kimberlite sample with $CuCl_2$-$2H_2O$, Magnafloc 366 and a combination of the latter.

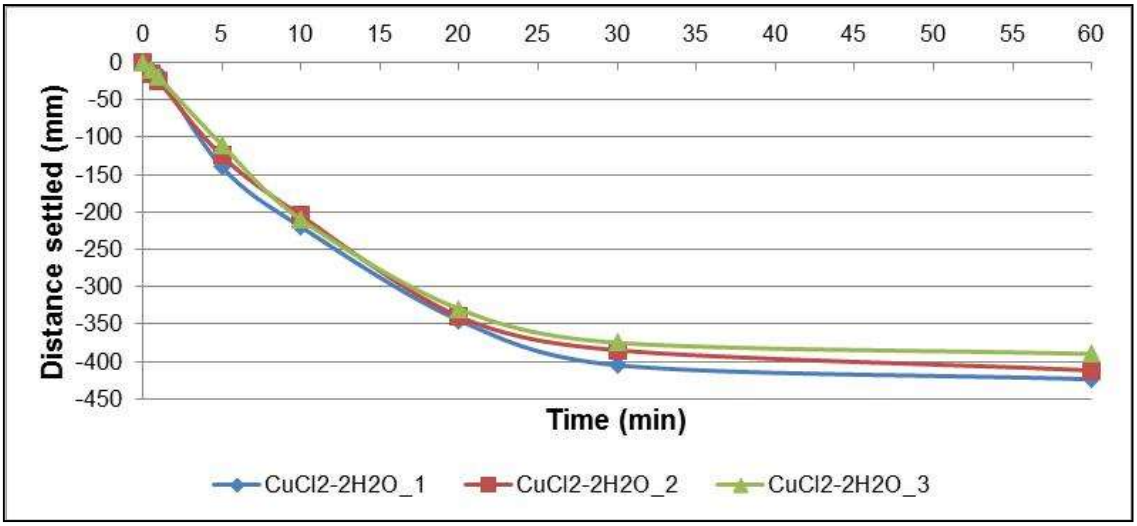

Figure 131: Repeatability of the settling tests was done in triplicate with 0.005M copper concentration. Tests were done on the AO 322 kimberlite sample.

The results in Figure 131, Figure 132 and Figure 133 show that all results consistently fall in a 5% interval for the settling rates and a 2% interval for the slurry bed weight percentage.

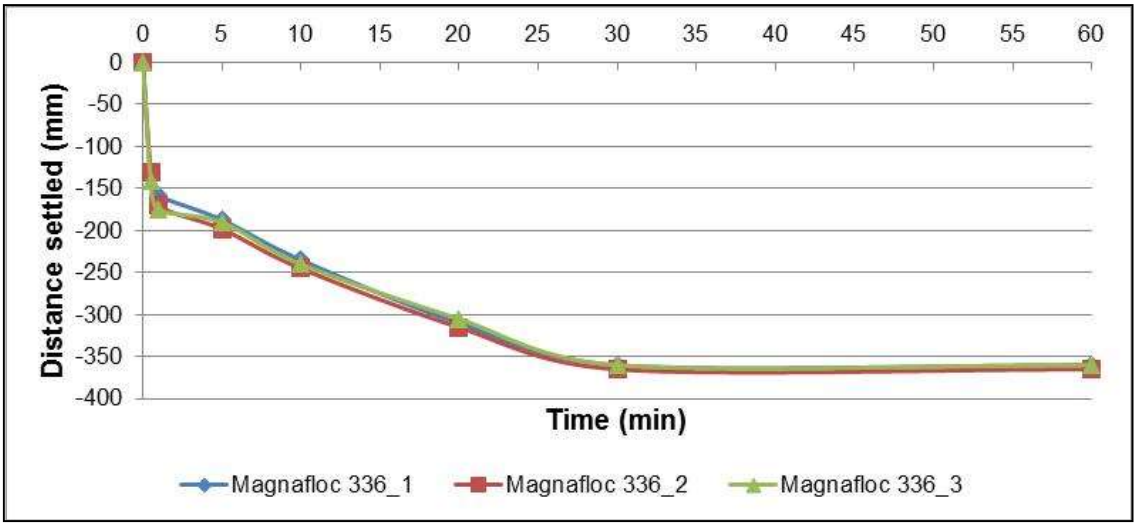

Figure 132: Repeatability of the settling tests was done in triplicate with 0.025% Magnafloc 336. Tests were done on the AO 322 kimberlite sample.

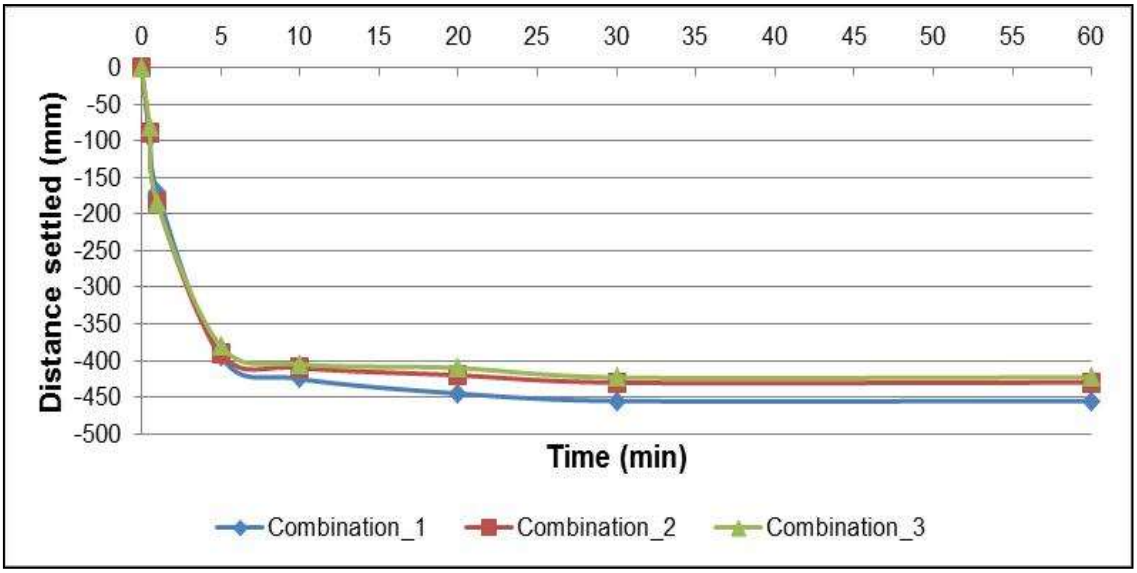

Figure 133: Repeatability of the settling tests was done in triplicate with a combination 0.005M copper and 0.025% Magnafloc 336. Tests were done on the AO 322 kimberlite sample.

6. Regression modelling

An online software package, Business Spreadsheets, Multiple Regression Analysis and Forecasting, was used for regression modelling of the coagulant and flocculant assisted settling of the kimberlite slurries. No regression modelling was possible with regards to natural settling as settling did not take place. The regression model was evaluated in terms of its standard error, σ, and R^2 adjusted where after the significance of the model was determined by the significance of F through the analysis of variance. The coefficients were evaluated on their respective P-values, where a P-value smaller than 5% was significant, based on a 95% confidence level. Coefficients with values larger than 5% were insignificant and the regression was run again with the remaining variables. This process was repeated until a significant model was found with significant coefficients.

The parameters that had the largest influence on the settling rate and slurry bed depth of the different kimberlite slurries were chosen to determine if a regression model exist that will predict how the slurries will react when cation, flocculant and a combination of both was used in the settling process.

Independent variables were chosen by evaluating the outside variables that had the largest influence on the settling process and evaluating the kimberlite characteristics that could have influenced the settling process. The dependent and independent variables that were chosen are listed in Table 19. The detailed data sheets are shown in Appendix 2.

Table 19: Dependent and Independent variables used for regression modelling

Dependent variables	**Independent variables**
Cation settling rate	Sodium percentage (Na) in kimberlite
Cation slurry bed depth	Potassium percentage (K) in kimberlite
Flocculant settling rate	Calcium percentage (Ca) in kimberlite
Flocculant slurry bed depth	Magnesium percentage (Mg) in kimberlite
Combined settling rate	Smectite percentage
Combined slurry bed depth	Cation exchange capacity (CEC)
	Exchangeable sodium percentage (ESP)
	pH of slurry solution
	Particle size distribution (PSD)

6.1 Cation settling rate regression model

No significant correlation could be found between cation settling and the nine independent variables. This indicates that a single parameter cannot be used to predict the settling behaviour of clay rich kimberlite slurries with cation addition.

6.2 Cation sediment bed depth

No significant correlation could be found between cation bed depth and the nine independent variables. This indicates that a single parameter cannot be used to predict the slurry bed depth of cation settled clay rich kimberlite slurries.

6.3 Flocculant settling rate

Two kimberlite samples, AC 56-5-1 and Venetia Red, did not settle out with any flocculant addition, but their data was included for regression modelling.

A significant correlation, F-Statistic of 6.89, was found between the flocculant settling rate of the kimberlite samples and the 9 independent variables. The adjusted R^2 was 0.75 with a standard error of 3.54. Only three variables, pH, and cumulative percentage passing 7.5 and 75 micron met the 95% confidence level, and these 3 variables were used in the next regression analysis. A significant correlation was found with the 3 independent variables with an improved F-statistic of 21.80, adjusted R^2 of 0.79 and a standard error of 0.55. The regression model for flocculant settling rate is shown in equation 12 and a comparison between the model and actual data is shown in Figure 134.

$$Flocculant\ settling\ rate\ (\frac{m}{h}) = -9.99pH - 0.92(7.5\ micron) + 0.63(75\ micron) + 89.52 \quad (12)$$

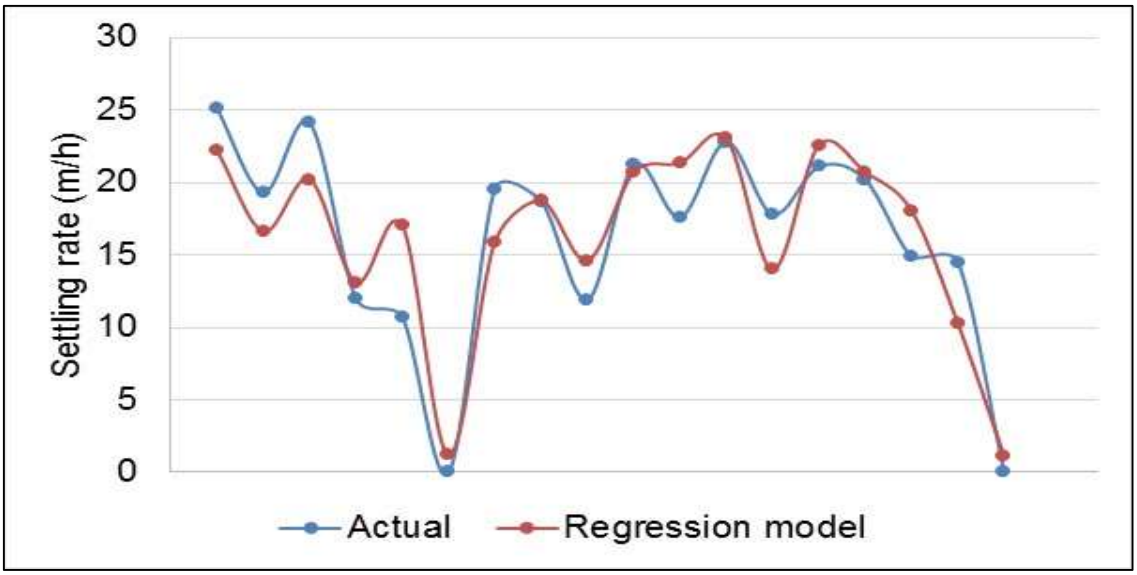

Figure 134: Regression model fit against actual data for the flocculant settling rate.

Particle size has the largest influence on the settling behaviour of kimberlite slurries with the addition of anionic flocculants and follows Stoke's law for settling behaviour.

6.4 Flocculant bed depth

Two kimberlite samples, AC 56-5-1 and Venetia Red, did not settle out with any flocculant addition, but their data was included for regression modelling.

The flocculant bed depth of the various kimberlite slurries had a significant correlation, F-statistic of 7.83, with the 9 independent variables with a standard error of 0.06 and an adjusted R^2 of 0.78. The pH of the slurries along with the cumulative percentage of particles passing 7.5 and 75 micron were the only independent variables that met the criteria of the 95% confidence level. It is interesting to note that the size of the slurry particles is significantly contributing to slurry bed depth, although two kimberlites, AC 56-5-1 and Venetia Red did not settle with any of the flocculants. A significant correlation was found with the 3 independent variables with an improved F-statistic of 25.56, adjusted R^2 of 0.81 and a standard error of 3.33. The regression model for flocculant settling rate is shown in equation 13 and a comparison between the model and actual data is shown in Figure 135.

$$Flocculant\ bed\ depth\ (\%) = -0.176pH - 0.016(7.5\ micron) + 0.012(75\ micron) + 1.513 \quad (13)$$

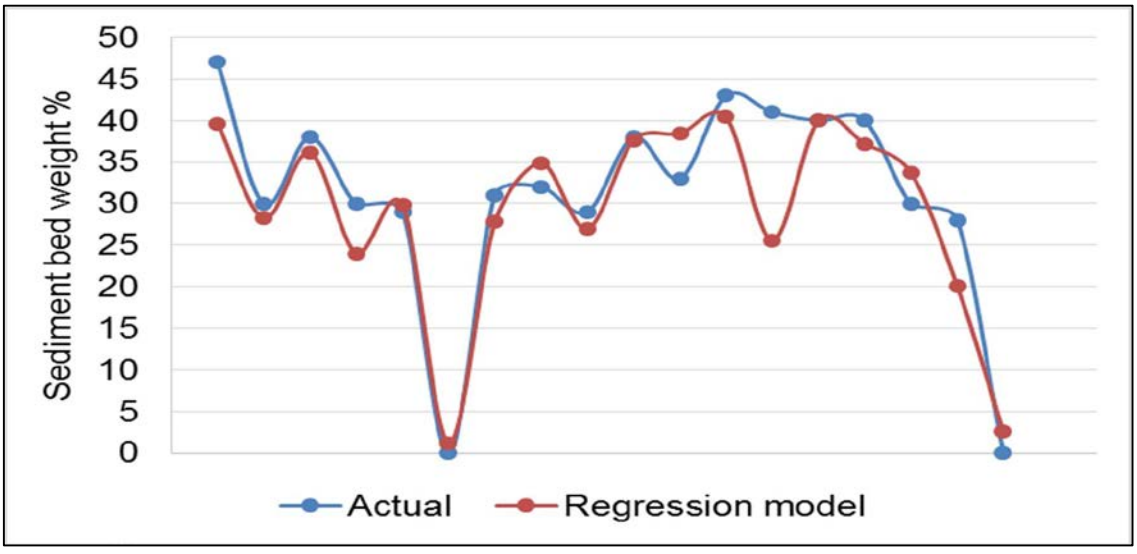

Figure 135: Regression model fit against actual data for the flocculant sediment bed.

Particle size has the largest influence on the slurry bed depth of kimberlite slurries with the addition of anionic flocculants.

6.5 Combined settling rate

No significant correlation could be found between cation bed depth and the 9 independent variables.

6.6 Combined sediment bed depth

The settling rate of the kimberlite slurry bed depth after settling with a combination of flocculants and cations showed a significant correlation with the 9 independent variables. The F-statistic was 9.37 with an adjusted R^2 of 0.82 and standard error of 0.06. The pH value of the kimberlite slurries, combined with the cumulative percentage of the particles smaller than 7.5 and 75 micron were significant independent variables based on the 95% confidence level. A significant correlation was found between the combined slurry bed depth and 3 independent variables with an F-statistic of 29.93, adjusted R^2 value of 0.84 and a standard error of 0.06. The regression model for the combined settling bed depth is shown in equation 14 and a comparison between the model and actual data is shown in Figure 136:

$$Combined\ bed\ depth\ (\%) = -0.208pH - 0.020(7.5\ micron) + 0.013(75\ micron) + 1.892 \quad (14)$$

Particle size has the largest influence on the slurry bed depth of kimberlite slurries with the addition of cations and anionic flocculants.

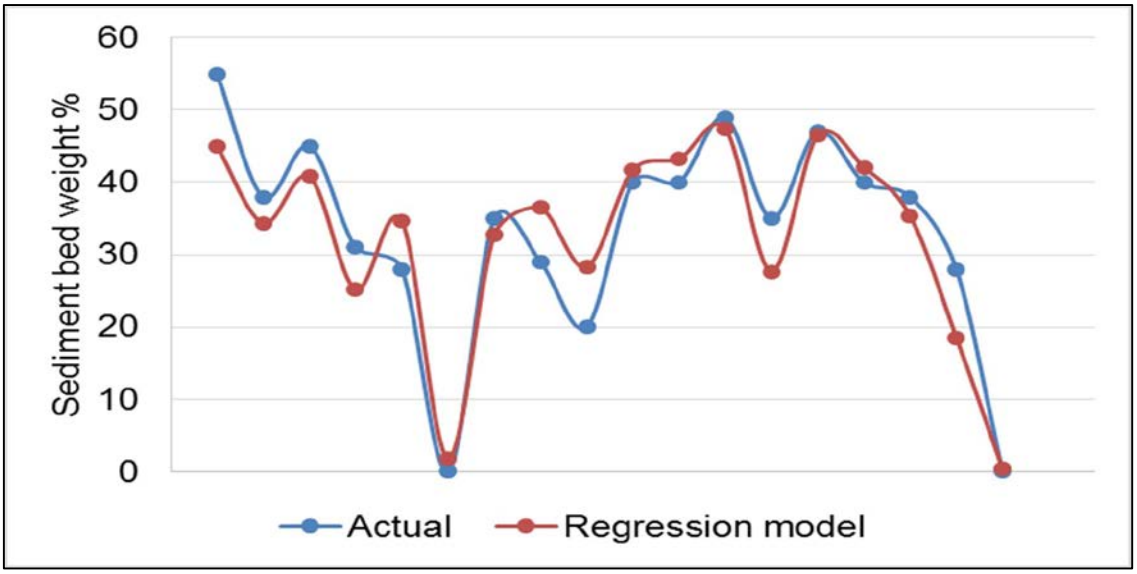

Figure 136: Regression model fit against actual data for the combined cation/flocculant sediment bed.

7. Conclusion

Settling behaviour is usually predicted from a theoretical point of view by the particle size distribution and Stokes law for single particles. It is usually assumed that a finer particle size distribution of the kimberlite slurry will be more difficult to settle.

In this study the settling behaviour of 17 kimberlites from Angola and 1 kimberlite from South Africa was investigated. For particle size analysis the Malvern results showed on average 27% of the slurry particles were passing 7.5 micron and 80% of the particles were passing 75 micron. Two kimberlites, AC 1-1-1 and AC 5-5-1, settled out naturally with 27% of the fine particles passing 7.5 micron and 81% and 82% of the particles passing 75 micron.

Vietti (2004) proposed that kimberlites will experience colloidal stability during natural settling when the exchangeable sodium percentage in the kimberlite is higher than 15% and the pH of the slurry is between 9 and 11. The pH values of all eighteen kimberlite slurries were between 9 and 11 in this case. The exchangeable sodium percentage of the kimberlites however ranged from 0.6 % to 43 %. The two kimberlites that settled out naturally, AC 1-1-1 and AC 5-5-1, had ESP values of 2.1% and 2.9% respectively, which conforms to the proposed model of Vietti (2004). Six kimberlites experienced colloidal stability and had ESP values higher than 15% which fits the proposed model by Vietti (2004). The remaining 10 kimberlites had ESP values ranging between 0.6 % and 8 % and experienced colloidal stability during natural settling, contradicting the proposed model. These results indicate that the Exchangeable Sodium Percentage and pH model cannot be used to accurately predict natural settling of kimberlites.

The settling of colloidally stable slurries is only possible when the negative repulsive forces surrounding the particles are reduced by the addition of coagulants. The settling rate and slurry bed weight percentage for every kimberlite sample increased when di- and tri-valent cations, as opposed to monovalent cations, were used as coagulants. Settling rates of between 0.5 m/h and 2.5 m/h

were achieved for coagulant settling, which is less than the industry norm of 10 m/h. Slurry bed weight percentages ranged between 28% and 52% with an average slurry bed weight percentage of 40%, which is almost twice as much as the industry norm of 20% to 22%.

Flocculants are used in the industry to increase the settling rate of colloidally stable kimberlite samples. Anionic flocculants produced faster settling rates than the non-ionic flocculants, regardless of the smectite percentage in the kimberlite. Anionic flocculants produced acceptable settling rates of more than 10 m/h (Nguyen and Boger, 1998; de Kretser, 1995; O Gorman and Kitchener, 1974) for every kimberlite sample with the lowest settling rate of 12 m/h and the highest settling rate of 25 m/h. The slurry bed weight percentages ranged between 28% and 48% with an average slurry weight percentage of 35%, which is significantly higher than the industry norm of between 20% and 22% weight percentage (Nguyen and Boger, 1998; de Kretser, 1995; O Gorman and Kitchener, 1974). As the smectite percentage increase in the kimberlite, the slurry bed compaction decreased.

Flocculant and coagulant settling of colloidally stable slurries have different advantages and disadvantages associated with the process. A combination of the two processes could result in an overall superior outcome for the settling rate and the slurry bed depth of the kimberlite slurries. Cation coagulation along with anionic flocculation of kimberlites reduced the settling rate that was achieved with flocculant assisted settling alone. Faster settling rates were achieved when the anionic flocculant alone was used to settle the colloidally stable slurry. A 4 % to 7 % weight increase occurred in the slurry bed when cation coagulants were used together with the anionic flocculant to settle the colloidally stable slurry when compared to only flocculant settling - regardless of the percentage of smectite in the kimberlite. This can increase the water recovery and reduce the slurry dam footprint of diamond mines.

Regression modelling was done to identify if there are any critical parameters that can predict the settling characteristics of African kimberlites with the aid of coagulants and flocculants. For representation of the particle size two data points from the psd was utilised which represented the fine material and the coarser

material. These two data points were taken at 7.5 μm and 75 μm. The particle size and the pH of the slurry were identified as significant parameters in predicting flocculant assisted settling with an adjusted R^2 of 0.78 for the settling rate and an adjusted R^2 of 0.78 for the slurry bed depth. The regression fit equation for settling rate is given by:

$$Flocculant\ settling\ rate\ (\frac{m}{h}) = -9.99pH - 0.92(7.5\ micron) + 0.63(75\ micron) + 89.52$$

Particle size and pH of the slurry are significant parameters for predicting the slurry bed depth of the combined cation/flocculant assisted settling of kimberlite slurries with an adjusted R^2 of 0.82.

No significant relationships could be found for cationic settling of the kimberlite slurries and the resultant slurry bed depth or for the combined cation and flocculant settling rate of the kimberlite slurries.

A single parameter could not be isolated to predict the settling behaviour of clay-rich kimberlite slimes. The combined CEC and ESP value, a CEC value higher than 30 and an ESP value higher than 25%, could possibly be important to identify non-settling kimberlites (with flocculants).

The regression data showed a correlation between pH and the two particle size data points and these three values can be used as an indication of settling behaviour.

8. References

Addai–Mensah, J., 2007, *Enhanced flocculation and dewatering of clay mineral dispersions*, Powder Technology, Elsevier

Besra, L., Sengupta, D.K., Roy, S.K., Ay, P., 2002, *Studies of flocculation and dewatering of kaolin suspensions by anionic polyacrylamide flocculant in the presence some surfactants*, Journal of Minerals Processing 66, p.p. 1 – 28

Bland, W., Rolls, D., 1998, *Weathering: An introduction to the scientific principles*, Arnold Publishers

Box G.E.P., Hunter J.S., 1957, *Multi-factor experimental design for exploring response surfaces*, Annals of Mathematic Statistics, 28 (1), March, 195-241

Box G.E.P., Wilson K.B., 1951, *On the experimental attainment of optimum conditions,* J. Royal Stat. Soc., Series B, 13 (1), 1-45.

Bühmann, D., 1998, *Clay Workshop*, The mineralogical Association of South Africa, Council for Geoscience

Clark, IH, 1983, *The weathering of Venetia kimberlite*, DRL Report E65/002/001
Dawson, J.B., 1980, Kimberlites *and their Xenoliths*, Springer-Verlag, Berlin Heidelberg New York

Coe H.S., Clevenger G.H., 1916, *Methods for determining the capacities of slime settling tanks,* TRANS, AIME, 55, p.p. 356 - 384

Dawson, J.B., 1980, *Kimberlites and their Xenoliths*, Springer-Verlag, Berlin Heidelberg New York.

de Kretser R.G., 1995, *The rheological properties and de-watering of slurried coal mine tailings.* Ph.D. Dissertation, University of Melbourne, Melbourne, Australia

Department of Water Affairs and Forestry (1996) South African Water Quality Guidelines, Second Edition, Volume 1: Domestic use

Derjaguin, B.V., Landau, L.D., 1941, *Theory of the Stability of Strongly Charged Lyophobic Sols and of the adhesion of Strongly Charged Particles in Solutions of Electrolytes*, Acta Physico-chimica of the USSR 14: p.p. 633 -622

Greenwood, N.N., Earnshaw, A., 1997, *Chemistry of the elements*, Second edition, Butterworth-Heinemann

Gregory, J., 1985, *The use of polymeric flocculants*, Proceedings of the Engineering Foundation Conference on Flocculation, Sedimentation and Consolidation, The Clister Sea Island, Georgia, USA, p.p. 125 – 137

Gregory, J., 1987, *Flocculation by polymers and polyelectrolytes*, Tadros, Th.F (Ed.), Solid/liquid Dispersions, Academic Press, London, p.p. 163 – 181

Grim, R.E., 1968, *Clay Mineralogy*, Mcgraw Hill

Harlow, G.E., 1998, *The nature of diamonds*, Cambridge University Press in association with the American museum of Natural History

Healy, T.W., 1969, *Research in Colloid and Surface Chemistry*, Department of Physical Chemistry, University of Melbourne, Melbourne, Australia

Hodgson, I.M.J., 1981, *Hydrothermal Alteration of Kimberlite*, Imperial College of Science and Technology (LONDON SW7 2BP), Thesis in fulfilment of degree of Doctor of Philosophy, Department of Mineral Resource Engineering

Hopwood, JS., Pretorius, Webb, SM. 1975a. *The accelerated weathering of kimberlite*, De Beers Research Laboratory (DRL), Report no. DRL 75/9/2

Huang, J.Y., Dixon, J.B., 2000, *Flocculation behaviour and properties of Na-montmorillonite treated with four organic polymers*, Clay Science 11, p.p. 137 – 146

James, R.O., Healy, T.W.J., 1972a, *Adsorption of hydrolysable metal ions at the oxide – water interface: 11 Charge reversal of SiO2 and TiO_2 colloids by adsorbed Co(11), La(11) and Th(1V) as models system, Journal of Colloid and Interface Science 40, p.p. 53 – 63*

James, R.O., Healy, T.W.J., 1972b, *Adsorption of hydrolysable metal ions at the oxide – water interface: 111 A thermodynamic Model of Adsorption, Journal of Colloid and Interface Science 40, p.p. 65 – 81*

Johnson, S.B., Dixon, D.R., Scales, P.J., 1999, *The electrokinetic and shear yield stress properties of kaolinite in the presence of aluminium ions ,* Colloids and Surfaces 146, p.p. 281 -291

Kemmer, F.N., 1988, *The Nalco Water Handbook,* Second Edition, Nalco Chemical Company, McGraw – Hill

Klein, C., Hurlbut, CS., 1993, *Manual of Mineralogy*, Twenty-first Edition, John Wiley and Sons

Klimpel, R.R., 1997, *Introduction to chemicals used in particle systems*, ERC Particle Science and Technology, University of Florida

Krause, B., 2008, *Solid-Liquid separation technology selection considerations for a shear sensitive ore,* Technical note, Ticor South Africa

Kosmulski, M., Dahlsten, P., 2006, *High ionic strength electrokinetics of clay minerals*, Colloids and Surfaces A: Physiochem. Eng. Aspects 291, p.p. 212 – 218

Lagaly, G., 1993, *From clay mineral crystals to colloidal clay mineral dispersions*, Coagulation and Flocculation: Theory and Applications, p.p. 427 – 493, B. Dobias (Ed)

Lester D.R., Usher S.P., Scales P.J, 2005, *Estimation of the hindered settling function (φ) from batch-settling tests,* AIChE Journal 51, p.p. 1158 – 1168

Luckham, P.F., Rossi, S., 1999, *The colloidal and rheological properties of bentonite suspensions*, Advances in Colloid and Interface Science 82, p.p. 43 – 92

Madsen, F.T., Müller-Vonmoos, M., 1989, *The swelling behaviour of clays*, Applied Clay Science 4, p.p. 143-156, Elsevier Science Publishers

McFarlane, A., Bremmel, K., Addai-Mensah, J., 2005a, *Microstructure, rheology and dewatering behaviour of smectite dispersions during orthokinetic flocculation*, Minerals Engineering 18, p.p. 1173 – 1182

McFarlane, A., Bremmel, K., Addai-Mensah, J., 2005b, *Optimising the dewatering behaviour of clay tailings through interfacial chemistry, orthokinetic flocculation and controlled shear*, Powder Technology 160, p.p. 27 – 34

McFarlane, A., Bremmel, K., Addai-Mensah, J., 2006, Improved dewatering behaviour of clay minerals dispersions via interfacial chemistry and particle interactions optimisation, Journal of Colloid and Interface Science 293, p.p. 116–127

Mitchell RH, 1986, *Kimberlites: Mineralogy, Geochemistry and Petrology*, New York Plenum Press.

Moore, D. M., Reynolds, R.C., 1989, *X-Ray Diffraction and the identification and analysis of Clay minerals*, Oxford University Press

Morkel J, 2005, *Kimberlite weathering: Mineralogy and Mechanism*, Dissertation for Philosophae doctorate, University of Pretoria, Pretoria, South Africa

Moss, N. & Dymond, B., 1978, *Flocculation: Theory and application*, Mine and Quarry Journal

Mpofu, P., Addai-Mensah, J., Ralston, R., 2003a, *Investigation of polymer structure type on flocculation, rheology and dewatering behaviour of kaolinite dispersions*, International Journal of Mineral Processing 71, p.p. 247 – 268

Mpofu, P., Addai-Mensah, J., Ralston, R., 2003b, *The influence of hydrolysable metal ions in the interfacial chemistry, particle interactions and dewatering behaviour of kaolinite dispersions*, Journal of Colloid and Interface Science 261, p.p. 349 – 359

Mpofu, P., Addai-Mensah, J., Ralston, R., 2004, *Flocculation and dewatering behaviour of smectite dispersions: effect of polymer structure type*, Minerals Engineering 17, p.p. 411 – 423

Mpofu, P., Addai-Mensah, J., Ralston, R., 2005, *Interfacial chemistry, particle interactions and improved dewatering behaviour of smectite clay dispersions*, International Journal of Mineral Processing 75, p.p. 155 – 171

Napier-Munn, TJ, 2008, *An Introduction to Comparative Statistics and Experimental Design for Mineral Engineers*, Course notes, 2nd Edition Version 6.2, p.p 40 - 55

Nguyen, Q.D., Boger, D.V., 1985, *Direct yield stress measurement with the vane technique,* Journal of Rheology 29, p.p. 335 – 347

Nguyen, Q.D., Boger, D.V., 1998, *Rheology to solving tailings disposal problems,* International Journal of Mineral Processing 54, p.p. 217 – 233

O' Gorman J.V. and Kitchener, J.A., 1972, *An Investigation of the Colliodal Properties and De-watering of Kimberlite Slimes*, Fine Particle Technology Project, Dept. of Mining and Mineral Technology, Imperial College, London

O' Gorman J.V. and Kitchener, J.A., 1974, *The flocculation and de-watering of kimberlite clay slimes*, International Journal of Minerals Processing 1, p.p. 33 – 49

Olivier, W, 2006, *Investigating the settling of kimberlite in the presence of cation salts,* Final year thesis, University of Pretoria, Pretoria, South Africa

Pieters, R, 2006, *The effect of organic compounds on kimberlite weathering,* Final year thesis, University of Pretoria, Pretoria, South Africa

Rawle, A, 2012, *Basic principles of particle size analysis,* ATA Scientific publication, Australia

Richens, D.T., 1997, *The Chemistry of Aqua Ions: Synthesis, structure and reactivity*, John Wiley and Sons, United Kingdom

Richards, L.A., 1969, *Diagnosis and improvement of saline and alkali soils,* US Department Agriculture Handbook No. 60

Schlegal, M.L., Charlet, L., Manceau, A., 1999, *Sorption of Metal Ions on Clay Minerals: 11. Mechanism of Co Sorption on Hectorite at High and Low Ionic Strength and Impact on the Sorbent Stability*, Journal of Colloid and Interface Science 220, p.p. 392 – 405

Sheiner, B.J., Smelly, A.G., 1984, *Dewatering of fine particles mining wastes using polyethylene oxide flocculant*, Minerals and Metallurgical Processing, p.p. 71 -75

Skinner E.M.W., Clement C.R., 1979, *Mineralogical classification of southern African kimberlites*, in Boyd FR, Meyer HOA, eds, Kimberlites, Diatremes and Diamonds: Their geology, petrology and Geochemistry, American Geophysical Union, Washington

Sposito, G., 1984, *The Surface Chemistry of Soils*, Oxford University Press, Oxford, England

Svarovsky, L., 1981, *Solid – Liquid separation,* Second Edition, Butterworth's, London

Talmage W.P., Fitch E.B., 1955, *Determining thickener unit areas,* Industrial Engineering Chemistry 47, p.p. 38 - 41

Van Olphen, H., 1977, *An introduction to clay colloidal chemistry*, John Wiley & Sons, New York

Vatta, L, 2001, *Water quality standards and guidelines for wastewater discharge,* DRL interim report, R2001.02.03

Verwey, E.J.W, Overbeek, J.T.G, 1948, *Theory of the stability of Lyophobic Colloids,* Elsievier Amsterdam

Vietti, A.J., 1994, *Clay – Water – Flocculant Interaction*, De Beers Diamond Research Laboratory, Report no. E66/005/006

Vietti, A.J., Dunn, F., 2003, *Paste and Thickened Tailings Disposal Handbook*, De Beers Technical Support Services: p.p. 25 – 69

Vietti, A.J., 2004, *Know you chemistry-Suspension and Compaction behaviour of Paste*, International seminar on Paste and Thickened Tailings, Cape Town, South Africa

Wang, C.C., Juang, L.C., Lee, C.K., Hsu, T.C., Lee, J.F., Chao, H.P., 2004, *Effects of exchanged surfactant cations on the pore structure and adsorption characteristics of montmorillonite*, Journal of Colloid and Interface Science 280, p.p. 27 – 35

Wills B.A., 1997, *Mineral Processing Technology*, 6th edition, p.p. 369 – 375

Wilson, M.G.C., Anhaeusser, C.R., 1998, *The mineral resources of South Africa*, Sixth Edition, Handbook 16, Council for Geoscience, p.p. 232-258.

Yamanaka S, Brindley GW, 1977, *Hydroxy-nickel interlayering in montmorillonite by the titration method,* Clays and Clay Minerals, Vol. 26, No. 1, p.p. 21-24, 1978

Yamanaka S, Numata K, Hattori M, 1987, *Hydroxy-copper interlayering in montmorrilonite by the titration method,* Proceedings of the International Clay Conference, Denver, pp 273-276

Ye, C., Wang, D., Shi, B., Yu, J., Qu, J., Edwards, M., Tang, H., 2006, *Alkalinity effect of coagulation with polyaluminum chlorides: Role of electrostatic patch*, Colloids and Surfaces A: Physiochem. Eng. Aspects 294, p.p. 163 - 173

Appendix A

Table 20: Sample classification and depth from which the sample were extracted from

Sample number	Kimberlite type	From (m)	To (m)	Hole number
AC-1-1-1	Hypabyssal kimberlite			
AC-4-1A-1	Tuffisitic kimberlite			
AC-5-5-1	Hypabyssal kimberlite			
AC-5-5-2	Tuffisitic kimberlite			
AC-16-11-1	Tuffisitic kimberlite			
AC-56-5-1	Resedimented Volcaniclastic kimberlite			
AC-197-1-1	Volcaniclastic kimberlite			
Venetia Red	Red kimberlite			
AO 319	Primary Volcaniclastic kimberlite	115,43	116.41	TCH031H06
AO 320	Resedimented Volcaniclastic kimberlite	29,56	30,37	TCH031H06
AO 321	Volcaniclastic kimberlite	136,36	137.16	TCH032H01
AO 322	Sandy Resedimented Volcaniclastic kimberlite	91,72	92,56	TCH032H01
AO 323	Crater Facies Sediment	29,56	30,59	TCH032H01
AO 324	Primary Volcaniclastic kimberlite	339,70	340.98	ITE066H01
AO 325	Crater Facies Sediment	103,74	104,56	ITE066H01
AO 326	Primary Volcaniclastic kimberlite	89,41	90.76	ITE064H01
AO 327	Resedimented Volcaniclastic kimberlite	100,36	101.14	TCH030H01
AO 328	Primary Volcaniclastic kimberlite	163,03	163,64	TCH030H01

Table 21: Results of XRF analysis done at the University of Pretoria on the ore samples tested (proportions by mass).

Sample name	Na_2O	MgO	Al_2O_3	SiO_2	P_2O_5	K_2O	CaO	TiO_2	Fe_2O_3	MnO
	%	%	%	%	%	%	%	%	%	%
AC-1-1-1	0.01	20.63	4.10	25.54	1.36	0.61	15.34	4.70	15.18	0.27
AC-4-1A-1	0.01	17.47	2.71	62.81	0.15	0.23	3.19	0.86	5.25	0.06
AC-5-5-1	0.01	29.35	3.73	35.33	0.66	0.15	5.91	1.03	9.49	0.14
AC-5-5-2	0.01	25.82	4.12	38.99	0.56	0.25	7.19	0.90	8.50	0.10
AC-16-11-1	0.00	24.52	2.30	41.29	0.18	0.26	6.73	1.44	9.60	0.18
AC-56-5-1	0.58	18.92	7.15	51.10	0.34	1.68	4.54	1.16	6.27	0.10
AC-197-1-1	0.00	20.68	2.89	26.01	1.19	0.21	17.24	1.35	9.50	0.47
AO319	0.60	18.69	6.16	44.45	0.20	0.82	5.72	2.16	13.70	0.18
AO320	0.55	17.86	4.57	43.71	0.49	1.47	8.16	1.99	11.07	0.23
AO321	1.98	4.14	10.99	65.44	0.09	1.96	2.89	0.54	8.80	0.06
AO322	0.85	10.97	7.12	56.61	0.14	1.25	5.37	0.56	8.51	0.12
AO323	0.82	0.65	8.65	80.49	0.23	4.05	0.81	0.34	2.38	0.05
AO324	0.98	15.29	6.96	41.59	0.66	0.46	11.77	1.89	12.35	0.16
AO325	0.97	2.53	7.24	80.04	<0.01	1.89	2.23	0.26	2.20	0.03
AO326	0.72	15.70	6.93	52.37	0.14	2.49	3.89	0.84	9.58	0.11
AO327	0.88	1.77	12.72	65.29	0.07	5.40	3.86	0.53	4.82	0.08
AO328	0.11	16.10	6.04	45.15	0.21	0.75	10.12	1.21	14.11	0.18
Venetia Red	1.09	19.60	8.37	51.10	0.18	1.86	4.46	0.72	8.79	0.10

Table 22: The XRD analyses on the Alto Cuilo kimberlites done at the University of Pretoria

Sample	Mineral group / mineral identified	Probable mineral	Estimated Quantity[Mass %]
AC 1-1-1	Smectite		40 - 50
	Chlorite		30 -35
	Calcite		10 - 15
	Pyroxene	Diopside	~ 5
	Serpentine	Lizardite	~ 5
AC 4-1A-1	Smectite		70 - 75
	Quartz		~ 10
	Annite		6 - 8
	Calcite		~ 6
	Kaolinite		< 4
	Hematite		< 3
AC 5-5-1	Smectite		40 - 50
	Chlorite		30 -35
	Calcite		10 - 15
	Pyroxene	Diopside	~ 5
	Serpentine	Lizardite	~ 5
	Hematite		~ 5
AC 5-5-2	Smectite		60 - 70
	Kaolinite		~ 10
	Calcite		< 10
	Annite		< 10
	Pyroxene	Diopside	~ 5
	Orthoclase		< 5
	Plagioclase		< 2

AC 16-11-1	Smectite		65 - 70
	Chlorite		10 - 15
	Calcite		~ 10
	Annite		~ 5
	Serpentine	Lizardite	< 5
	Hematite		< 2
	Quartz		~ 1
AC 56-5-1	Smectite		55 - 65
	Talc		~ 8
	Annite		~ 7
	Quartz		~ 7
	Calcite		~ 5
	Plagioclase		~ 5
	Orthoclase		~ 3
	Hematite		2 – 3
	Diopside		2 – 3
	Chlorite		~ 2
	Kaolinite		< 1
AC 197-1-1	Smectite		35 – 40
	Calcite		25 - 30
	Chlorite		5 - 10
	Kaolinite		5 - 8
	Hematite		~ 5
	Serpentine	Lizardite	< 5
	Pyroxene	Diopside	< 3
	Annite		< 3
	Orthoclase		< 2

Table 23: The XRD analyses on the Itengo/Tchegi kimberlites done at the University of Pretoria

AO 319	Smectite		55 - 60
	Pyroxene	Diopside	10 – 15
	Actinolite		~ 10
	Annite		~ 10
	Calcite		~ 3
	Orthoclase		~ 3
	Plagioclase		< 3
AO 320	Smectite		55 - 60
	Annite		~ 10
	Pyroxene	Diopside	~10
	Actinolite		6 - 8
	Calcite		~ 6
	Orthoclase		< 5
	Plagioclase		< 5
	Hematite		< 3
AO 321	Smectite		30 - 35
	Plagioclase		30 - 35
	Quartz		20 - 25
	Pyroxene	Diopside	~ 4
	Annite		~ 4
	Hematite		~ 3
	Calcite		2 - 3
AO 322	Smectite		55 - 60
	Quartz		~ 13
	Plagioclase		~ 10

	Calcite		~ 7
	Annite		~ 6
	Pyroxene	Diopside	~ 3
	Orthoclase		~ 3
	Hematite		~ 2
AO 323	Quartz		40 - 50
	Orthoclase		~ 20
	Smectite		~ 15
	Plagioclase		10 - 15
	Annite		~ 3
	Pyroxene	Diopside	~ 2
	Hematite		< 2
AO 324	Smectite		50 - 55
	Pyroxene	Diopside	20 -25
	Annite		~ 10
	Calcite		~ 5
	Plagioclase		< 5
	Hematite		< 4
	Actinolite		< 3
	Orthoclase		< 2
	Quartz		< 1
AO 325	Quartz		45 - 50
	Smectite		~ 30
	Plagioclase		10 -15
	Calcite		~ 5
	Orthoclase		< 4
	Pyroxene	Diopside	< 2

	Hematite		< 2
AO 326	Smectite		50 - 55
	Talc		10 – 20 ?
	Annite		~ 8
	Plagioclase		5 – 10
	Orthoclase		~ 5
	Pyroxene	Diopside	~ 5
	Actinolite		< 5
	Calcite		~ 3
AO 327	Quartz		~ 25
	Smectite		20 – 25
	Plagioclase		15 – 20
	Orthoclase		15 – 20
	Calcite		~ 5
	Annite		~ 5
	Pyroxene	Diopside	< 3
	Actinolite		< 3
	Hematite		< 2
AO 328	Smectite		55 - 60
	Pyroxene	Diopside	~ 15
	Actinolite		10 - 12
	Annite		~ 9
	Calcite		~ 4
	Orthoclase		< 4
	Hematite		~ 2
	Plagioclase		< 2

Venetia Red	Smectite		~ 40
	Quartz		~ 25
	Calcite		~ 10
	Feldspar	Albite	~ 10
	Serpentine	Lizardite	~ 10
	Mica	Phlogopite	~ 5
	Amphibole	Tremolite	< 5
	Magnetite		< 5

Table 24: Cation exchange capacity (CEC) and exchangeable sodium percentage (ESP) of the kimberlites

cmol(+)/kg	Na	K	Ca	Mg	T- Value (CEC)	ESP %	Clarity
AC-1-1-1	0.112	0.169	12.259	6.405	5.29	2.1	Good
AC-4-1A-1	0.333	0.645	35.109	20.891	45.17	0.7	Poor
AC-5-5-1	0.301	0.261	16.228	7.722	10.336	2.9	Good
AC-5-5-2	0.302	0.352	42.11	7.874	47.942	0.6	Poor
AC-16-11-1	1.8	0.534	26.601	13.408	31.351	5.7	Poor
AC-56-5-1	16.285	0.753	37.746	5.397	53.723	30.3	Poor
AC-197-1-1	3.16	0.224	19.846	6.773	18.622	17.0	Poor
AO319	13.772	1.114	51.233	5.948	66.898	20.6	Poor
AO320	1.852	1.631	47.862	19.102	59.177	3.1	Poor
AO321	3.446	0.956	62.698	12.756	67.933	5.1	Poor
AO322	0.576	0.735	28.007	10.263	30.964	1.9	Poor
AO323	0.173	0.681	8.706	4.054	12.955	1.3	Poor
AO324	9.718	0.502	52.932	4.15	56.311	17.3	Poor
AO325	0.344	0.473	24.066	6.453	21.733	1.6	Poor
AO326	1.582	0.863	46.369	14.814	53.283	3.0	Poor
AO327	1.465	1.815	21.827	4.92	18.316	8.0	Poor
AO328	15.809	1.11	53.633	10.645	76.646	20.6	Poor
Venetia Red	14	0.878	22.566	3.902	32.386	43.2	Poor

Table 25: The critical coagulant concentrations of the Alto Cuilo kimberlites and Venetia Red as reference kimberlite

		Cationic salt					
Sample	**Molar**	**KCl**	**CaCl2**	**MgCl2-6H2O**	**CuCl2-2H2O**	**FeCl3-6H2O**	**AlCl3**
AC1-1-1	**0.005**	++	++	++	+	++	++
	0.01	++	++	++	++	++	++
	0.02	++	++	++	++	++	-
	0.035	++	++	++	++	-	-
	0.05	++	++	++	++	-	-
AC4-1A-1	**0.005**	++	++	++	++	++	++
	0.01	++	++	++	++	++	++
	0.02	++	++	++	++	++	++
	0.035	++	++	++	++	++	++
	0.05	++	++	++	++	++	++
AC5-5-1	**0.005**	++	++	++	++	+	+
	0.01	++	++	++	++	++	++
	0.02	++	++	++	++	++	-
	0.035	++	++	++	++	-	-
	0.05	++	++	++	++	-	-
AC5-5-2	**0.005**	++	++	++	++	++	++
	0.01	++	++	++	++	++	++
	0.02	++	++	++	++	++	++
	0.035	++	++	++	++	++	++
	0.05	++	++	++	++	++	++
AC16-1-1	**0.005**	++	++	++	++	++	++
	0.01	++	++	++	++	++	++
	0.02	++	++	++	++	++	++
	0.035	++	++	++	++	++	++
	0.05	++	++	++	++	++	++

AC56-5-1	0.005	+	++	++	++	++	++
	0.01	++	++	++	++	++	++
	0.02	++	++	++	++	++	++
	0.035	++	++	++	++	++	++
	0.05	++	++	++	++	++	++
AC197-1-1	0.005	++	++	++	++	++	++
	0.01	++	++	++	++	++	++
	0.02	++	++	++	++	++	++
	0.035	++	++	++	++	++	++
	0.05	++	++	++	++	++	++
Venetia Red	0.005	-	++	+	++	++	++
	0.01	-	++	++	++	++	++
	0.02	+	++	++	++	++	++
	0.035	+	++	++	++	++	+
	0.05	++	++	++	++	++	+

Table 26: The critical coagulant concentrations of the Itengo/Tchegi kimberlites

		Cationic salt					
Sample	Molar	KCl	$CaCl_2$	$MgCl_2$-6H2O	$CuCl_2$-2H2O	$FeCl_3$-6H2O	$AlCl_3$
AO319	0.005	-	+	+	++	++	++
	0.01	+	++	++	++	++	++
	0.02	++	++	++	++	++	++
	0.035	++	++	++	++	-	++
	0.05	++	++	++	++	-	++
AO320	0.005	++	++	++	++	++	++
	0.01	++	++	++	++	++	++
	0.02	++	++	++	++	++	++
	0.035	++	++	++	++	++	++
	0.05	++	++	++	++	++	++
AO321	0.005	+	++	++	++	++	++
	0.01	++	++	++	++	++	++
	0.02	++	++	++	++	++	++
	0.035	++	++	++	++	++	++
	0.05	++	++	++	++	+	+

AO322	0.005	+	++	++	++	++	++
	0.01	+	++	++	++	++	++
	0.02	+	++	++	++	++	++
	0.035	++	++	++	++	++	++
	0.05	++	++	++	++	++	++
AO323	0.005	-	++	++	++	++	++
	0.01	+	++	++	++	++	++
	0.02	+	++	++	++	++	++
	0.035	+	++	++	++	++	++
	0.05	++	++	++	++	++	++
AO324	0.005	+	++	++	++	++	++
	0.01	++	++	++	++	++	++
	0.02	++	++	++	++	++	++
	0.035	++	++	++	++	++	++
	0.05	++	++	++	++	++	++
AO325	0.005	++	++	++	++	++	++
	0.01	++	++	++	++	++	++
	0.02	++	++	++	++	++	++
	0.035	++	++	++	++	++	++
	0.05	++	++	++	++	++	++
AO326	0.005	++	++	++	++	++	++
	0.01	++	++	++	++	++	++
	0.02	++	++	++	++	++	++
	0.035	++	++	++	++	++	++
	0.05	++	++	++	++	++	++
AO327	0.005	+	++	++	++	++	++
	0.01	+	++	++	++	++	++
	0.02	++	++	++	++	++	+
	0.035	++	++	++	++	+	-
	0.05	++	++	++	++	-	-
AO328	0.005	-	+	++	++	++	++
	0.01	+	++	++	++	++	++
	0.02	++	++	++	++	++	++
	0.035	++	++	++	++	++	++
	0.05	++	++	++	++	++	++

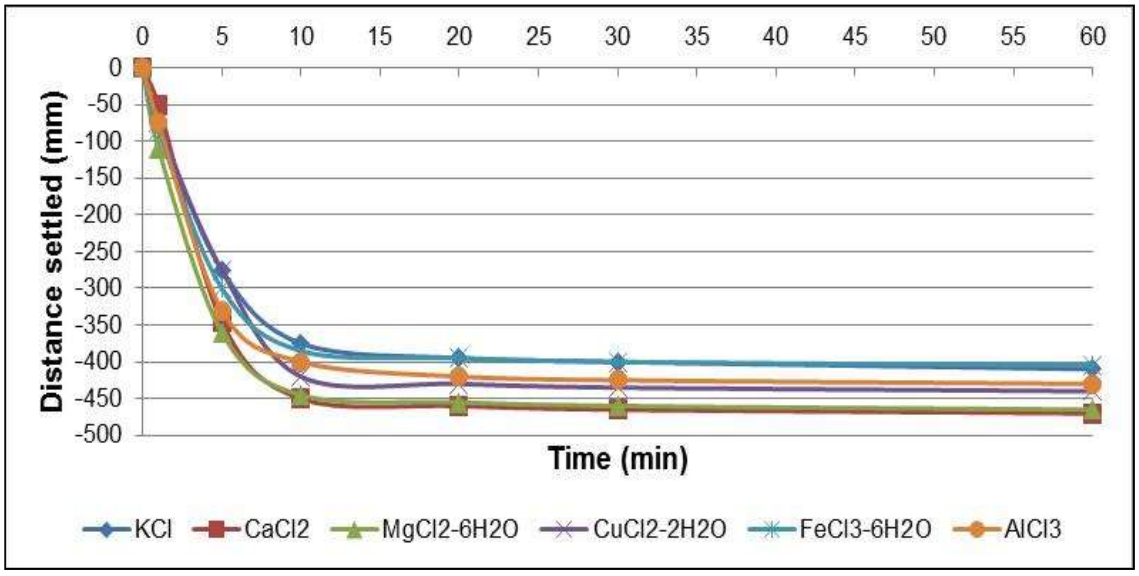

Figure 137: Critical coagulant concentration settling graphs for AC 1-1-1

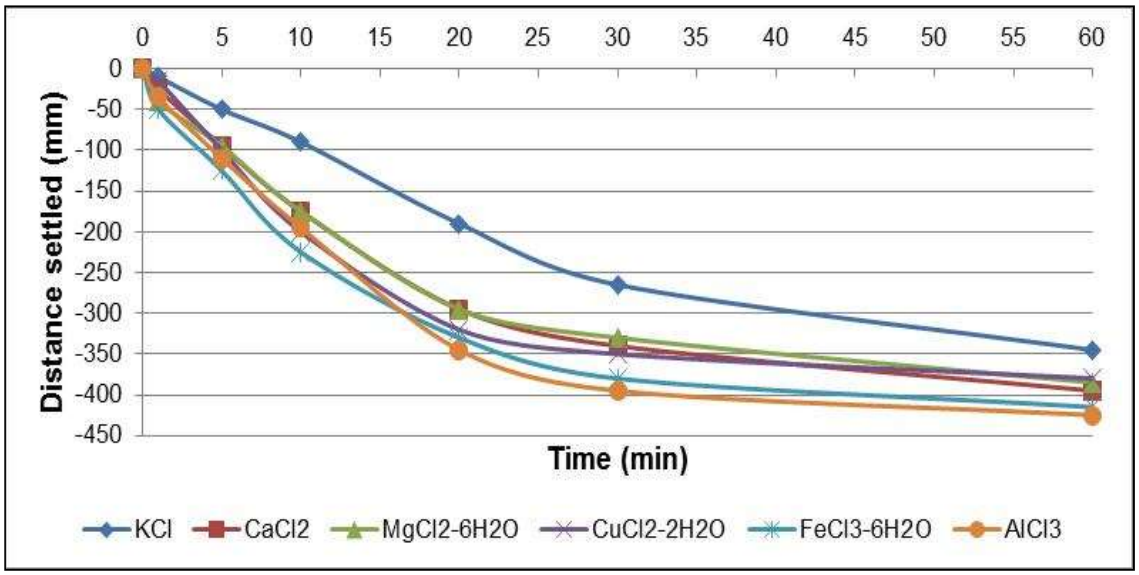

Figure 138: Critical coagulant concentration settling graphs for AC 4-1A-1

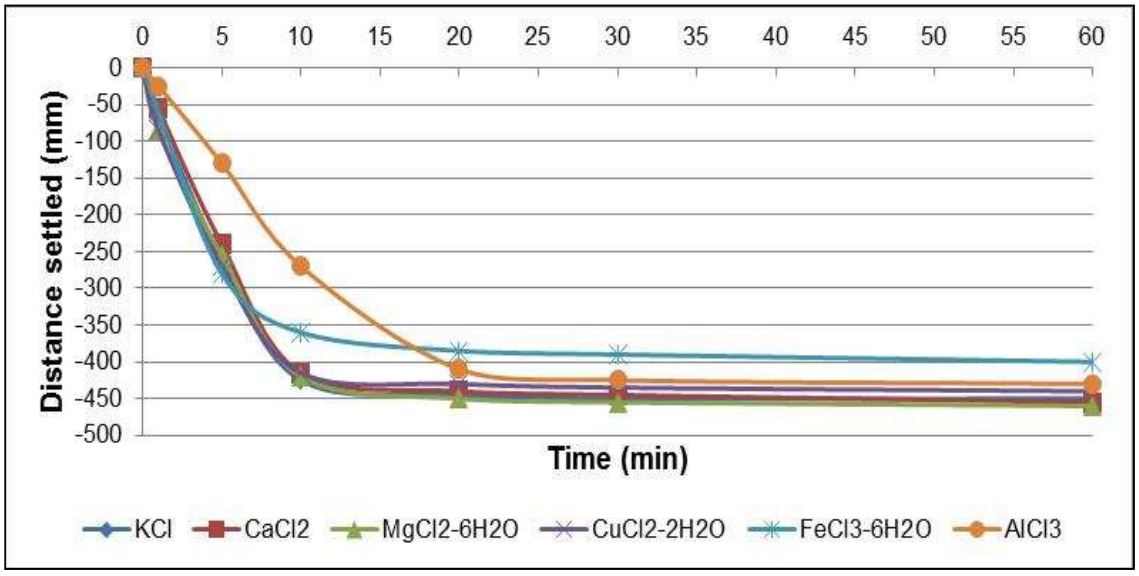

Figure 139: Critical coagulant concentration settling graphs for AC 5 -5-1

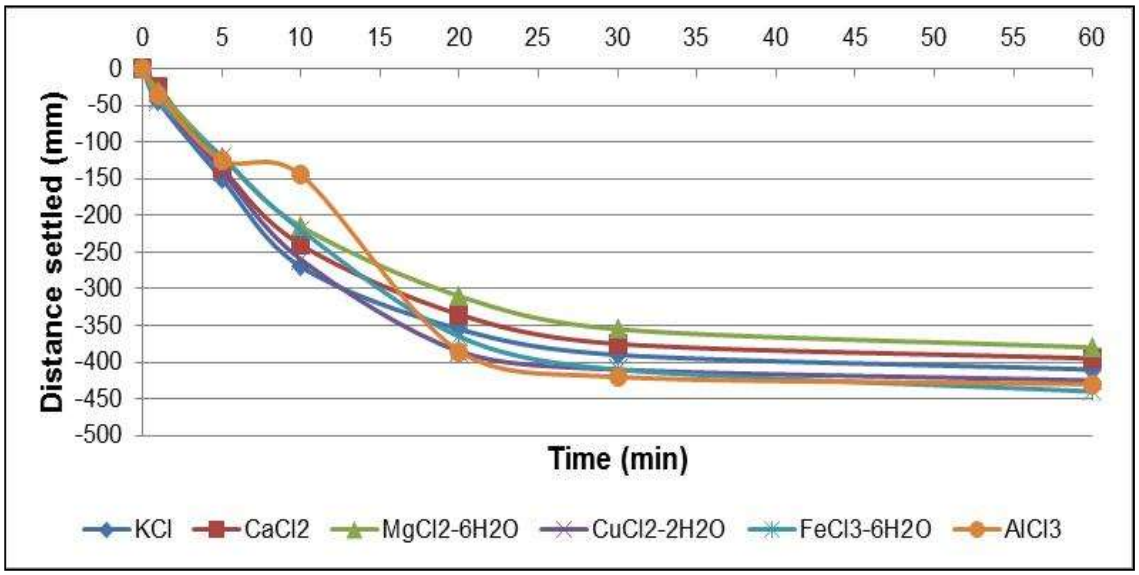

Figure 140: Critical coagulant concentration settling graphs for AC 5 -5-2

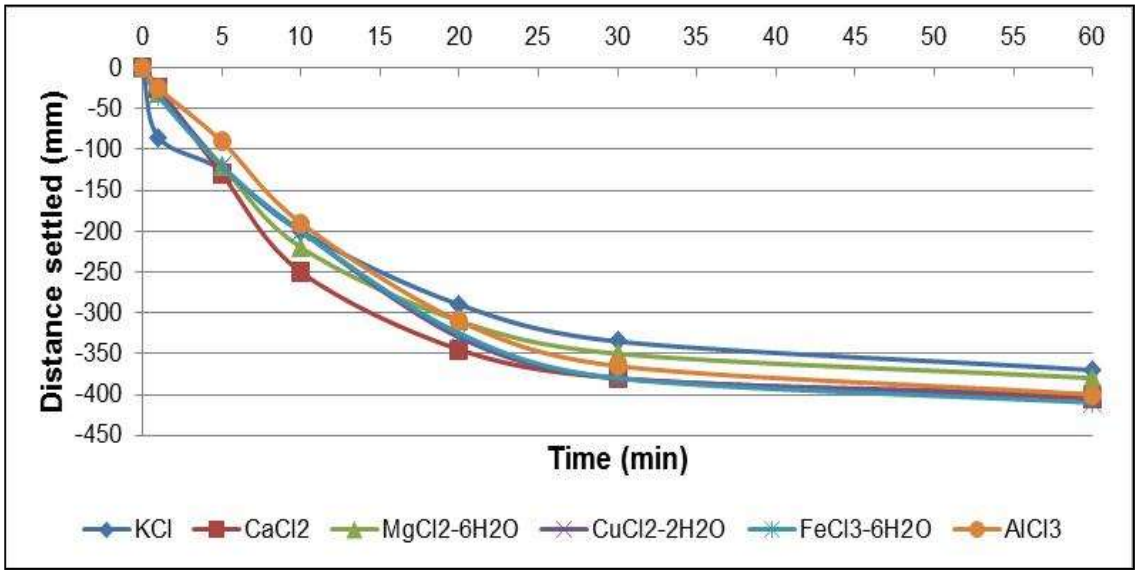

Figure 141: Critical coagulant concentration settling graphs for AC 16-1-1

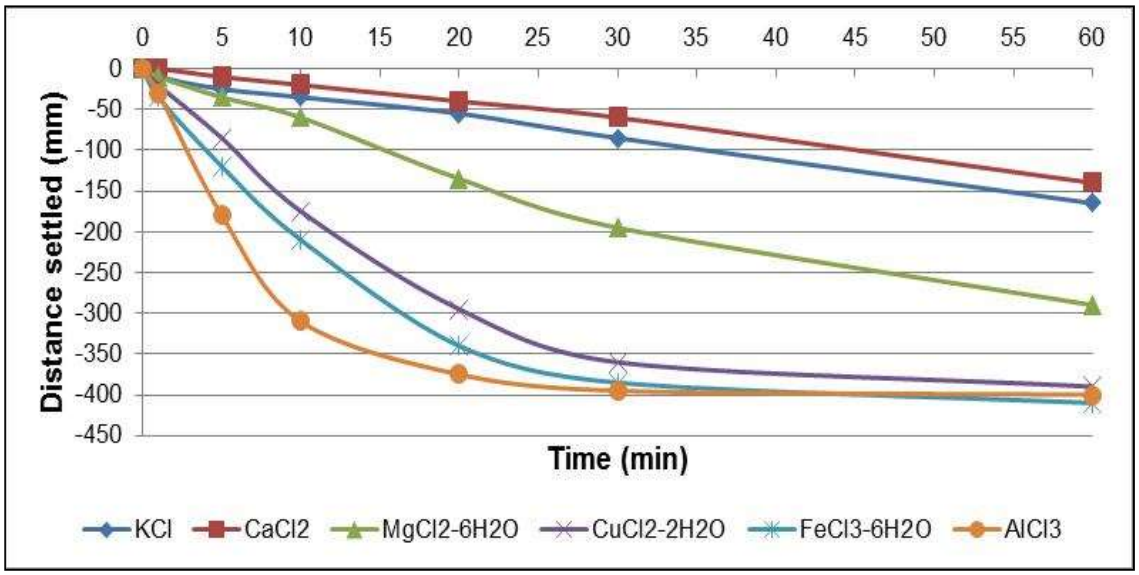

Figure 142: Critical coagulant concentration settling graphs for AC 56-5-1

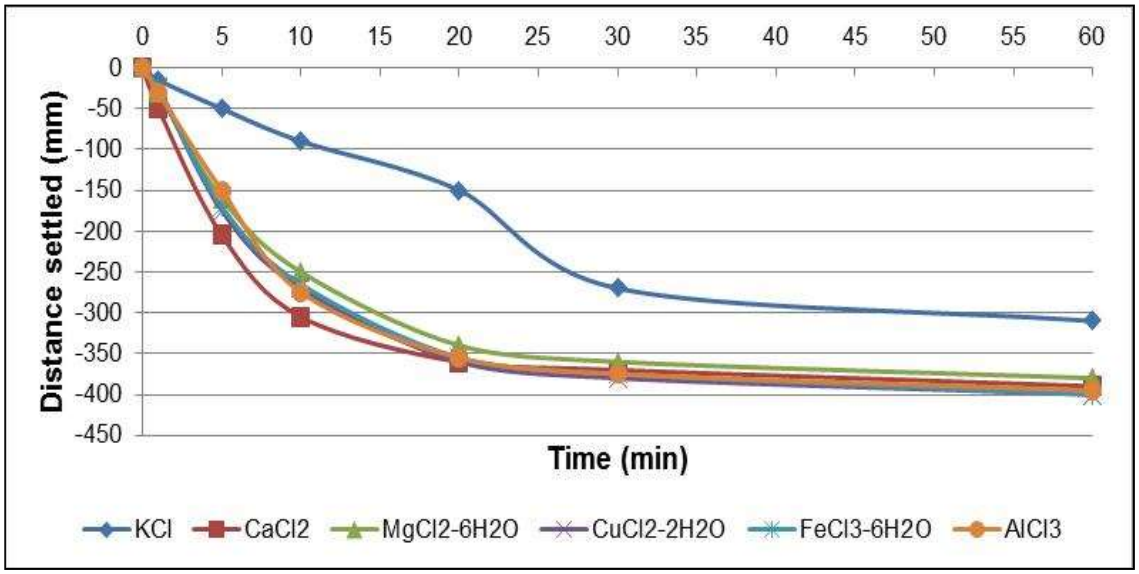

Figure 143: Critical coagulant concentration settling graphs for AC 197-1-1

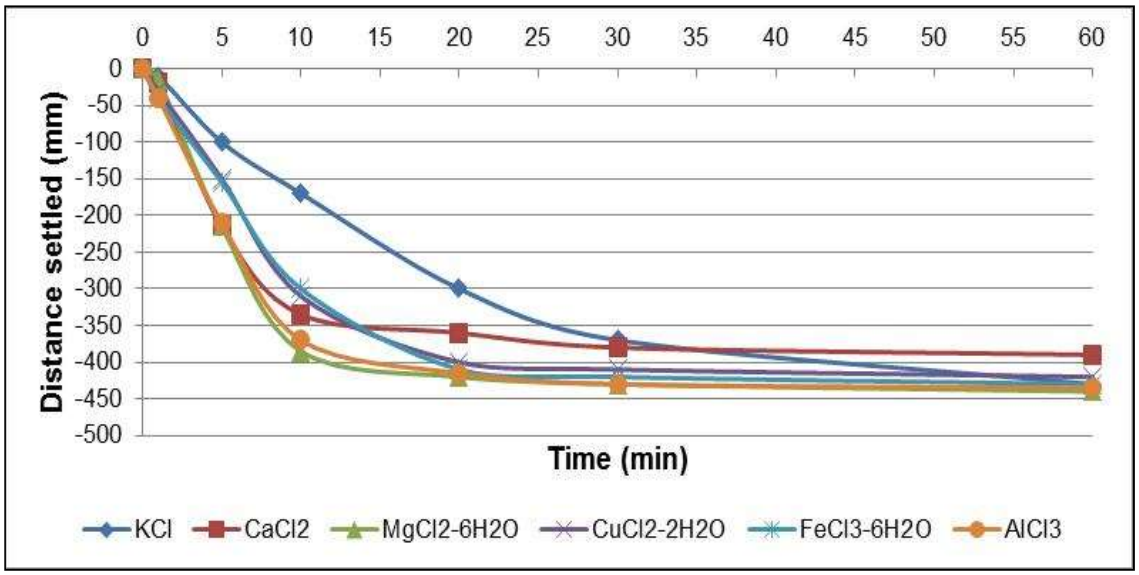

Figure 144: Critical coagulant concentration settling graphs for Venetia Red

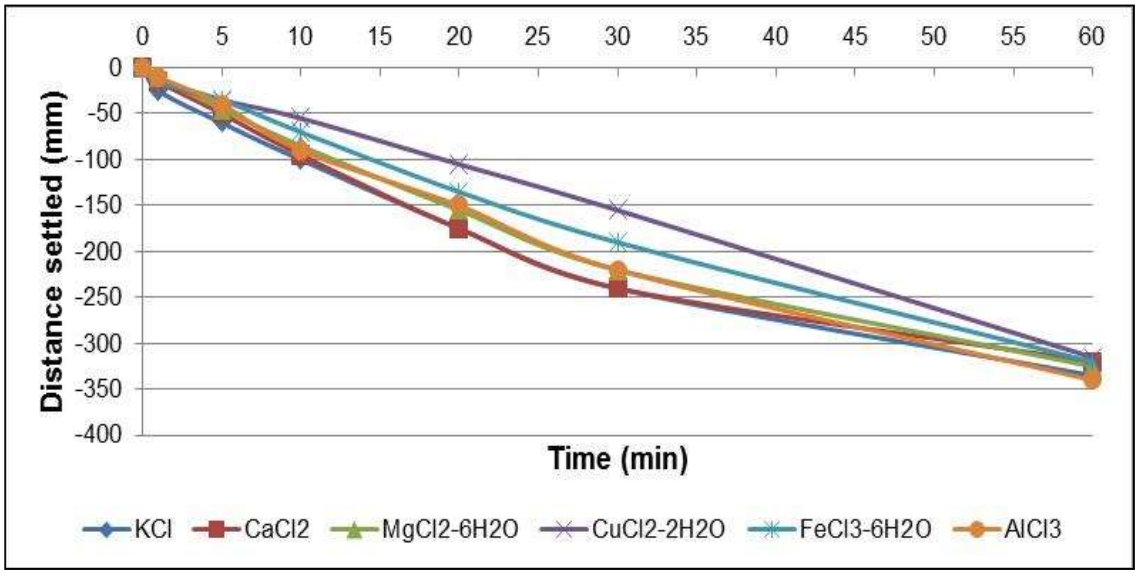

Figure 145: Critical coagulant concentration settling graphs for AO 319

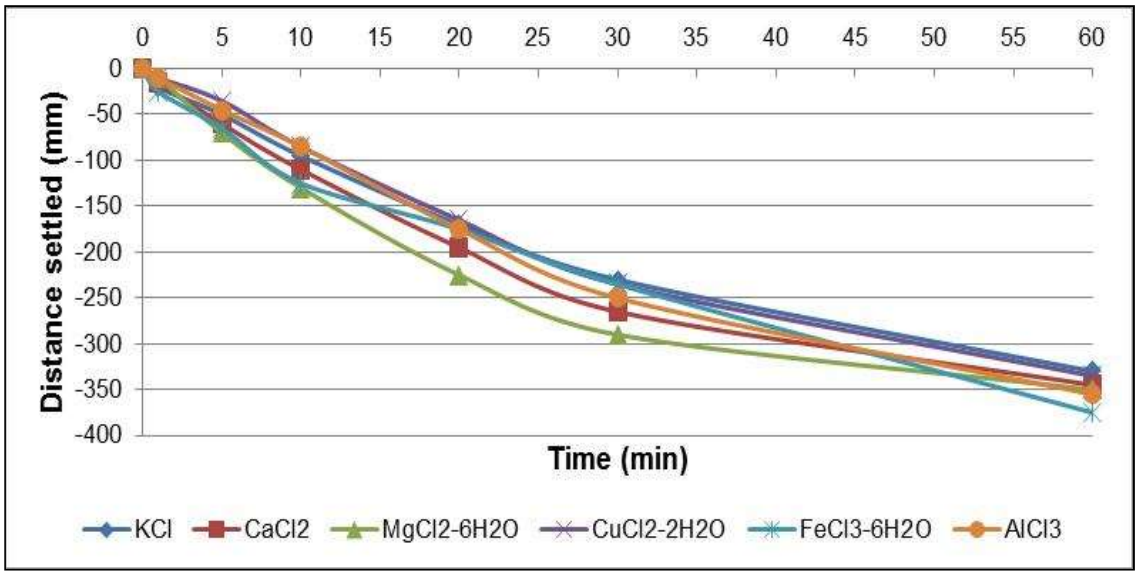

Figure 146: Critical coagulant concentration settling graphs for AO 320

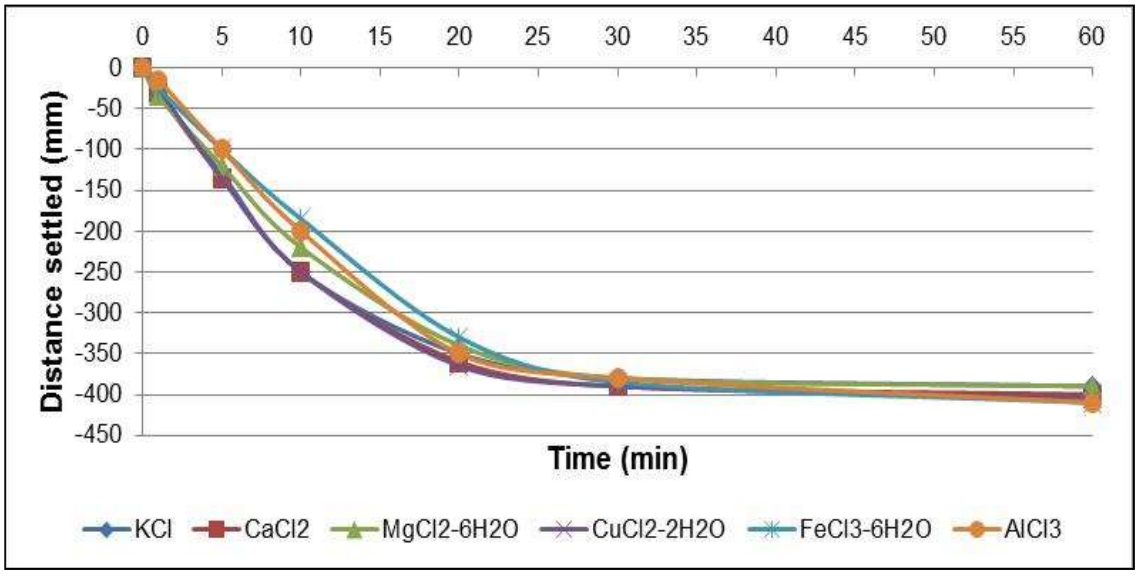

Figure 147: Critical coagulant concentration settling graphs for AO 321

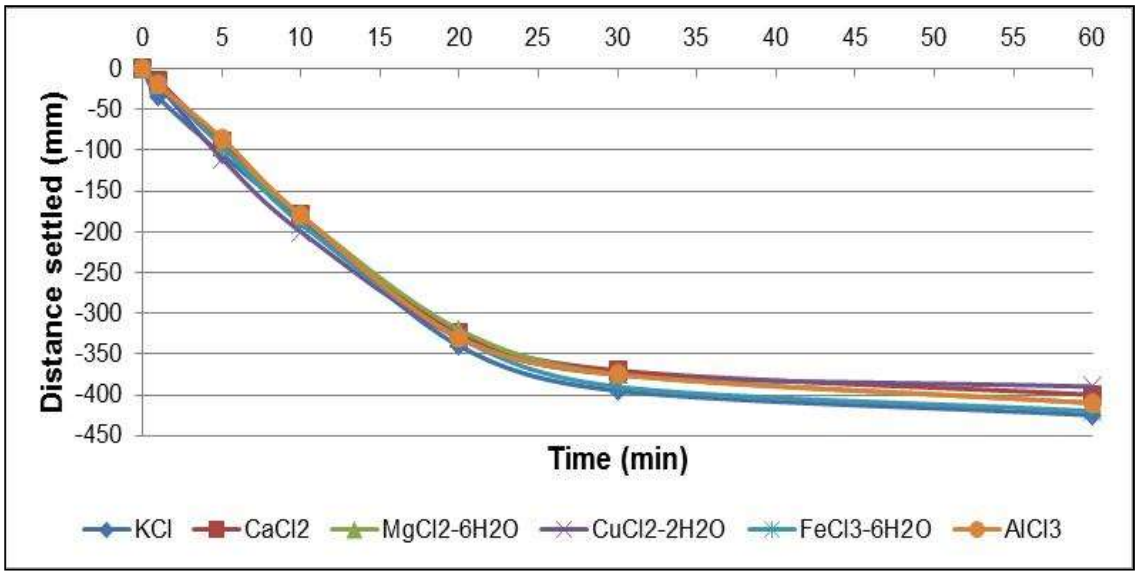

Figure 148: Critical coagulant concentration settling graphs for AO 322

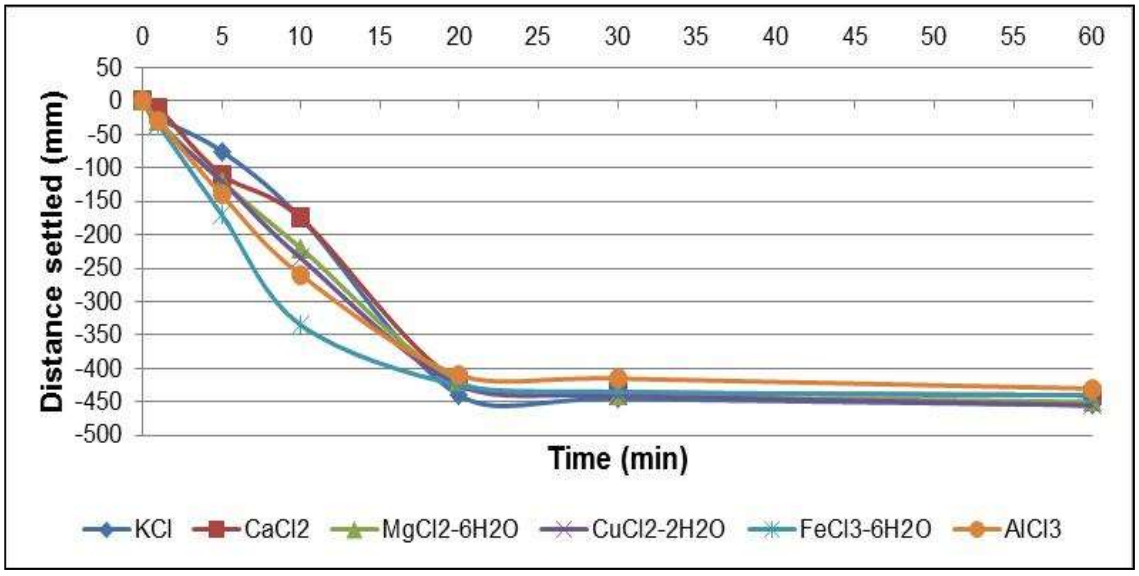

Figure 149: Critical coagulant concentration settling graphs for AO 323

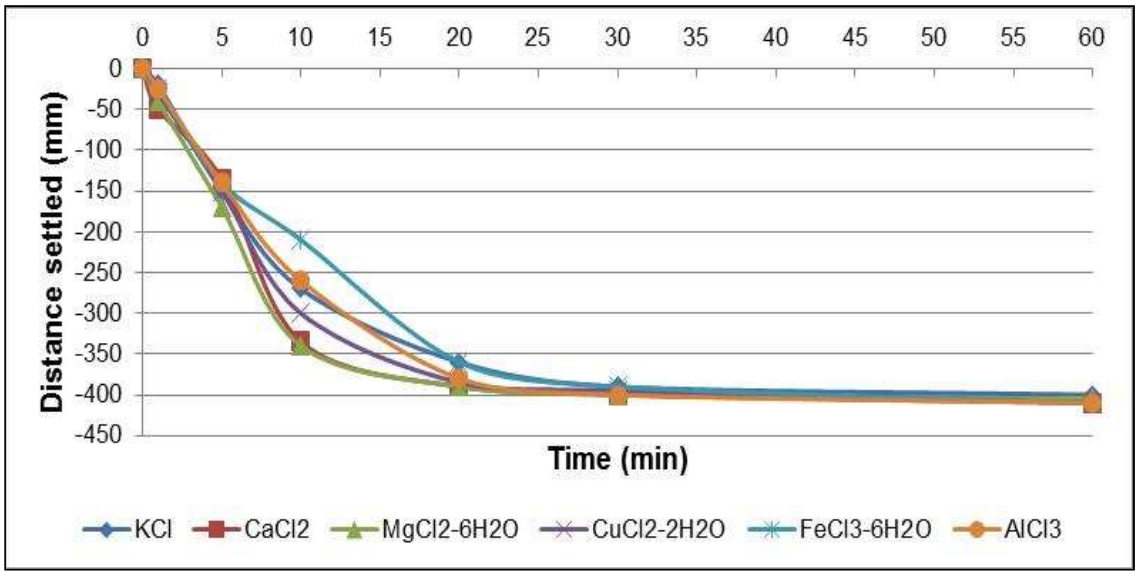

Figure 150: Critical coagulant concentration settling graphs for AO 324

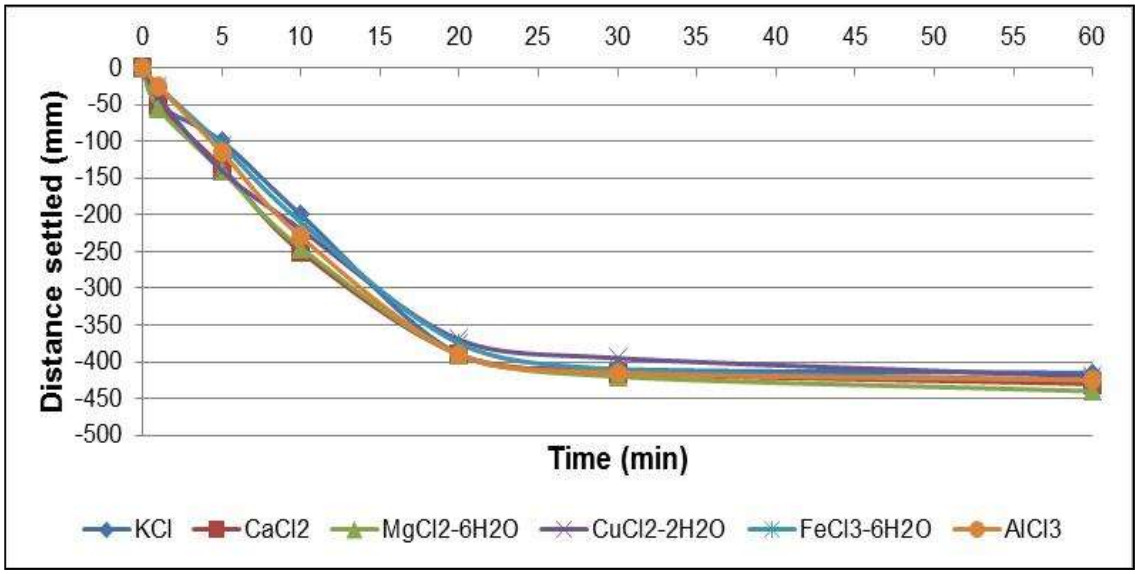

Figure 151: Critical coagulant concentration settling graphs for AO 325

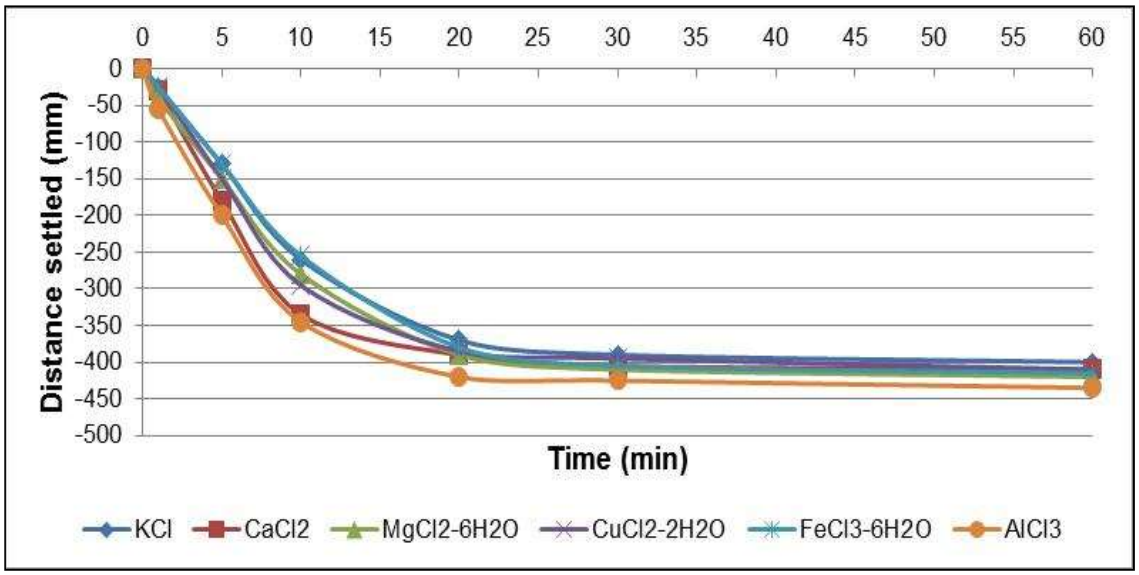

Figure 152: Critical coagulant concentration settling graphs for AO 326

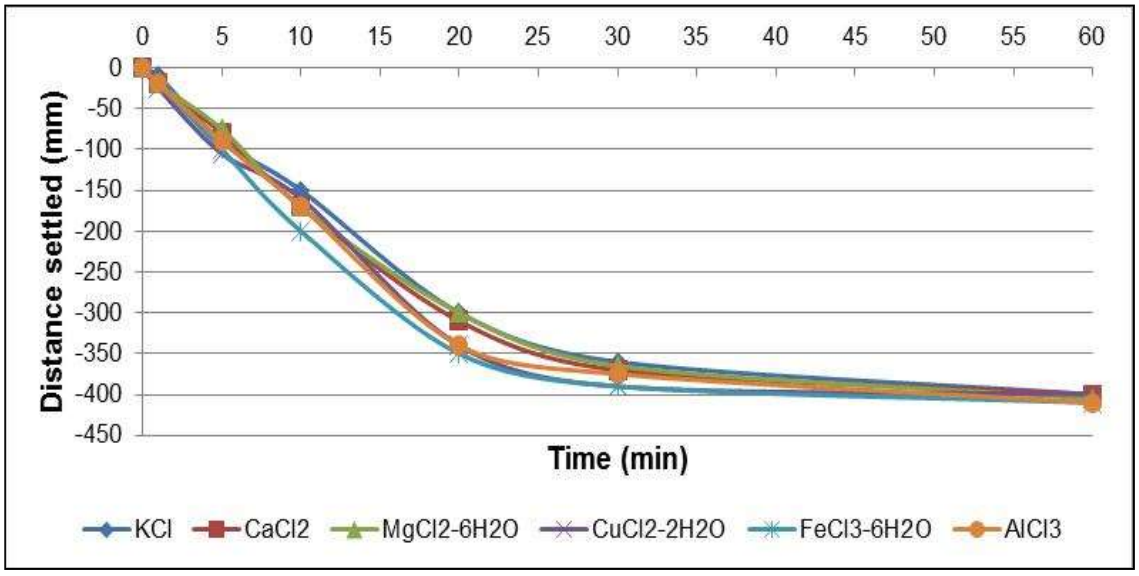

Figure 153: Critical coagulant concentration settling graphs for AO 327

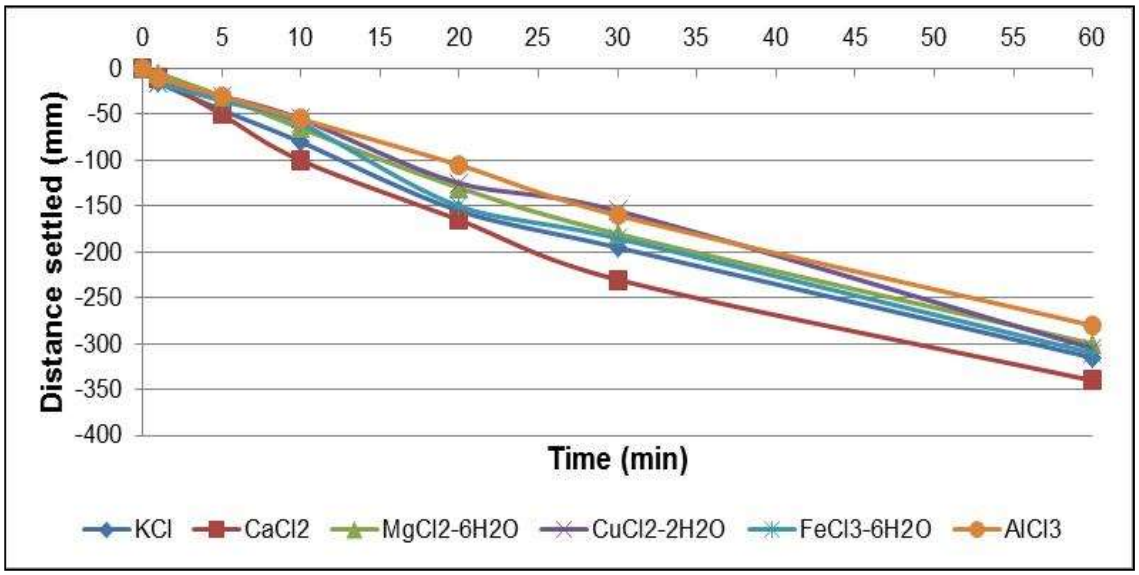

Figure 154: Critical coagulant concentration settling graphs for AO 328

Table 27: The critical coagulant concentration settling rates and final slurry volume for the Alto Cuilo and Venetia Red kimberlites

Sample	Cationic salt	Molar	Initial settling rate – m/h	Slurry bed depth - mm
AC1-1-1	KCl	0.005	2.25	65
	$CaCl_2$	0.005	**2.7**	**55**
	$MgCl_2$-6H2O	0.005	2.67	60
	$CuCl_2$-2H2O	0.01	2.52	60
	$FeCl_3$-6H2O	0.01	2.31	95
	$AlCl_3$	0.005	2.4	75
AC4-1A-1	KCl	0.005	0.54	155
	$CaCl_2$	0.005	1.05	130
	$MgCl_2$-6H2O	0.005	1.05	130
	$CuCl_2$-2H2O	0.005	1.2	120
	$FeCl_3$-6H2O	0.005	**1.35**	**110**
	$AlCl_3$	0.005	1.17	100
AC5-5-1	KCl	0.005	2.55	75
	$CaCl_2$	0.005	2.49	60
	$MgCl_2$-6H2O	0.005	**2.52**	**65**
	$CuCl_2$-2H2O	0.005	2.49	70
	$FeCl_3$-6H2O	0.01	2.16	80
	$AlCl_3$	0.005	1.62	70
AC5-5-2	KCl	0.005	1.62	115
	$CaCl_2$	0.005	1.44	120
	$MgCl_2$-6H2O	0.005	1.29	120
	$CuCl_2$-2H2O	0.005	**1.56**	**105**
	$FeCl_3$-6H2O	0.005	1.32	100
	$AlCl_3$	0.005	0.87	95
AC16-1-1	KCl	0.005	1.2	130
	$CaCl_2$	0.005	**1.5**	**120**
	$MgCl_2$-6H2O	0.005	1.32	120
	$CuCl_2$-2H2O	0.005	1.2	120
	$FeCl_3$-6H2O	0.005	1.2	120
	$AlCl_3$	0.005	1.14	110
AC56-5-1	KCl	0.01	0.21	360
	$CaCl_2$	0.005	0.12	370
	$MgCl_2$-6H2O	0.005	0.36	220
	$CuCl_2$-2H2O	0.005	1.05	140
	$FeCl_3$-6H2O	0.005	1.26	120
	$AlCl_3$	0.005	**1.86**	**110**

AC197-1-1	KCl	0.005	0.54	190
	$CaCl_2$	0.005	**1.83**	**100**
	$MgCl_2$-6H2O	0.005	1.5	110
	$CuCl_2$-2H2O	0.005	1.62	100
	$FeCl_3$-6H2O	0.005	1.59	100
	$AlCl_3$	0.005	1.65	80
Venetia Red	KCl	0.05	1.02	70
	$CaCl_2$	0.01	2.01	80
	$MgCl_2$-6H2O	0.01	**2.31**	**75**
	$CuCl_2$-2H2O	0.005	1.86	80
	$FeCl_3$-6H2O	0.005	1.8	70
	$AlCl_3$	0.005	2.22	65

Table 28: The critical coagulant concentration settling rates and final slurry volume for the Itengo/Tchegi kimberlites

Sample	Cationic salt	Molar	Initial settling rate – m/h	Slurry bed depth - mm
AO319	KCl	0.02	0.6	190
	$CaCl_2$	0.01	0.57	180
	$MgCl_2$-6H2O	0.01	0.51	180
	$CuCl_2$-2H2O	0.005	0.33	190
	$FeCl_3$-6H2O	0.005	0.42	210
	$AlCl_3$	0.005	**0.54**	**150**
AO320	KCl	0.005	0.57	190
	$CaCl_2$	0.005	0.66	170
	$MgCl_2$-6H2O	0.005	**0.78**	**150**
	$CuCl_2$-2H2O	0.005	0.51	175
	$FeCl_3$-6H2O	0.005	0.75	150
	$AlCl_3$	0.005	0.51	150
AO321	KCl	0.01	1.5	110
	$CaCl_2$	0.005	1.5	110
	$MgCl_2$-6H2O	0.005	1.32	110
	$CuCl_2$-2H2O	0.005	**1.5**	**90**
	$FeCl_3$-6H2O	0.005	1.11	90
	$AlCl_3$	0.005	1.2	90
AO322	KCl	0.035	1.11	100
	$CaCl_2$	0.005	1.08	100
	$MgCl_2$-6H2O	0.005	1.08	100
	$CuCl_2$-2H2O	0.005	**1.2**	**90**

	$FeCl_3$-6H2O	0.005	1.14	100
	$AlCl_3$	0.005	1.08	90
AO323	KCl	0.05	1.05	70
	$CaCl_2$	0.005	1.05	70
	$MgCl_2$-6H2O	0.005	1.32	70
	$CuCl_2$-2H2O	0.005	1.41	70
	$FeCl_3$-6H2O	0.005	**2.01**	**70**
	$AlCl_3$	0.005	1.56	70
AO324	KCl	0.01	1.62	100
	$CaCl_2$	0.005	**2.04**	**90**
	$MgCl_2$-6H2O	0.005	**2.04**	**90**
	$CuCl_2$-2H2O	0.005	1.8	90
	$FeCl_3$-6H2O	0.005	1.26	90
	$AlCl_3$	0.005	1.56	90
AO325	KCl	0.005	1.2	85
	$CaCl_2$	0.005	**1.5**	**80**
	$MgCl_2$-6H2O	0.005	**1.5**	**80**
	$CuCl_2$-2H2O	0.005	1.32	80
	$FeCl_3$-6H2O	0.005	1.26	75
	$AlCl_3$	0.005	1.38	80
AO326	KCl	0.005	1.56	100
	$CaCl_2$	0.005	2.01	100
	$MgCl_2$-6H2O	0.005	1.68	100
	$CuCl_2$-2H2O	0.005	1.77	90
	$FeCl_3$-6H2O	0.005	1.53	90
	$AlCl_3$	0.005	**2.07**	**90**
AO327	KCl	0.02	0.9	100
	$CaCl_2$	0.005	1.02	100
	$MgCl_2$-6H2O	0.005	1.02	95
	$CuCl_2$-2H2O	0.005	0.96	100
	$FeCl_3$-6H2O	0.005	**1.2**	**90**
	$AlCl_3$	0.005	1.02	90
AO328	KCl	0.02	0.48	210
	$CaCl_2$	0.01	**0.6**	**170**
	$MgCl_2$-6H2O	0.01	0.39	200
	$CuCl_2$-2H2O	0.005	0.33	200
	$FeCl_3$-6H2O	0.005	0.36	200
	$AlCl_3$	0.005	0.33	210

Table 29: AC 1-1-1 Flocculant screening

AC 1-1-1				
Flocculant - Magnafloc	**Time settling 30mm**	**Settling rate (m/h)**	**Floc structure**	**Clarity**
10	3	36.00	large	46
336	3.16	34.18	large	46
1011	3.5	30.86	large	46
340	3.57	30.25	large	46
356	3.66	29.51	large	46
342	3.72	29.03	large	46
351	3.97	27.20	large	46
333	4.12	26.21	large	46
6260	4.13	26.15	large	46
155	4.16	25.96	large	46
5250	4.16	25.96	large	46
919	5.04	21.43	large	46
345	5.19	20.81	large	46

Table 30: AC 4-1A-1 Flocculant screening

AC 4-1A-1				
Flocculant - Magnafloc	**Time settling 30mm**	**Settling rate (m/h)**	**Floc structure**	**Clarity**
336	6.62	16.31	large	46
5250	7.1	15.21	large	46
6260	7.12	15.17	large	46
155	7.35	14.69	large	46
1011	7.69	14.04	large	46
342	8.69	12.43	large	46
340	9.62	11.23	large	46
919	11.94	9.05	large	46
10	12.78	8.45	medium	46
345	15.18	7.11	medium	46
333	29.69	3.64	small	good
351	35.91	3.01	small	poor
356	0	0.00	-	-

Table 31: AC 5-5-1 Flocculant screening

AC 5-5-1				
Flocculant - Magnafloc	**Time settling 30mm**	**Settling rate (m/h)**	**Floc structure**	**Clarity**
340	2.75	39.27	large	46
5250	3.25	33.23	large	46
6260	3.31	32.63	large	46
155	3.41	31.67	medium	46
10	3.84	28.13	large	46
336	4.16	25.96	large	46
342	4.22	25.59	large	46
1011	4.63	23.33	large	46
333	4.66	23.18	medium	46
351	5.5	19.64	medium	46
919	5.65	19.12	large	46
345	6.22	17.36	medium	46
356	6.57	16.44	medium	46

Table 32: AC 5-5-2 Flocculant screening

AC 5-5-2				
Flocculant - Magnafloc	**Time settling 30mm**	**Settling rate (m/h)**	**Floc structure**	**Clarity**
6260	7.16	15.08	large	46
5250	9.19	11.75	large	46
342	9.88	10.93	large	46
336	11.16	9.68	large	46
1011	11.32	9.54	large	46
340	11.59	9.32	large	46
155	12.5	8.64	large	46
10	15.34	7.04	large	46
345	17.52	6.16	large	46
351	22.03	4.90	medium	46
356	25.81	4.18	medium	46
333	28.25	3.82	medium	46
919	33.1	3.26	small	46

Table 33: AC 16-1-1 Flocculant screening

AC 16-1-1				
Flocculant - Magnafloc	**Time settling 30mm**	**Settling rate (m/h)**	**Floc structure**	**Clarity**
1011	10.06	10.74	large	46
5250	11.19	9.65	large	46
340	12.16	8.88	medium	46
342	12.75	8.47	medium	46
336	13.33	8.10	medium	46
345	13.66	7.91	medium	46
155	13.82	7.81	large	46
915	14.81	7.29	medium	46
6260	16.22	6.66	medium	46
10	29.13	3.71	small	good
356	49.44	2.18	small	poor
333	101.22	1.07	small	poor
351	110.5	0.98	small	poor

Table 34: AC 56-5-1 Flocculant screening

AC 56-5-1				
Flocculant - Magnafloc	**Time settling 30mm**	**Settling rate (m/h)**	**Floc structure**	**Clarity**
10	9.47	11.40	medium	poor
340	10.22	10.57	medium	poor
6260	10.31	10.48	medium	poor
919	13.97	7.73	medium	poor
342	16.53	6.53	small	poor
345	20.96	5.15	small	poor
336	23.01	4.69	small	poor
155	0	0.00	-	-
333	0	0.00	-	-
351	0	0.00	-	-
356	0	0.00	-	-
1011	0	0.00	-	-
5250	0	0.00	-	-

Table 35: AC 197-1-1 Flocculant screening

AC 197-1-1				
Flocculant - Magnafloc	**Time settling 30mm**	**Settling rate (m/h)**	**Floc structure**	**Clarity**
6260	6.75	16.00	large	46
1011	7.22	14.96	large	46
340	8.44	12.80	large	46
5250	9.72	11.11	large	46
336	11.76	9.18	large	46
345	12.15	8.89	large	46
342	13.12	8.23	large	46
10	13.43	8.04	large	46
919	14.19	7.61	large	46
155	16.47	6.56	large	46
351	25.37	4.26	small	46
333	26.03	4.15	small	46
356	28.85	3.74	small	46

Table 36: Venetia Red Flocculant screening

Venetia Red				
Flocculant - Magnafloc	**Time settling 30mm**	**Settling rate (m/h)**	**Floc structure**	**Clarity**
351	9.06	11.92	small	poor
356	21.16	5.10	small	poor
333	22.06	4.90	small	poor
10	0	0.00	-	-
155	0	0.00	-	-
336	0	0.00	-	-
340	0	0.00	-	-
342	0	0.00	-	-
345	0	0.00	-	-
919	0	0.00	-	-
1011	0	0.00	-	-
5250	0	0.00	-	-
6260	0	0.00	-	-

Table 37: AO 319 Flocculant screening

AO319				
Flocculant - Magnafloc	**Time settling 30mm**	**Settling rate (m/h)**	**Floc structure**	**Clarity**
336	5.72	18.88	medium	good
10	6.25	17.28	large	46
340	6.94	15.56	medium	good
919	7.12	15.17	medium	good
342	7.13	15.15	medium	good
6260	7.31	14.77	medium	good
5250	7.82	13.81	medium	good
1011	8.9	12.13	medium	good
155	9.38	11.51	medium	good
345	9.84	10.98	medium	good
356	37.12	2.91	small	poor
333	0	0.00	-	-
351	0	0.00	-	-

Table 38: AO 320 Flocculant screening

AO320				
Flocculant - Magnafloc	**Time settling 30mm**	**Settling rate (m/h)**	**Floc structure**	**Clarity**
5250	14.12	7.65	medium	46
1011	17.37	6.22	medium	good
336	19.47	5.55	medium	good
340	23.28	4.64	small	good
342	23.37	4.62	small	good
155	24.22	4.46	small	good
919	35.63	3.03	small	good
345	37	2.92	small	good
6260	41.09	2.63	small	poor
10	58.12	1.86	small	poor
333	0	0.00	-	-
351	0	0.00	-	-
356	0	0.00	-	-

Table 39: AO 321 Flocculant screening

AO321				
Flocculant - Magnafloc	**Time settling 30mm**	**Settling rate (m/h)**	**Floc structure**	**Clarity**
336	4.25	25.41	large	46
1011	4.72	22.88	large	46
6260	4.85	22.27	large	46
340	4.87	22.18	large	46
5250	4.94	21.86	large	46
342	5.19	20.81	large	46
919	5.91	18.27	large	46
155	6.38	16.93	large	good
345	7.38	14.63	large	46
10	9.03	11.96	medium	good
356	29.66	3.64	small	poor
351	42.34	2.55	small	poor
333	45.78	2.36	small	poor

Table 40: AO 322 Flocculant screening

AO322				
Flocculant - Magnafloc	**Time settling 30mm**	**Settling rate (m/h)**	**Floc structure**	**Clarity**
336	3.44	31.40	large	46
5250	3.59	30.08	large	46
6260	4.32	25.00	large	46
340	4.38	24.66	large	46
1011	4.56	23.68	large	46
919	4.6	23.48	large	46
155	4.75	22.74	large	46
345	6.44	16.77	large	46
342	6.56	16.46	large	46
10	6.57	16.44	large	46
356	13.59	7.95	small	poor
333	14.28	7.56	small	good
351	14.77	7.31	medium	good

Table 41: AO 323 Flocculant screening

AO 323				
Flocculant - Magnafloc	**Time settling 30mm**	**Settling rate (m/h)**	**Floc structure**	**Clarity**
6260	2.54	42.52	medium	46
155	2.72	39.71	medium	46
340	2.84	38.03	medium	46
5250	2.86	37.76	medium	46
336	2.94	36.73	medium	46
342	3.34	32.34	medium	46
1011	3.44	31.40	medium	46
919	3.57	30.25	medium	46
10	3.59	30.08	medium	46
345	3.76	28.72	medium	46
333	5.87	18.40	medium	46
351	6.12	17.65	medium	46
356	7.19	15.02	medium	46

Table 42: AO 324 Flocculant screening

AO 324				
Flocculant - Magnafloc	**Time settling 30mm**	**Settling rate (m/h)**	**Floc structure**	**Clarity**
10	5.47	19.74	large	46
155	5.66	19.08	medium	good
342	6.43	16.80	large	46
6260	7.09	15.23	large	46
919	7.19	15.02	medium	good
340	7.25	14.90	medium	good
336	7.47	14.46	medium	poor
345	8.28	13.04	medium	good
1011	10.1	10.69	small	poor
5250	12.13	8.90	small	poor
351	17.15	6.30	small	good
333	18.97	5.69	small	poor
356	21.63	4.99	small	poor

Table 43: AO 325 Flocculant screening

AO325				
Flocculant - Magnafloc	**Time settling 30mm**	**Settling rate (m/h)**	**Floc structure**	**Clarity**
5250	3.19	33.86	large	46
336	3.22	33.54	large	46
6260	3.25	33.23	large	46
1011	3.65	29.59	large	46
340	3.68	29.35	large	46
919	4	27.00	large	46
155	4.5	24.00	medium	46
342	4.56	23.68	medium	46
345	4.63	23.33	medium	46
10	4.87	22.18	medium	46
351	8.41	12.84	medium	46
333	8.97	12.04	medium	46
356	9.16	11.79	medium	46

Table 44: AO 326 Flocculant screening

AO326				
Flocculant - Magnafloc	**Time settling 30mm**	**Settling rate (m/h)**	**Floc structure**	**Clarity**
1011	3.06	35.29	large	46
5250	4.53	23.84	large	46
6260	5.1	21.18	large	46
336	5.13	21.05	large	46
340	5.53	19.53	large	46
919	6	18.00	large	46
155	7.34	14.71	large	46
345	7.35	14.69	large	46
342	8.22	13.14	large	46
10	12.5	8.64	large	46
356	24.63	4.38	medium	46
333	25.31	4.27	small	46
351	27.1	3.99	small	46

Table 45: AO 327 Flocculant screening

AO 327				
Flocculant - Magnafloc	**Time settling 30mm**	**Settling rate (m/h)**	**Floc structure**	**Clarity**
6260	2.78	38.85	large	good
336	4.16	25.96	large	good
1011	4.16	25.96	large	good
5250	4.22	25.59	large	good
340	4.25	25.41	large	good
919	5.09	21.22	large	good
342	5.18	20.85	large	good
10	5.68	19.01	large	good
345	5.82	18.56	large	good
155	6.06	17.82	large	good
356	16.94	6.38	small	poor
351	17.79	6.07	small	poor
333	17.94	6.02	small	poor

Table 46: AO 328 Flocculant screening

AO 328				
Flocculant - Magnafloc	**Time settling 30mm**	**Settling rate (m/h)**	**Floc structure**	**Clarity**
10	6.6	16.36	large	good
342	7.4	14.59	medium	poor
6260	9.28	11.64	small	poor
919	9.66	11.18	medium	poor
340	10.66	10.13	small	poor
345	19.2	5.63	small	poor
155	21.53	5.02	small	poor
336	28.34	3.81	small	poor
1011	41.88	2.58	small	poor
5250	43.03	2.51	small	poor
333	0	0.00	-	-
351	0	0.00	-	-
356	0	0.00	-	-

Table 47: The fastest three flocculant settling rates and final slurry volume for the Alto Cuilo kimberlites

Sample	Flocculant	Strength	Initial settling rate m/h	Slurry bed depth - mm
AC1-1-1	Magnafloc 10	0.025%	**25.1**	**75**
	Magnafloc 336	0.025%	22.9	85
	Magnafloc 1011	0.025%	22.0	80
AC4-1A-1	Magnafloc 5250	0.025%	16.4	115
	Magnafloc 6260	0.025%	**19.3**	**135**
	Magnafloc 336	0.025%	14.4	135
AC5-5-1	Magnafloc 6260	0.025%	**24.1**	**100**
	Magnafloc 5250	0.025%	21.0	90
	Magnafloc 340	0.025%	21.2	90
AC5-5-2	Magnafloc 6260	0.025%	10.3	140
	Magnafloc 5250	0.025%	**12.0**	**135**
	Magnafloc 342	0.025%	8.0	155
AC16-1-1	Magnafloc 5250	0.025%	**10.7**	**140**
	Magnafloc 1011	0.025%	10.0	145
	Magnafloc 340	0.025%	9.6	145
AC56-5-1	Magnafloc 6260	0.025%	No settling	No settling
	Magnafloc 10	0.025%	No settling	No settling
	Magnafloc 340	0.025%	No settling	No settling
AC197-1-1	Magnafloc 6260	0.025%	13.3	120
	Magnafloc 340	0.025%	16.7	120
	Magnafloc 1011	0.025%	**19.6**	**130**
Venetia Red	Magnafloc 333	0.025%	No settling	No settling
	Magnafloc 351	0.025%	No settling	No settling
	Magnafloc 356	0.025%	No settling	No settling

Table 48: The fastest three flocculant settling rates and final slurry volumes for the Itengo/Tchegi kimberlites

Sample	Flocculant	Strength	Initial settling rate m/h	Slurry bed depth - mm
AO 319	Magnafloc 10	0.025%	**18.7**	**125**
	Magnafloc 336	0.025%	18.7	130
	Magnafloc 340	0.025%	12.8	145
AO 320	Magnafloc 5250	0.025%	6.1	150
	Magnafloc 1011	0.025%	**11.9**	**140**
	Magnafloc 336	0.025%	10.2	145
AO 321	Magnafloc 6260	0.025%	19.8	100
	Magnafloc 336	0.025%	**21.2**	**100**
	Magnafloc 1011	0.025%	19.4	105
AO 322	Magnafloc 6260	0.025%	15.4	120
	Magnafloc 336	0.025%	**17.6**	**120**
	Magnafloc 5250	0.025%	14.6	115
AO 323	Magnafloc 6260	0.025%	20.4	85
	Magnafloc 155	0.025%	**22.8**	**85**
	Magnafloc 340	0.025%	22.3	80
AO 324	Magnafloc 342	0.025%	**17.8**	**110**
	Magnafloc 155	0.025%	13.4	125
	Magnafloc 10	0.025%	16.7	115
AO 325	Magnafloc 5250	0.025%	**21.1**	**95**
	Magnafloc 6260	0.025%	19.3	100
	Magnafloc 336	0.025%	20.5	95
AO 326	Magnafloc 6260	0.025%	15.1	110
	Magnafloc 5250	0.025%	**20.2**	**95**
	Magnafloc 1011	0.025%	19.7	110
AO 327	Magnafloc 6260	0.025%	13.1	130
	Magnafloc 336	0.025%	13.8	130
	Magnafloc 1011	0.025%	**14.9**	**135**
AO 328	Magnafloc 6260	0.025%	8.0	190
	Magnafloc 342	0.025%	13.8	160
	Magnafloc 10	0.025%	**14.5**	**150**

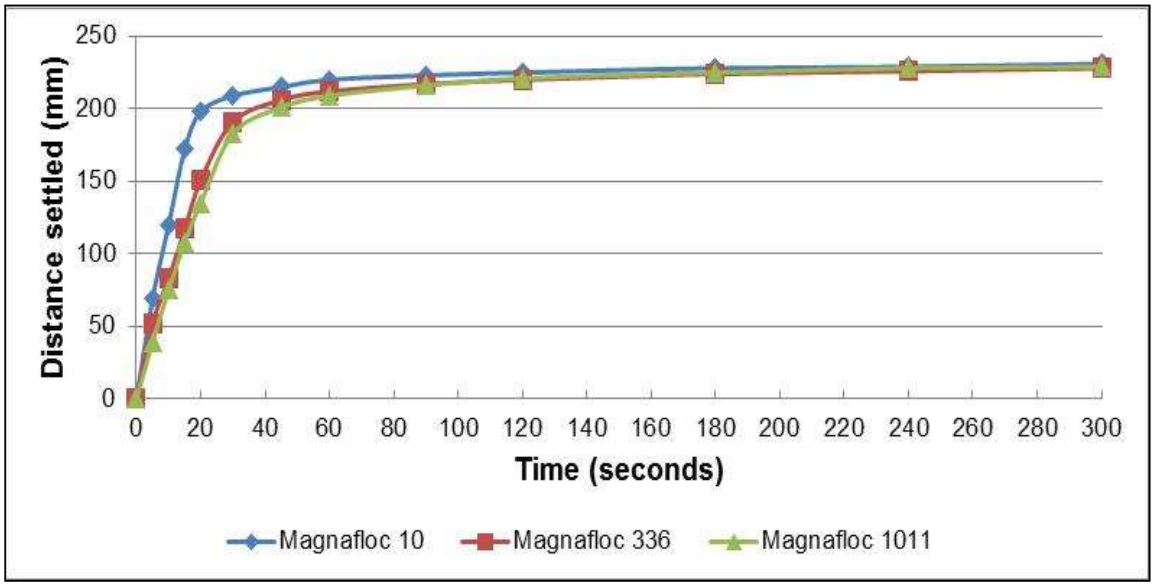

Figure 155: The settling rate curves of AC 1-1-1 with 0.025% of Magnafloc 10, 336 and 1011

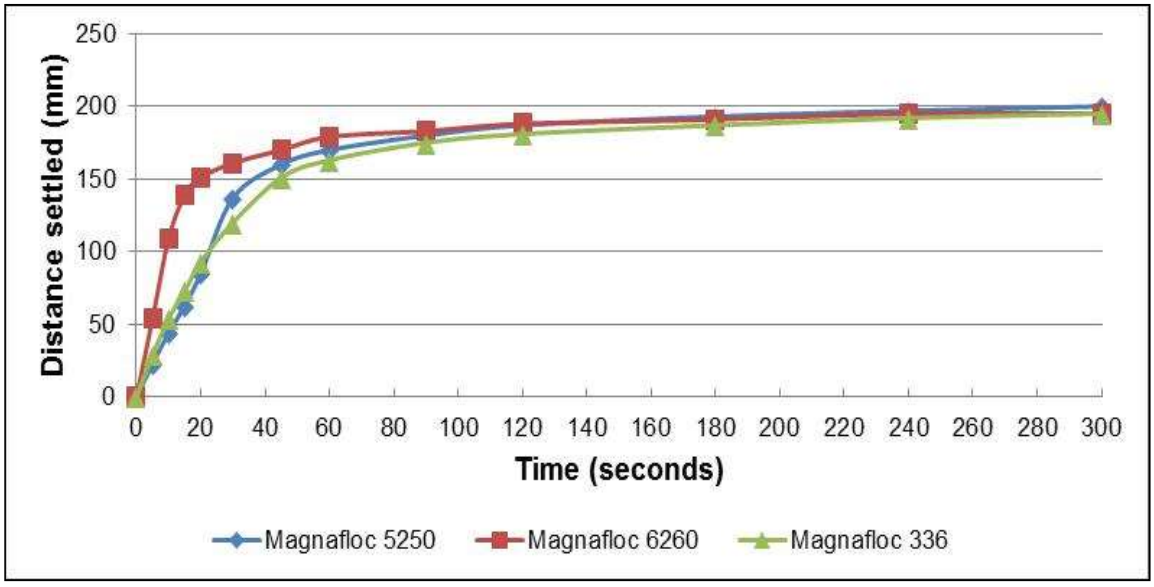

Figure 156: The settling rate curves of AC 4-1A-1 with 0.025% of Magnafloc 5250, 6260 and 336

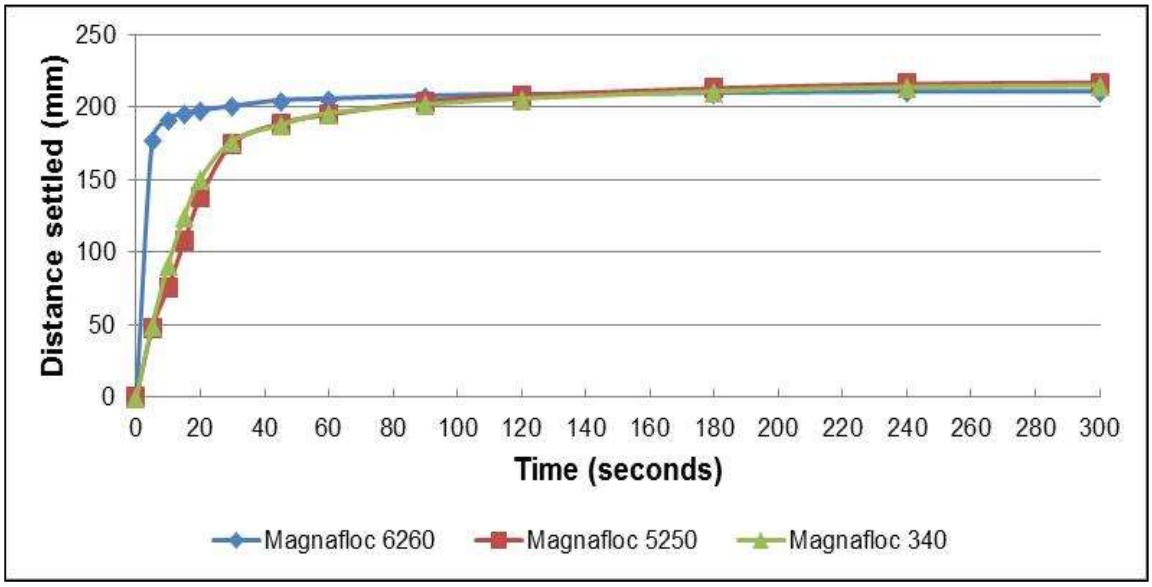

Figure 157: The settling rate curves of AC 5-5-1 with 0.025% of Magnafloc 6260, 5250 and 340

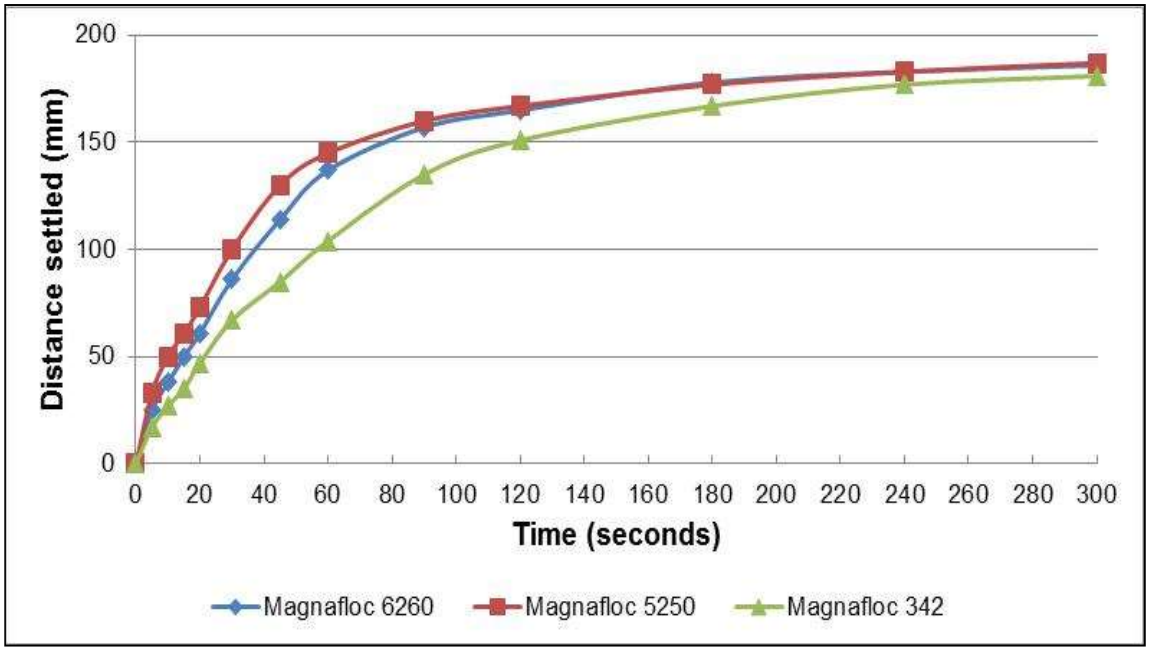

Figure 158: The settling rate curves of AC 5-5-2 with 0.025% of Magnafloc 6260, 5250 and 342

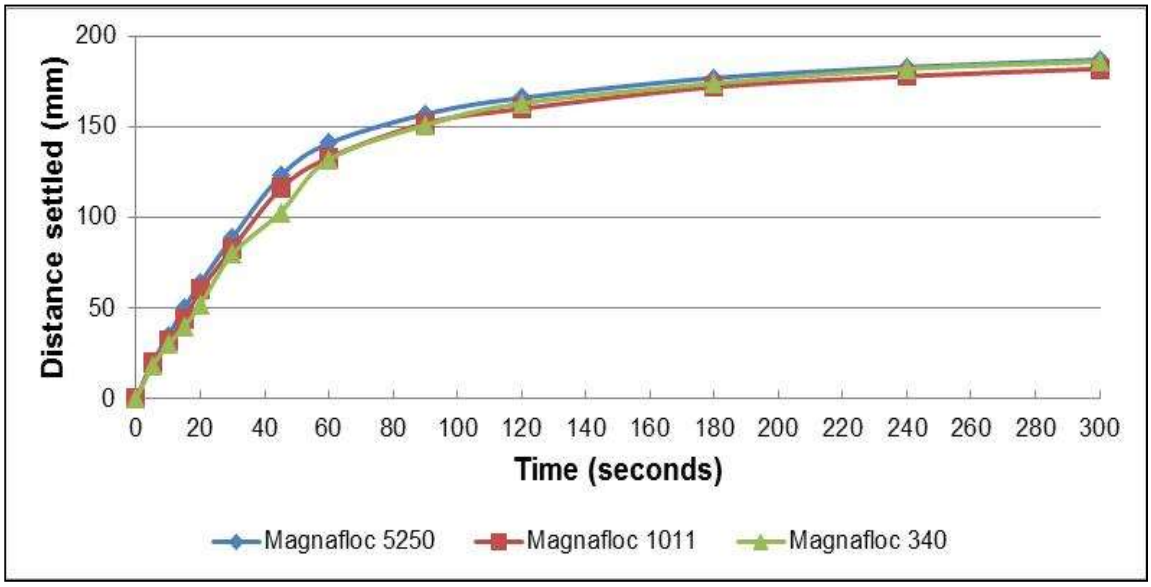

Figure 159: The settling rate curves of AC 16-1-1 with 0.025% of Magnafloc 5250, 1011 and 340

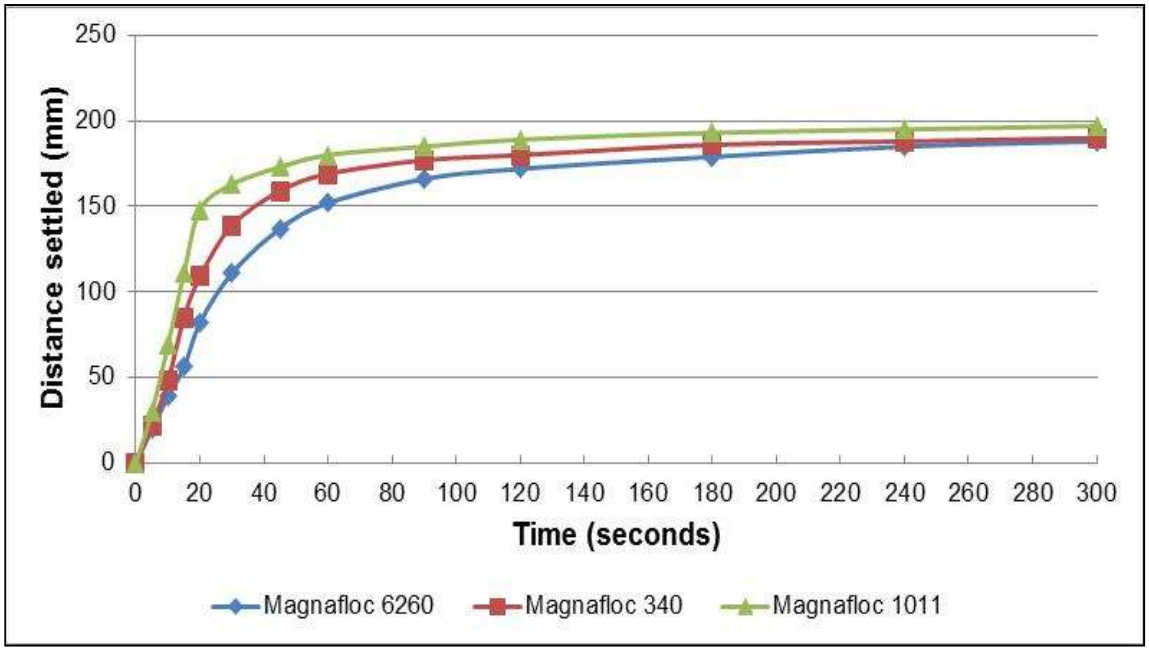

Figure 160: The settling rate curves of AC 197-1-1 with 0.025% of Magnafloc 6260, 340 and 1011

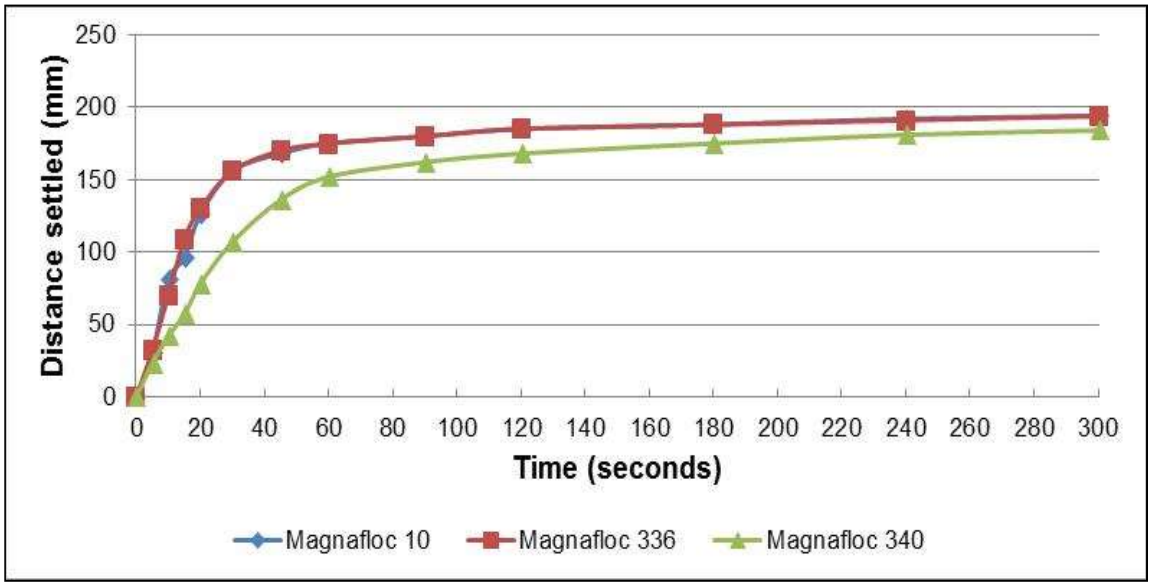

Figure 161: The settling rate curves of AO 319 with 0.025% of Magnafloc 10, 336 and 340

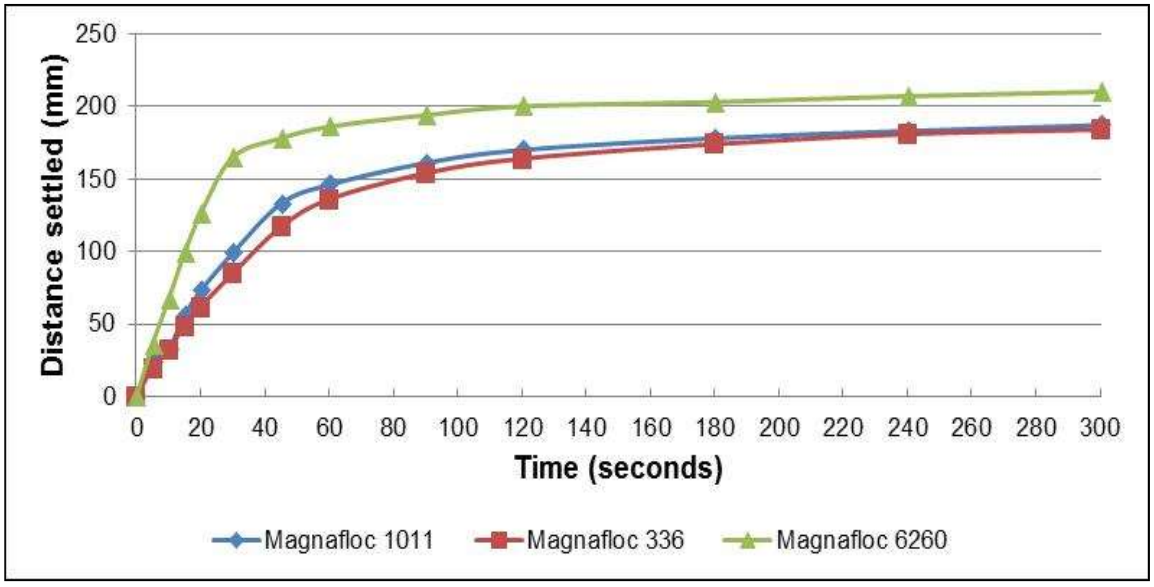

Figure 162: The settling rate curves of AO 320 with 0.025% of Magnafloc 5250, 1011 and 336

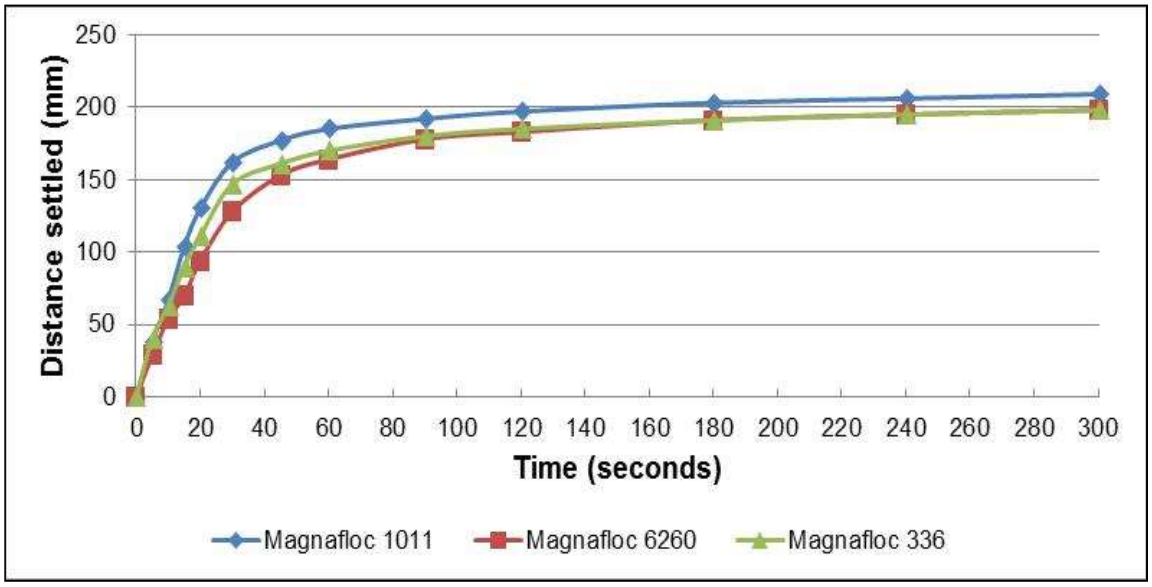

Figure 163: The settling rate of AO 321 with 0.025% of Magnafloc 6260, 336 and 1011

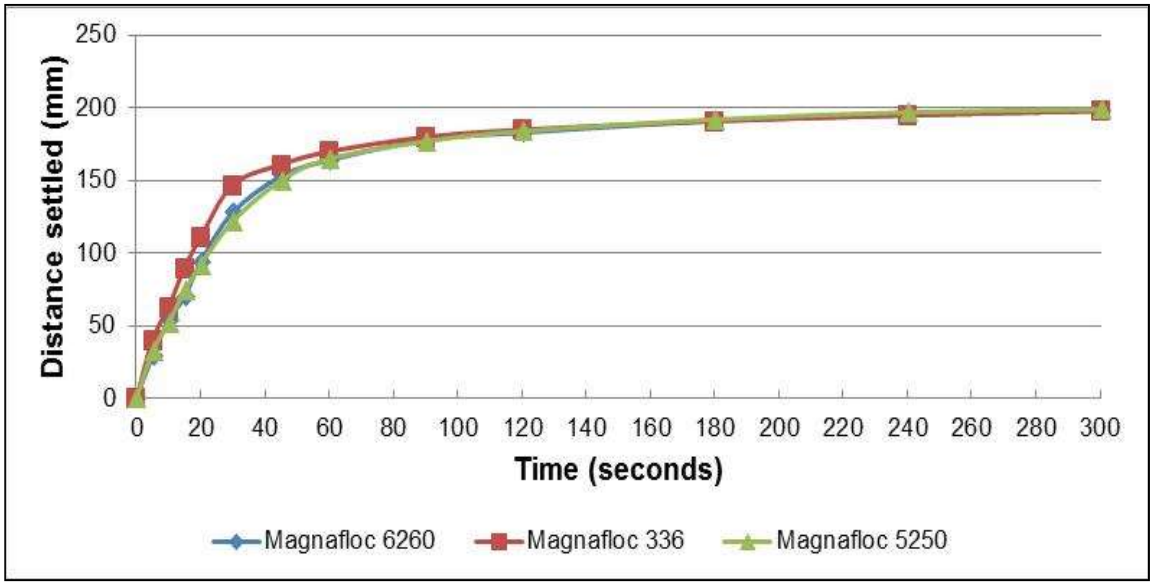

Figure 164: The settling rate curves of AO 322 with 0.025% of Magnafloc 6260, 336 and 5250

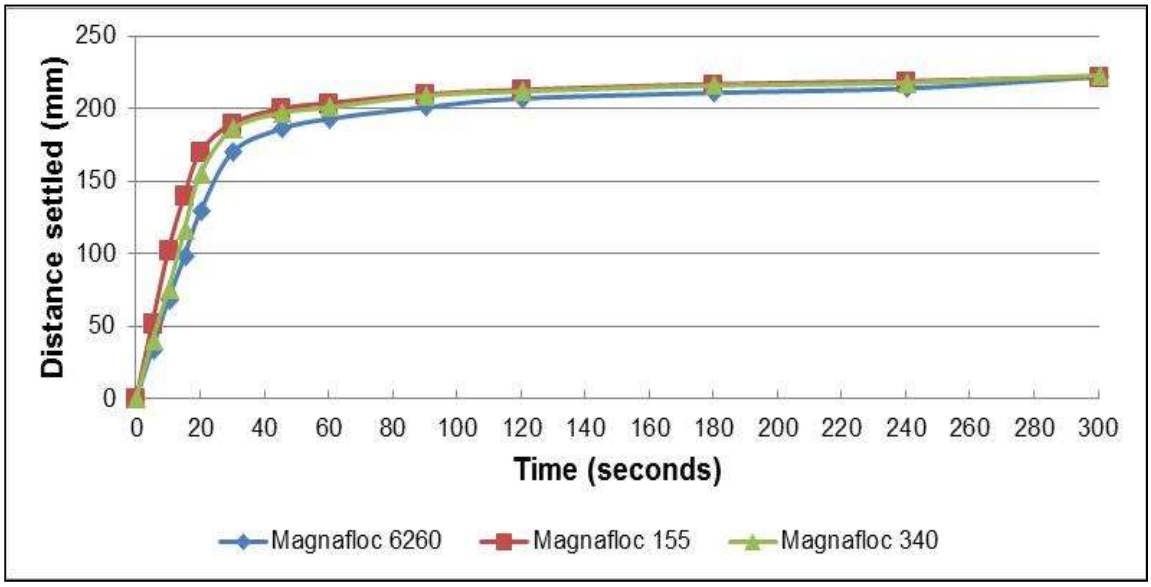

Figure 165: The settling rate curves of AO 323 with 0.025% of Magnafloc 6260, 155 and 340

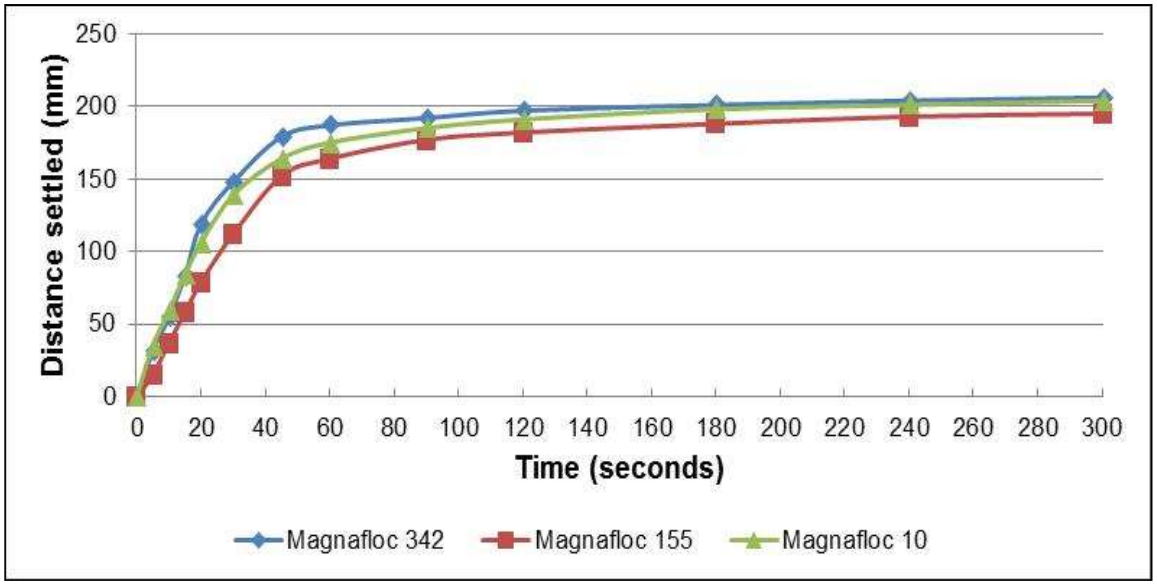

Figure 166: The settling rate curves of AO 324 with 0.025% of Magnafloc 342, 155 and 10

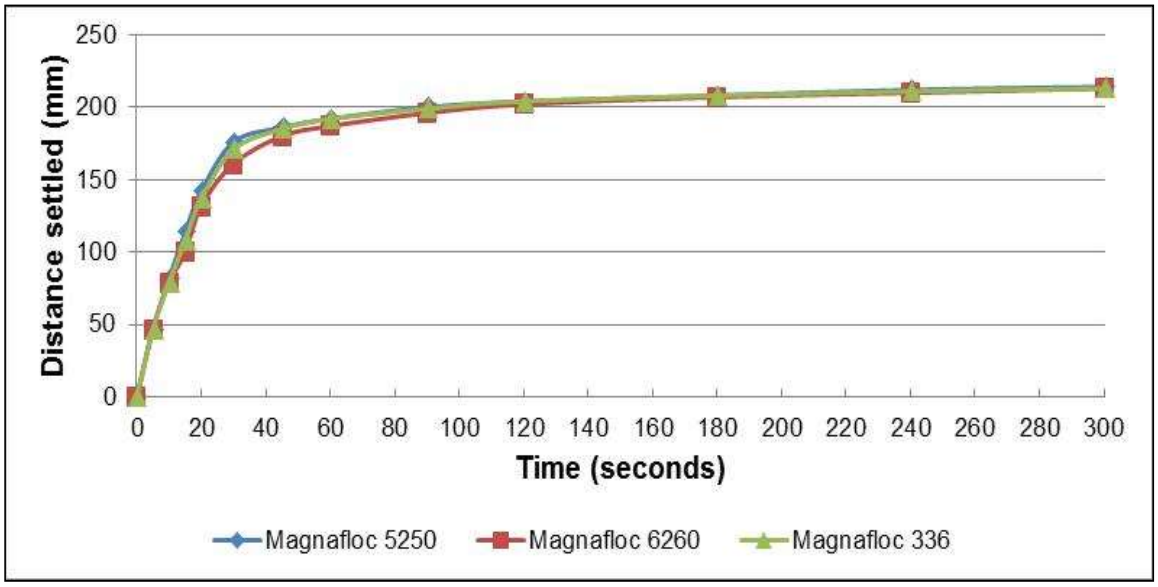

Figure 167: The settling rate curves of AO 325 with 0.025% of Magnafloc 5250, 6260 and 336

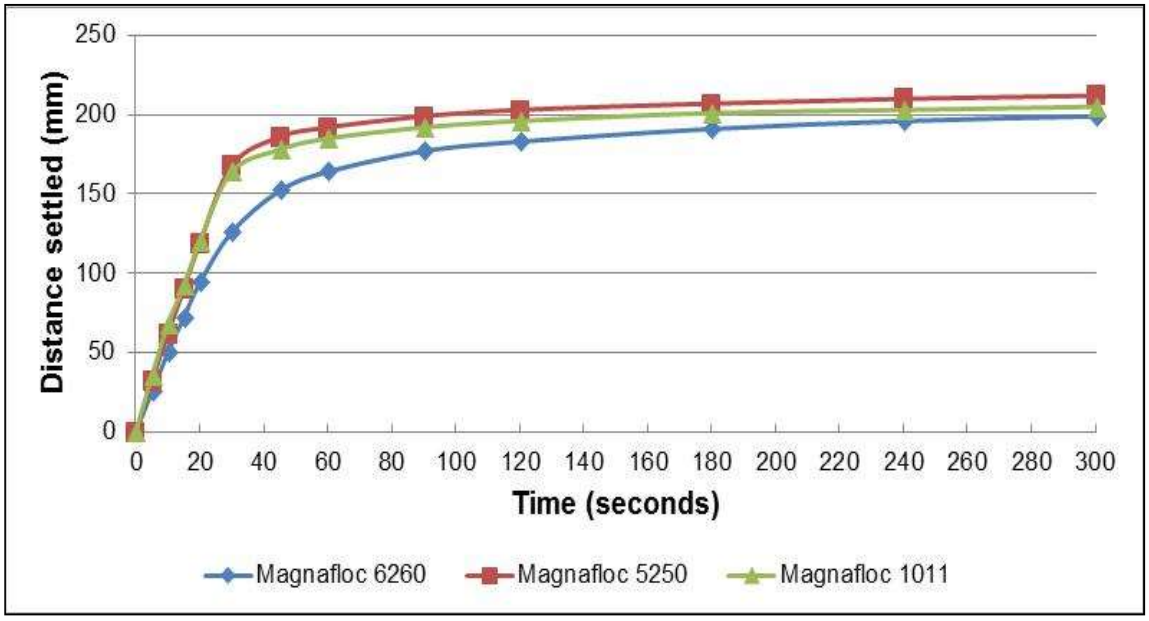

Figure 168: The settling rate curves of AO 326 with 0.025% of Magnafloc 6260, 5250 and 1011

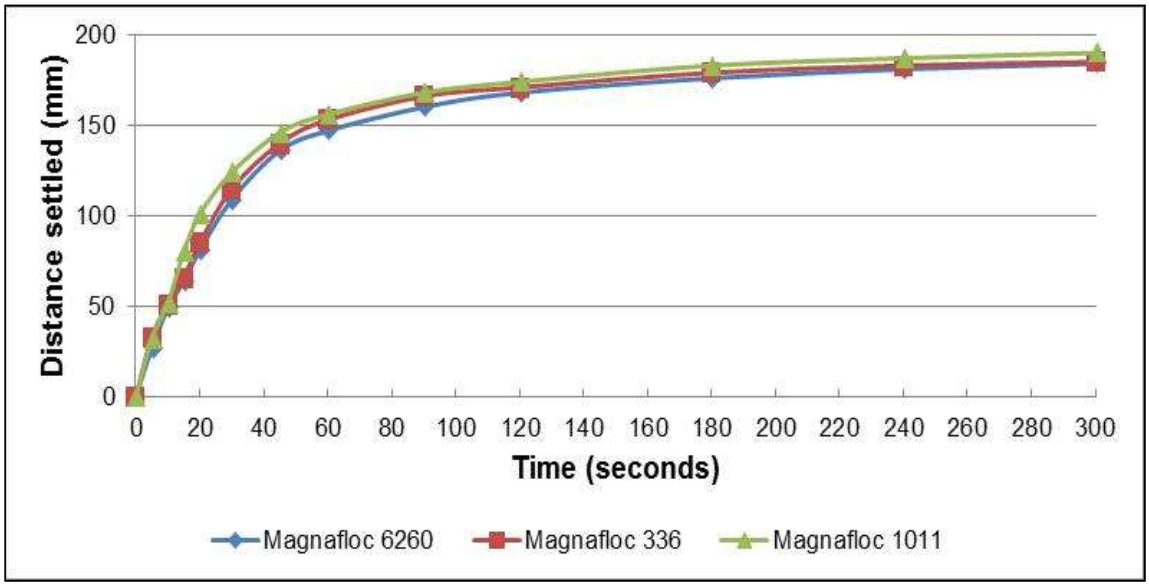

Figure 169: The settling rate curves of AO 327 with 0.025% of Magnafloc 6260, 336 and 1011

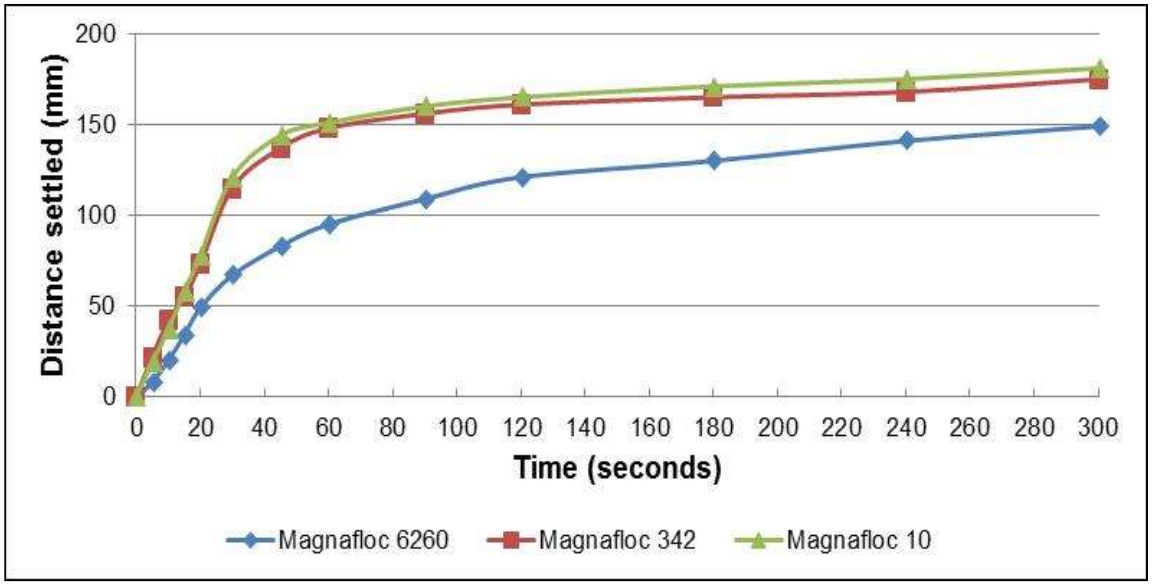

Figure 170: The settling rate curves of AO 328 with 0.025% of Magnafloc 6260, 342 and 10

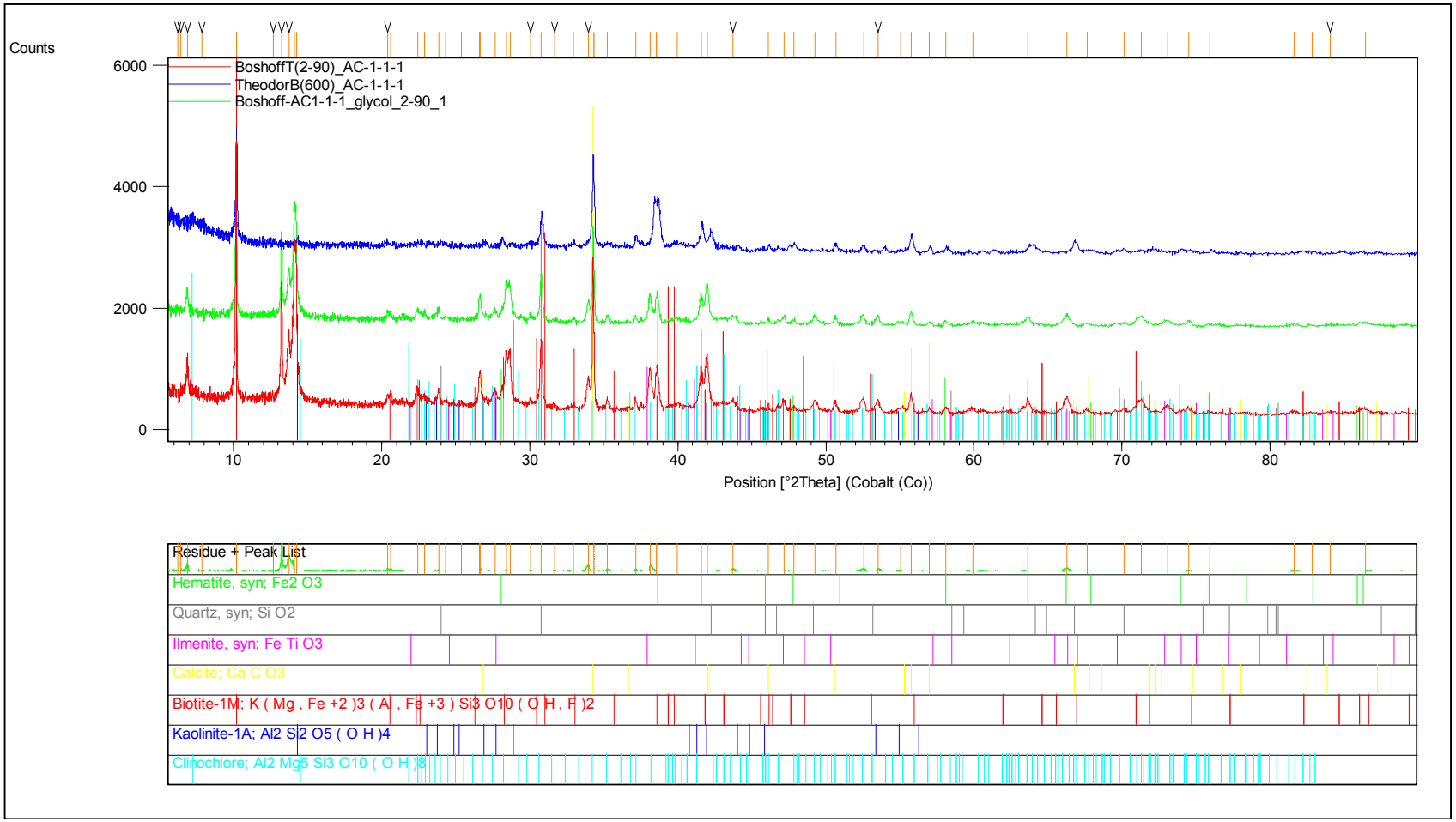

Figure 171: XRD Scan done on AC 1 - 1 - 1 at the University of Pretoria

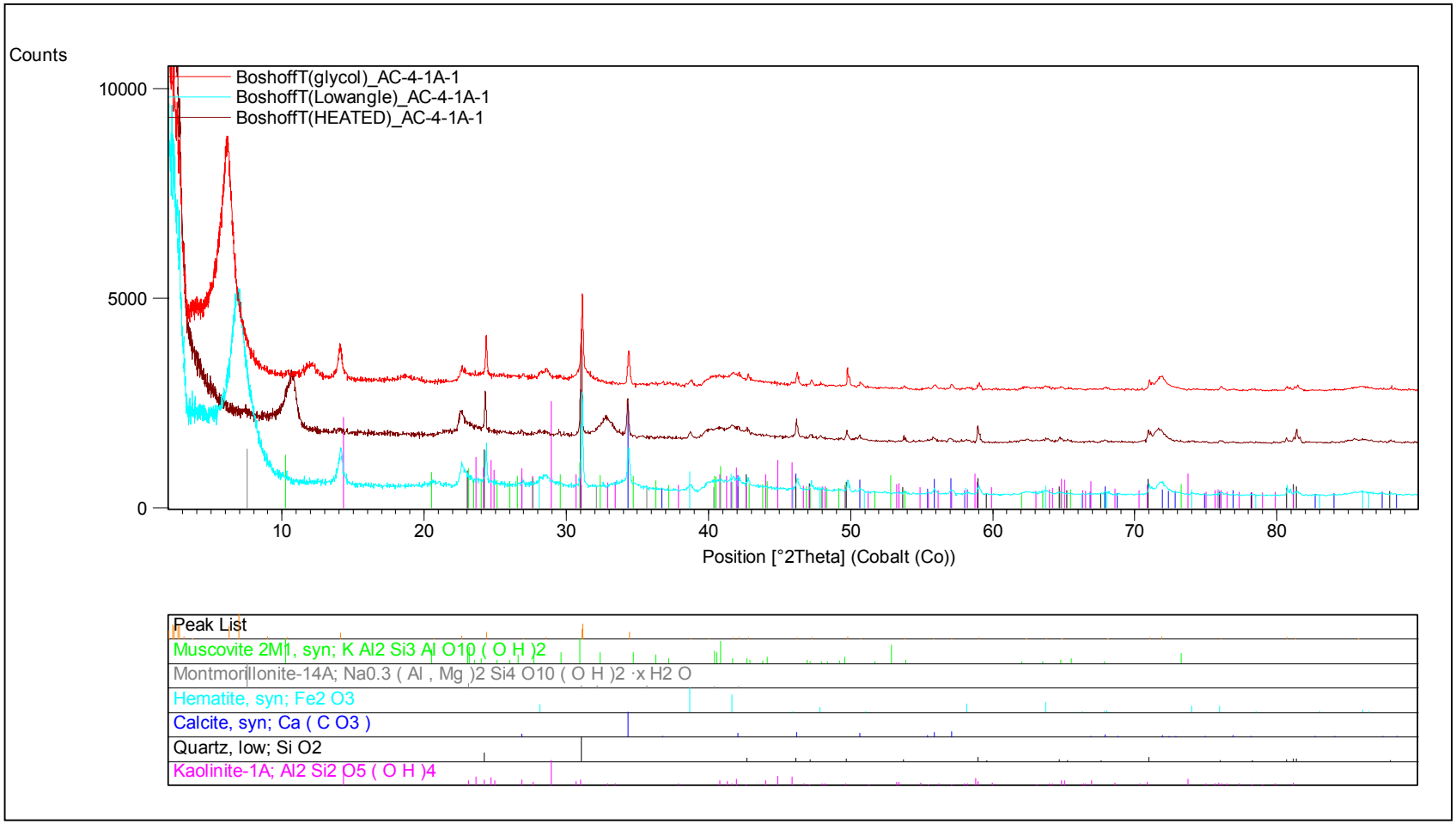

Figure 172: XRD Scan done on AC 4 – 1A -1 at the University of Pretoria

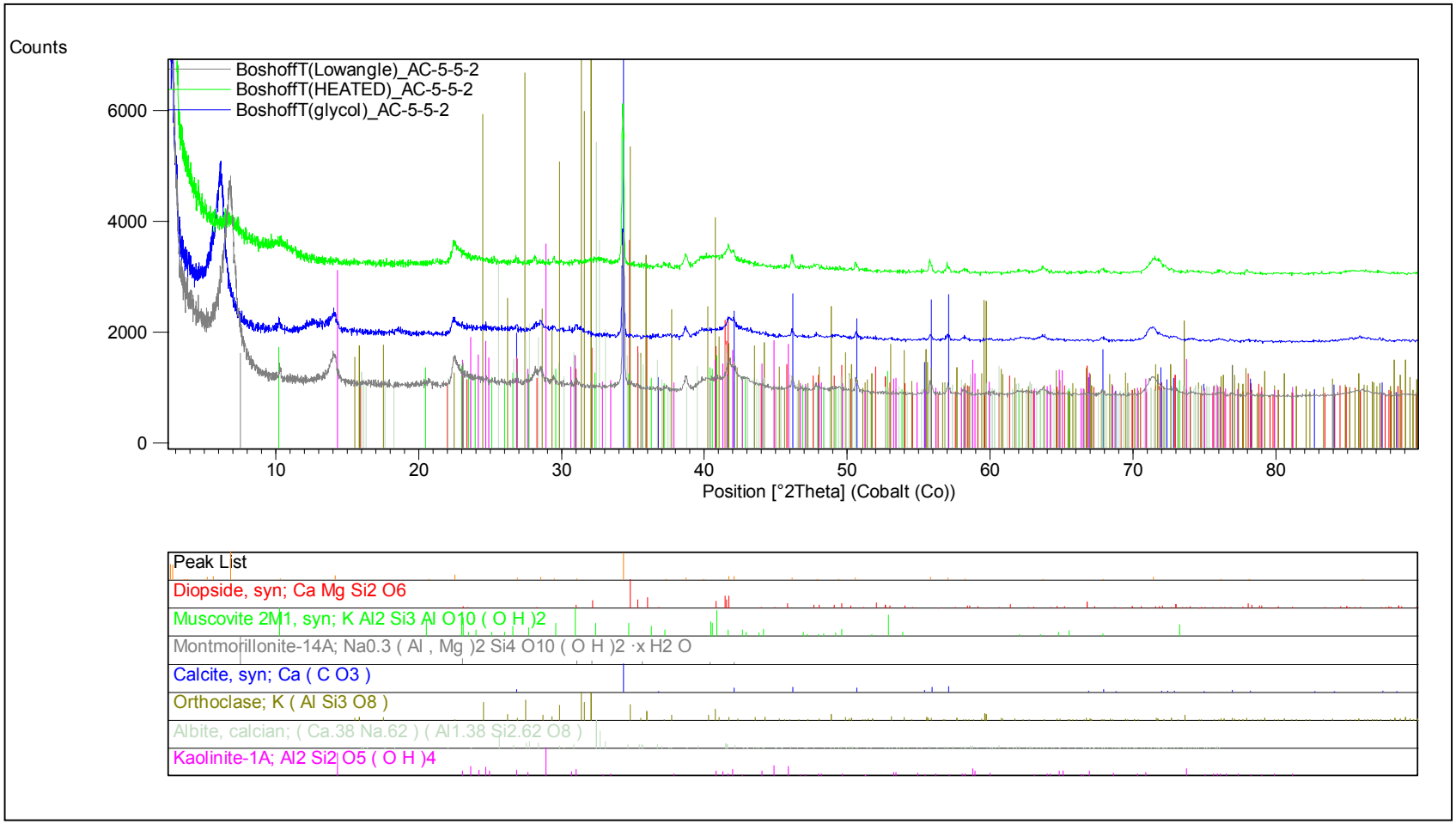

Figure 173: XRD Scan done on AC 5-5-2 at the University of Pretoria

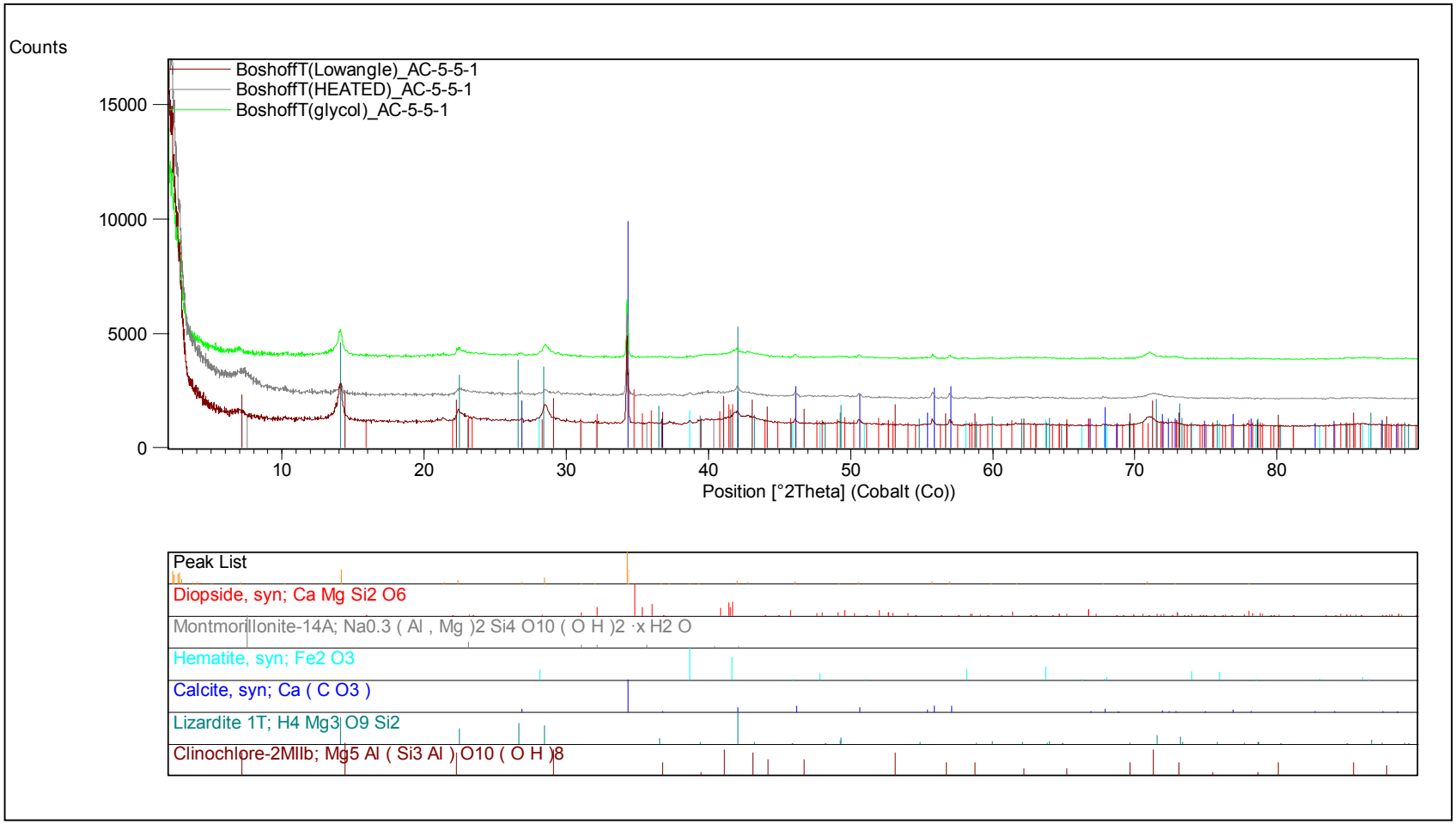

Figure 174: XRD Scan done on AC 5 – 5 - 1 at the University of Pretoria

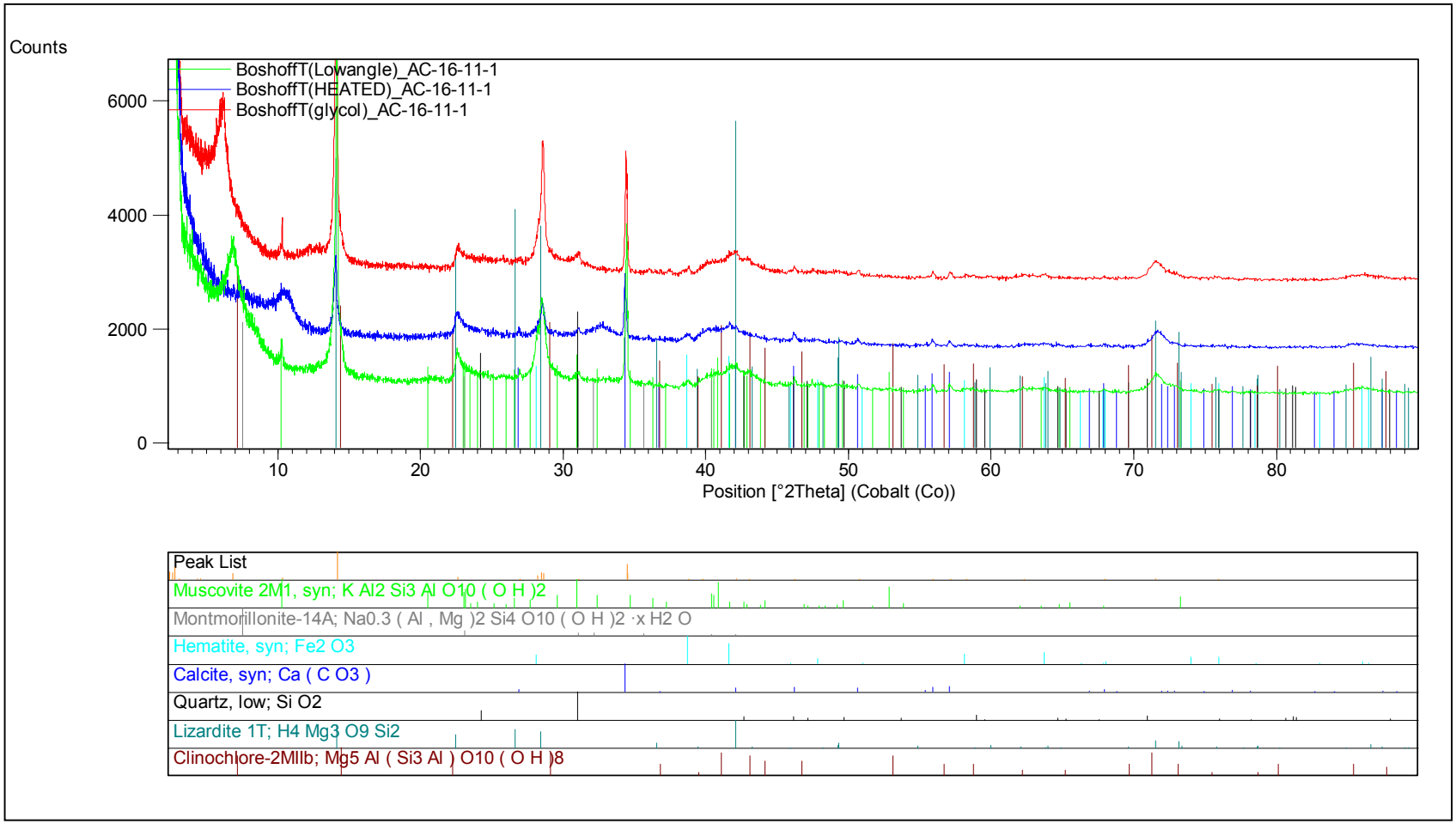

Figure 175: XRD Scan done on AC 16 – 11 -1 at the University of Pretoria

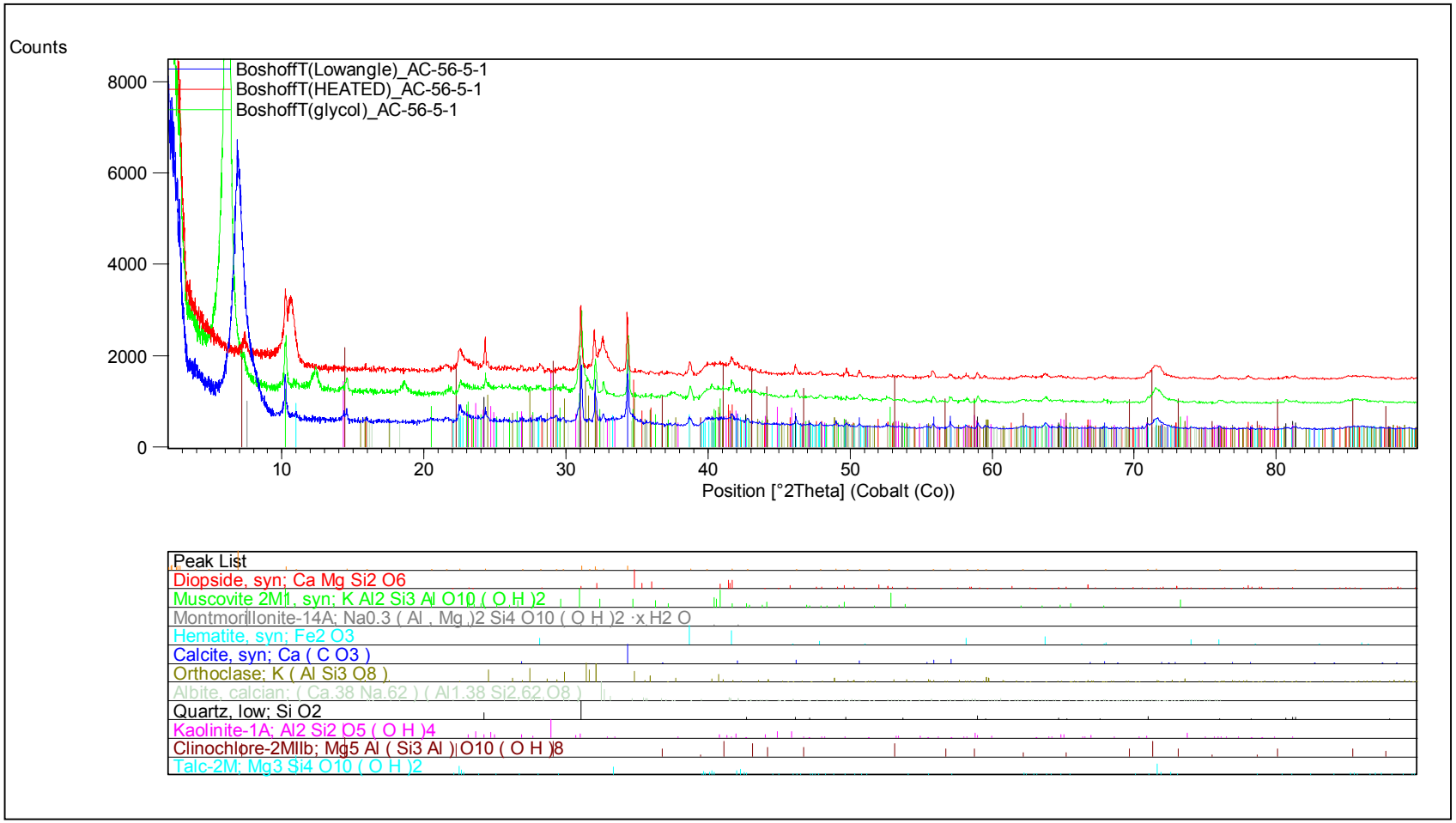

Figure 176: XRD Scan done on AC 56 – 5 -1 at the University of Pretoria

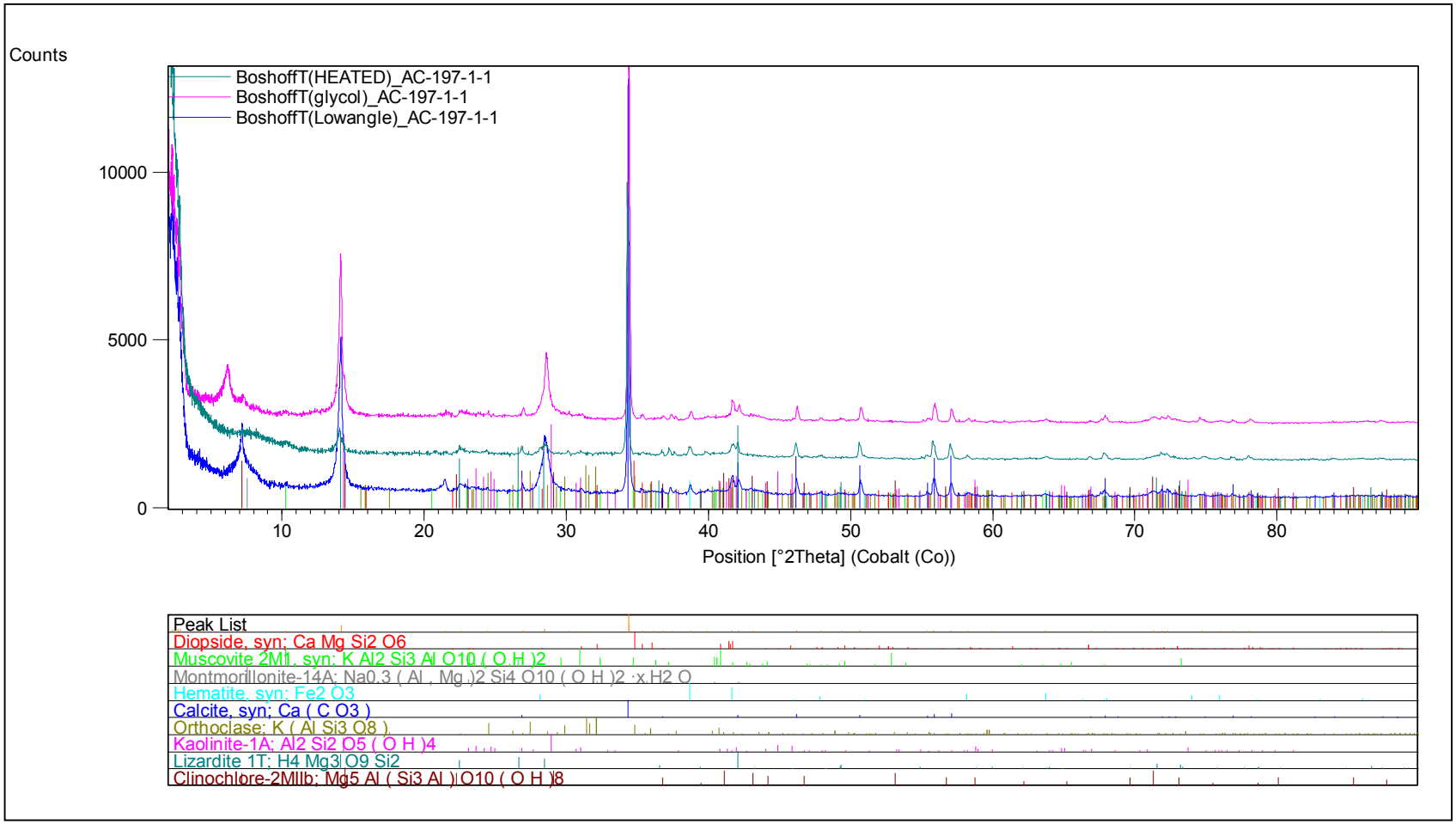

Figure 177: XRD Scan done on AC 197 – 1 - 1 at the University of Pretoria

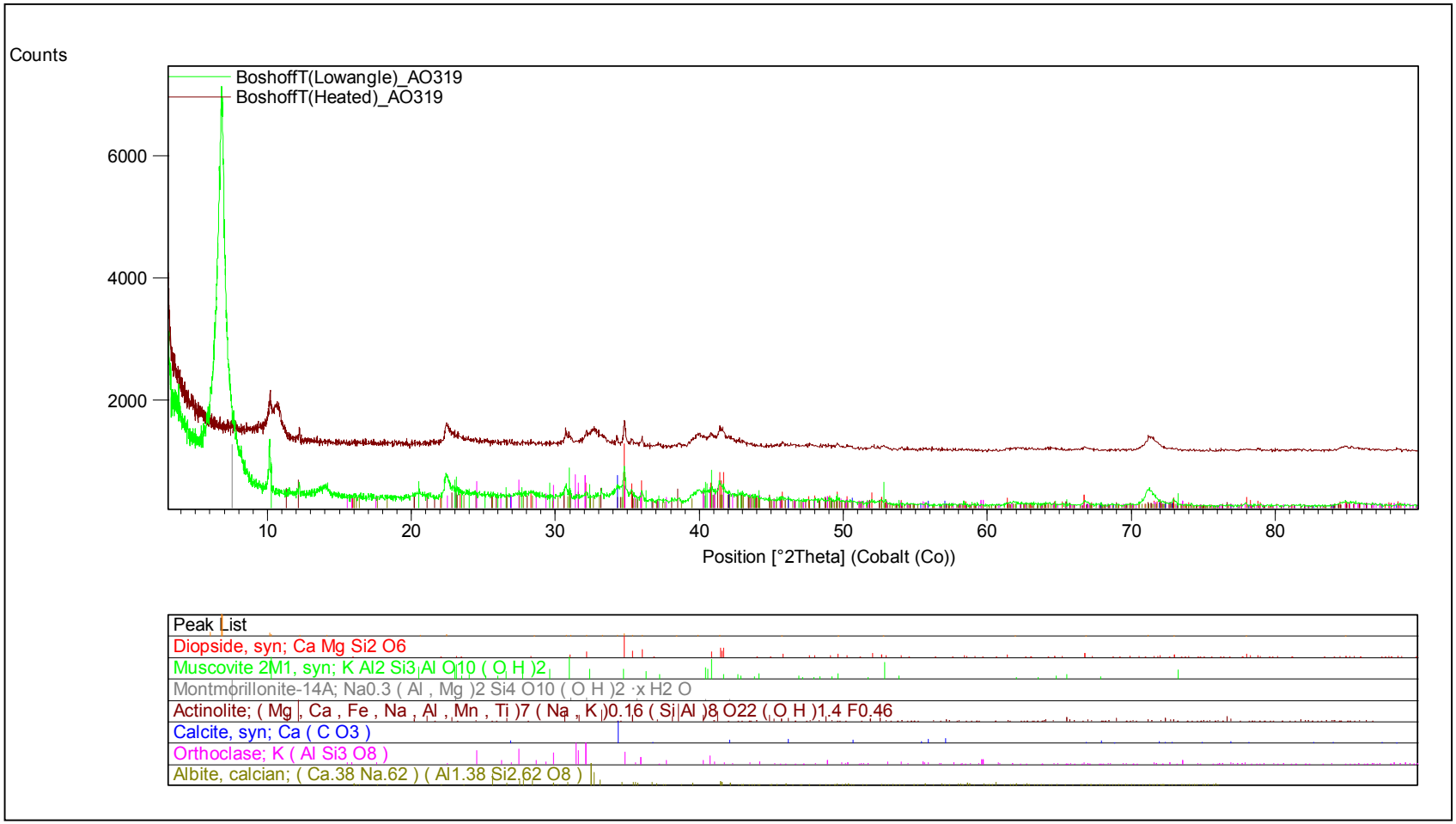

Figure 178: XRD Scan done on AO 319 at the University of Pretoria

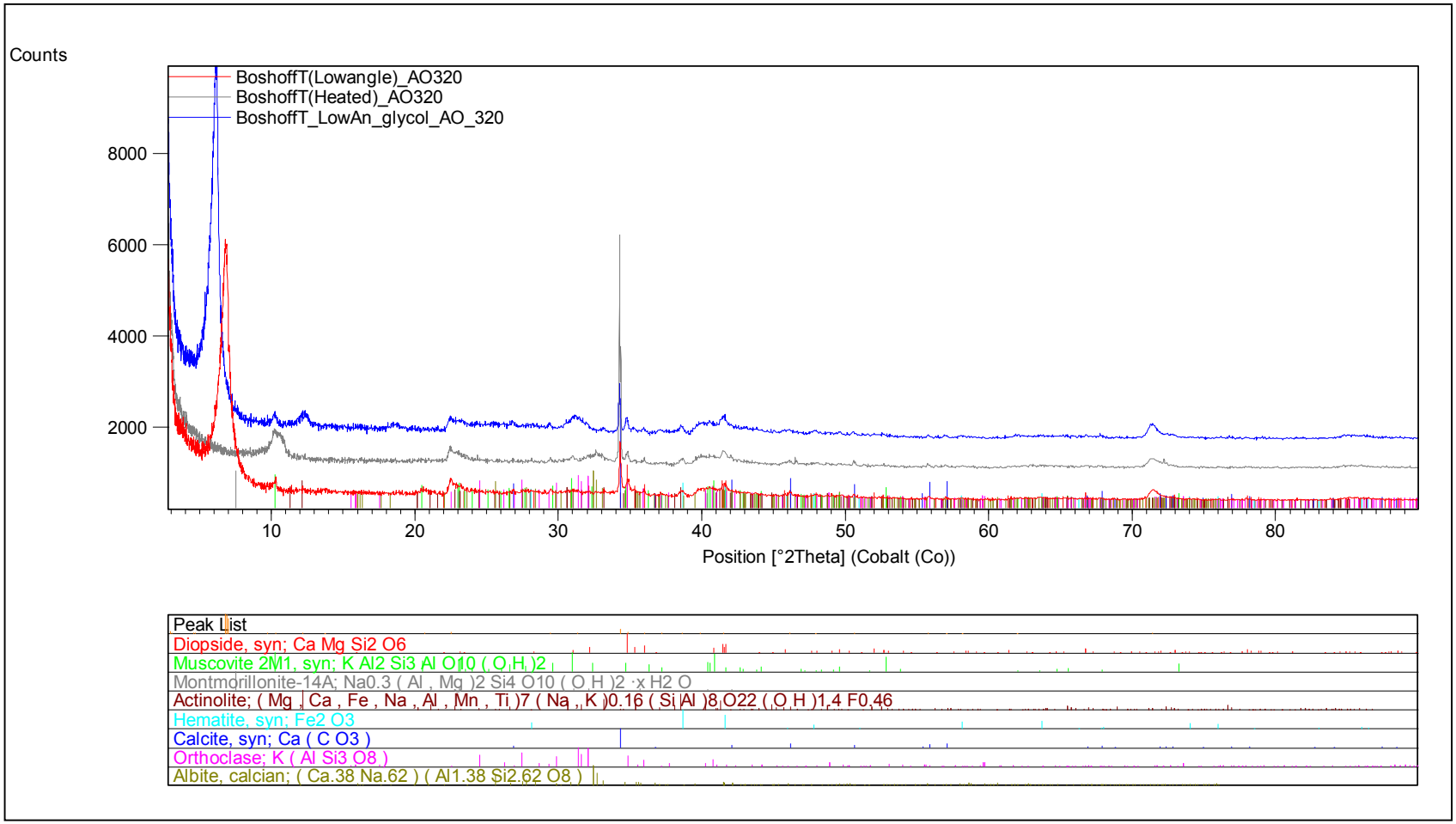

Figure 179: XRD Scan done on AO 320 at the University of Pretoria

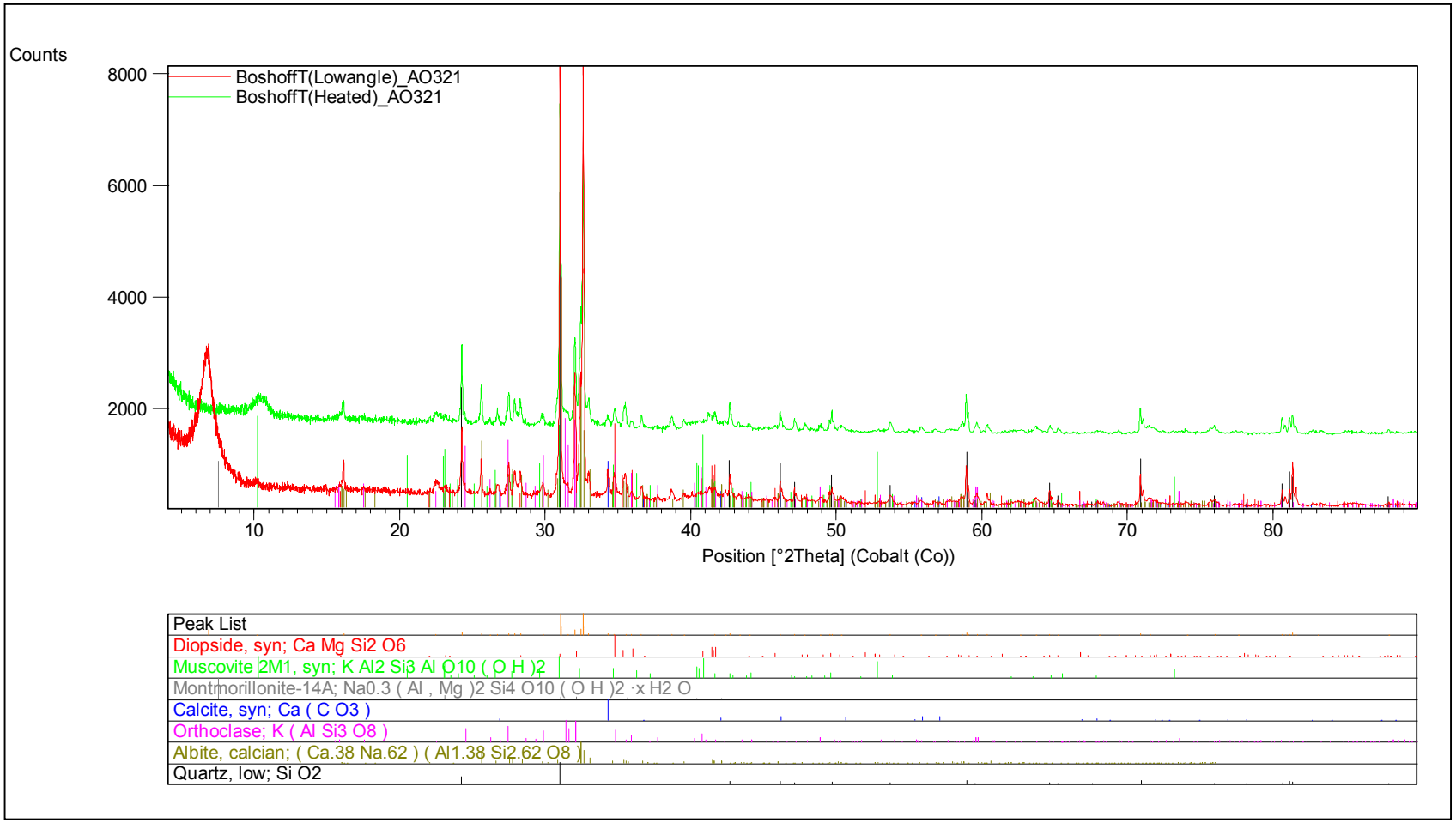

Figure 180: XRD Scan done on AO 321 at the University of Pretoria

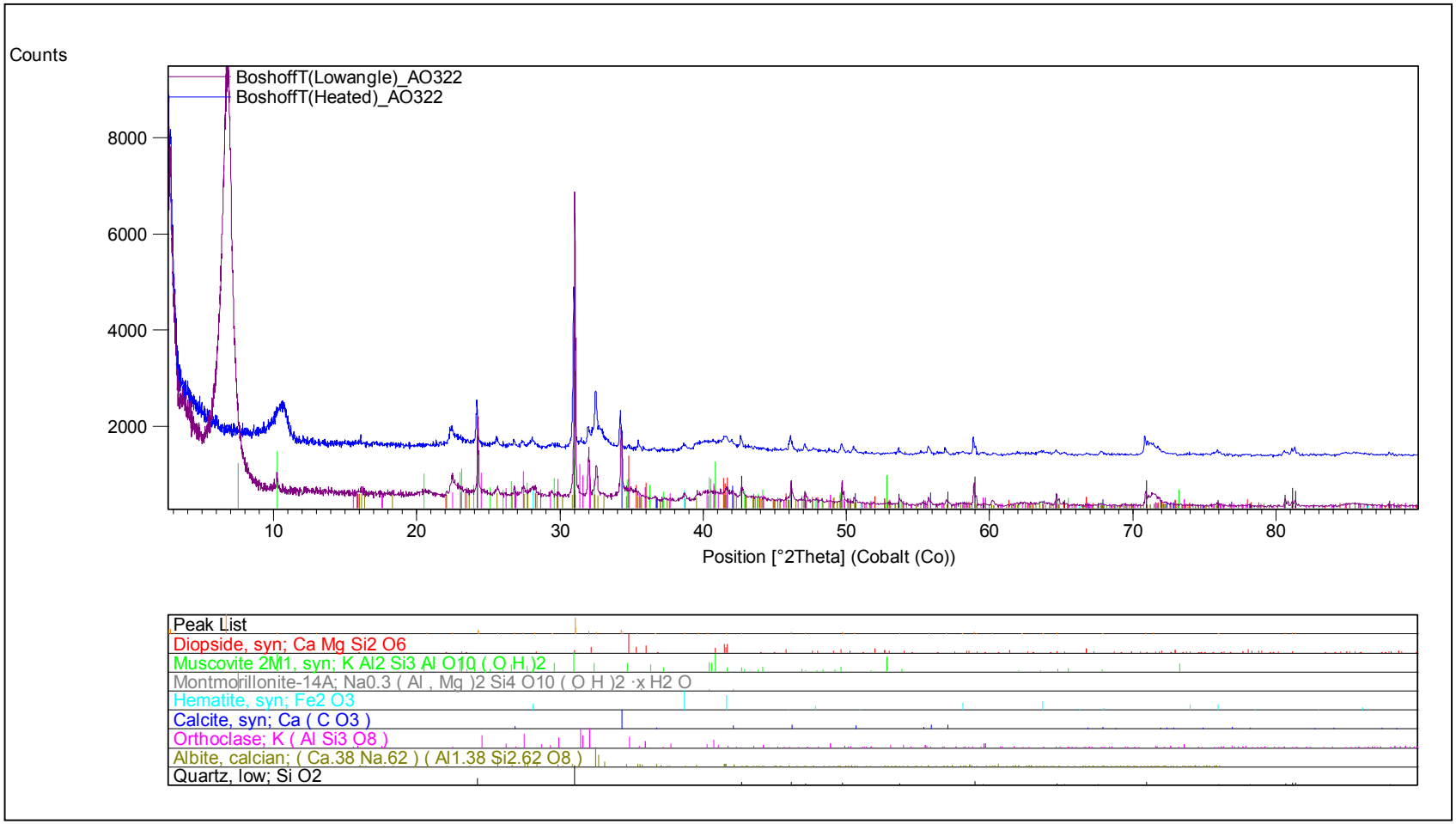

Figure 181: XRD Scan done on AO 322 at the University of Pretoria

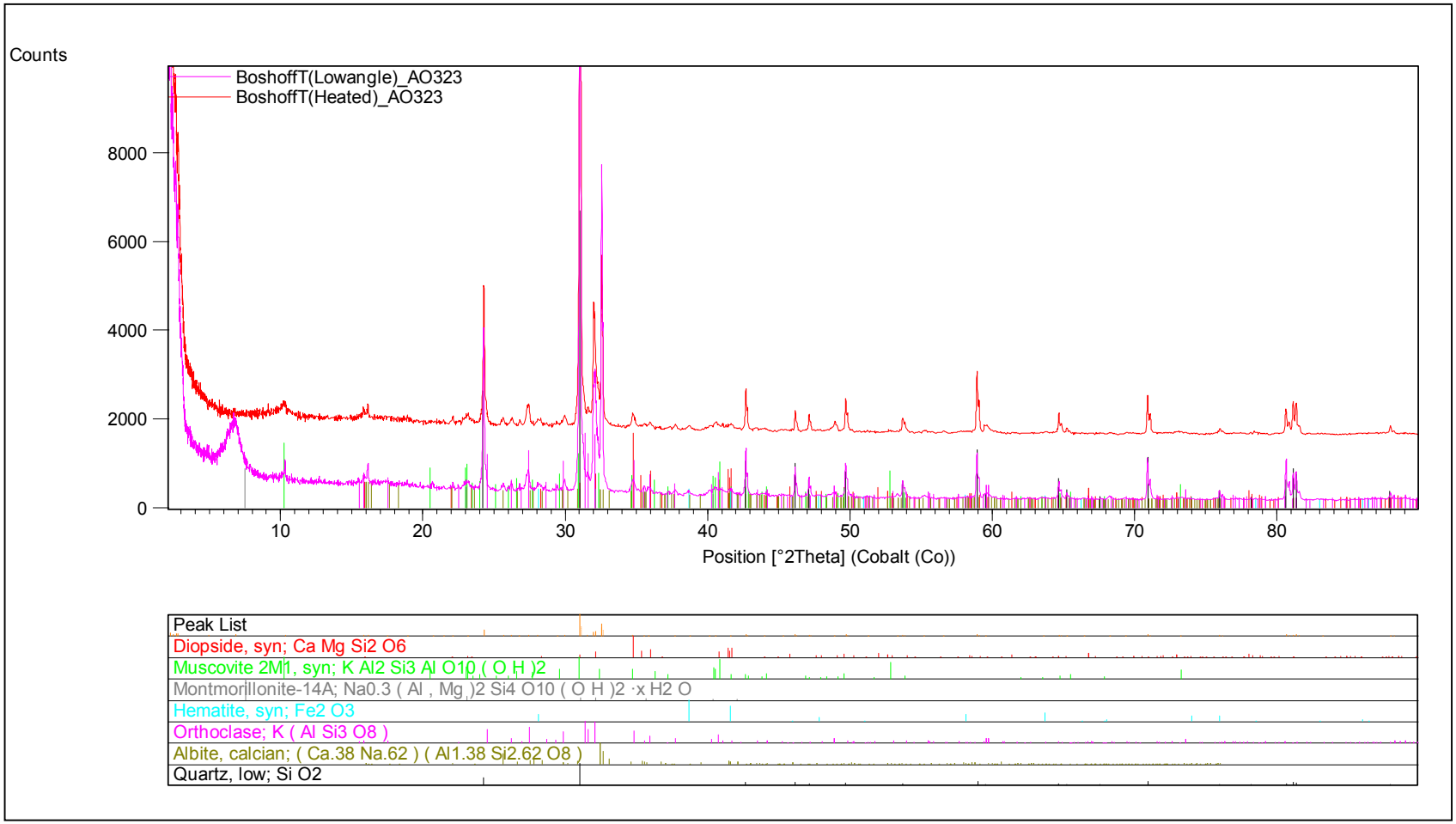

Figure 182: XRD Scan done on AO 323 at the University of Pretoria

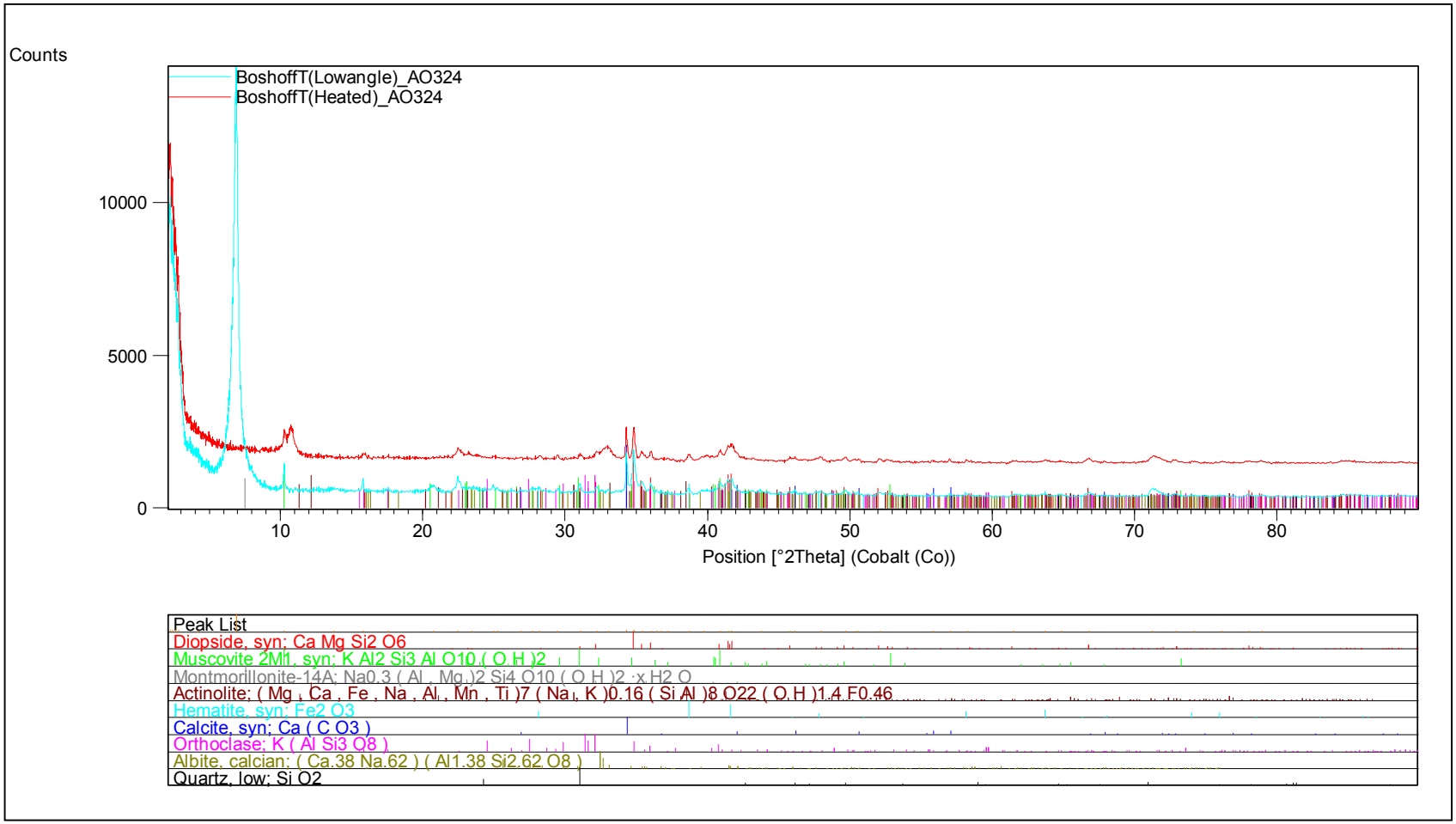

Figure 183: XRD Scan done on AO 324 at the University of Pretoria

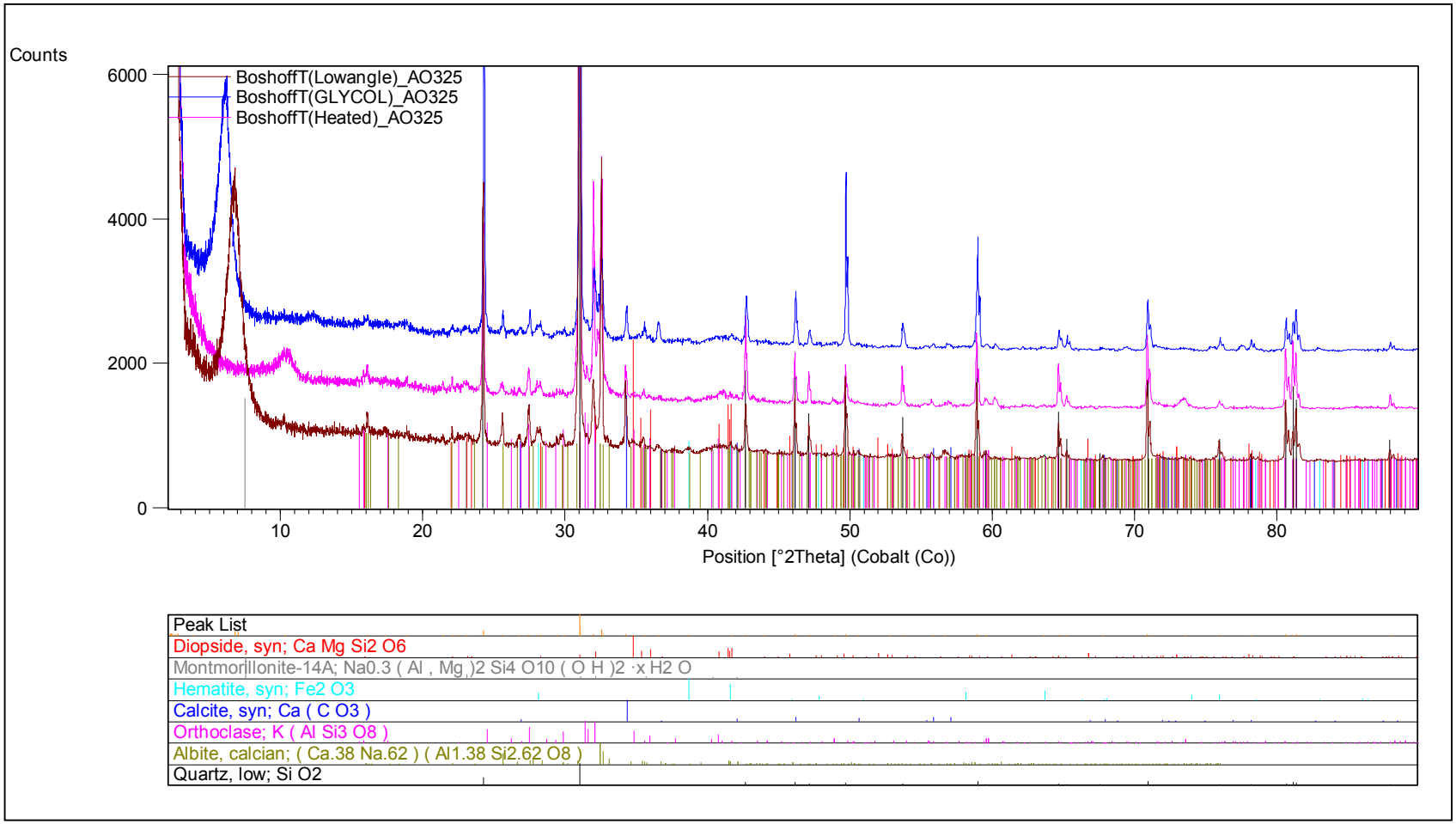

Figure 184: XRD Scan done on AO 325 at the University of Pretoria

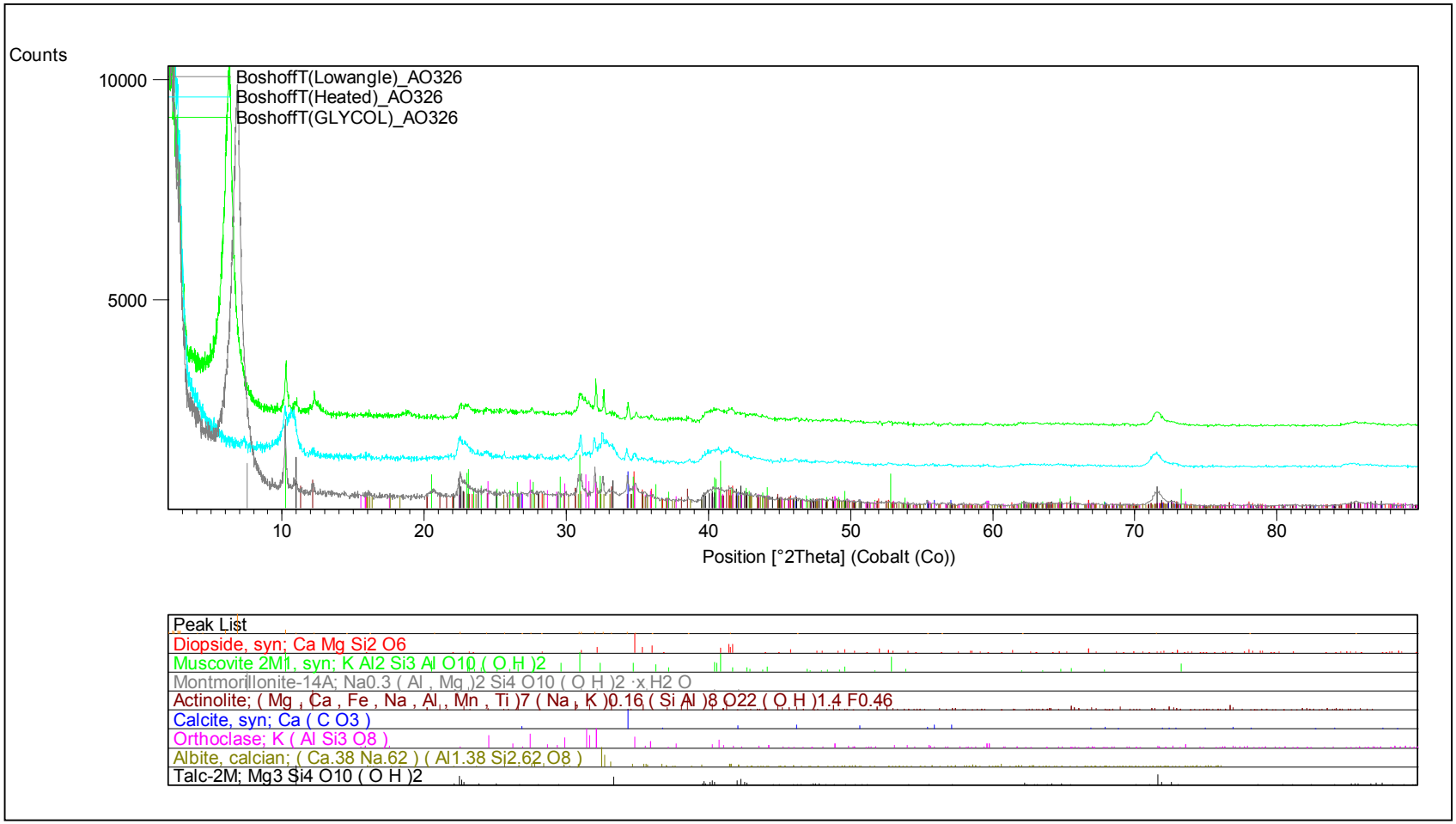

Figure 185: XRD Scan done on AO 326 at the University of Pretoria

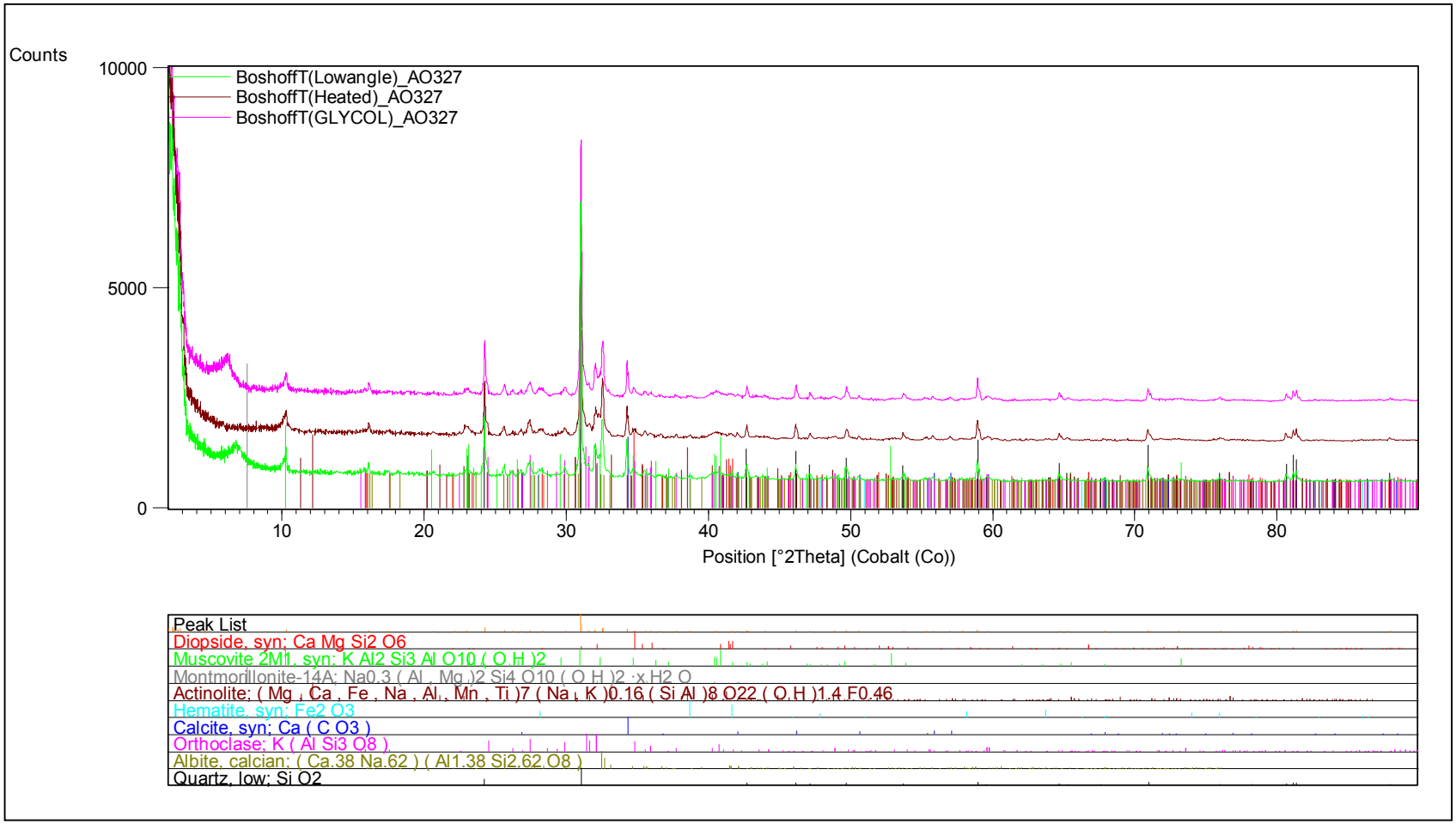

Figure 186: XRD Scan done on AO 327 at the University of Pretoria

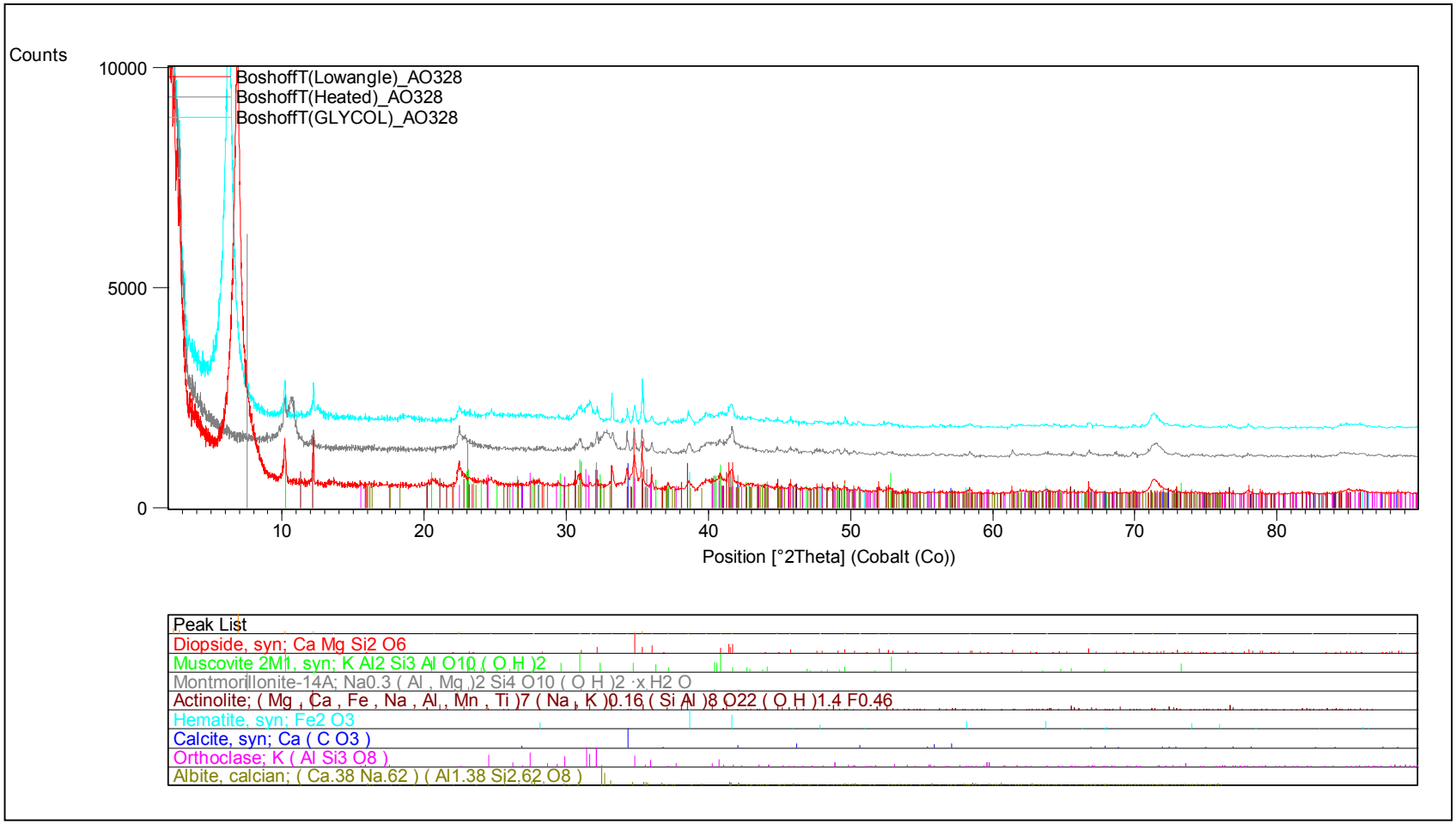

Figure 187: XRD Scan done on AO 328 at the University of Pretoria

Equation Parameters																				
R Squared	0.4461	44.61% of the change in cation settling rate can be explained by the change in the 9 Independent Variables																		
Adjusted R Squared	-0.1771	Adjusted for Sample Size bias						2.27419	Durbin-Watson Statistic		Critical D-W Values: Lower (Dl)=0.71; Upper (Du)=2.06									
Standard Error	0.6651	to +/- on result of Regression Equation							Therefore Negative Autocorrelation maybe present at 95% Confidence											
F - Statistic	0.7159	Therefore analysis IS NOT Significant						2.49429	Critical F-Statistic at 95% Confidence						(Significance holds to 31.1% Confidence)					

Multiple Regression Equation					Independent Analysis			Correlation	Tests for Multicollinearity between Independent Variables										
	Coefficients	Standard Error	t Stat	p Value	R Squared	Gradient	Intercept	Dl=1.16 Du=1.39 DW-Stat	Adjusted R-Squared against other	Independent R-Square Matrix									
Intercept	-5.534	8.133	-0.680	51.54%															
Ca	-0.007	0.011	-0.652	53.28%	9.90%	0.00	1.13	1.82	72.00%	100%	78%	2%	15%	36%	4%	11%	6%	2%	Ca
Mg	0.019	0.018	1.025	33.52%	15.92%	0.01	1.32	1.97	80.99%	78%	100%	0%	33%	42%	2%	21%	13%	10%	Mg
Smectite %	-0.002	0.017	-0.113	91.29%	0.64%	0.00	1.76	2.91	39.17%	2%	0%	100%	0%	22%	38%	0%	7%	0%	Smectite %
pH	0.770	0.850	0.906	39.16%	0.37%	0.09	0.73	1.69	61.39%	15%	33%	0%	100%	11%	1%	63%	2%	0%	pH
CEC	-0.010	0.018	-0.580	57.79%	18.61%	-0.01	2.09	2.55	67.77%	36%	42%	22%	11%	100%	23%	7%	34%	26%	CEC
K	-0.078	0.140	-0.558	59.19%	0.00	-0.02	1.66	2.67	44.61%	4%	2%	38%	1%	23%	100%	2%	1%	5%	K
ESP %	-0.002	0.031	-0.056	95.69%	0.00	0.00	1.61	1.07	65.10%	11%	21%	0%	63%	7%	2%	100%	11%	0%	ESP %
7.5 micron	-0.021	0.062	-0.344	73.95%	0.23	-0.04	2.81	1.57	73.37%	6%	13%	7%	2%	34%	1%	11%	100%	59%	7.5 micron
75 micron	0.012	0.038	0.315	76.08%	0.19	-0.03	3.85	1.93	63.81%	2%	10%	0%	0%	26%	5%	0%	59%	100%	75 micron

Figure 188: Regression modelling for the cation settling rate of kimberlite slurries.

Equation Parameters																				
R Squared	0.4797	47.97% of the change in cation bed depth can be explained by the change in the 9 Independent Variables																		
Adjusted R Squared	-0.1056	Adjusted for Sample Size bias						0.13312	Durbin-Watson Statistic		Critical D-W Values: Lower (Dl)=0.71; Upper (Du)=2.06									
Standard Error	0.0927	to +/- on result of Regression Equation							Therefore Positive Autocorrelation detected at 95% Confidence											
F - Statistic	0.8196	Therefore analysis IS NOT Significant						2.49429	Critical F-Statistic at 95% Confidence						(Significance holds to 39.3% Confidence)					

Multiple Regression Equation					Independent Analysis			Auto Correlation	Tests for Multicollinearity between Independent Variables										
	Coefficients	Standard Error	t Stat	p Value	R Squared	Gradient	Intercept	Dl=1.16 Du=1.39 DW-Stat	Adjusted R-Squared against other Indep	Independent R-Square Matrix									
Intercept	-0.623	1.134	-0.550	59.75%															
Ca	-0.002	0.001	-1.035	33.11%	14.28%	0.00	0.32	1.82	72.00%	100%	78%	2%	15%	36%	4%	11%	6%	2%	Ca
Mg	0.003	0.003	1.310	22.66%	19.85%	0.00	0.36	1.97	80.99%	78%	100%	0%	33%	42%	2%	21%	13%	10%	Mg
Smectite %	-0.001	0.002	-0.579	57.86%	9.93%	0.00	0.49	2.91	39.17%	2%	0%	100%	0%	22%	38%	0%	7%	0%	Smectite %
pH	0.092	0.119	0.773	46.16%	0.94%	-0.02	0.60	1.69	61.39%	15%	33%	0%	100%	11%	1%	63%	2%	0%	pH
CEC	-0.003	0.002	-1.053	32.30%	27.83%	0.00	0.49	2.55	67.77%	36%	42%	22%	11%	100%	23%	7%	34%	26%	CEC
K	-0.014	0.019	-0.738	48.19%	0.04	0.01	0.38	2.67	44.61%	4%	2%	38%	1%	23%	100%	2%	1%	5%	K
ESP %	0.000	0.004	-0.023	98.19%	0.01	0.00	0.41	1.07	65.10%	11%	21%	0%	63%	7%	2%	100%	11%	0%	ESP %
7.5 micron	-0.002	0.009	-0.214	83.55%	0.11	0.00	0.52	1.57	73.37%	6%	13%	7%	2%	34%	1%	11%	100%	59%	7.5 micron
75 micron	0.005	0.005	1.003	34.53%	0.03	0.00	0.52	1.93	63.81%	2%	10%	0%	0%	26%	5%	0%	59%	100%	75 micron

Figure 189: Regression modelling for cation bed depth for kimberlite slurries after settling with cations.

Equation Parameters																					
R Squared	0.8857	88.57% of the change in Flocculant settling rate m/s can be explained by the change in the 9 Independent Variables																			
Adjusted R Squared	0.7572	Adjusted for Sample Size bias							0.05990	Durbin-Watson Statistic		Critical D-W Values: Lower (Dl)=0.71; Upper (Du)=2.06									
Standard Error	3.5411	to +/- on result of Regression Equation								Therefore Positive Autocorrelation detected at 95% Confidence											
F - Statistic	6.8910	Therefore analysis IS Significant							2.49429	Critical F-Statistic at 95% Confidence		(Significance holds to 99.9% Confidence)									

Multiple Regression Equation					Independent Analysis			Auto Correlation	Tests for Multicollinearity between Independent Variables											
	Coefficients	Standard Error	t Stat	p Value	R Squared	Gradient	Intercept	Dl=1.16 Du=1.39	Adjusted R-Squared against other Indep	Independent R-Square Matrix										
Intercept	93.670	43.296	2.163	6.25%				DW-Stat												
Ca	0.016	0.056	0.288	78.04%	18.12%	0.08	8.63	1.82	72.00%	100%	78%	2%	15%	36%	4%	11%	6%	2%	Ca	
Mg	0.048	0.098	0.492	63.56%	21.99%	0.12	12.18	1.97	80.99%	78%	100%	0%	33%	42%	2%	21%	13%	10%	Mg	
Smectite %	-0.079	0.090	-0.876	40.68%	5.40%	-0.10	21.27	2.91	39.17%	2%	0%	100%	0%	22%	38%	0%	7%	0%	Smectite %	
pH	-10.651	4.527	-2.353	4.65%	49.21%	-12.01	134.03	1.69	61.39%	15%	33%	0%	100%	11%	1%	63%	2%	0%	pH	
CEC	0.055	0.095	0.586	57.40%	5.45%	-0.08	19.20	2.55	67.77%	36%	42%	22%	11%	100%	23%	7%	34%	26%	CEC	
K	-0.669	0.744	-0.900	39.45%	0.00	0.17	15.76	2.67	44.61%	4%	2%	38%	1%	23%	100%	2%	1%	5%	K	
ESP %	0.074	0.165	0.449	66.55%	0.51	-0.43	20.57	1.07	65.10%	11%	21%	0%	63%	7%	2%	100%	11%	0%	ESP %	
7.096	-0.920	0.331	-2.777	2.41%	0.10	-0.33	25.50	1.57	73.37%	6%	13%	7%	2%	34%	1%	11%	100%	59%	7.096	
70.963	0.659	0.205	3.217	1.23%	0.03	0.12	6.66	1.93	63.81%	2%	10%	0%	0%	26%	5%	0%	59%	100%	70.963	

Figure 190: Regression modelling for the flocculant settling rate of the kimberlite slurries.

Equation Parameters																					
R Squared	0.8237	82.37% of the change in Flocculant settling rate m/s can be explained by the change in the 3 Independent Variables																			
Adjusted R Squared	0.7859	Adjusted for Sample Size bias							2.05470	Durbin-Watson Statistic		Critical D-W Values: Lower (Dl)=0.93; Upper									
Standard Error	3.3254	to +/- on result of Regression Equation								Therefore No Autocorrelation detected at 95% Confidence											
F - Statistic	21.7998	Therefore analysis IS Significant							3.19678	Critical F-Statistic at 95% Confidence											(Significance holds to

Multiple Regression Equation					Independent Analysis			Correlation	Tests for Multicollinearity between Independent Variables											
	Coefficients	Standard Error	t Stat	p Value	R Squared	Gradient	Intercept	Dl=1.16 Du=1.39	Adjusted R-Squared against other	Independent R-Square Matrix										
Intercept	89.515	21.161	4.230	0.08%				DW-Stat												
pH	-9.988	1.968	-5.076	0.02%	49.21%	-12.01	134.03	1.69	-8.12%	100%	2%	0%							pH	
7.5 micron	-0.917	0.187	-4.904	0.02%	10.07%	-0.33	25.50	1.57	55.79%	2%	100%	59%							7.5 micron	
75 micron	0.634	0.133	4.755	0.03%	2.55%	0.12	6.66	1.93	54.81%	0%	59%	100%							75 micron	

Figure 191: Regression modelling of the flocculant settling rate of the kimberlite slurries with the most significant independent variables.

Equation Parameters																					
R Squared	0.8980	89.80% of the change in floc bed depth can be explained by the change in the 9 Independent Variables																			
Adjusted R Squared	0.7833	Adjusted for Sample Size bias						0.06364	Durbin-Watson Statistic	Critical D-W Values: Lower (Dl)=0.71; Upper (Du)=2.06											
Standard Error	0.0587	to +/- on result of Regression Equation							Therefore Positive Autocorrelation detected at 95% Confidence												
F - Statistic	7.8267	Therefore analysis IS Significant						2.49429	Critical F-Statistic at 95% Confidence							(Significance holds to 99.9% Confidence)					
Multiple Regression Equation					**Independent Analysis**			Correlation	**Tests for Multicollinearity between Independent Variables**												
	Coefficients	Standard Error	t Stat	p Value	R Squared	Gradient	Intercept	Dl=1.16 Du=1.39 DW-Stat	Adjusted R-Squared against other	Independent R-Square Matrix										
Intercept	1.060	0.718	1.476	17.83%																	
Ca	0.001	0.001	0.596	56.75%	15.25%	0.00	0.19	1.82	72.00%	100%	78%	2%	15%	36%	4%	11%	6%	2%	Ca
Mg	0.000	0.002	-0.011	99.13%	16.58%	0.00	0.25	1.97	80.99%	78%	100%	0%	33%	42%	2%	21%	13%	10%	Mg
Smectite %	-0.001	0.002	-0.753	47.33%	3.24%	0.00	0.38	2.91	39.17%	2%	0%	100%	0%	22%	38%	0%	7%	0%	Smectite %
pH	-0.123	0.075	-1.644	13.89%	48.89%	-0.21	2.37	1.69	61.39%	15%	33%	0%	100%	11%	1%	63%	2%	0%	pH
CEC	0.000	0.002	0.159	87.75%	2.86%	0.00	0.35	2.55	67.77%	36%	42%	22%	11%	100%	23%	7%	34%	26%	CEC
K	-0.015	0.012	-1.188	26.87%	0.00	0.00	0.30	2.67	44.61%	4%	2%	38%	1%	23%	100%	2%	1%	5%	K
ESP %	-0.002	0.003	-0.884	40.27%	0.63	-0.01	0.40	1.07	65.10%	11%	21%	0%	63%	7%	2%	100%	11%	0%	ESP %
7.5 micron	-0.012	0.005	-2.131	6.57%	0.06	0.00	0.43	1.57	73.37%	6%	13%	7%	2%	34%	1%	11%	100%	59%	7.5 micron
75 micron	0.011	0.003	3.127	1.41%	0.06	0.00	0.05	1.93	63.81%	2%	10%	0%	0%	26%	5%	0%	59%	100%	75 micron

Figure 192: Regression modelling for the flocculant bed depth of the kimberlite slurries.

Equation Parameters																					
R Squared	0.8456	84.56% of the change in floc bed depth can be explained by the change in the 3 Independent Variables																			
Adjusted R Squared	0.8125	Adjusted for Sample Size bias						2.44477	Durbin-Watson Statistic	Critical D-W Values: Lower (Dl)=0.93; Upper (Du)=1.69											
Standard Error	0.0546	to +/- on result of Regression Equation							Therefore Negative Autocorrelation maybe present at 95% Confidence												
F - Statistic	25.5618	Therefore analysis IS Significant						3.19678	Critical F-Statistic at 95% Confidence							(Significance holds to 99.9% Confidence)					
Multiple Regression Equation					**Independent Analysis**			Correlation	**Tests for Multicollinearity between Independent Variables**												
	Coefficients	Standard Error	t Stat	p Value	R Squared	Gradient	Intercept	Dl=1.16 Du=1.39 DW-Stat	Adjusted R-Squared against other	Independent R-Square Matrix										
Intercept	1.513	0.348	4.352	0.07%																	
pH	-0.176	0.032	-5.444	0.01%	48.89%	-0.21	2.37	1.69	-8.12%	100%	2%	0%							pH
7.5 micron	-0.016	0.003	-5.111	0.02%	5.64%	0.00	0.43	1.57	55.79%	2%	100%	59%							7.5 micron
75 micron	0.012	0.002	5.538	0.01%	6.37%	0.00	0.05	1.93	54.81%	0%	59%	100%							75 micron

Figure 193: Regression modelling of the flocculant bed depth of the kimberlite slurries with the most significant independent variables.

Equation Parameters																				
R Squared	0.6136	61.36% of the change in combined settling rate can be explained by the change in the 9 Independent Variables																		
Adjusted R Squared	0.1788	Adjusted for Sample Size bias						0.10882	Durbin-Watson Statistic		Critical D-W Values: Lower (Dl)=0.71; Upper (Du)=2.06									
Standard Error	5.8033	to +/- on result of Regression Equation							Therefore Positive Autocorrelation detected at 95% Confidence											
F - Statistic	1.4113	Therefore analysis IS NOT Significant						2.49429	Critical F-Statistic at 95% Confidence						(Significance holds to 74.1% Confidence)					

Multiple Regression Equation					Independent Analysis			Auto Correlation	Tests for Multicollinearity between Independent Variables										
	Coefficients	Standard Error	t Stat	p Value	R Squared	Gradient	Intercept	Dl=1.16 Du=1.39 DW-Stat	Adjusted R-Squared against other	Independent R-Square Matrix									
Intercept	-36.559	70.955	-0.515	62.03%															
Ca	0.037	0.092	0.400	69.97%	18.22%	0.07	0.61	1.82	72.00%	100%	78%	2%	15%	36%	4%	11%	6%	2%	Ca
Mg	0.025	0.161	0.157	87.91%	16.02%	0.09	4.32	1.97	80.99%	78%	100%	0%	33%	42%	2%	21%	13%	10%	Mg
Smectite %	0.073	0.148	0.492	63.62%	1.88%	-0.05	10.04	2.91	39.17%	2%	0%	100%	0%	22%	38%	0%	7%	0%	Smectite %
pH	1.538	7.419	0.207	84.09%	8.74%	-4.51	51.61	1.69	61.39%	15%	33%	0%	100%	11%	1%	63%	2%	0%	pH
CEC	-0.007	0.155	-0.044	96.58%	7.18%	-0.08	10.44	2.55	67.77%	36%	42%	22%	11%	100%	23%	7%	34%	26%	CEC
K	-0.049	1.219	-0.040	96.90%	0.00	0.18	6.93	2.67	44.61%	4%	2%	38%	1%	23%	100%	2%	1%	5%	K
ESP %	-0.064	0.271	-0.235	81.99%	0.27	-0.27	10.18	1.07	65.10%	11%	21%	0%	63%	7%	2%	100%	11%	0%	ESP %
7.5 micron	-0.958	0.543	-1.765	11.56%	0.17	-0.38	18.20	1.57	73.37%	6%	13%	7%	2%	34%	1%	11%	100%	59%	7.5 micron
75 micron	0.612	0.336	1.823	10.57%	0.00	0.02	5.45	1.93	63.81%	2%	10%	0%	0%	26%	5%	0%	59%	100%	75 micron

Figure 194: Regression modelling for the combined settling rate of the kimberlite slurries.

Equation Parameters																				
R Squared	0.9133	91.33% of the change in combined bed depth can be explained by the change in the 9 Independent Variables																		
Adjusted R Squared	0.8158	Adjusted for Sample Size bias						0.05999	Durbin-Watson Statistic		Critical D-W Values: Lower (Dl)=0.71; Upper (Du)=2.06									
Standard Error	0.0633	to +/- on result of Regression Equation							Therefore Positive Autocorrelation detected at 95% Confidence											
F - Statistic	9.3670	Therefore analysis IS Significant						2.49429	Critical F-Statistic at 95% Confidence						(Significance holds to 99.9% Confidence)					

Multiple Regression Equation					Independent Analysis			Correlation	Tests for Multicollinearity between Independent Variables										
	Coefficients	Standard Error	t Stat	p Value	R Squared	Gradient	Intercept	Dl=1.16 Du=1.39 DW-Stat	Adjusted R-Squared against other	Independent R-Square Matrix									
Intercept	1.094	0.774	1.412	19.55%															
Ca	0.001	0.001	0.508	62.48%	25.07%	0.00	0.15	1.82	72.00%	100%	78%	2%	15%	36%	4%	11%	6%	2%	Ca
Mg	0.000	0.002	0.138	89.40%	28.00%	0.00	0.24	1.97	80.99%	78%	100%	0%	33%	42%	2%	21%	13%	10%	Mg
Smectite %	-0.001	0.002	-0.675	51.87%	8.21%	0.00	0.46	2.91	39.17%	2%	0%	100%	0%	22%	38%	0%	7%	0%	Smectite %
pH	-0.126	0.081	-1.556	15.84%	51.28%	-0.25	2.80	1.69	61.39%	15%	33%	0%	100%	11%	1%	63%	2%	0%	pH
CEC	-0.001	0.002	-0.589	57.18%	15.10%	0.00	0.43	2.55	67.77%	36%	42%	22%	11%	100%	23%	7%	34%	26%	CEC
K	-0.012	0.013	-0.927	38.09%	0.04	0.01	0.30	2.67	44.61%	4%	2%	38%	1%	23%	100%	2%	1%	5%	K
ESP %	-0.003	0.003	-0.863	41.33%	0.64	-0.01	0.43	1.07	65.10%	11%	21%	0%	63%	7%	2%	100%	11%	0%	ESP %
7.5 micron	-0.014	0.006	-2.369	4.53%	0.13	-0.01	0.55	1.57	73.37%	6%	13%	7%	2%	34%	1%	11%	100%	59%	7.5 micron
75 micron	0.012	0.004	3.301	1.08%	0.02	0.00	0.18	1.93	63.81%	2%	10%	0%	0%	26%	5%	0%	59%	100%	75 micron

Figure 195: Regression modelling for the combined bed depth of the kimberlite slurries.

Equation Parameters																
R Squared	0.8651	86.51% of the change in combined bed depth can be explained by the change in the 3 Independent Variables														
Adjusted R Squared	0.8362	Adjusted for Sample Size bias						1.56412	Durbin-Watson Statistic	Critical D-W Values: Lower (Dl)=0.93; Upper (Du)=1.68						
Standard Error	0.0597	to +/- on result of Regression Equation						Therefore Positive Autocorrelation maybe present at 95% Confidence								
F - Statistic	29.9336	Therefore analysis IS Significant						3.19678	Critical F-Statistic at 95% Confidence							

Multiple Regression Equation					Independent Analysis			Auto Correlation	Tests for Multicollinearity between Independent Variables						
	Coefficients	Standard Error	t Stat	p Value	R Squared	Gradient	Intercept	Dl=1.16 Du=1.39 DW-Stat	Adjusted R-Squared against other	Independent R-Square Matrix					
Intercept	1.892	0.380	4.979	0.02%											
pH	-0.208	0.035	-5.885	0.00%	51.28%	-0.25	2.80	1.69	-8.12%	100%	2%	0%			pH
7.5 micron	-0.020	0.003	-5.886	0.00%	13.13%	-0.01	0.55	1.57	55.79%	2%	100%	59%			7.5 micron
75 micron	0.013	0.002	5.438	0.01%	1.59%	0.00	0.18	1.93	54.81%	0%	59%	100%			75 micron

Figure 196: Regression modelling of the combined bed depth of the kimberlite slurries with the most significant independent variables.

Appendix B

Coagulant settling tests

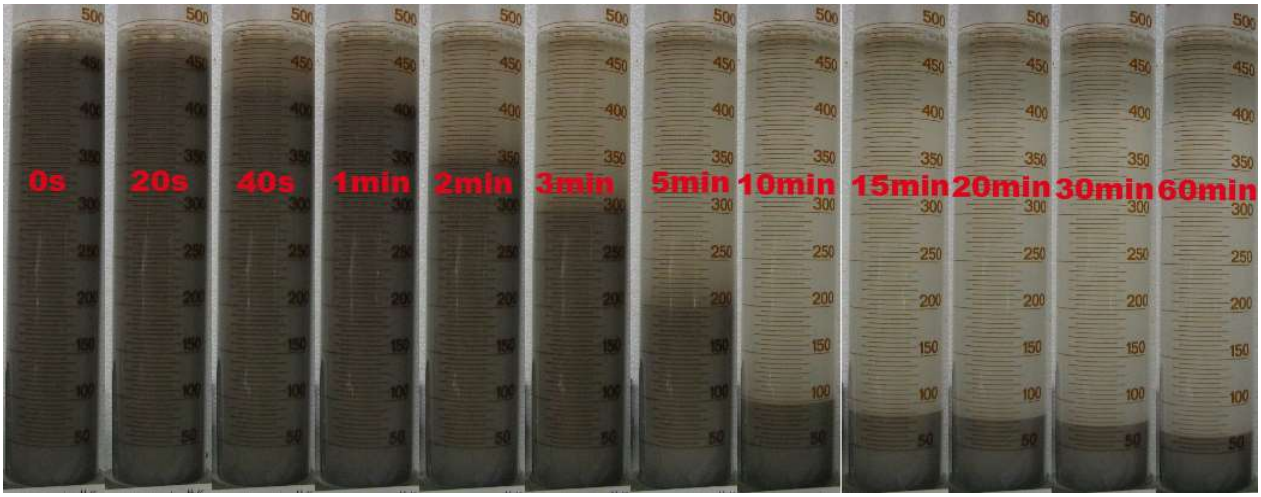

Figure 197: AC 1-1-1 0.005M KCl

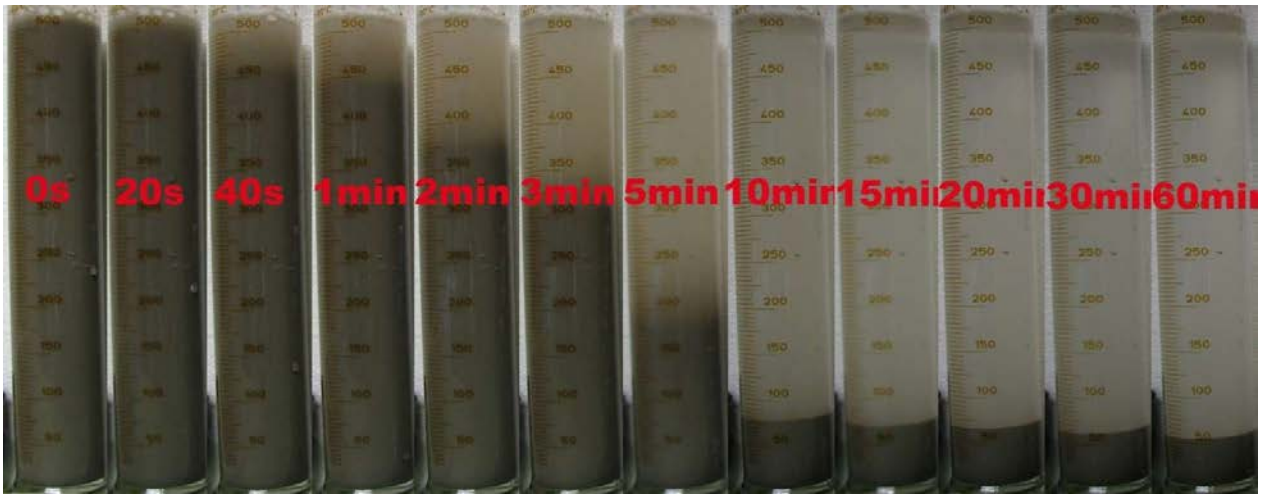

Figure 198: AC 1-1-1 0.005M $CaCl_2$

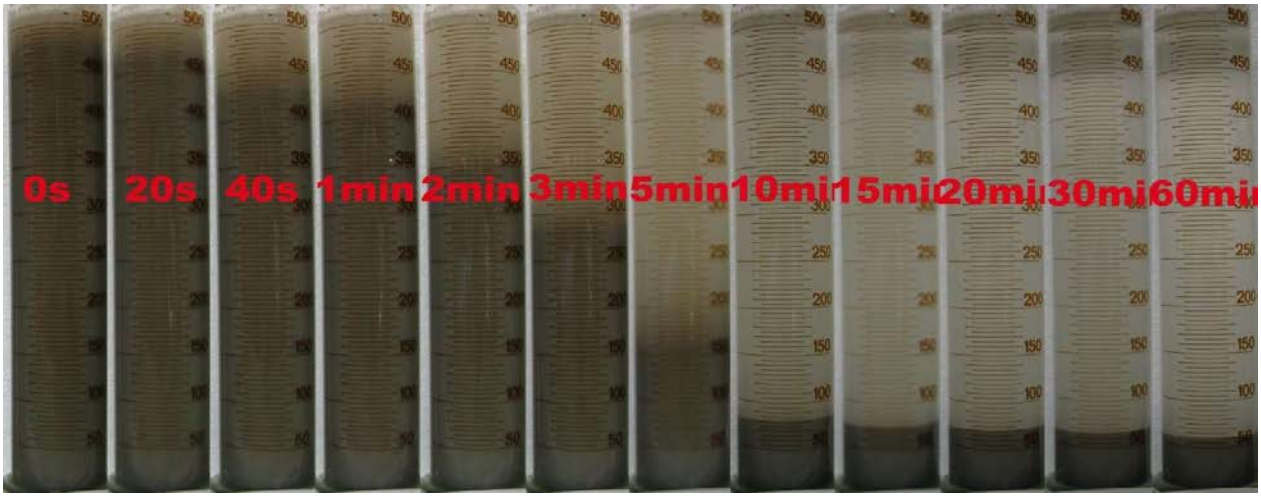

Figure 199: AC 1-1-1 0.005M $MgCl_2$

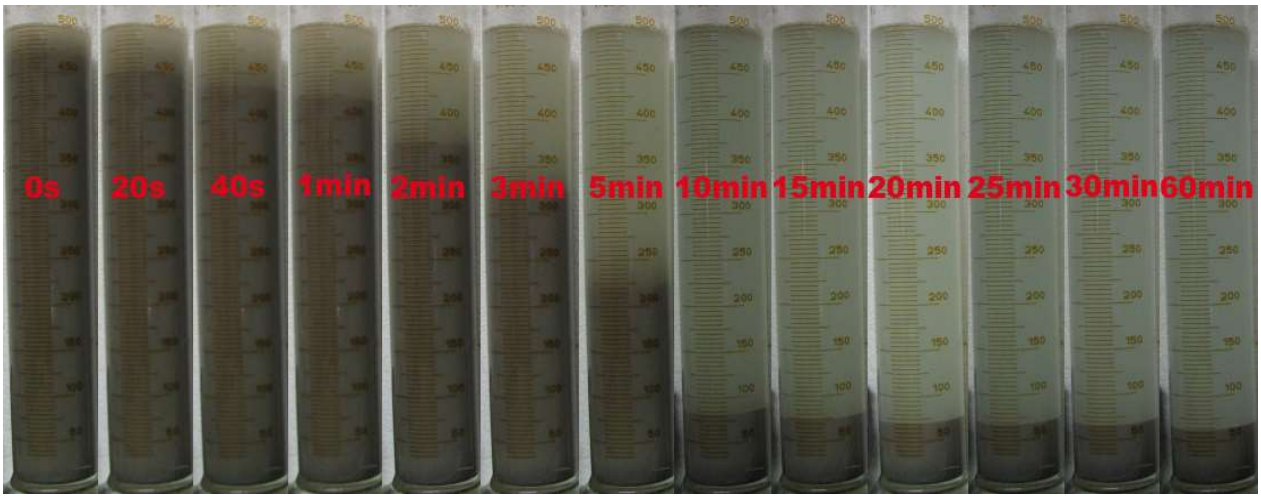

Figure 200: AC 1-1-1 0.01M $CuCl_2$

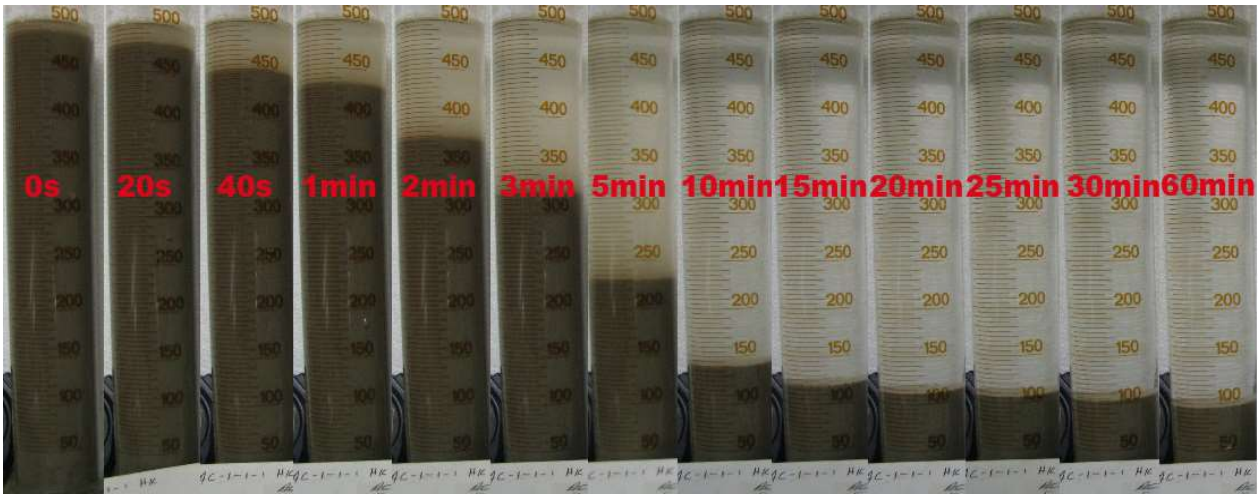

Figure 201: AC 1-1-1 0.01M $FeCl_3$

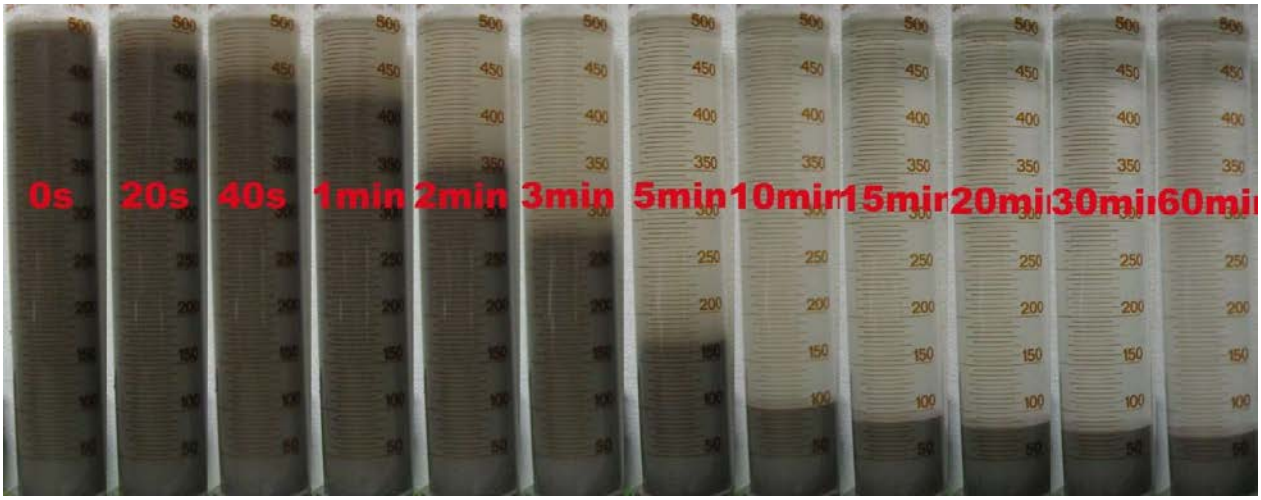

Figure 202: AC 1-1-1 0.005M $AlCl_3$

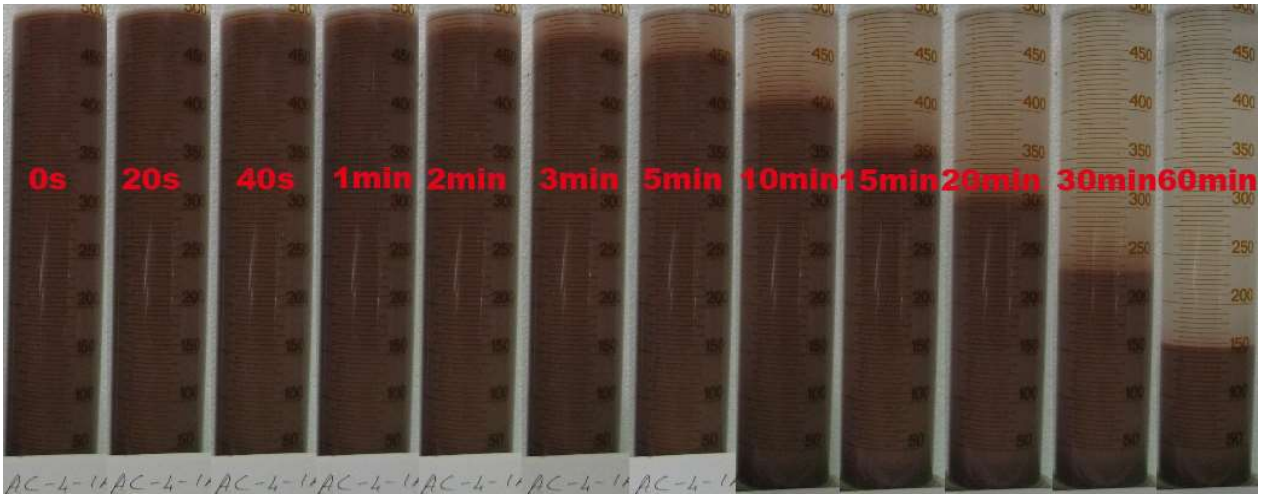

Figure 203: AC 4-1A-1 0.005M KCl

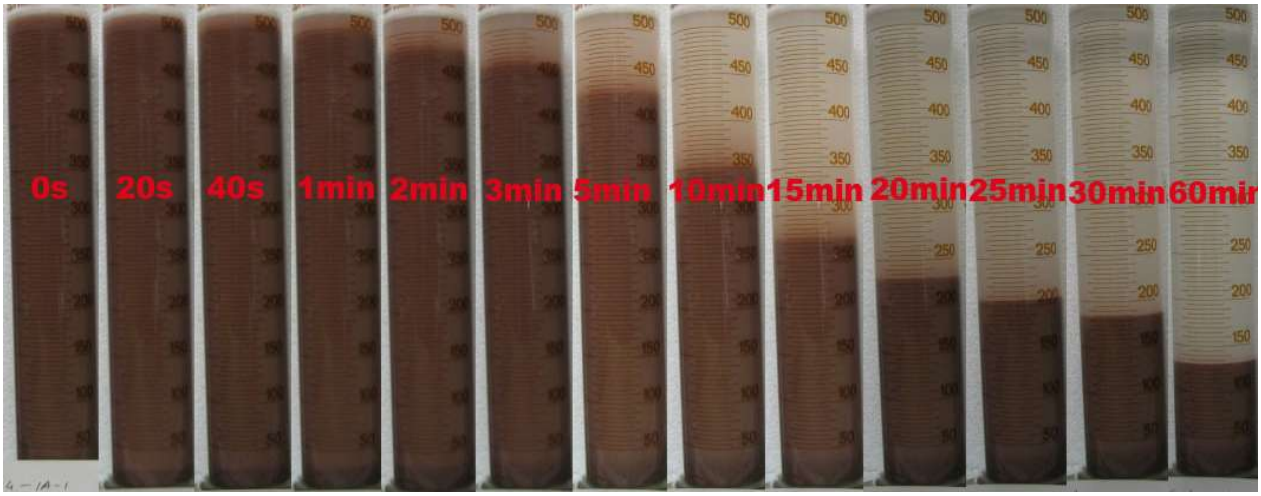

Figure 204: AC 4-1A-1 0.005M $CaCl_2$

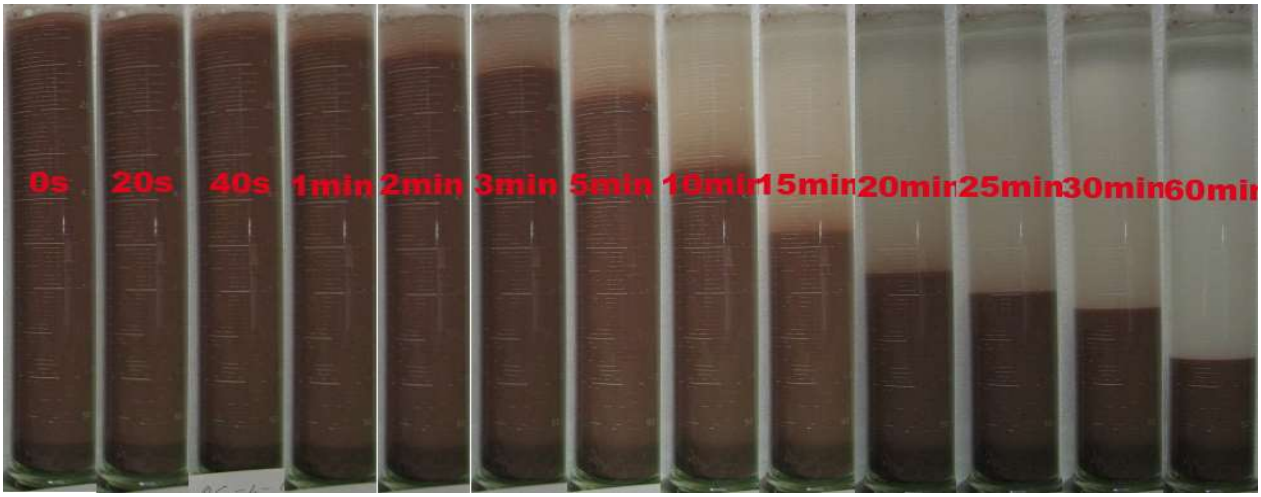

Figure 205: AC 4-1A-1 0.005M $MgCl_2$

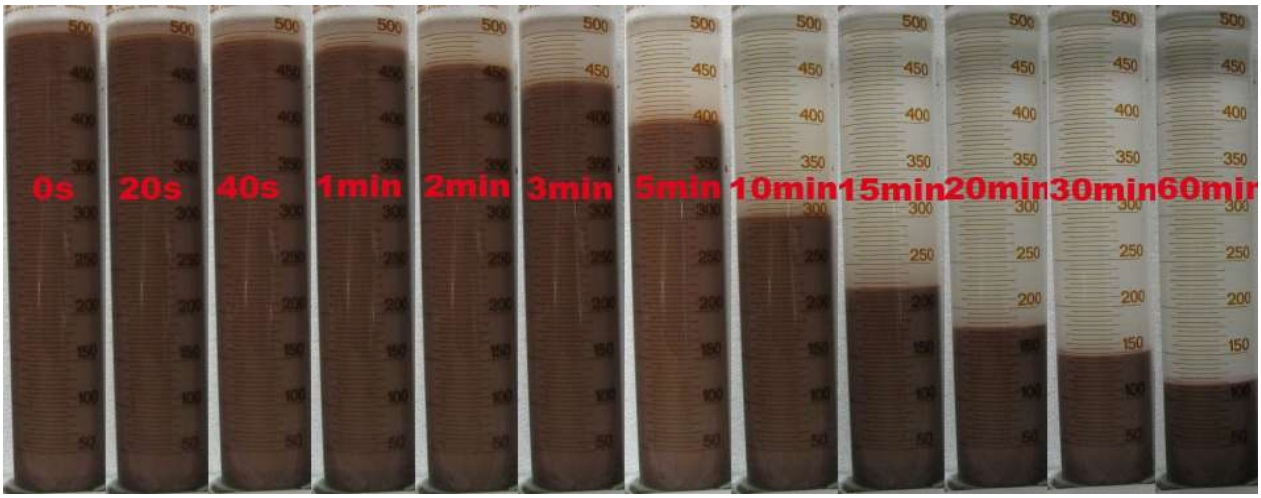

Figure 206: AC 4-1A-1 0.005M $CuCl_2$

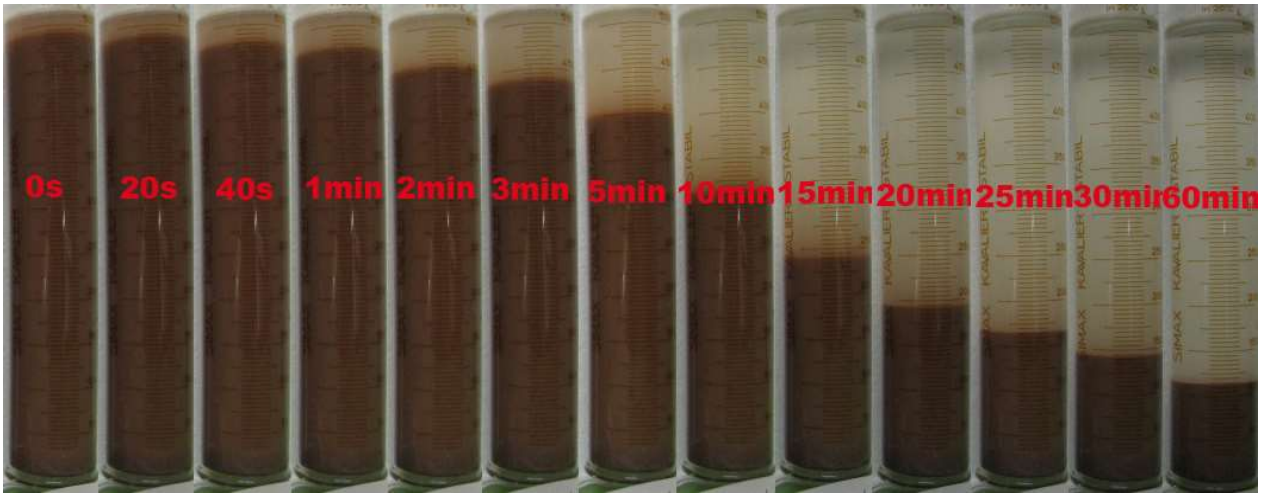

Figure 207: AC 4-1A-1 0.005M $FeCl_3$

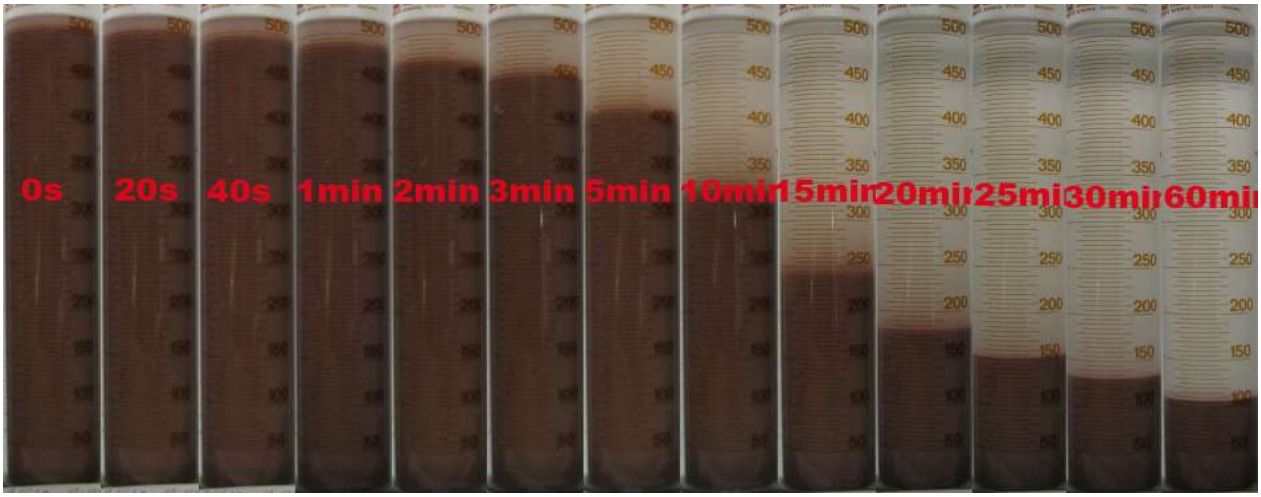

Figure 208: AC 4-1A-1 0.005M $AlCl_3$

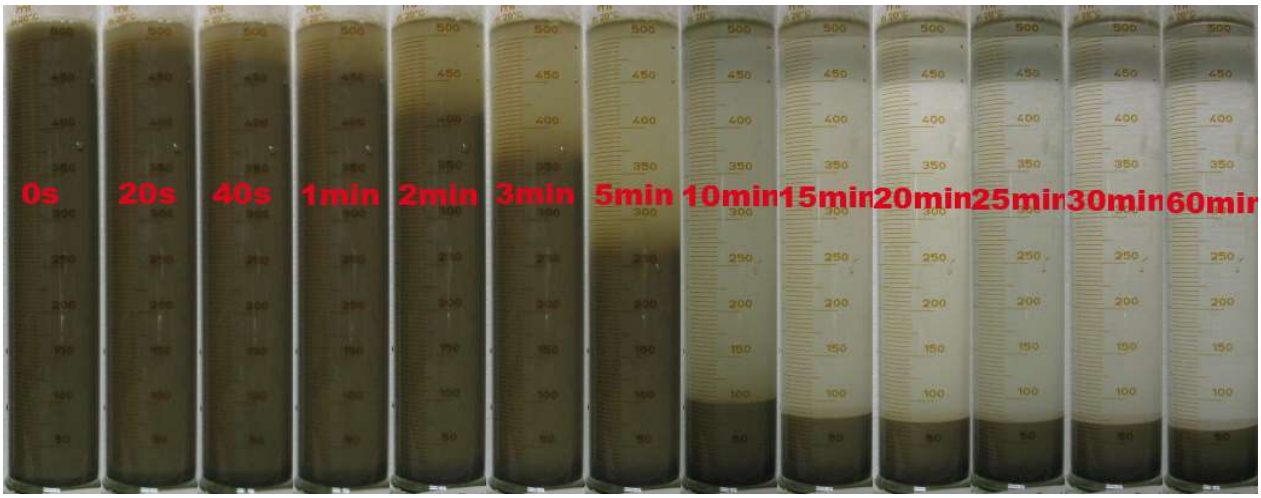

Figure 209: AC 5-5-1 0.005M KCl

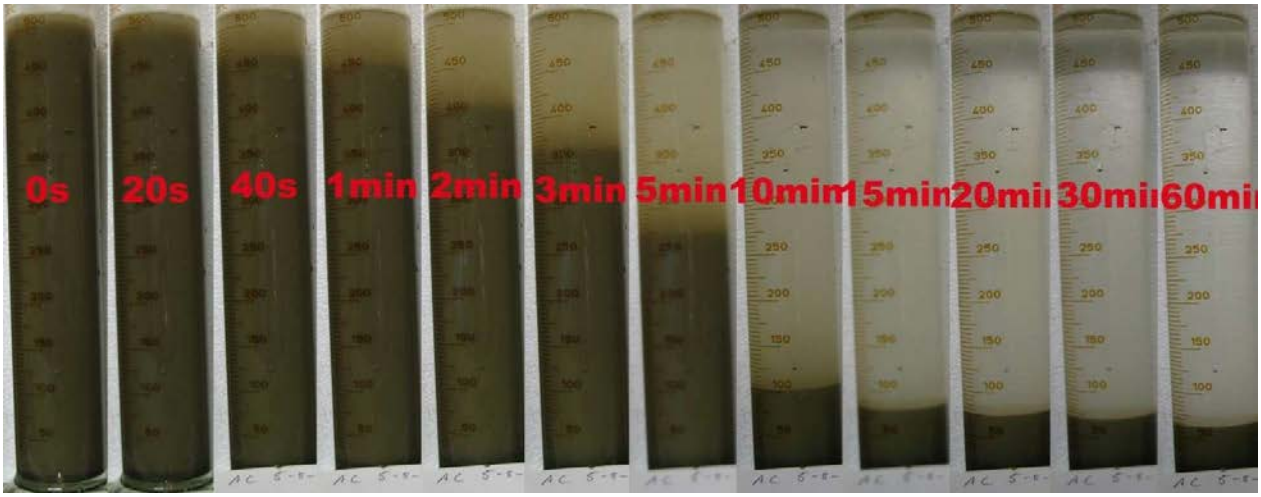

Figure 210: AC 5-5-1 0.005M $CaCl_2$

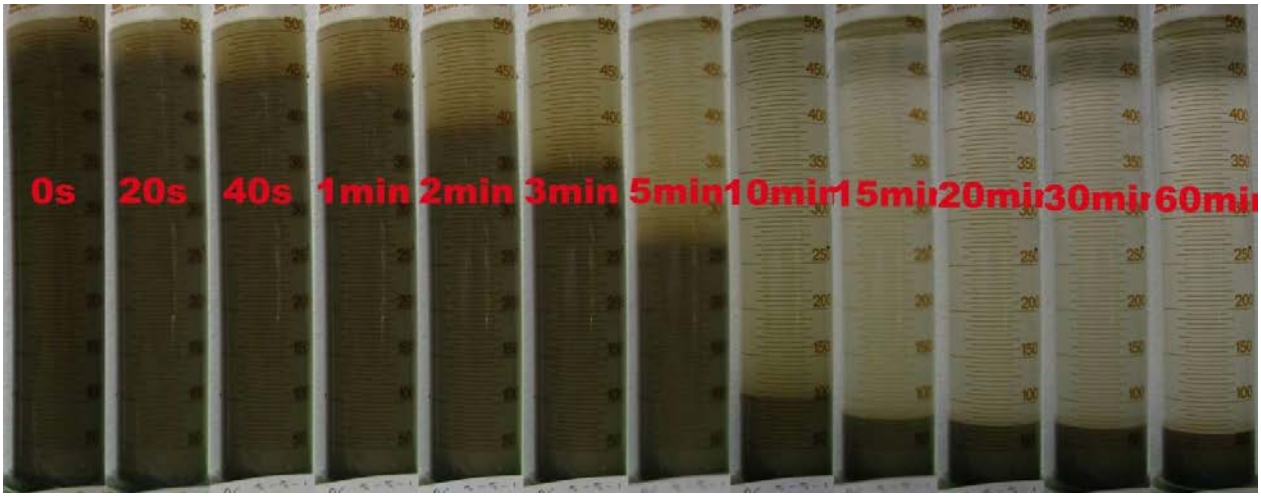

Figure 211: AC 5-5-1 0.005M $MgCl_2$

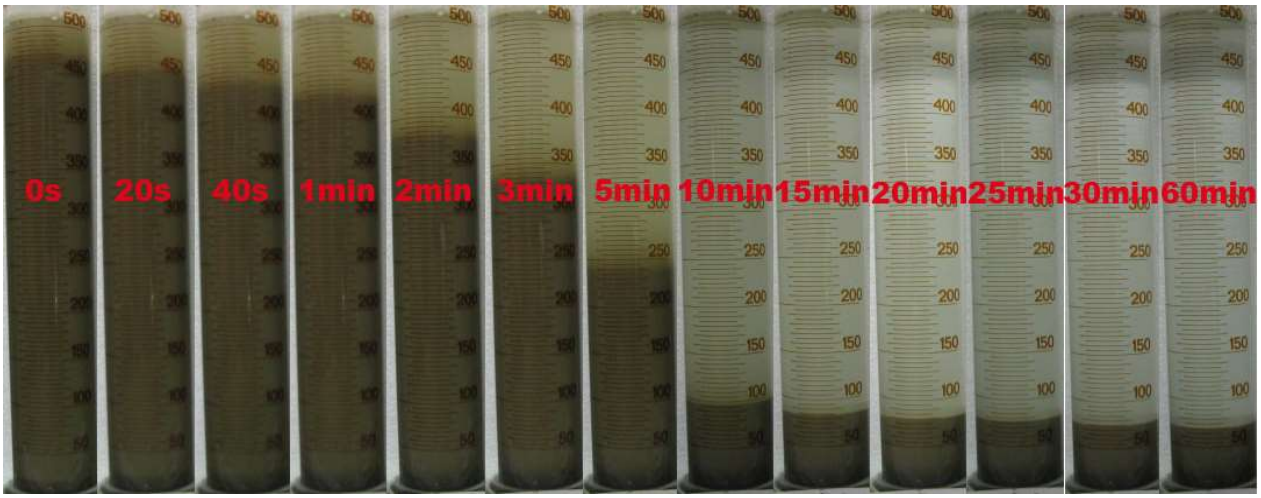

Figure 212: AC 5-5-1 0.01M $CuCl_2$

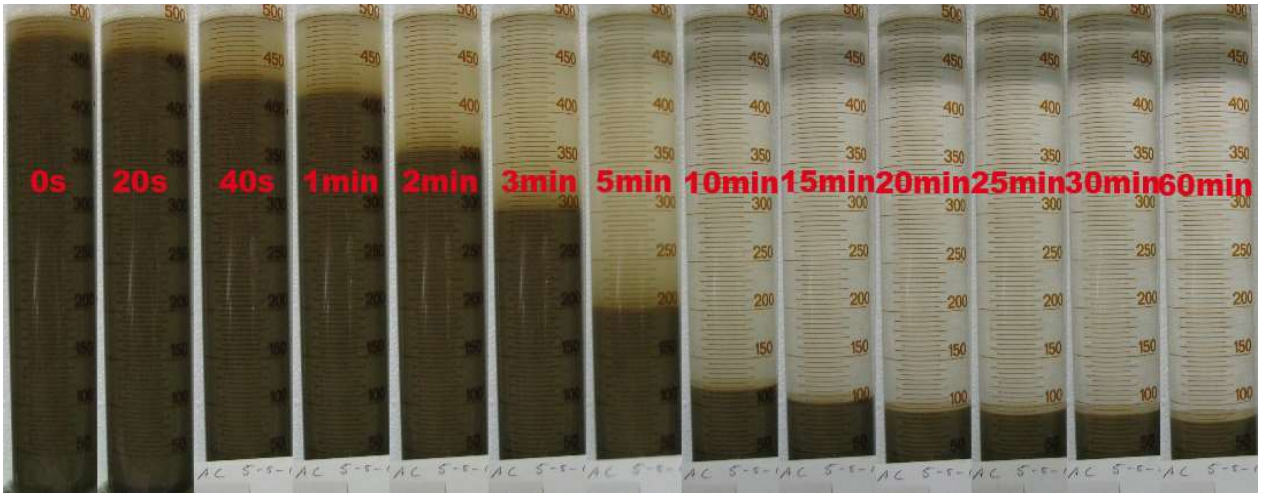

Figure 213: AC 5-5-1 0.01M $FeCl_3$

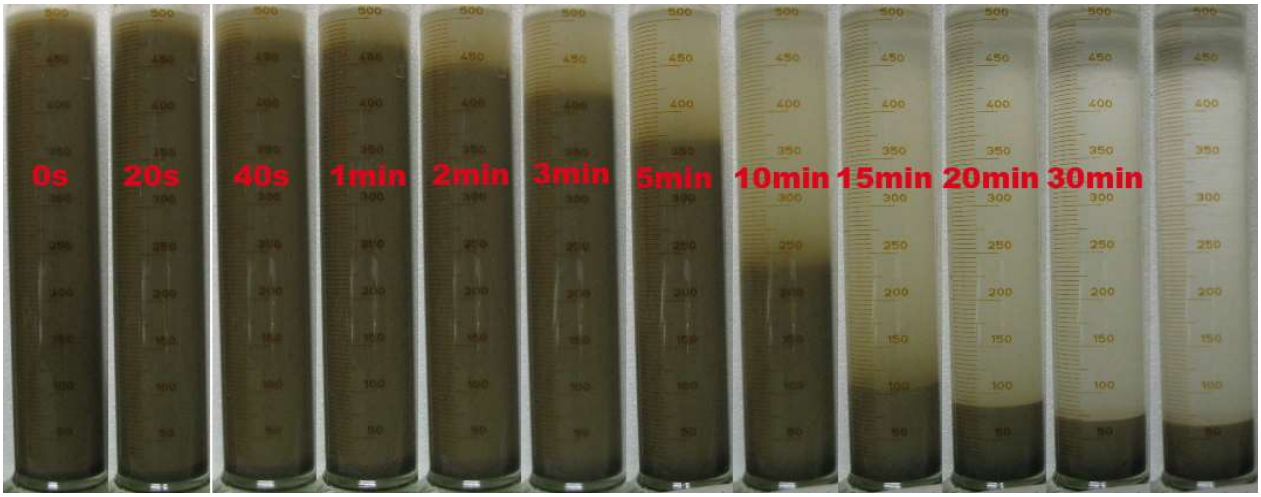

Figure 214: AC 5-5-1 0.005M $AlCl_3$

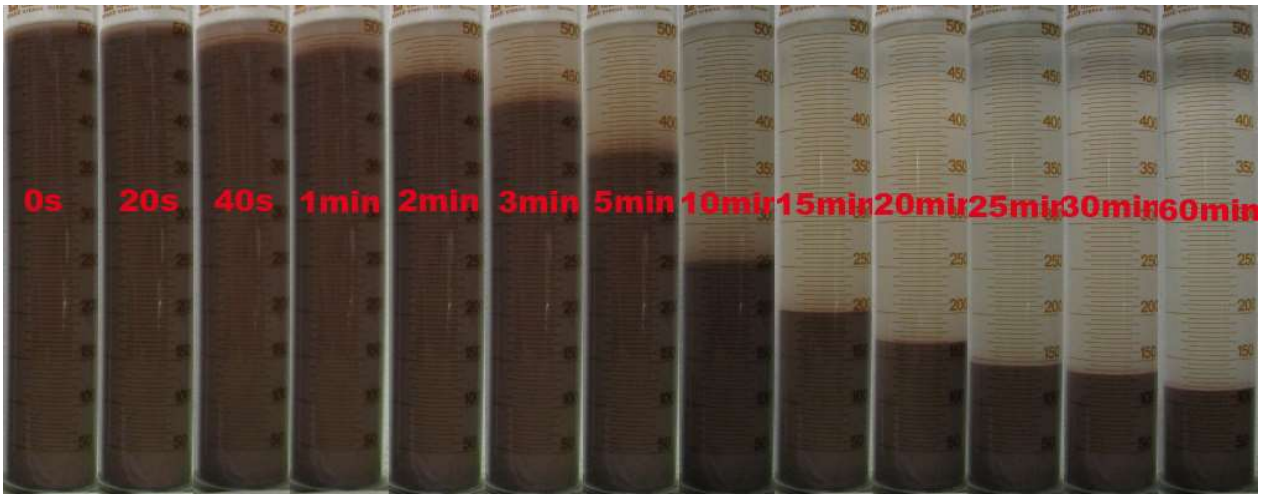

Figure 215: AC 5-5-2 0.005M KCl

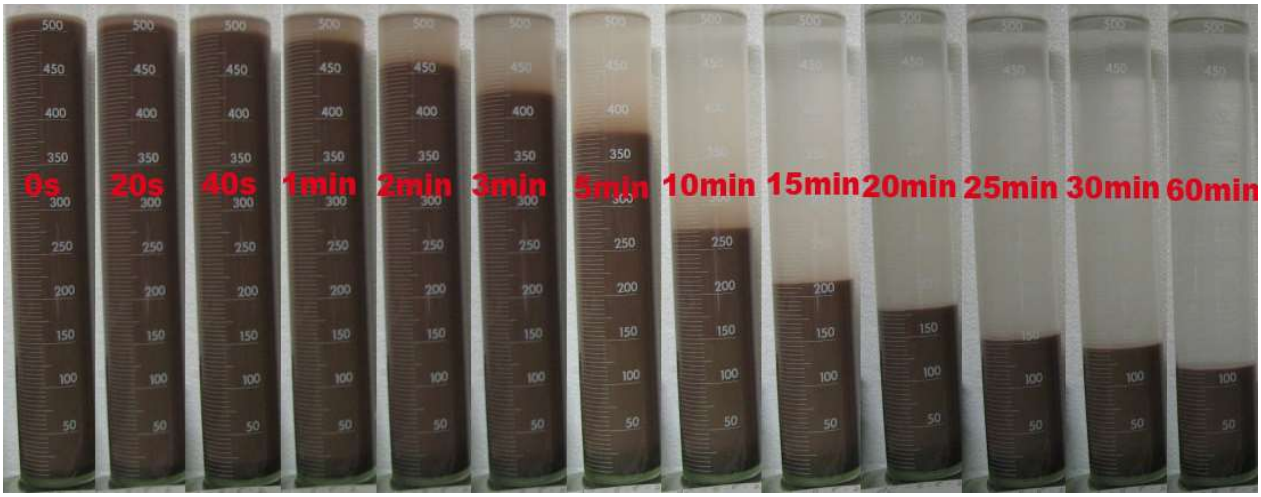

Figure 216: AC 5-5-2 0.005M $CaCl_2$

Figure 217: AC 5-5-2 0.005M $MgCl_2$

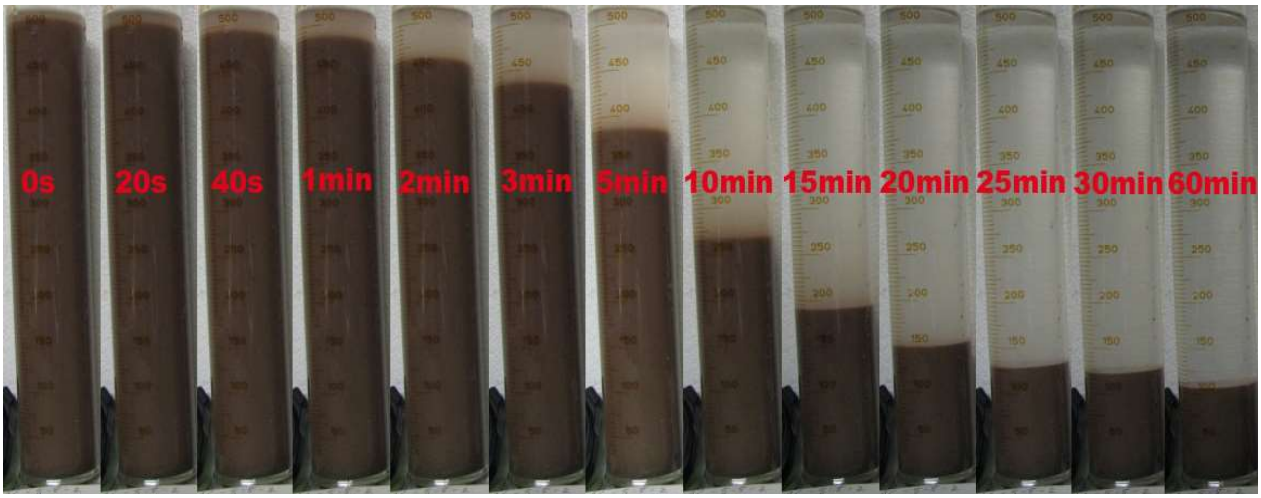

Figure 218: AC 5-5-2 0.005M $CuCl_2$

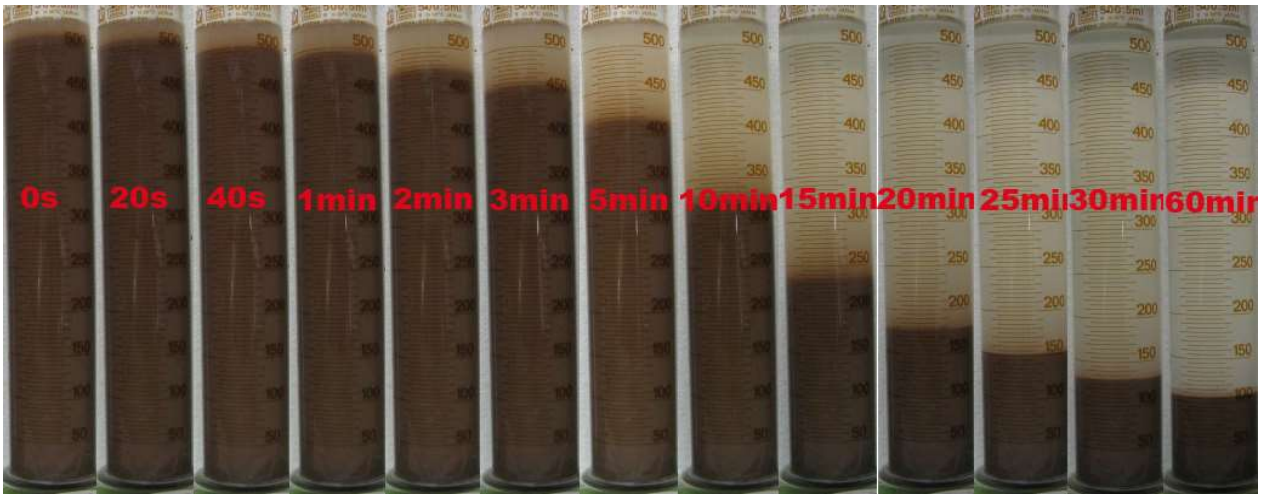

Figure 219: AC 5-5-2 0.005M $FeCl_3$

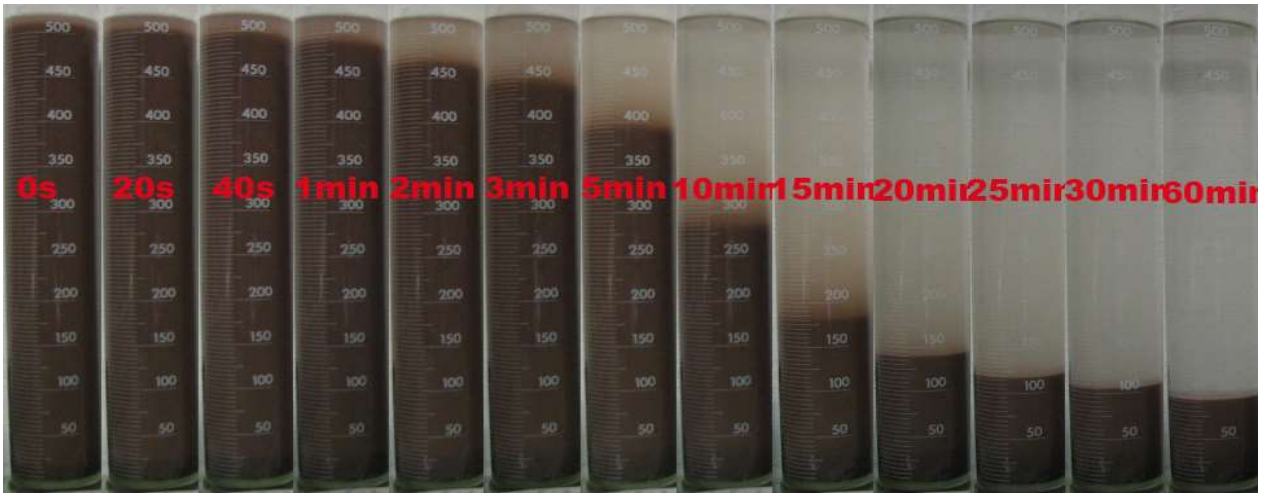

Figure 220: AC 5-5-2 0.005M $AlCl_3$

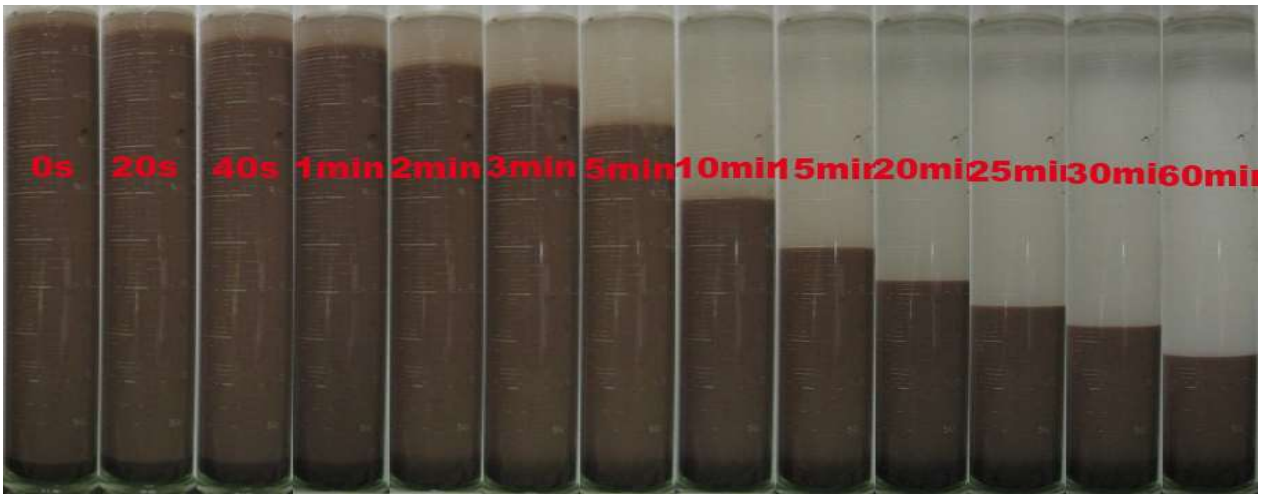

Figure 221: AC 16-1-1 0.005M KCl

Figure 222: AC 16-1-1 0.005M $CaCl_2$

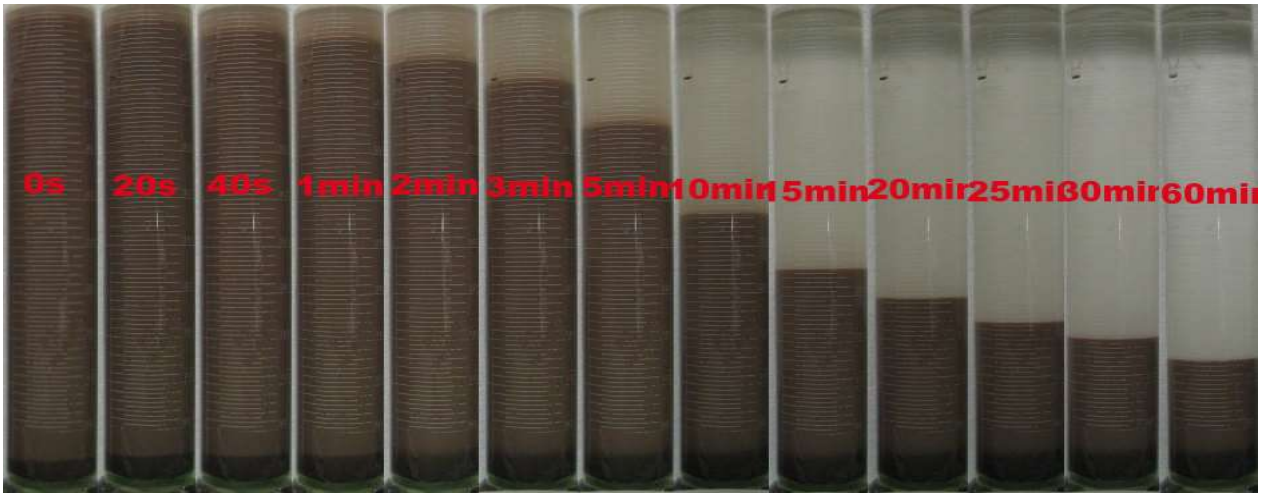

Figure 223: AC 16-1-1 0.005M $MgCl_2$

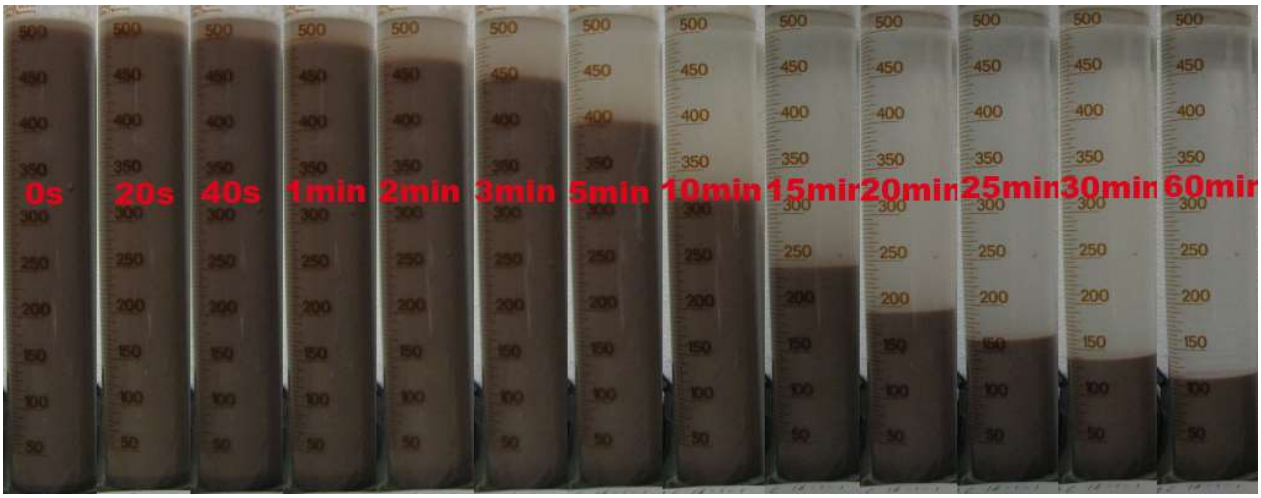

Figure 224: AC 16-1-1 0.005M $CuCl_2$

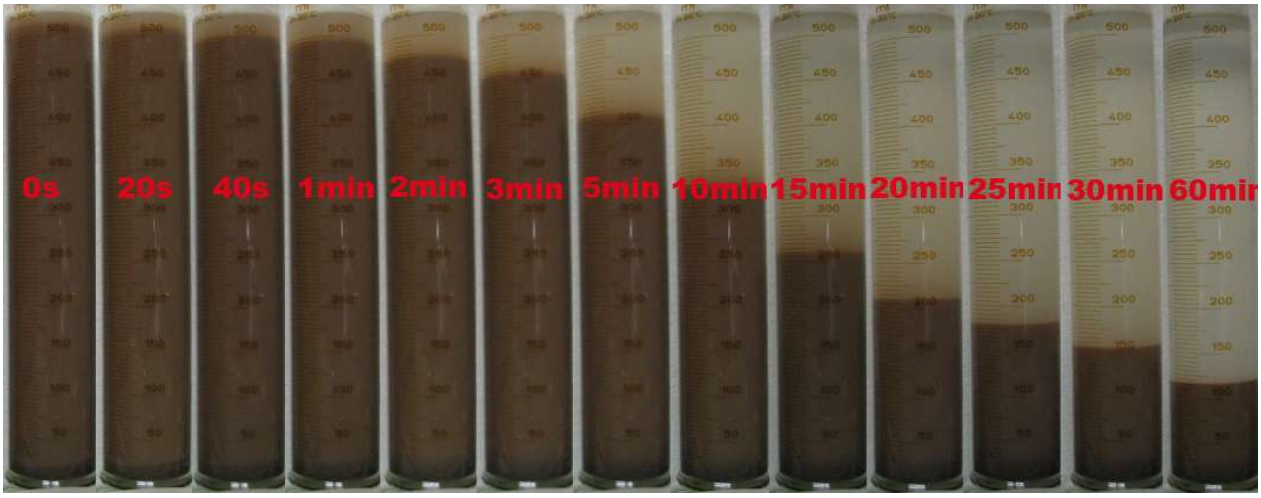

Figure 225: AC 16-1-1 0.005M $FeCl_3$

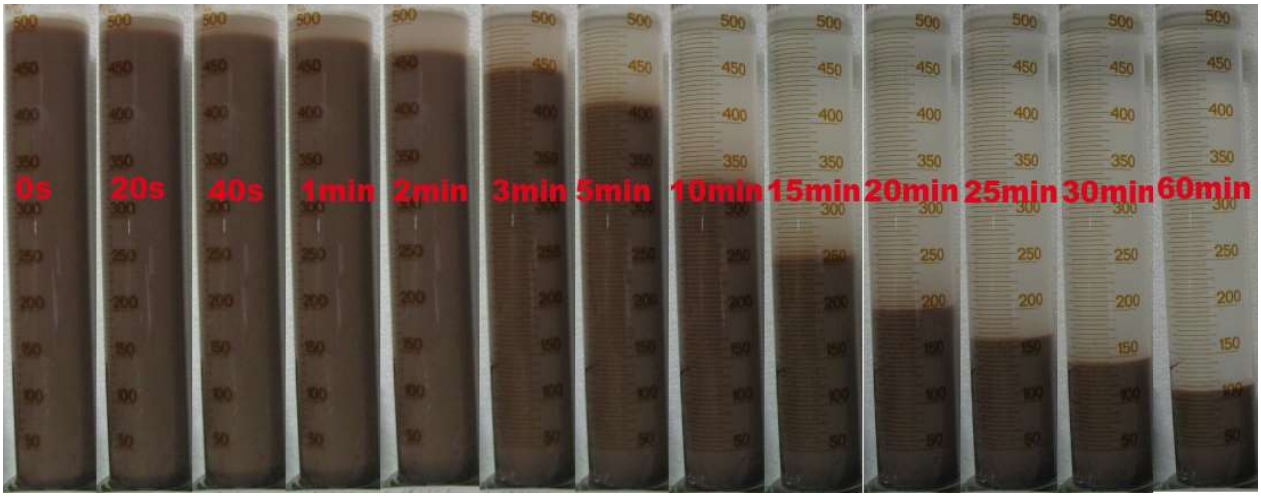

Figure 226: AC 16-1-1 0.005M $AlCl_3$

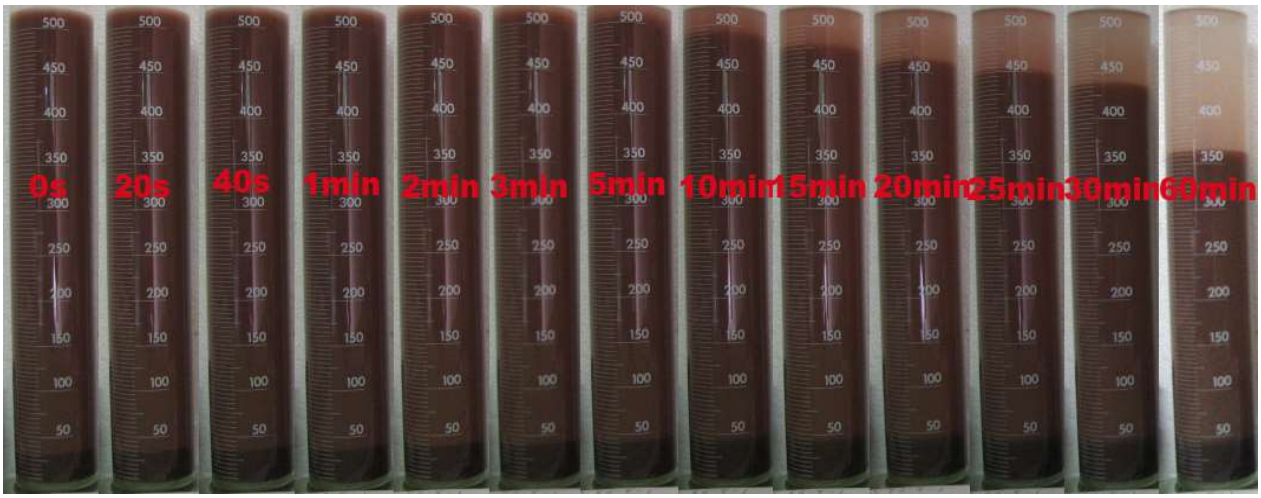

Figure 227: AC 56-5-1 0.005M KCl

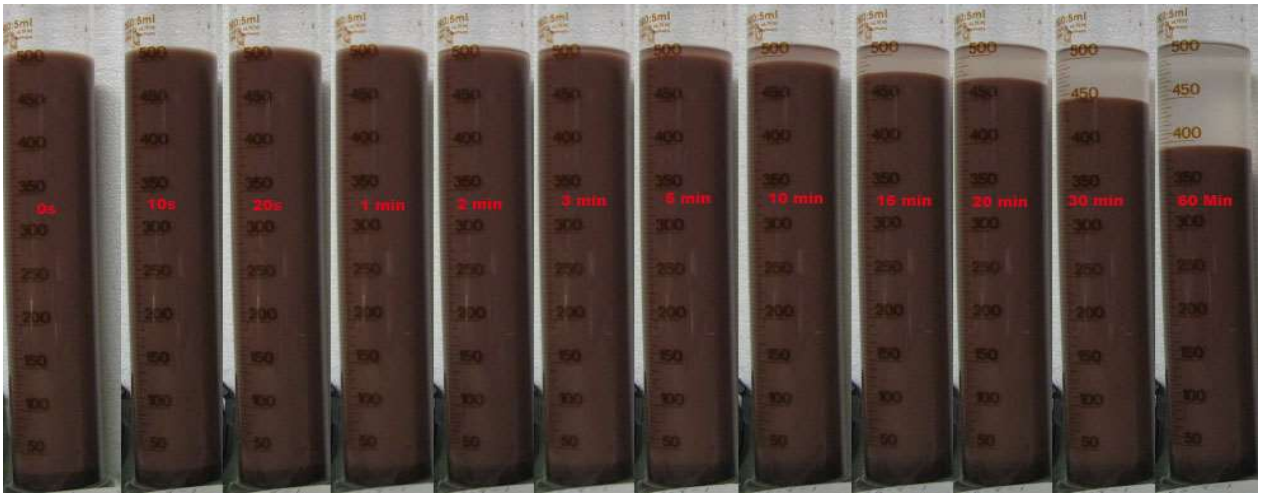

Figure 228: AC 56-5-1 0.005M $CaCl_2$

Figure 229: AC 56-5-1 0.005M $MgCl_2$

Figure 230: AC 56-5-1 0.005M $CuCl_2$

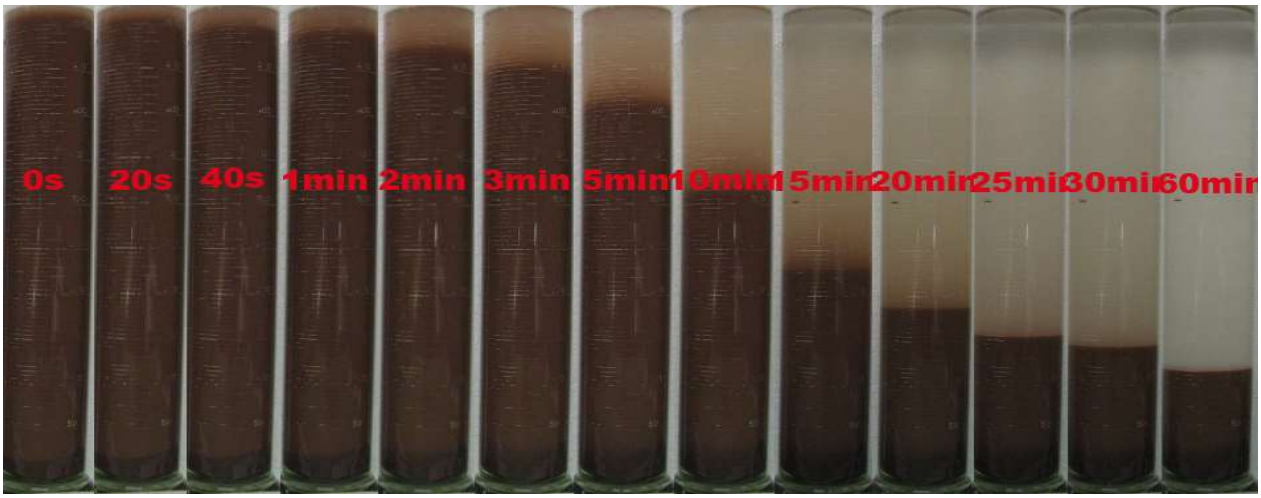

Figure 231: AC 56-5-1 0.005M $FeCl_3$

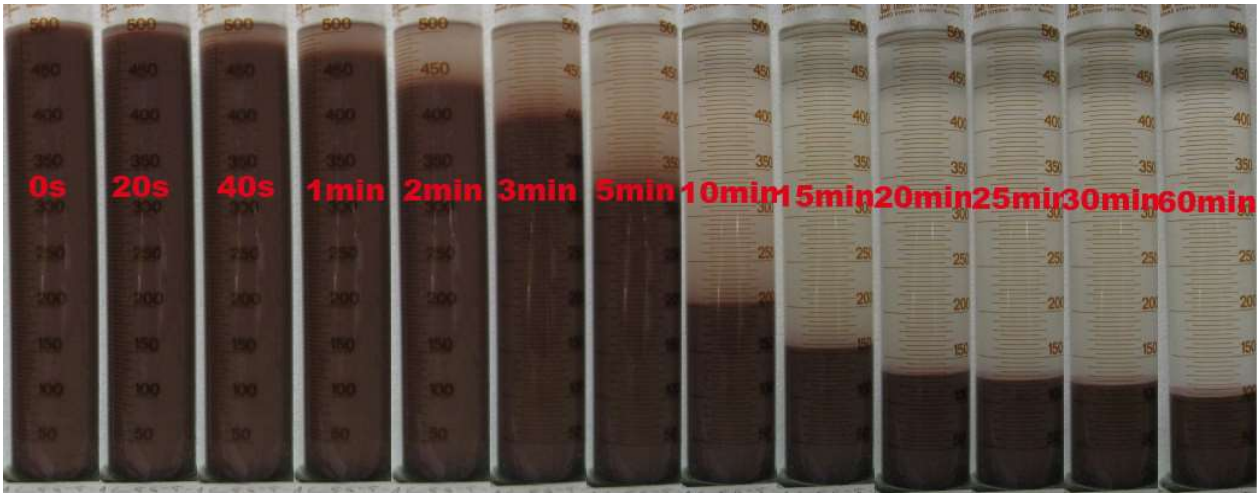

Figure 232: AC 56-5-1 0.005M $AlCl_3$

Figure 233: AC 197-1-1 0.005M KCl

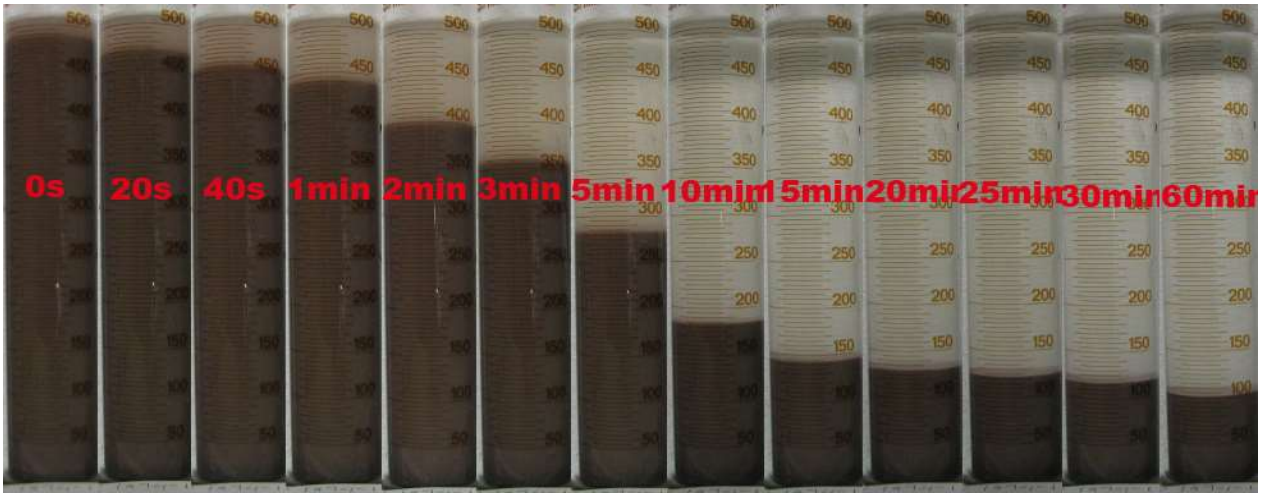

Figure 234: AC 197-1-1 0.005M $CaCl_2$

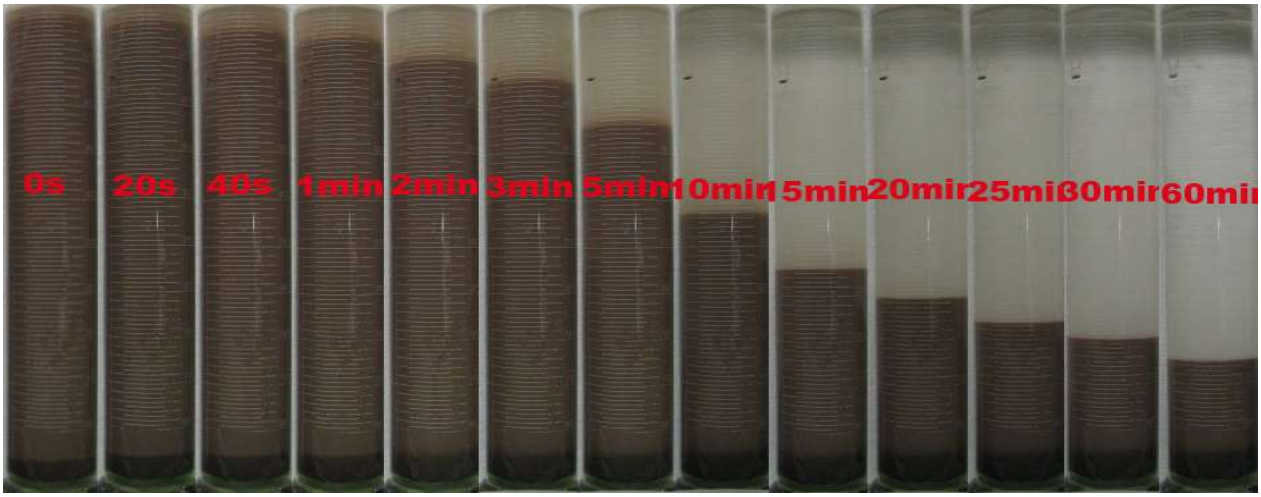

Figure 235: AC 197-1-1 0.005M $MgCl_2$

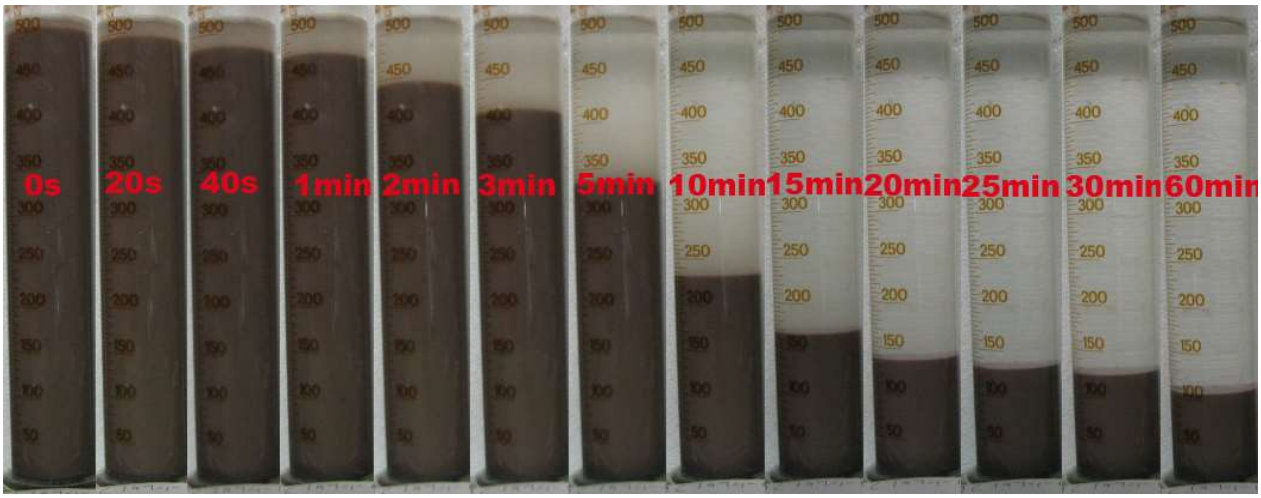

Figure 236: AC 197-1-1 0.005M $CuCl_2$

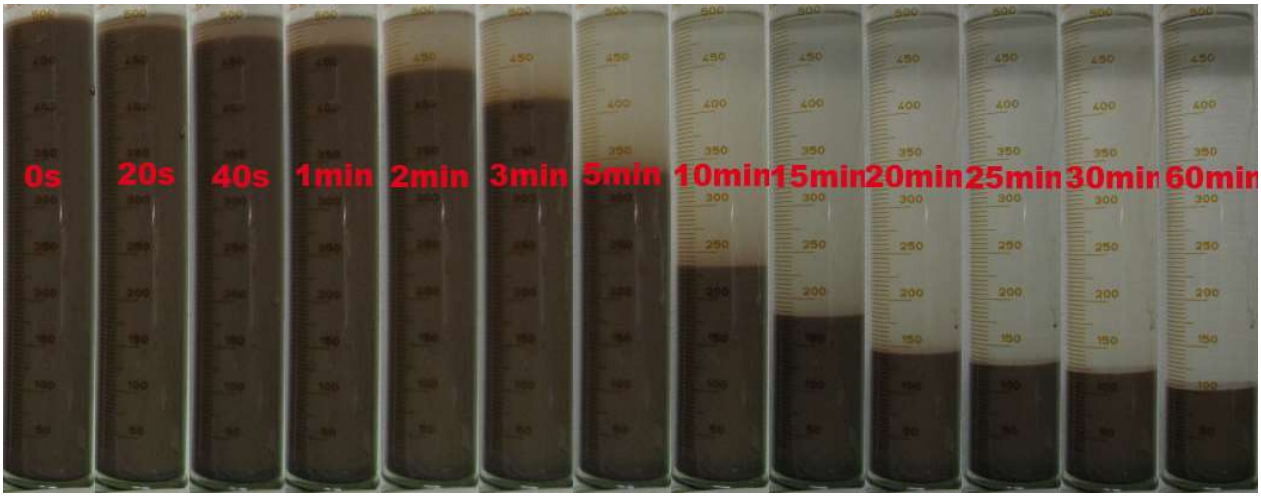

Figure 237: AC 197-1-1 0.005M $FeCl_3$

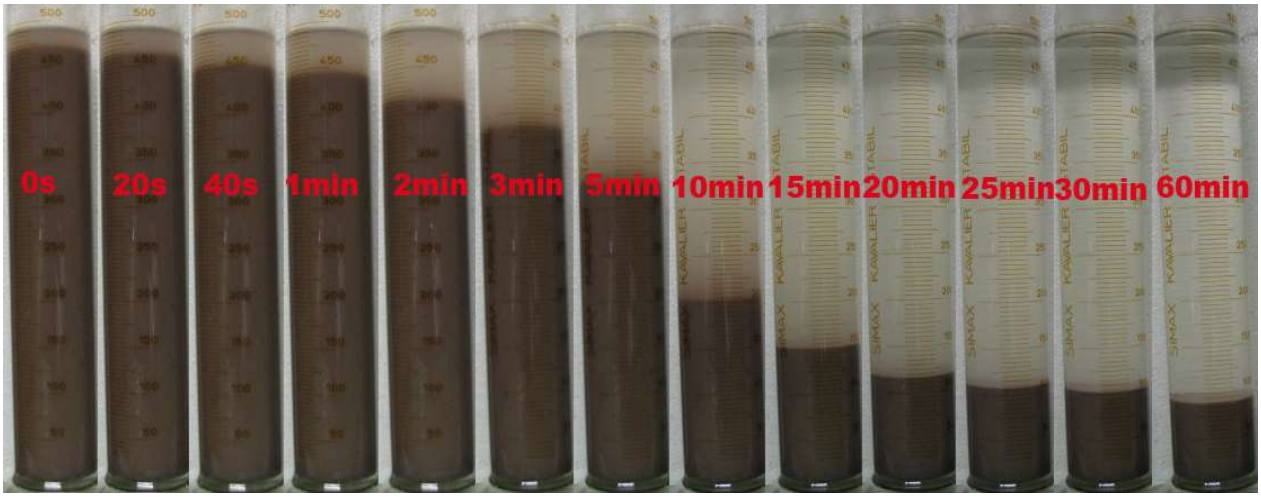

Figure 238: AC 197-1-1 0.005M $AlCl_3$

Figure 239: VR 0.05M KCl

Figure 240: VR 0.01M $CaCl_2$

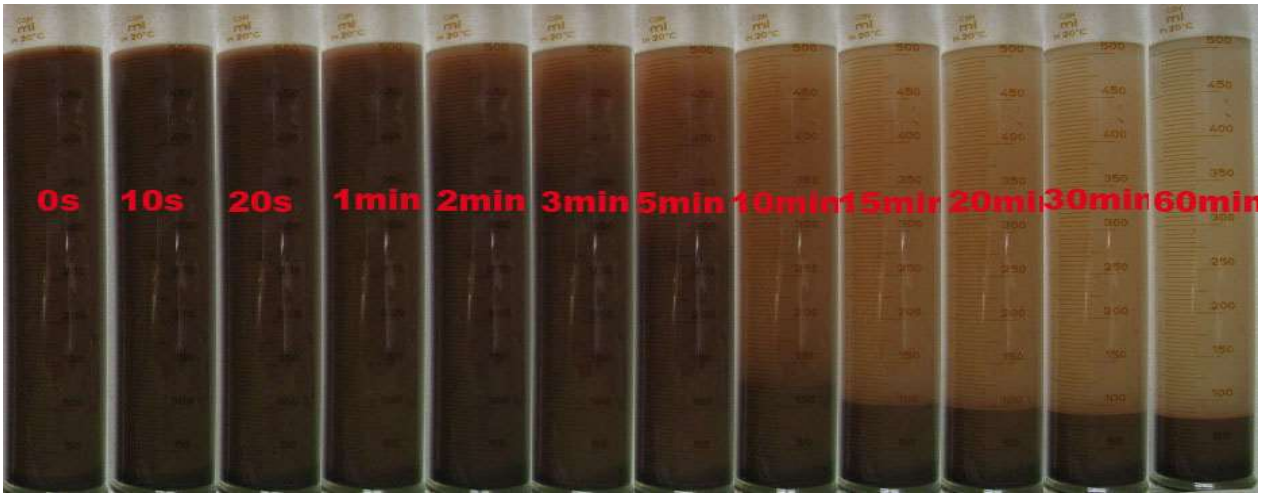

Figure 241: VR 0.01M $MgCl_2$

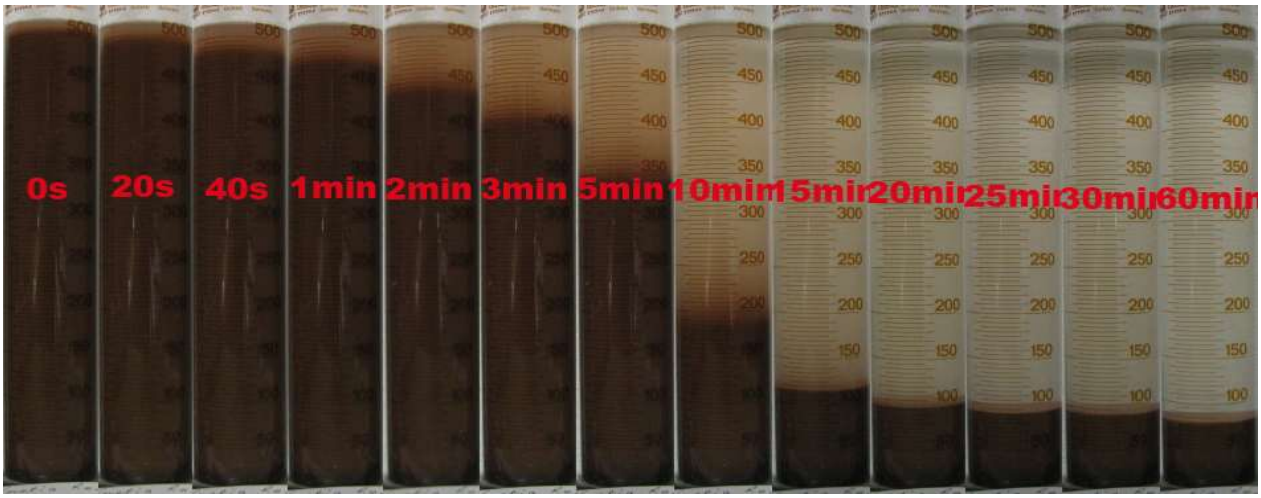

Figure 242: VR 0.005M $CuCl_2$

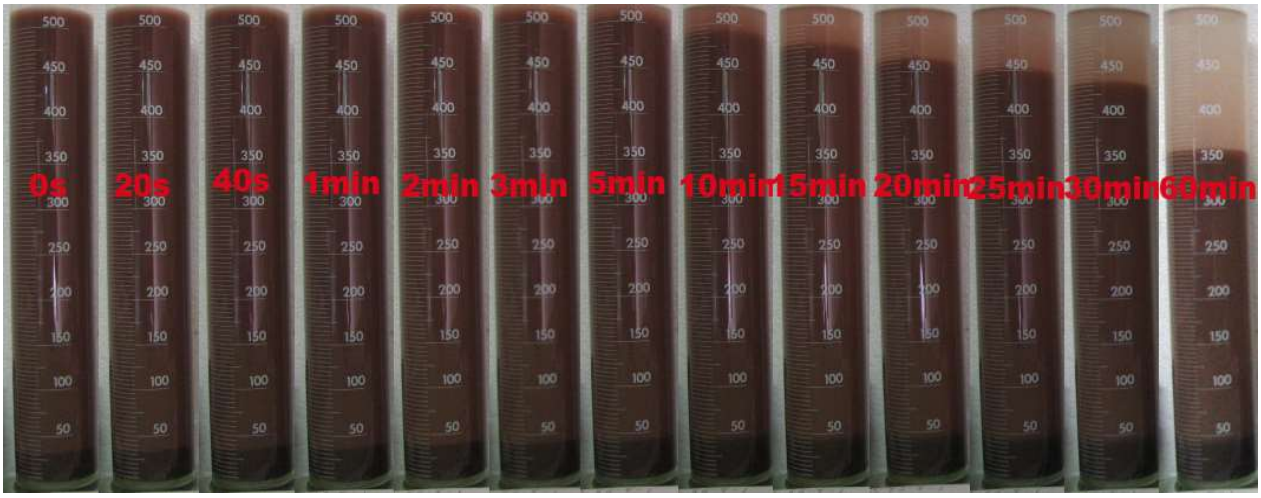

Figure 243: VR 0.005M $FeCl_3$

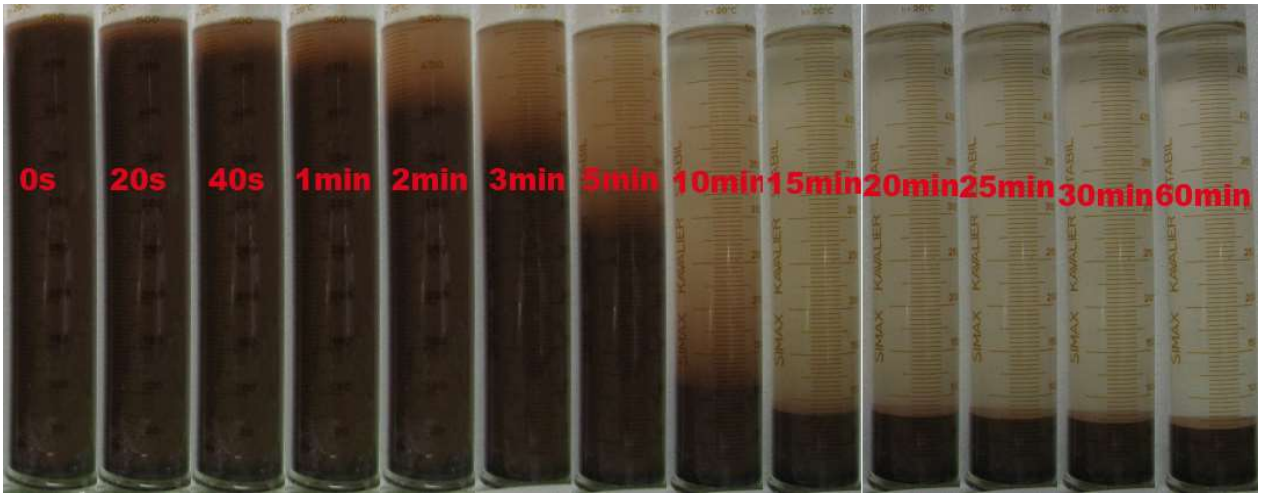

Figure 244: VR 0.005M $AlCl_3$

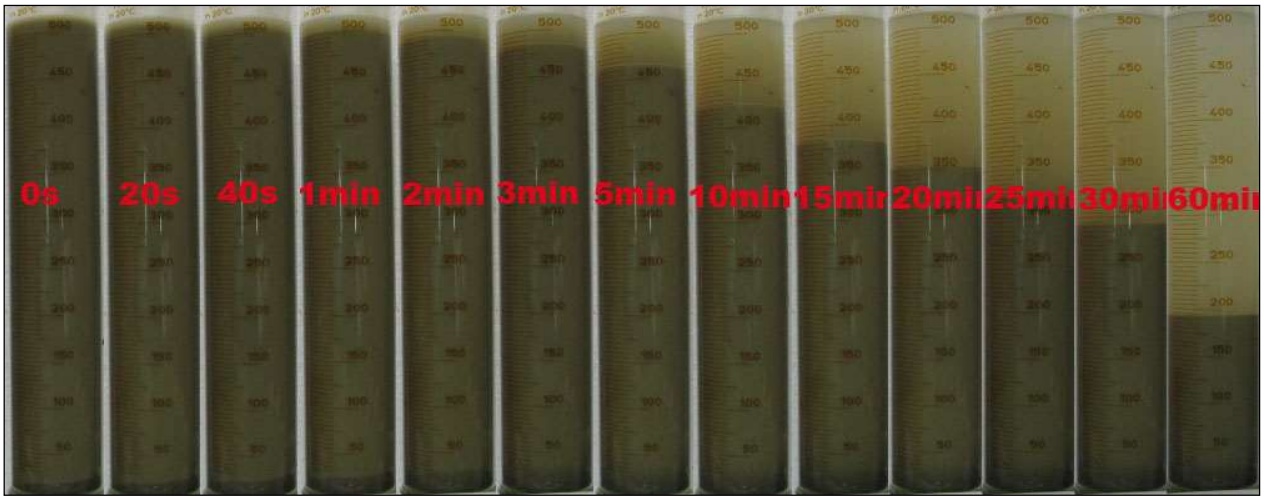

Figure 245: AO319 – 0.02M KCl

Figure 246: AO319 – 0.01M $CaCl_2$

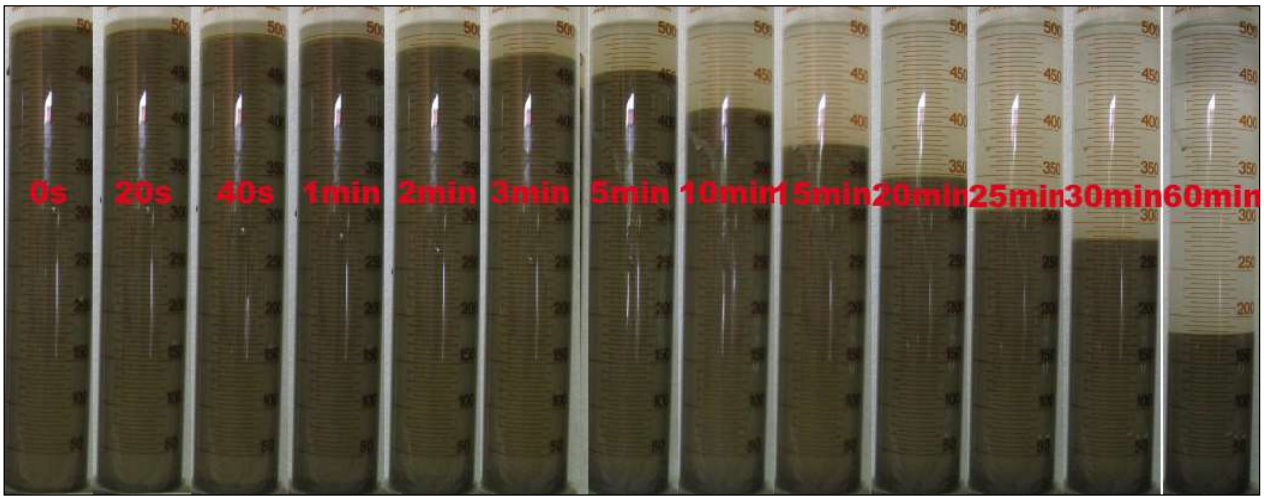

Figure 247: AO319 – 0.01M $MgCl_2$

Figure 248: AO319 – 0.005M $CuCl_2$

Figure 249: AO319 – 0.01M $FeCl_3$

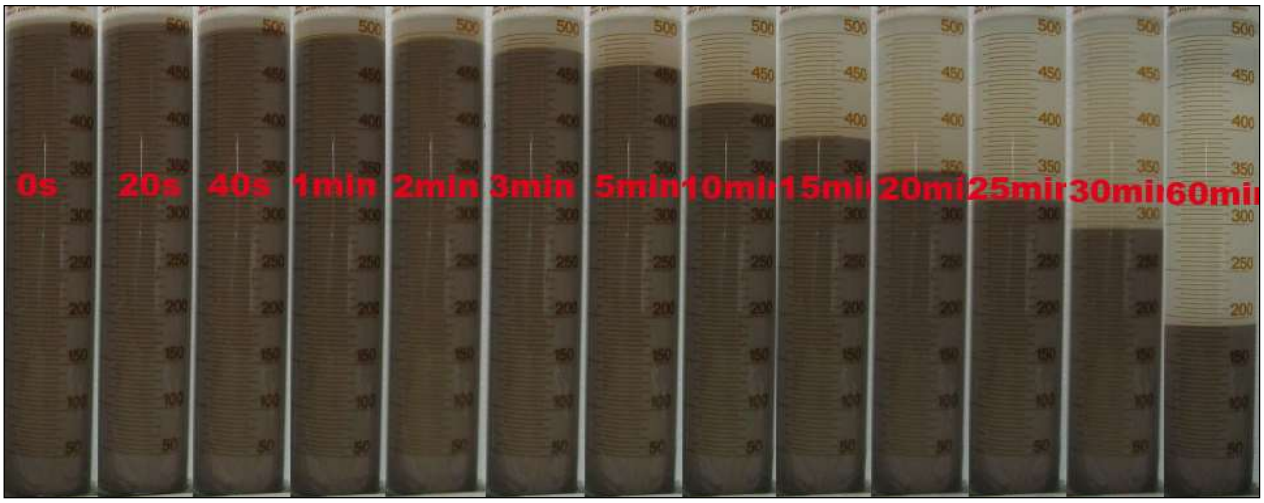

Figure 250: AO320 – 0.005M KCl

Figure 251: AO320 – 0.005M $CaCl_2$

Figure 252: AO320 – 0.005M $MgCl_2$

Figure 253: AO320 – 0.005M $CuCl_2$

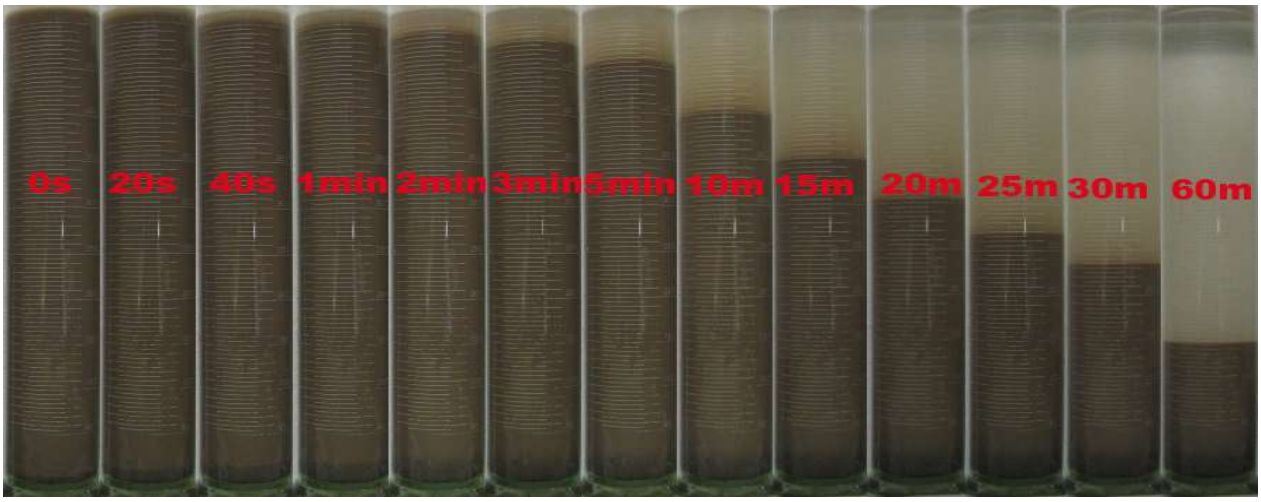

Figure 254: AO320 – 0.005M $FeCl_3$

Figure 255: AO320 – 0.005M $AlCl_3$

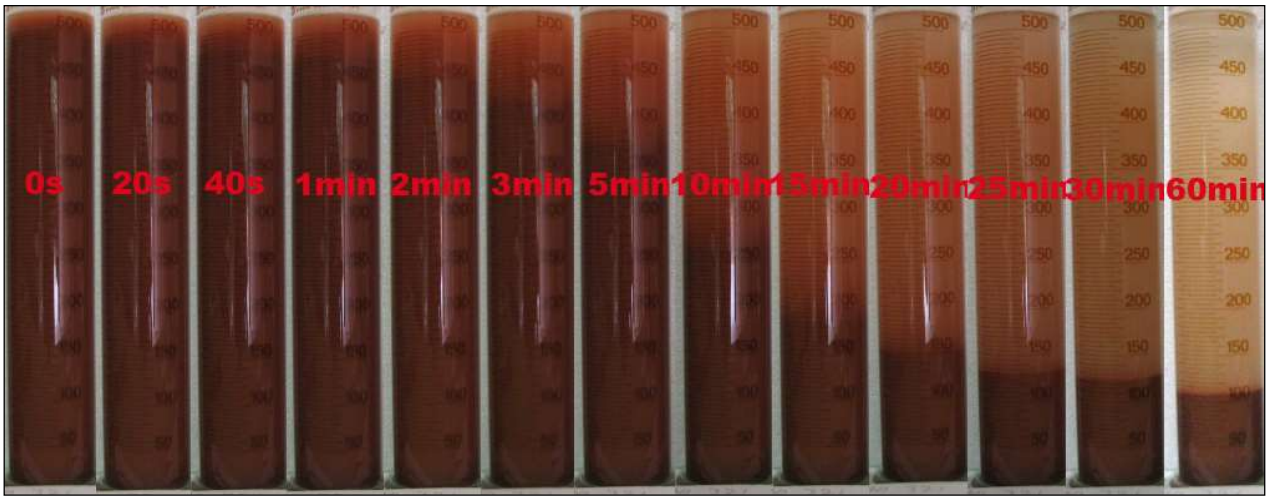

Figure 256: AO321 – 0.01M KCl

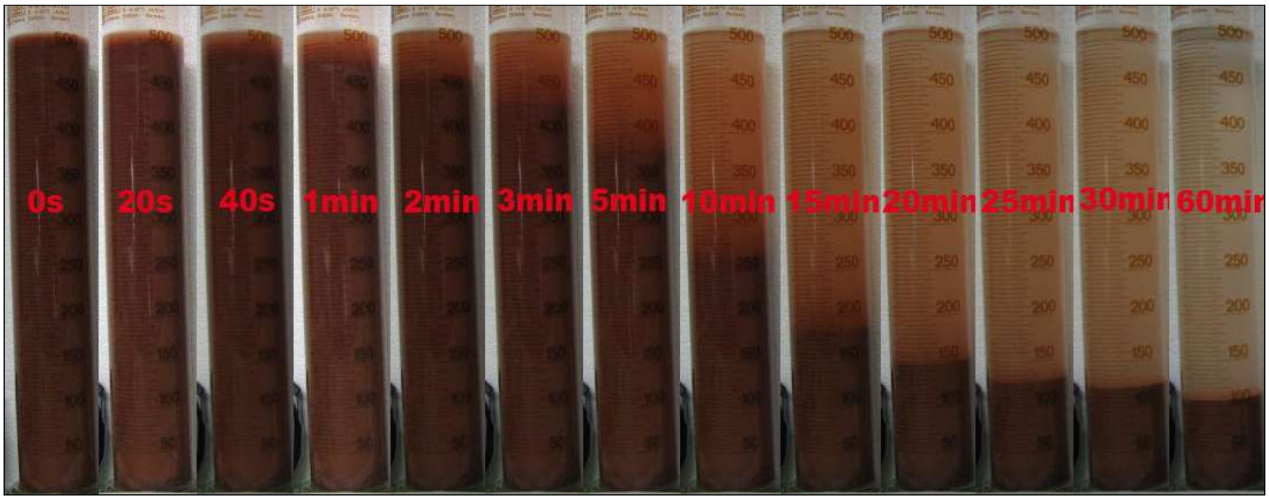

Figure 257: AO321 – 0.005M $CaCl_2$

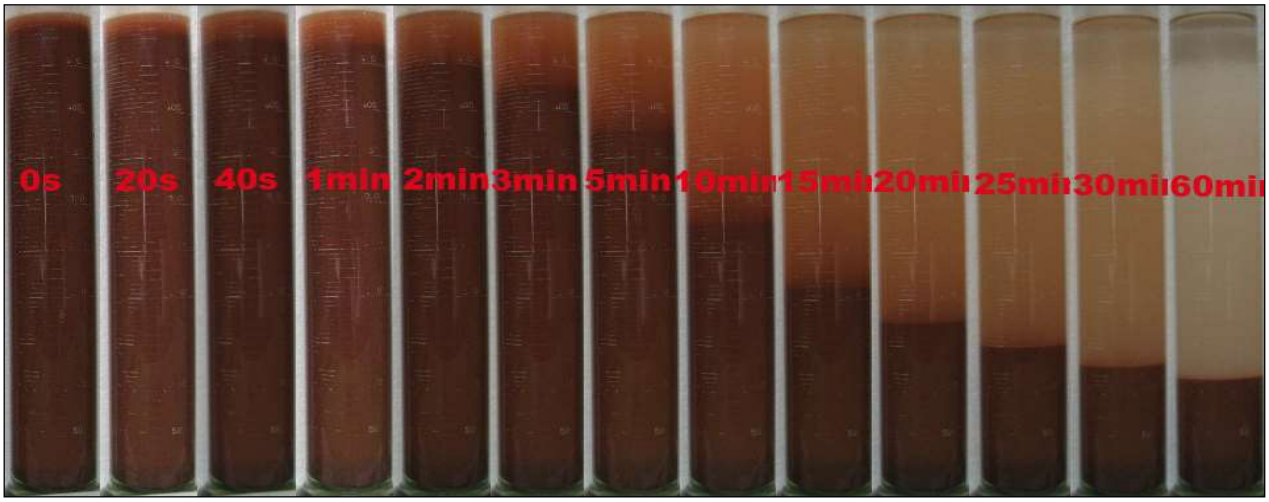

Figure 258: AO321 – 0.005M $MgCl_2$

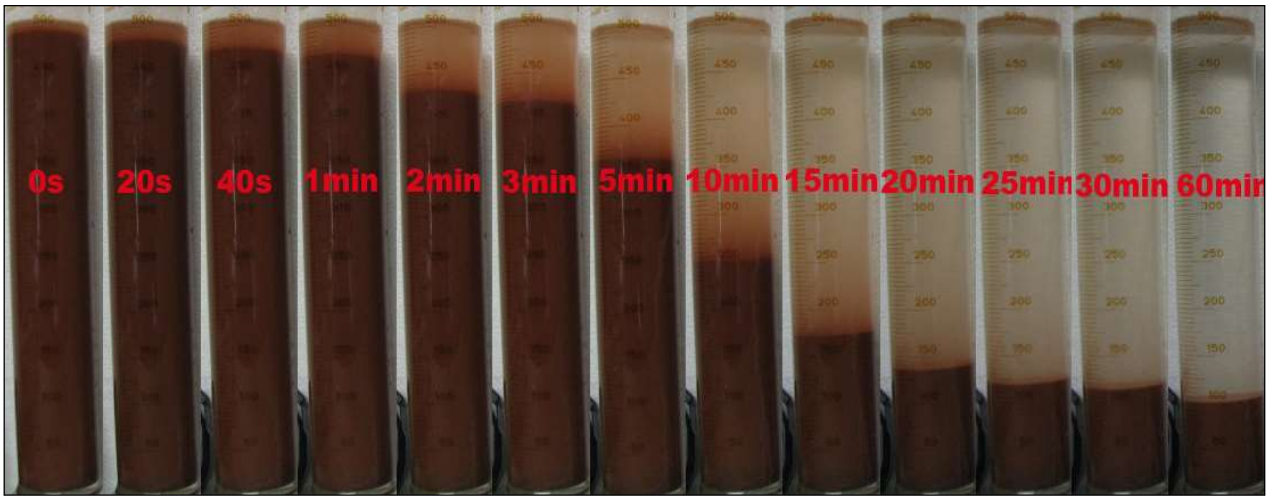

Figure 259: AO321 – 0.005M $CuCl_2$

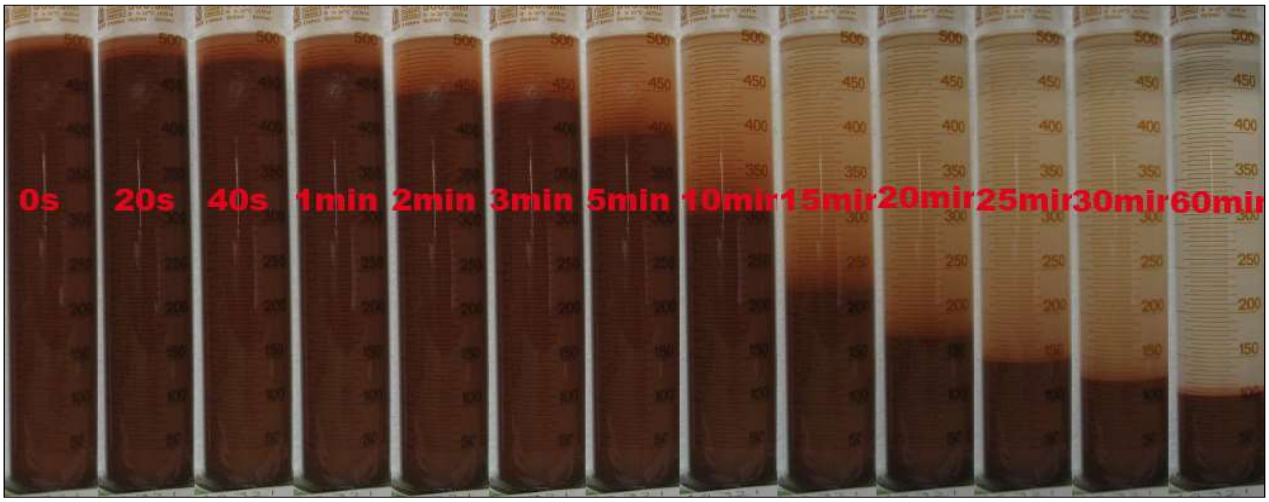

Figure 260: AO321 – 0.005M $FeCl_3$

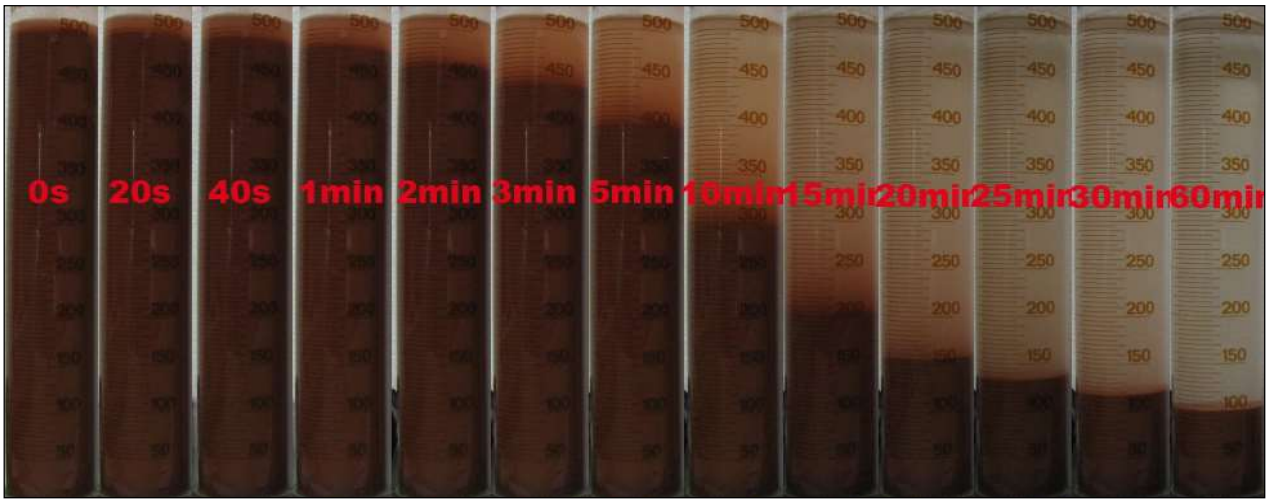

Figure 261: AO321 – 0.005M $AlCl_3$

Figure 262: AO322 – 0.035M KCl

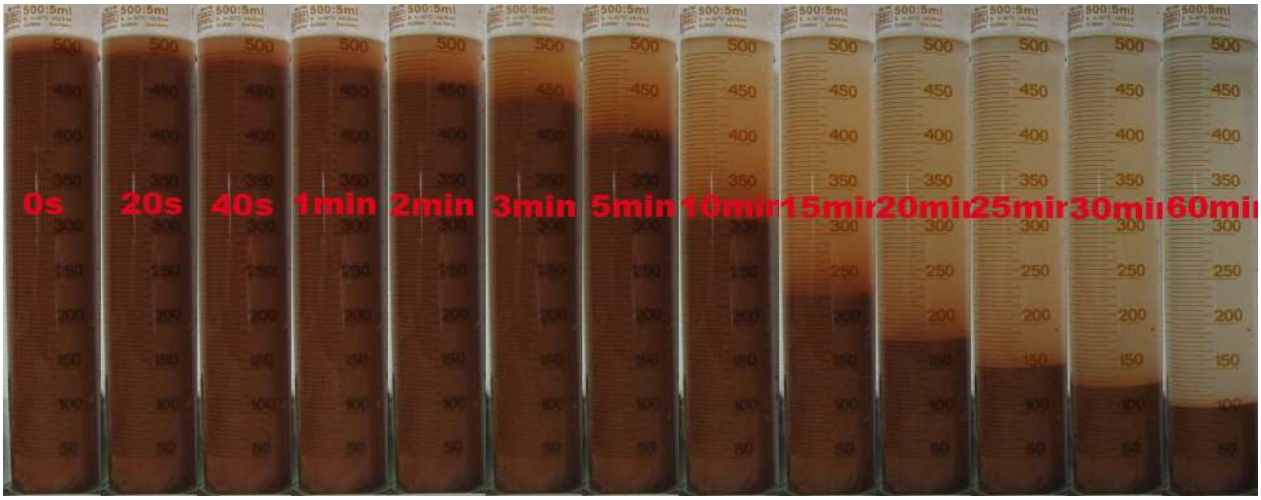

Figure 263: AO322 – 0.005M $CaCl_2$

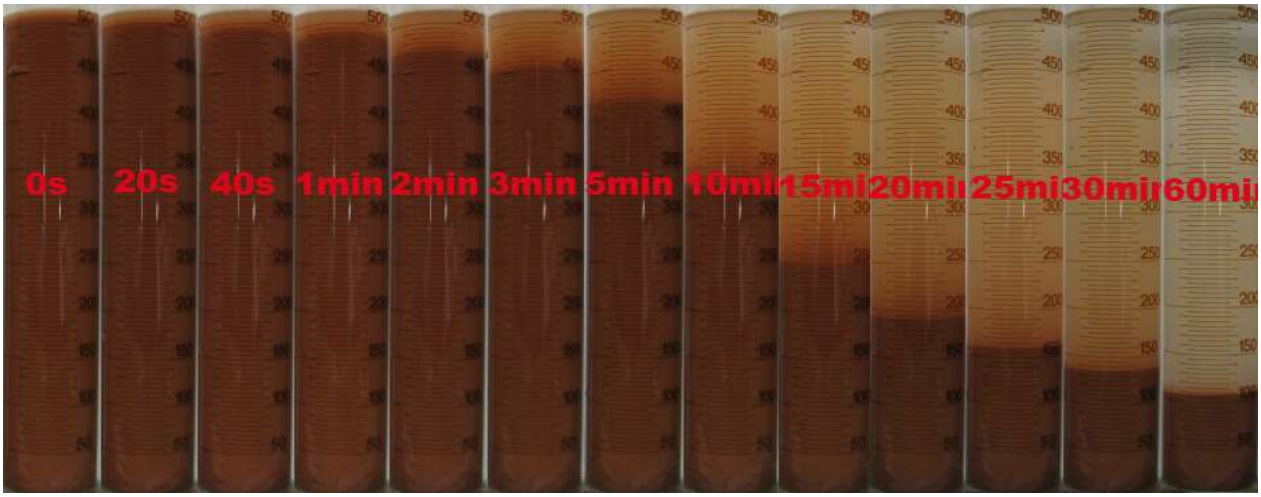

Figure 264: AO322 – 0.005M $MgCl_2$

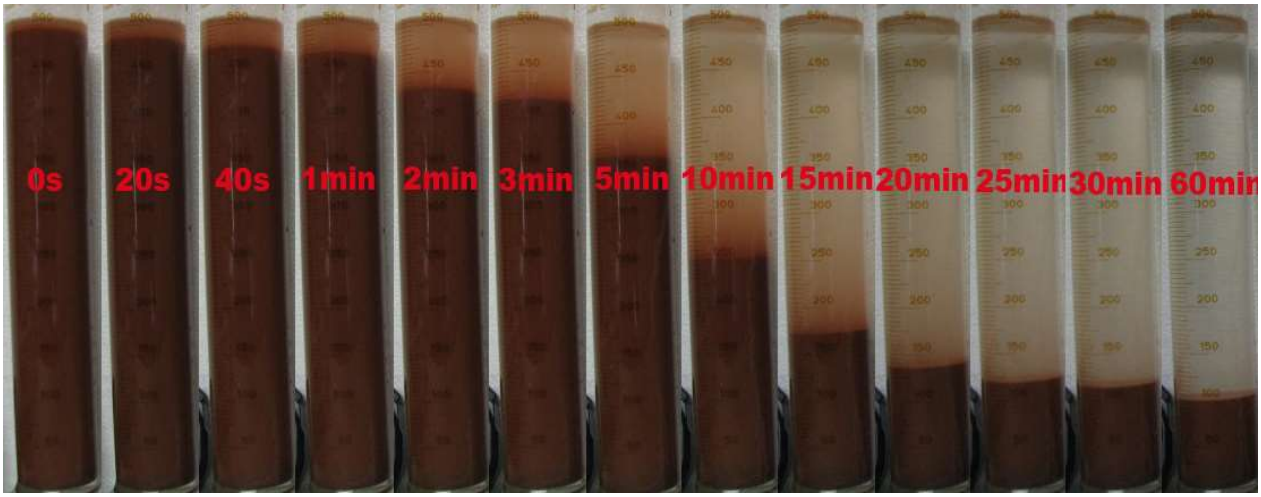

Figure 265: AO322 – 0.005M $CuCl_2$

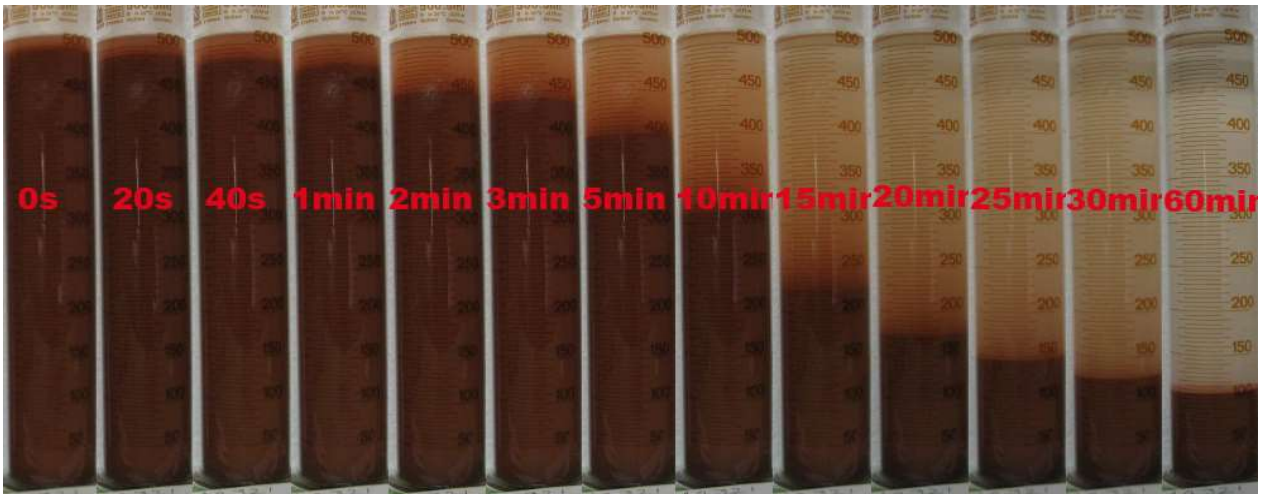

Figure 266: AO322 – 0.005M $FeCl_3$

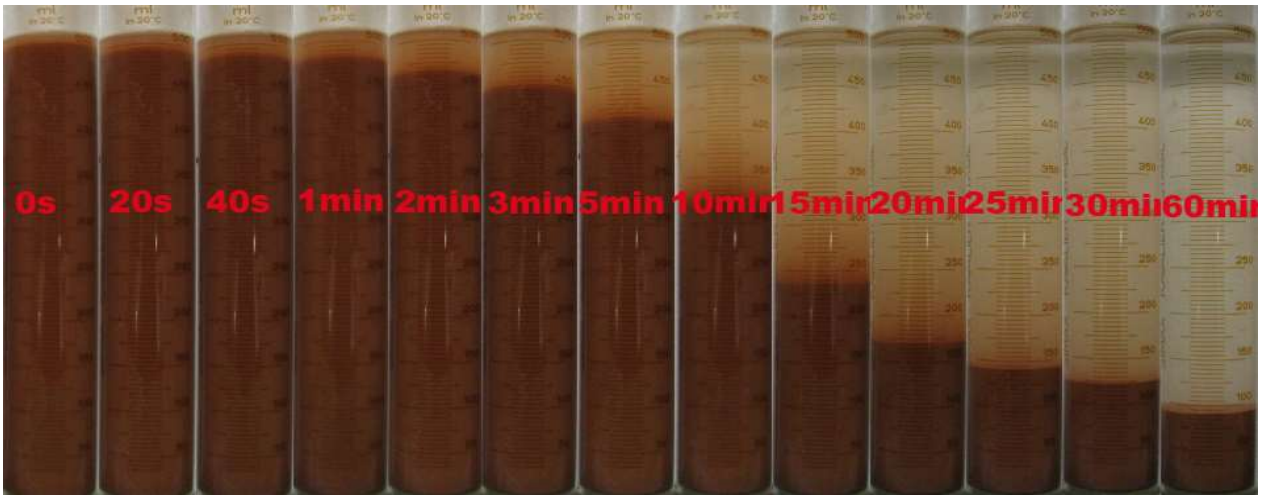

Figure 267: AO322 – 0.005M $AlCl_3$

Figure 268: AO323 – 0.05M KCl

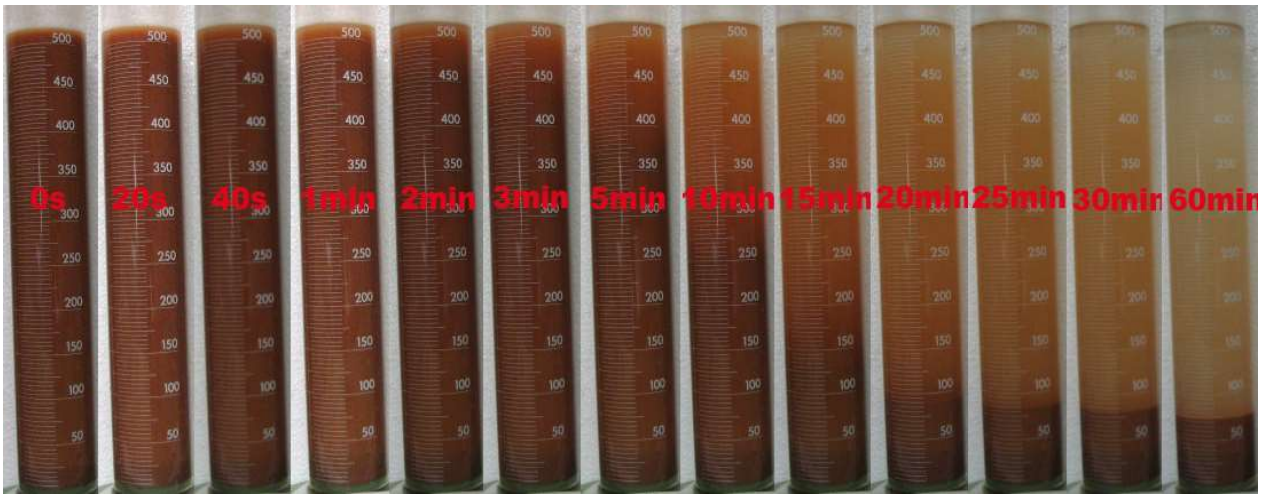

Figure 269: AO323 – 0.005M $CaCl_2$

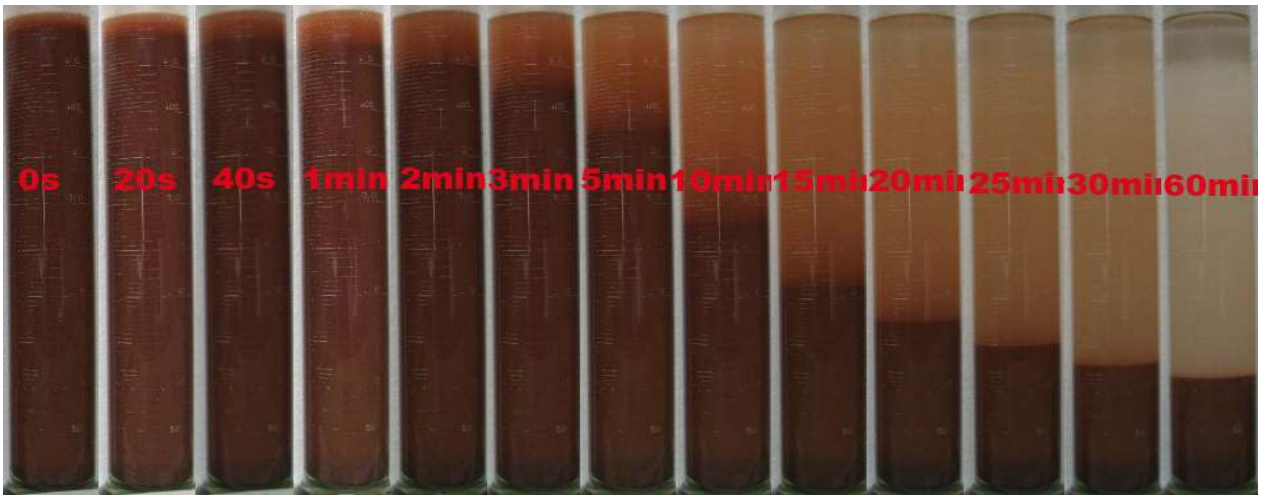

Figure 270: AO323 – 0.005M $MgCl_2$

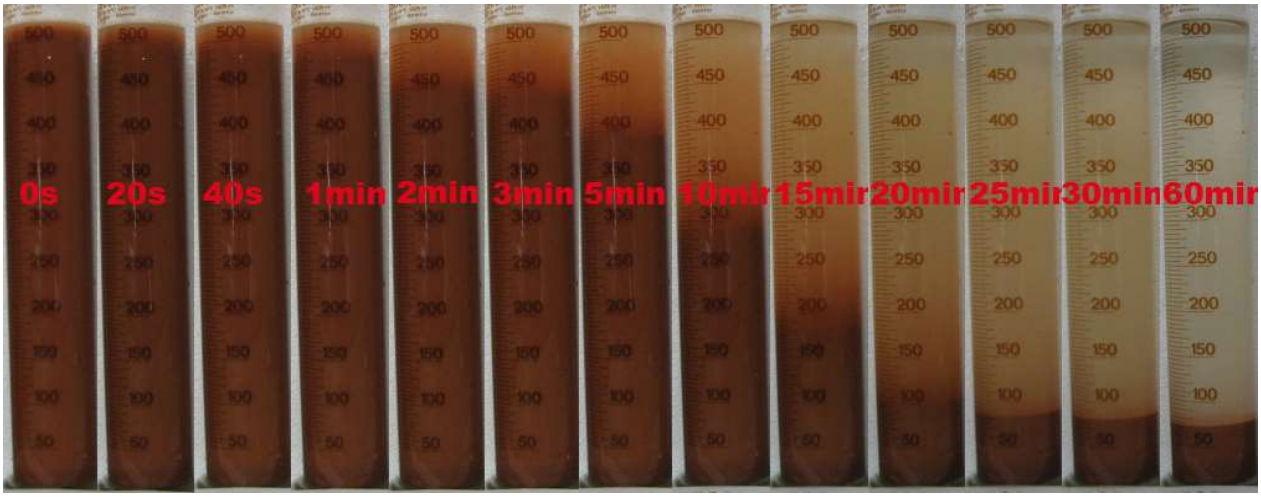

Figure 271: AO323 – 0.005M $CuCl_2$

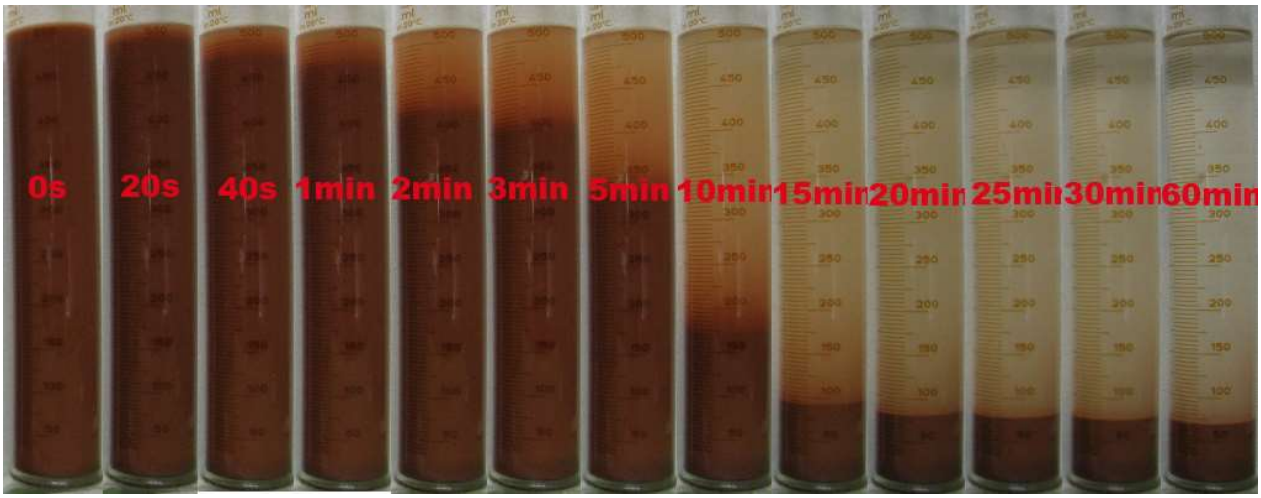

Figure 272: AO323 – 0.005M $FeCl_3$

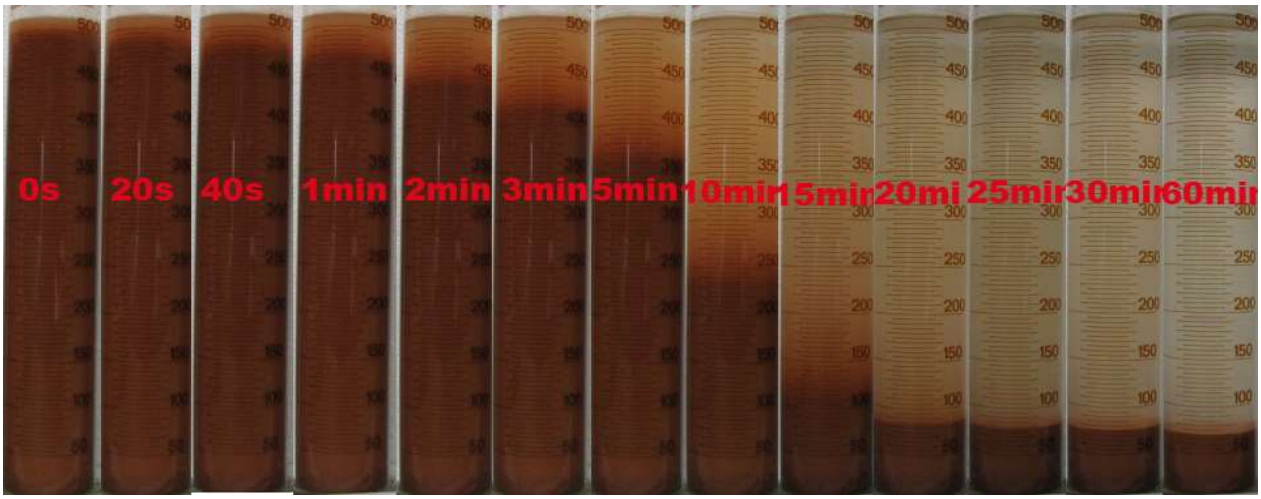

Figure 273: AO323 – 0.005M $AlCl_3$

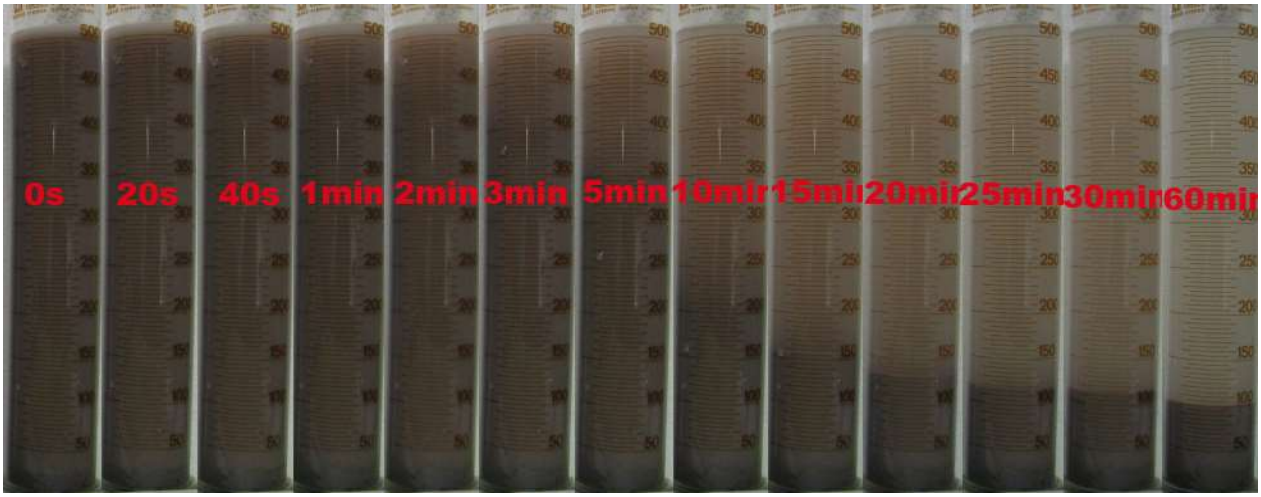

Figure 274: AO324 – 0.01M KCl

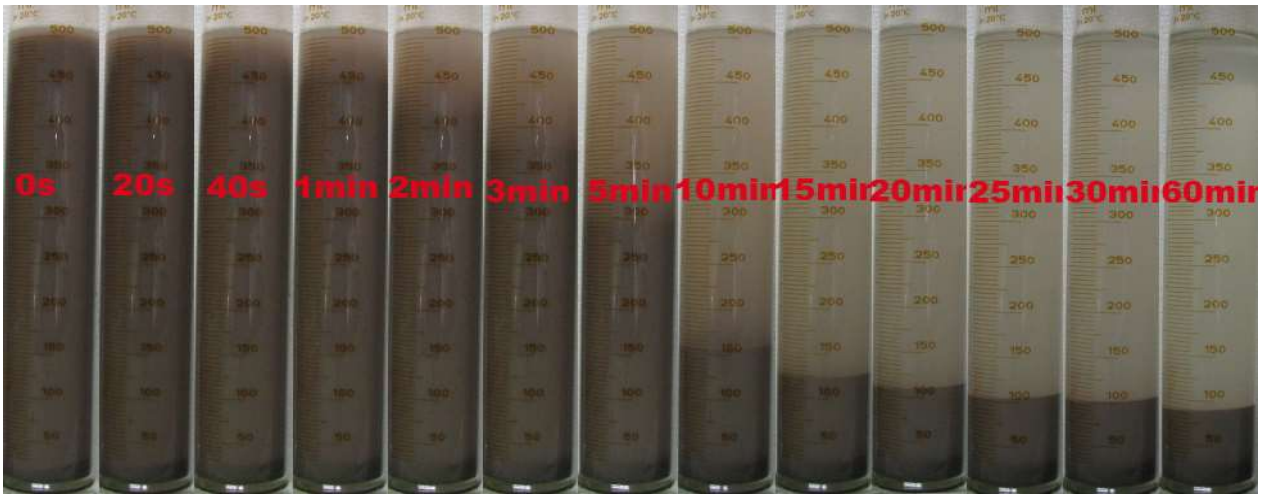

Figure 275: AO324 – 0.005M $CaCl_2$

Figure 276: AO324 – 0.005M $MgCl_2$

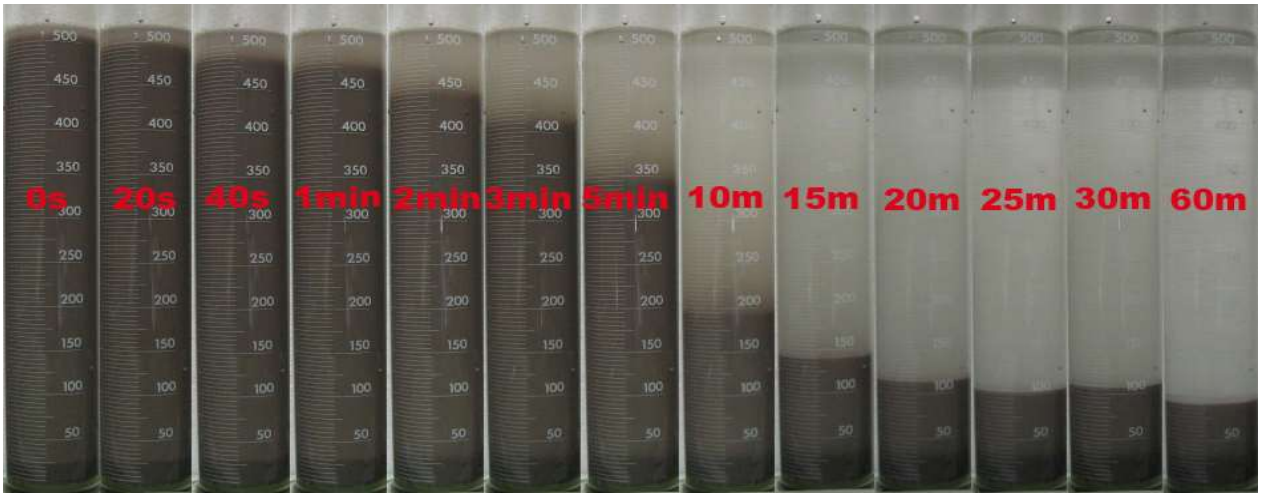

Figure 277: AO324 – 0.005M $CuCl_2$

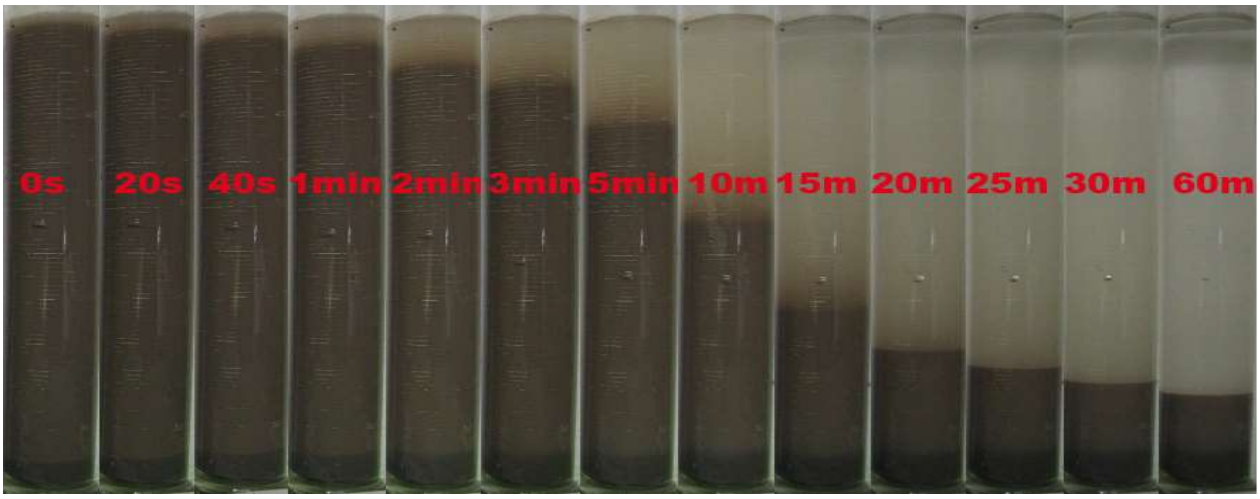

Figure 278: AO324 – 0.005M $FeCl_3$

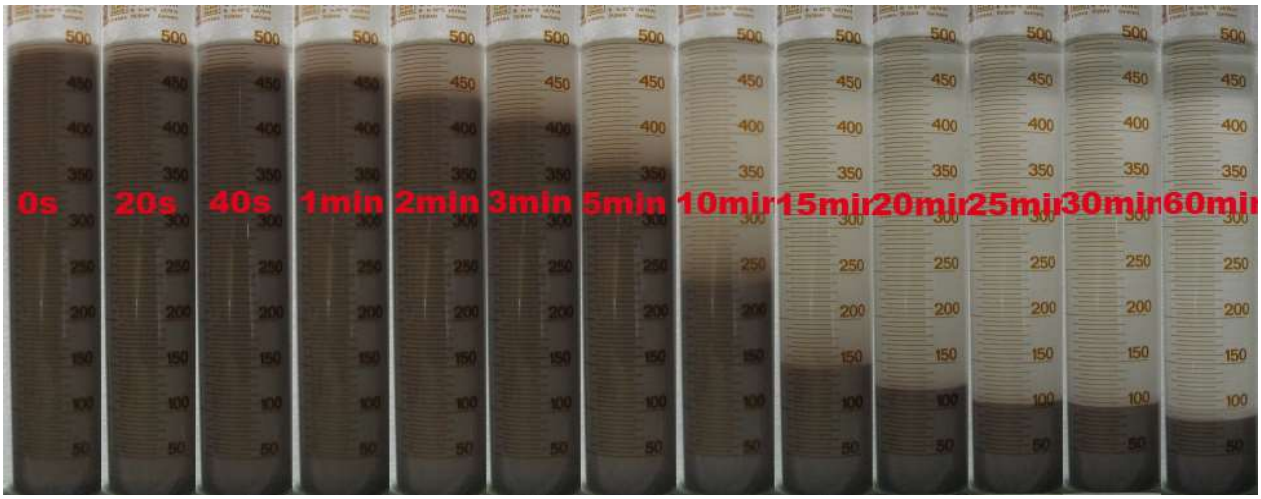

Figure 279: AO324 – 0.005M $AlCl_3$

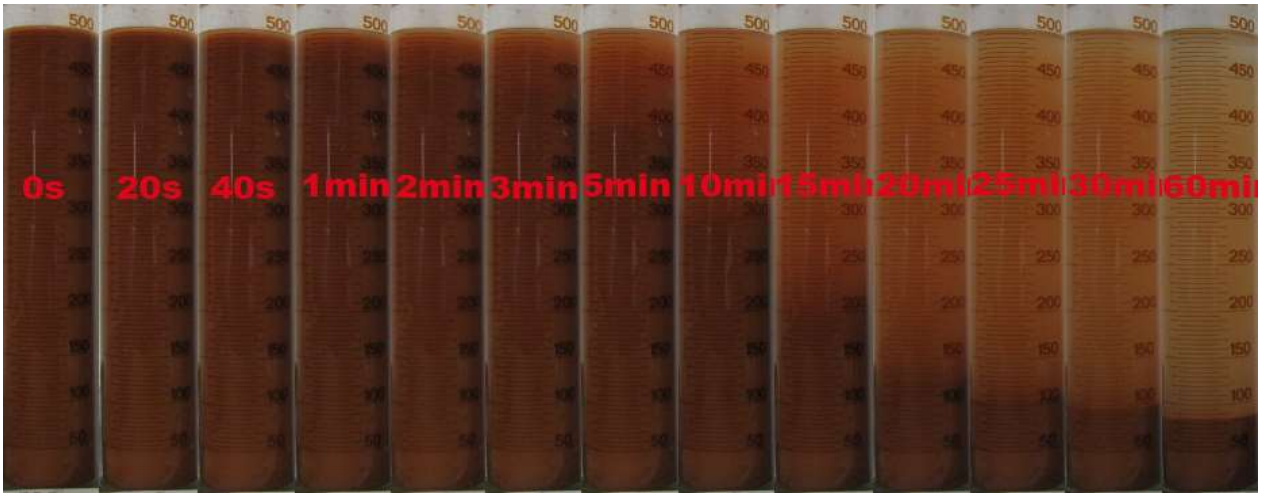

Figure 280: AO 325 – 0.005M KCl

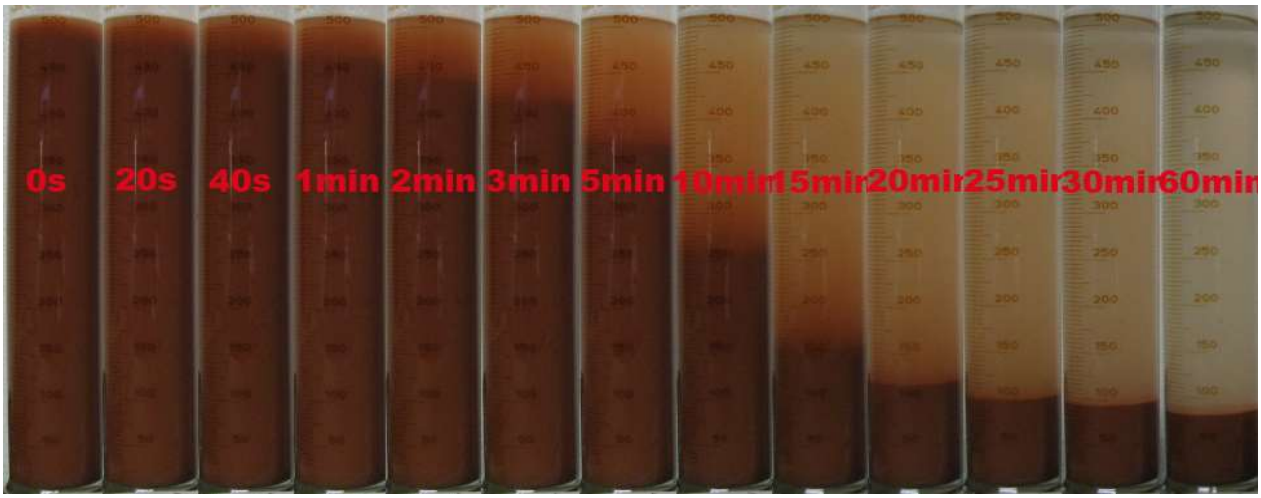

Figure 281: AO325 – 0.005M $CaCl_2$

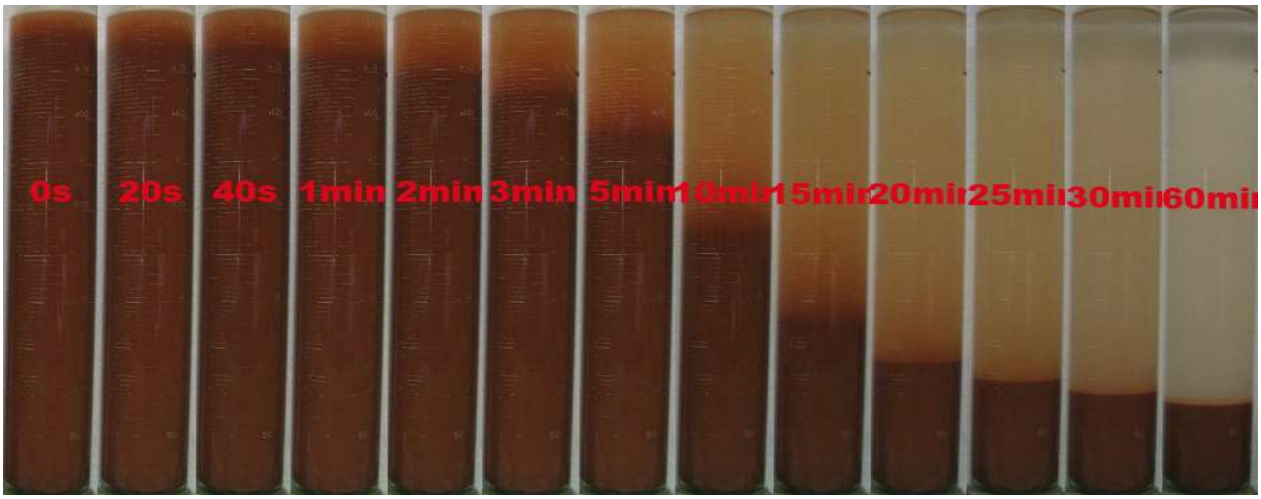

Figure 282: AO325 – 0.005M $MgCl_2$

Figure 283: AO325 – 0.005M $CuCl_2$

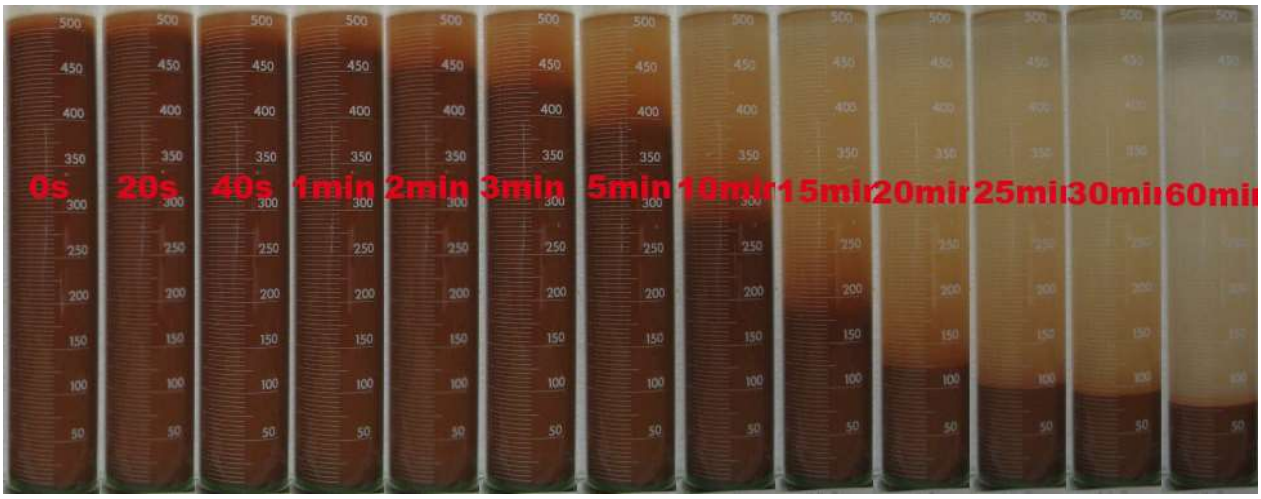

Figure 284: AO325 – 0.005M $FeCl_3$

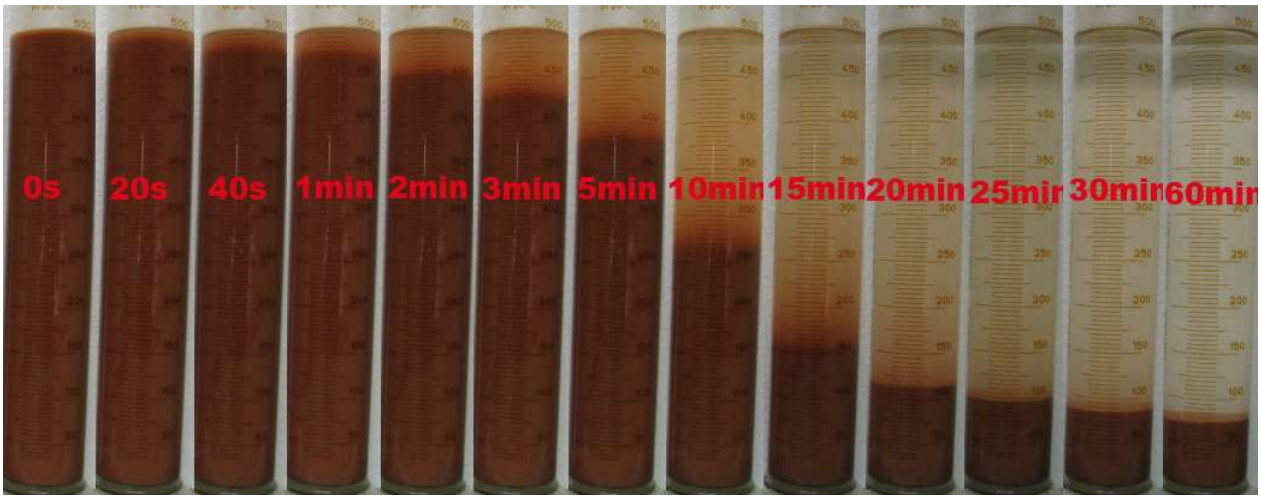

Figure 285: AO325 – 0.005M $AlCl_3$

Figure 286: AO 326 – 0.01M KCl

Figure 287: AO 326 – 0.005M $CaCl_2$

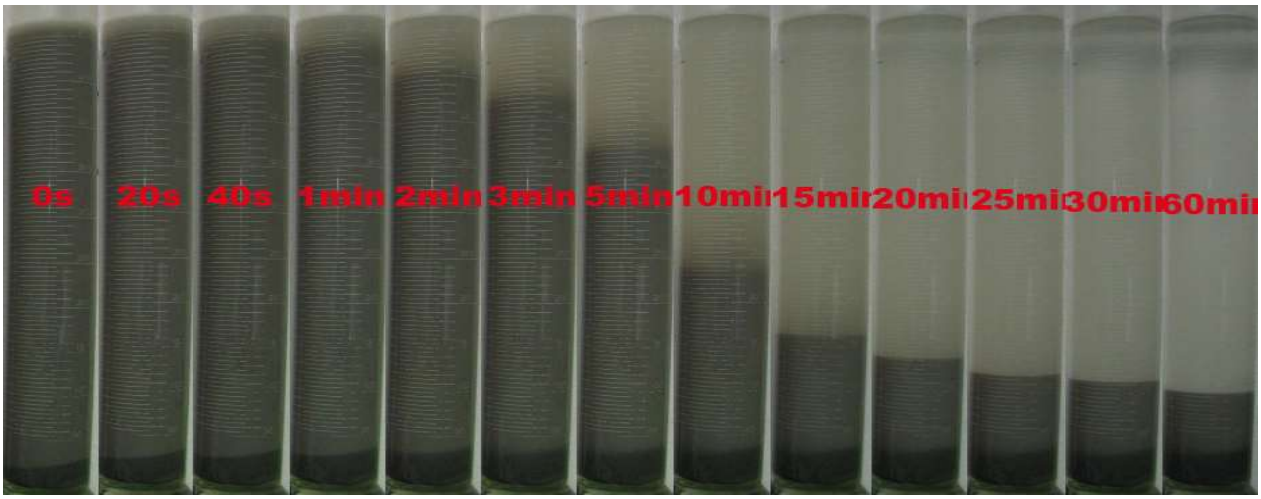

Figure 288: AO 326 – 0.005M $MgCl_2$

Figure 289: AO 326 – 0.005M $CuCl_2$

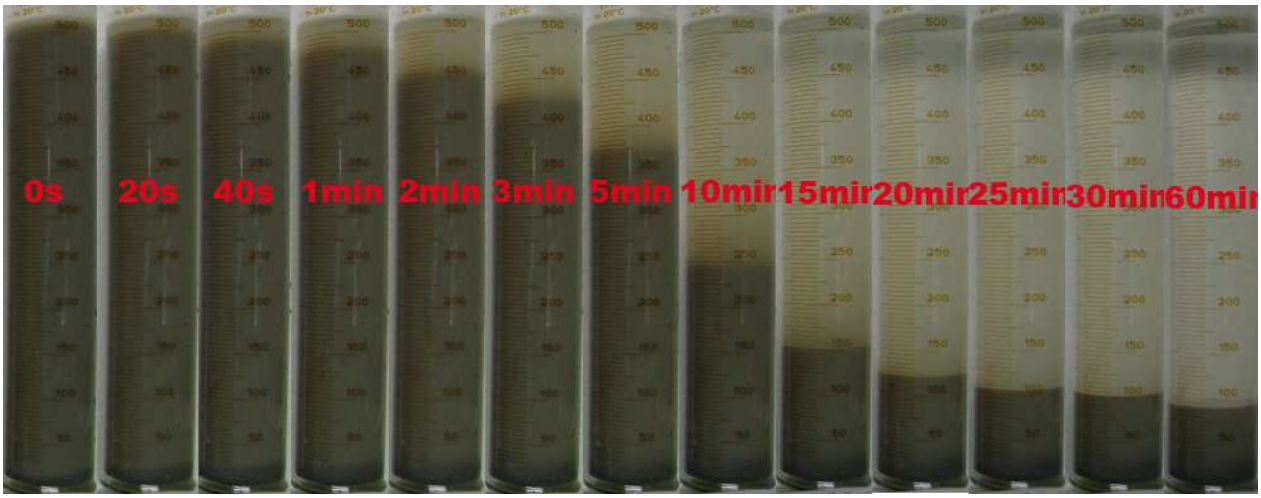

Figure 290: AO 326 – 0.005M $FeCl_3$

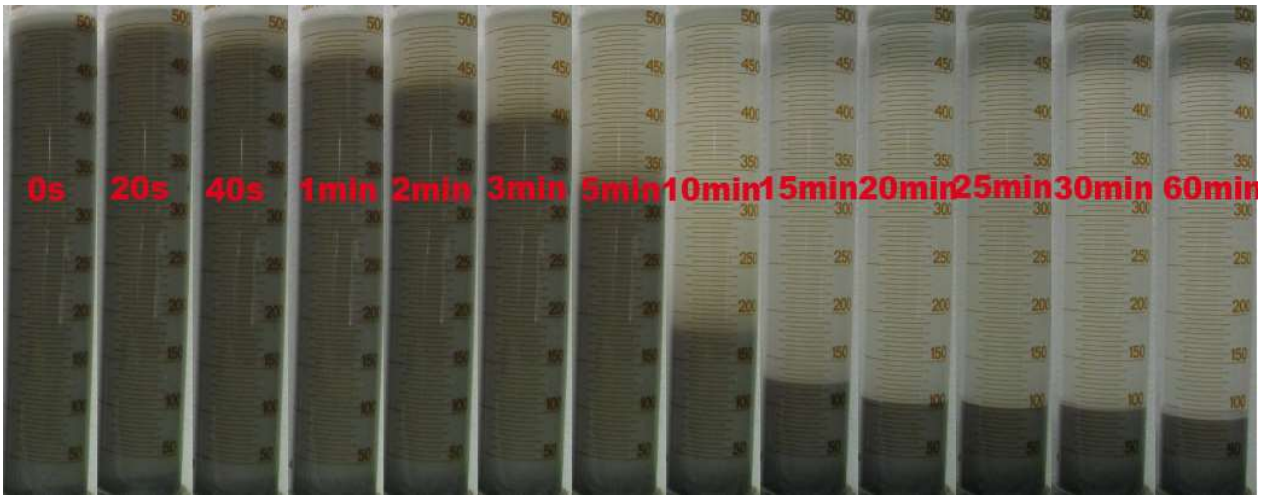

Figure 291: AO 326 – 0.005M $AlCl_3$

Figure 292: AO 327 – 0.02M KCl

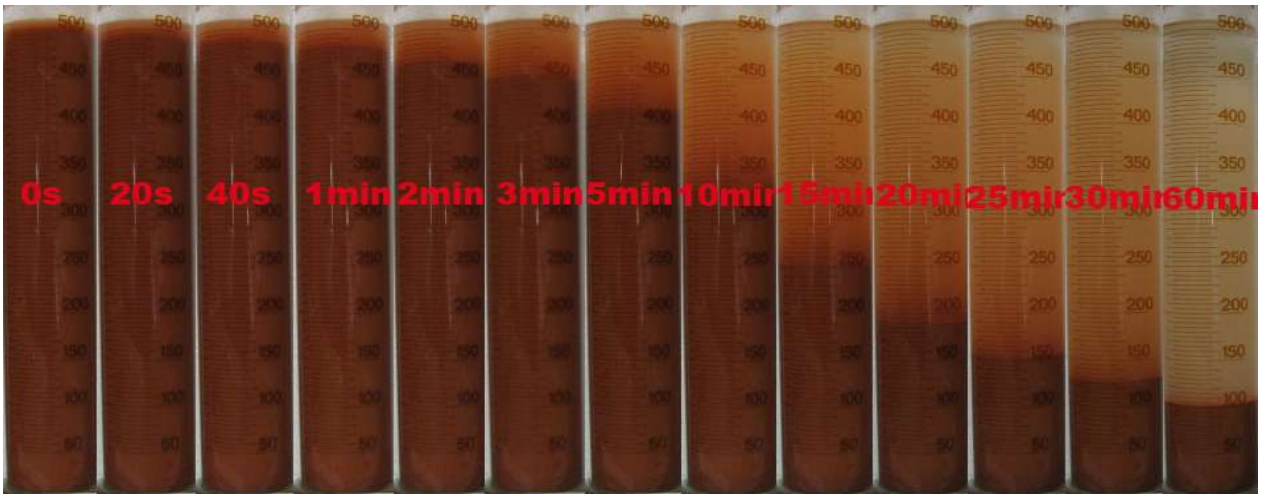

Figure 293: AO 327 – 0.005M $CaCl_2$

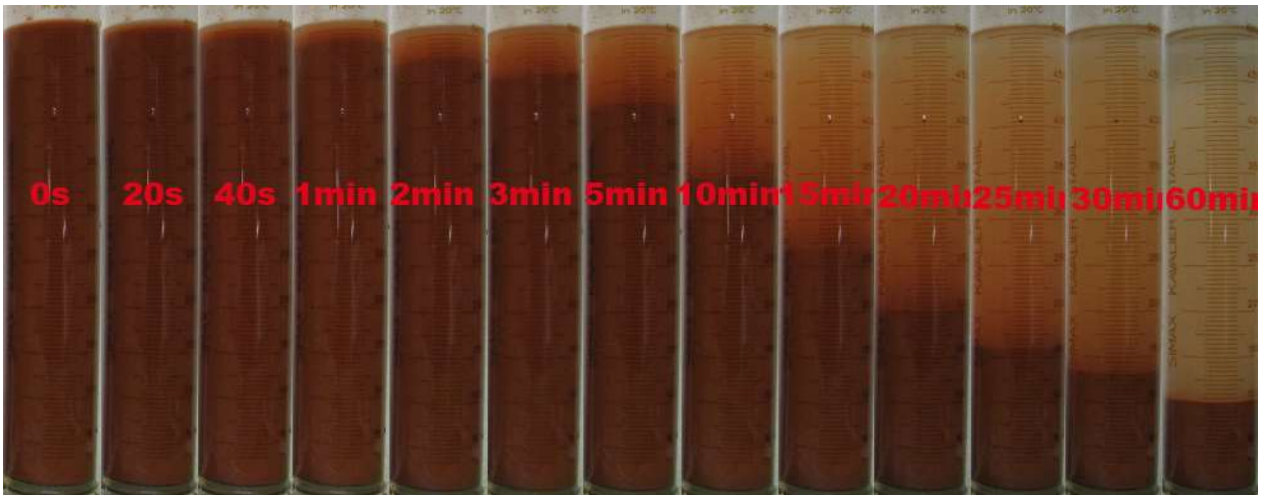

Figure 294: AO 327 – 0.005M $MgCl_2$

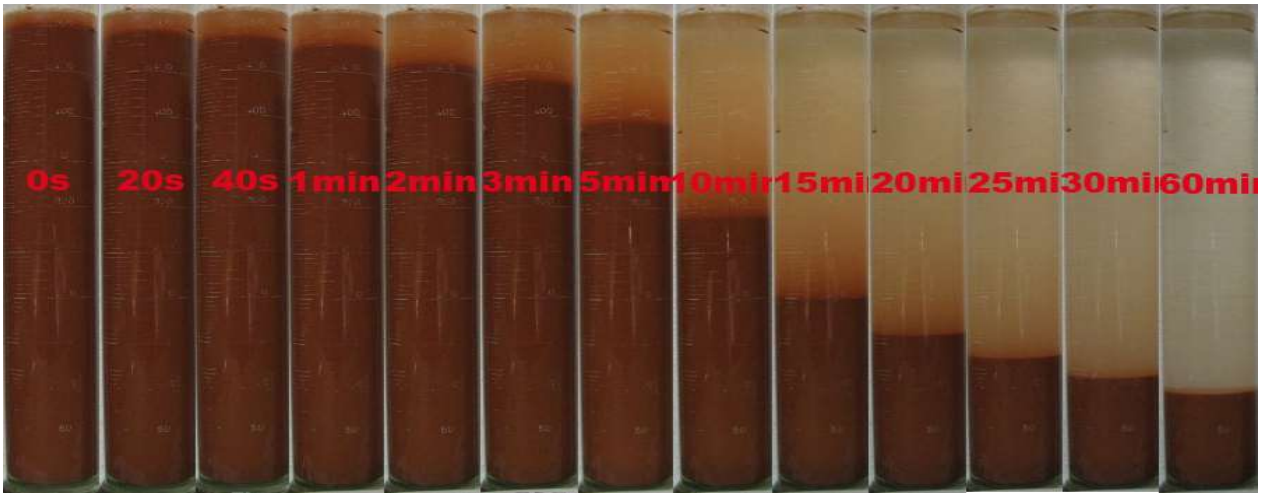

Figure 295: AO 327 – 0.005M $CuCl_2$

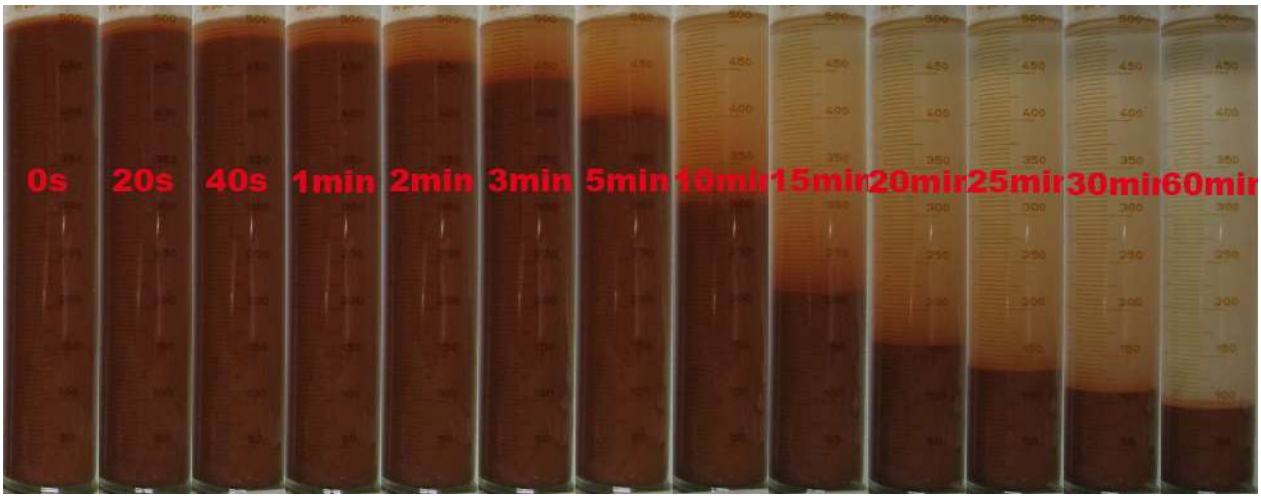

Figure 296: AO 327 – 0.005M $FeCl_3$

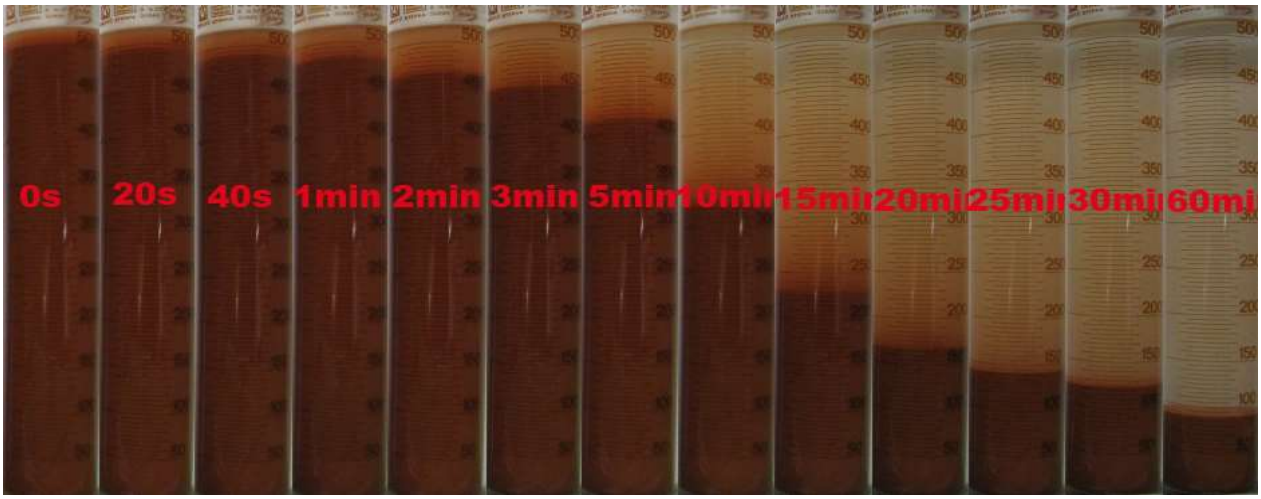

Figure 297: AO 327 – 0.005M $AlCl_3$

Figure 298: AO328 – 0.02M KCl

Figure 299: AO328 - 0.01M $CaCl_2$

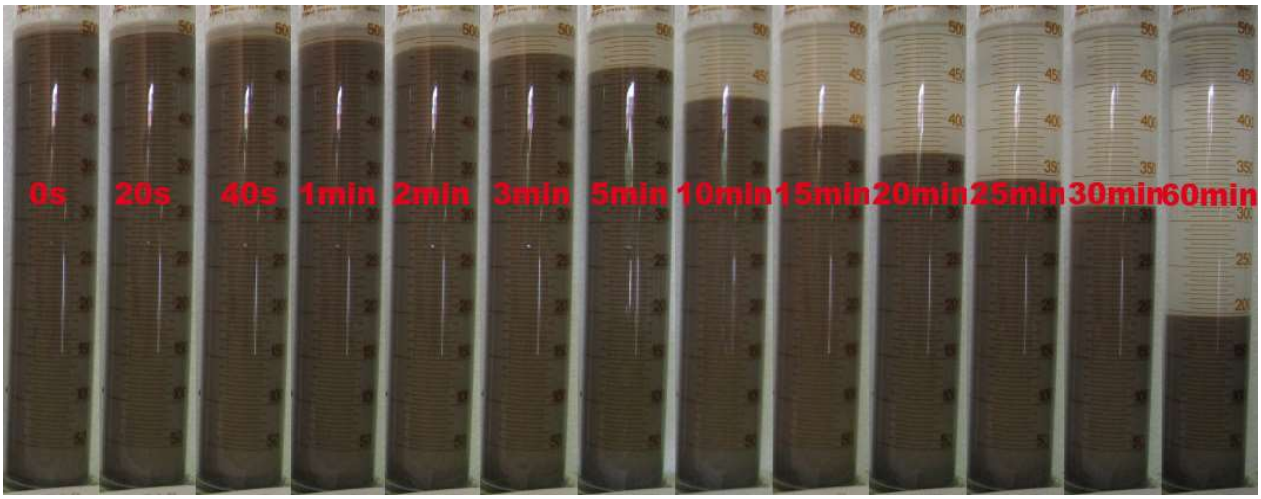

Figure 300: AO328 - 0.01M $MgCl_2$

Figure 301: AO328 - 0.005M $CuCl_2$

Figure 302: AO328 - 0.01M $FeCl_3$